ISSN: 0218 – 1274

INTERNATIONAL JOURNAL OF

BIFURCATION AND CHAOS

IN APPLIED SCIENCES AND ENGINEERING

THEME ISSUE – Part II

Volume 8 • Number 9 • September 1998

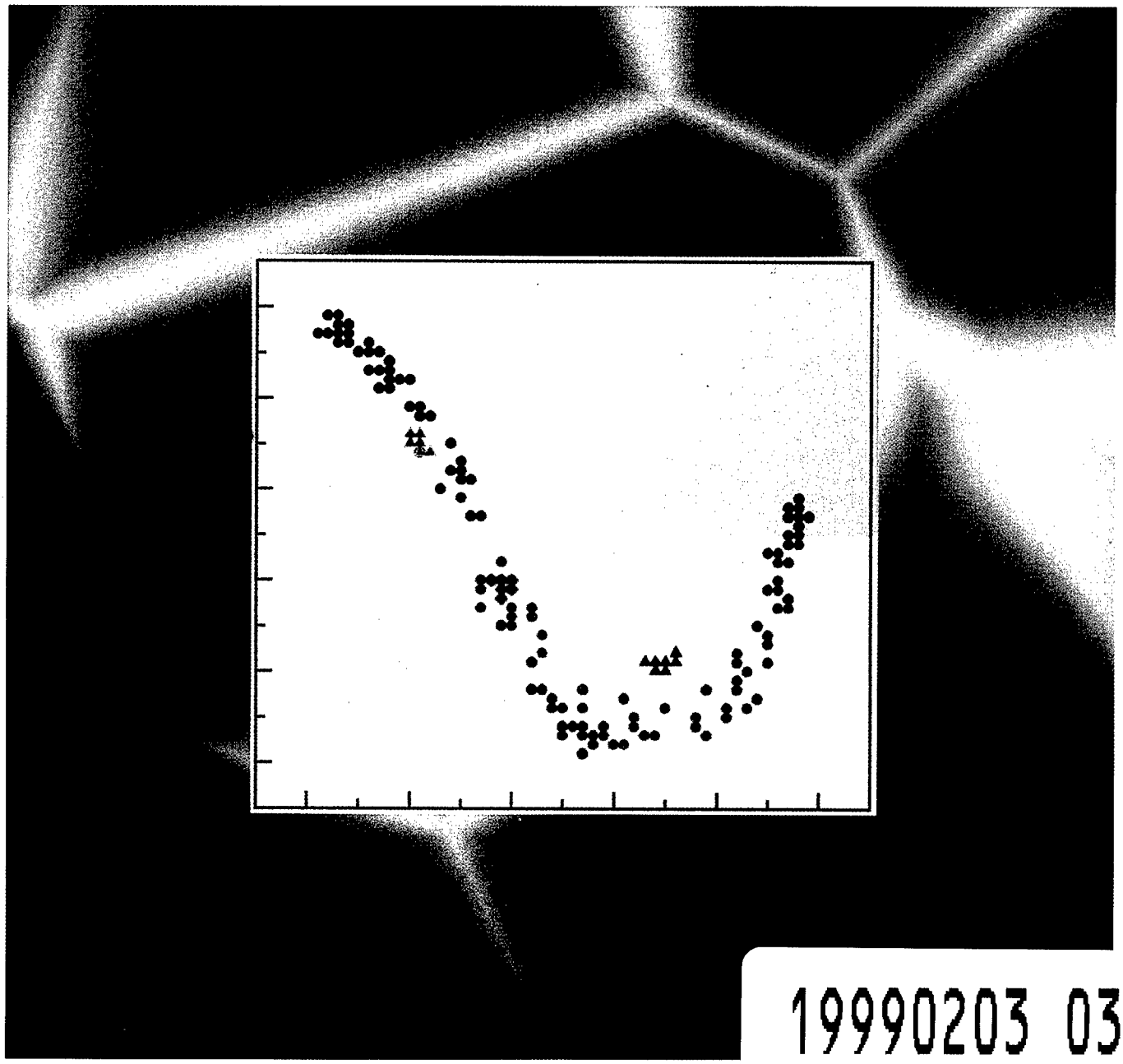

World Scientific
Singapore • New Jersey • London • Hong Kong

AIMS AND SCOPE

The discipline of *chaos* has created a universal paradigm, a scientific parlance, and a mathematical tool for grappling with *nonlinear* phenomena. In every field of the *applied sciences* (astronomy, atmospheric sciences, biology, chemistry, economics, geophysics, life and medical sciences, physics, social sciences, zoology, etc.) and *engineering* (aerospace, chemical, civil, computer, information, mechanical, software, telecommunication, etc.) the local and global manifestations of Chaos and Bifurcation have burst forth in an unprecedented universality, linking scientists heretofore unfamiliar with one another's fields, and offering an opportunity to reshape our grasp of reality.

The primary *objective* of this journal is to provide a single forum for this multidisciplinary discipline — a forum specifically designed for an interdisciplinary audience, a forum accessible and affordable to all. Real-world problems and applications will be emphasized. Our goal is to bring together, in one periodical, papers of the highest quality and greatest importance on every aspect of *nonlinear dynamics*, *phenomena*, *modeling*, and *complexity*, thereby providing a focus and catalyst for the timely dissemination and cross-fertilization of new ideas, principles, and techniques across a broad interdisciplinary front.

The *scope* of this journal encompasses *experimental*, *computational*, and *theoretical* aspects of **bifurcations**, **chaos** and **complexity** of biological, economic, engineering, fluid dynamic, neural, physical, social, and other dynamical systems. This broad but focused coverage includes, but is not restricted to, those areas of expertise provided by the members of the editorial board, whose composition will evolve continuously in order to respond to emerging new areas and directions in *nonlinear dynamics* and *complexity*. The philosophy and policy of this journal, as well as its commitment to readability and clarity, are articulated in an *Editorial* in the first issue (vol. 1, no. 1, 1991).

INFORMATION FOR AUTHORS

1. *International Journal of Bifurcation and Chaos* is a monthly journal consisting of
   - **papers**

     While the majority of papers will consist of original contributions, the Journal also welcomes well-written, incisive authoritative *tutorials* and *reviews* with long-lasting value to future researchers.
   - **letters to the Editor**

     These are mainly for the timely announcement of significant new results and discoveries (phenomena, algorithms, theorems, etc.). Though concise, letter manuscripts must include details and data so that referees can evaluate their validity and significance.
2. Once a paper or letter to the Editor is accepted for publication, the author is assumed to have transferred the copyright for it to the publisher.
3. Essential color pictures will be published at no cost to the authors.
4. There are no page charges for this journal.
5. 50 complimentary reprints will be given to the author(s) of each paper. For a multi-author paper, these will be sent to the author designated as the contact person. Orders for additional reprints may be made on forms which will be sent along with the proofs.

REPRODUCTION QUALITY NOTICE

This document is the best quality available. The copy furnished to DTIC contained pages that may have the following quality problems:

- Pages smaller or larger than normal.
- Pages with background color or light colored printing.
- Pages with small type or poor printing; and or
- Pages with continuous tone material or color photographs.

Due to various output media available these conditions may or may not cause poor legibility in the microfiche or hardcopy output you receive.

☑ If this block is checked, the copy furnished to DTIC contained pages with color printing, that when reproduced in Black and White, may change detail of the original copy.

REPORT DOCUMENTATION PAGE

Form Approved OMB No. 0704-0188

1. AGENCY USE ONLY (Leave blank)	2. REPORT DATE	3. REPORT TYPE AND DATES COVERED
	~~10 January 1999~~	Conference Proceedings

4. TITLE AND SUBTITLE

Control of Chaos: New Perspectives in Experimental and Theoretical Science

5. FUNDING NUMBERS

F6170897W0108

6. AUTHOR(S)

Conference Committee

7. PERFORMING ORGANIZATION NAME(S) AND ADDRESS(ES)

Instituto Nazionale di Ottica
Largo Enrico Fermi 6
Florence 50125
Italy

8. PERFORMING ORGANIZATION REPORT NUMBER

N/A

9. SPONSORING/MONITORING AGENCY NAME(S) AND ADDRESS(ES)

EOARD
PSC 802 BOX 14
FPO 09499-0200

10. SPONSORING/MONITORING AGENCY REPORT NUMBER

CSP 97-1053

11. SUPPLEMENTARY NOTES

2 Volumes

12a. DISTRIBUTION/AVAILABILITY STATEMENT

Approved for public release; distribution is unlimited.

12b. DISTRIBUTION CODE

A

13. ABSTRACT (Maximum 200 words)

The Final Proceedings for Control of Chaos: New Perspectives in Experimental and Theoretical Science, 16 May 1997 - 18 May 1997

nonlinear, adaptive and robust control; synchronization of chaotic processes; and applications of control of chaos in science and technology.

14. SUBJECT TERMS

EOARD, Control, Lasers, Non-linear Dynamics

15. NUMBER OF PAGES

16. PRICE CODE
N/A

17. SECURITY CLASSIFICATION OF REPORT	18. SECURITY CLASSIFICATION OF THIS PAGE	19. SECURITY CLASSIFICATION OF ABSTRACT	20. LIMITATION OF ABSTRACT
UNCLASSIFIED	UNCLASSIFIED	UNCLASSIFIED	UL

INTERNATIONAL JOURNAL OF

BIFURCATION AND CHAOS

IN APPLIED SCIENCES AND ENGINEERING

THEME ISSUE - Part II

Volume 8 • Number 9 • September 1998

CONTROL OF CHAOS: NEW PERSPECTIVES IN EXPERIMENTAL AND THEORETICAL NONLINEAR SCIENCE

Guest Editors

F. T. Arecchi

S. Boccaletti

M. Ciofini

G. Grebogi

R. Meucci

World Scientific

Singapore • New Jersey • London • Hong Kong

INTERNATIONAL JOURNAL OF
BIFURCATION AND CHAOS
IN APPLIED SCIENCES AND ENGINEERING
THEME ISSUE - Part II

Volume 8 • Numbers 8 & 9 • Aug & Sept 1998

CONTENTS (August 1998)

Editorial 1641

Tutorials and Reviews

The Control of Chaos: Theoretical Schemes and Experimental Realizations 1643
F. T. Arecchi, S. Boccaletti, M.Ciofini, R. Meucci and C. Grebogi

Applications of Chaotic Digital Code-Division Multiple Access (CDMA) to Cable Communication Systems 1657
T. Yang and L. O. Chua

Papers

Adaptive Mode Selection Using On–Off Switching of Chaos 1671
P. Davis

Parametric Resonant Control of Chaos 1675
R. Lima and M. Pettini

Adaptive Mode Selection Based on Chaotic Search in a Fabry–Perot Laser Diode 1685
Y. Liu and P. Davis

Controlling Chaos with Parametric Perturbations 1693
L. Fronzoni and M. Giocondo

On Optimal Stabilization of Periodic Orbits via Time Delayed Feedback Control 1699
M. Basso, R. Genesio, L. Giovanardi, A. Tesi and G. Torrini

Control of Chaotic Maps by Optimized Periodic Inputs 1707
R. Mettin

Clustering Bifurcation and Spatiotemporal Intermittency in RF-Driven Josephson Junction Series Arrays 1713
F. Xie and H. A. Cerdeira

Inhibition of Chaotic Escape by an Additional Driven Term 1719
F. Balibrea, R. Chacón and M. A. López

Simulation of Heartbeat Dynamics: A Nonlinear Model 1725
M. G. Signorini, S. Cerutti and D. di Bernardo

Letters

Desynchronization Transitions in Rings of Coupled Chaotic Oscillators 1733
I. P. Mariño, V. Pérez-Muñuzuri and M. A. Matías

Suppression and Excitation of Chaos: The Example of the Glow Discharge 1739
T. Braun

Fuzzy Control of Chaos 1743
O. Calvo and J. H. E. Cartwright

CONTENTS (September 1998)

Tutorials and Reviews

Control of Chaos in Lasers by Feedback and Nonfeedback Methods 1749
P. Glorieux

Papers

Experimental Techniques for Controlling Chaos in Lasers 1759
R. Meucci, A. Labate and M. Ciofini

Instabilities and Tracking of Travelling Wave Patterns in a Three-Level Laser 1769
W. Lu, D. Yu and R. G. Harrison

Experimental Switchings in Bistability Domains Induced by Resonant Perturbations 1777
V. N. Chizhevsky, R. Vilaseca and R. Corbalan

Dynamic Stabilization of Unstable Periodic Orbits in a CO_2 Laser by Slow Modulation of Cavity Detuning 1783
A. N. Pisarchik, R. Corbalán, V. N. Chizhevsky, R. Vilaseca and B. F. Kuntsevich

Chaos Control in External Cavity Laser Diodes Using Electronic Impulsive Delayed Feedback 1791
A. V. Naumenko, N. A. Loiko, S. I. Turovets, P. S. Spencer and K. A. Shore

Self-Pulsing and Chaos in an Extended-Cavity Diode Laser with Intracavity Atomic Absorber 1801
F. di Teodoro, E. Cerboneschi, D. Hennequin and E. Arimondo

Control of Turn-On in Class-B Lasers 1811
P. A. Porta, L. M. Hoffer, H. Grassi and G. L. Lippi

Synchronization of a Network of Chaotic Neurons Using Adaptive Control in Noisy Environments 1821
B. Cazelles

Nonlinearity Tests Using the Extrema of a Time Series 1831
A. di Garbo, R. Balocchi and S. Chillemi

Letters

Transmission of Signals via Synchronization of Chaotic Time-Delay Systems 1839
K. Pyragas

Control of Amplitude Turbulence in Delayed Dynamical Systems 1843
D. Maza, H. Mancini, S. Boccaletti, R. Genesio and F. T. Arecchi

Diffusion Parameter Control of Spatiotemporal Chaos 1849
R. Montagne and P. Colet

Cover Illustration: From page 1762 [Fig. 7], Volume 8, Number 9.
Cover inset design represents an experimental Poincarè map with chaos (blue circles), stabilized period-1 orbit (green squares) and stabilized period-2 orbit (red triangles).

Subscriptions, changes of address, single-copy orders should be addressed to Journal Department, World Scientific Publishing Co. Pte. Ltd., Farrer Road, P. O. Box 128, Singapore 912805, or Suite 1B, 1060 Main Street, River Edge, NJ 07661, USA, or 57 Shelton Street, Covent Garden, London WC2H 9HE, England.

The **International Journal of Bifurcation and Chaos** (ISSN 0218-1274) is published monthly by World Scientific Publishing Co. Pte. Ltd., Farrer Road, P. O. Box 128, Singapore 912805. Annual subscription rates are available upon request. Periodicals postage paid at Jamaica, N.Y. 11431.
US POST MASTER: Please send change of address to **International Journal of Bifurcation and Chaos**, c/o Publications Expediting Inc., 200 Meacham Avenue, Elmont, N.Y. 11003. Air freight & mailing in the US by Publications Expediting Inc., 200 Meacham Avenue, Elmont, N.Y. 11003 (Tel. 516-352-7300).

This journal is covered in *SciSearch®*, *Research Alert®*, *CompuMath Citation Index®* and *Science Citation Index®*.

International Journal of Bifurcation and Chaos, Vol. 8, No. 9 (1998) 1749–1758

CONTROL OF CHAOS IN LASERS BY FEEDBACK AND NONFEEDBACK METHODS

PIERRE GLORIEUX
Laboratoire de Spectroscopie Hertzienne, URA CNRS 249,
Centre d'Etudes et Recherches sur les Lasers et Applications,
Université des Sciences et Technologies de Lille,
F-59655 Villeneuve d'Ascq Cedex, France

Received July 31, 1997; Revised November 25, 1997

Analytical approaches of the theory of chaos control in class B lasers are presented in the cases of continuous delayed feedback and of subharmonic modulation. They are compared with experimental findings on a CO_2 laser and a Nd-doped fiber laser with modulated loss and pump respectively. In both cases, analytical theory allows one to predict the shift of the first period-doubling bifurcations. Numerical simulations show that subharmonic modulation may induce shifts, crises and new attractors in a laser with modulated parameters and that its phase relative to the main modulation allows one to control the laser dynamics. These results agree well with the experimental observations on control of chaos in CO_2 and fiber lasers.

1. Introduction

It is now conventional to separate among the methods used to control chaos those which rely on feedback from those based on nonfeedback techniques. In the former some information from the chaotic system is extracted and used to design a weak correction signal applied to some suitable control parameter. Following the seminal work of Ott, Grebogi and Yorke [Ott *et al.*, 1990], several algorithms have been proposed to control chaos by stabilizing a system on one of its unstable periodic orbits and applied to various systems including lasers [Roy *et al.*, 1994; Bielawski *et al.*, 1993]. In nonfeedback control, a small periodic perturbation or parametric modulation is shown to drastically alter the dynamics of the system under consideration [Bryant & Wiesenfeld, 1986] and this was applied to both monomode [Meucci *et al.*, 1994; Chizhevsky *et al.*, 1986; Gavrielides *et al.*, 1985] and multimode lasers [Otsuka *et al.*, 1997]. These two approaches are of completely different natures, but they share the concept of controlling dynamics through the use of small perturbations. The weakness of these perturbations suggests the existence of small parameters in both situations and therefore there is the possibility of applying perturbation methods to obtain analytical properties of the systems subjected to these control techniques and possibly to compare them with experimental findings.

In this paper we report on advances in the dynamics of class B lasers in presence of (i) delayed feedback [Bielawski *et al.*, 1994; Erneux *et al.*, 1995] and (ii) subharmonic modulation [Newell *et al.*, 1997; Dangoisse *et al.*, 1997]. These works show that singular perturbation methods and more precisely multiple timescale analysis is able to predict how the dynamics are altered by the control techniques and in particular to predict if bifurcation points are shifted by the use of the control techniques mentioned above and to describe how this is done. All these predictions are compared with experimental results on chaos control of class B lasers. This point of view is different from that developed in [Chizhevsky *et al.*, 1986] where the emphasis is on the fact that the nonfeedback control of chaos creates new attractors, a point which was already

discussed for a different system by Gavrielides *et al.* [1985].

Control of chaos by delayed feedback was proposed by Pyragas [Pyragas, 1992; Pyragas & Tamasevicius, 1993] and applied in the laser domain to loss modulated CO_2 lasers [Bielawski *et al.*, 1994; Erneux *et al.*, 1995]. Chaos may also be controlled by adding a small modulation which is resonant or nearly resonant with a subharmonic of the fundamental system frequency [Meucci *et al.*, 1994; Chizhevsky *et al.*, 1986; Braiman & Goldhirsch, 1991; Colet & Braiman, 1996; Ciofini *et al.*, 1995; Vohra *et al.*, 1995]. This technique was first applied to a magnetostrictive ribbon and soon after to lasers including CO_2 [Meucci *et al.*, 1994; Chizhevsky *et al.*, 1986], microchip [Otsuka *et al.*, 1997] and fiber [Dangoisse *et al.*, 1997] lasers. All these belong to the so-called class B lasers in which the relaxation time of the electric polarization is much shorter than the photon cavity lifetime which is itself much smaller than the population inversion relaxation time. Class B lasers have been used as test systems in this approach because they display well characterized chaos when they are subjected to periodic modulation of one of their parameters [Ivanov *et al.*, 1982; Arecchi *et al.*, 1982; Tredicce *et al.*, 1986; Chen *et al.*, 1985]. Moreover single-mode class B lasers are efficiently described by two-variable models suitable for fully analytical treatments. More specifically, doped fiber and CO_2 lasers have been used in the corresponding experiments. These particular lasers have been chosen for technical reasons linked to timescales and accessibility of parameters required for control. In fact the fiber laser is not a single mode laser but the standard class B model correctly describes its dynamics within some parameter range discussed in previous papers [Derozier *et al.*, 1992].

Chaos in class B lasers has long been observed when a suitable parameter is modulated at a frequency in the domain of the free running relaxation oscillations. In CO_2 lasers, chaos has been observed when the pump parameter [Biswas *et al.*, 1987], the cavity loss [Arecchi *et al.*, 1982; Tredicce *et al.*, 1986] or the cavity detuning [Midavaine *et al.*, 1985] have been sinusoidally modulated. The relative efficiency of these modulations has been discussed [Khanin, 1995] but technical arguments eventually determine which is the most efficient for a specific device. In doped fiber and YAG lasers, pump modulation has almost exclusively been used for the same technical reasons.

A single mode class B laser is essentially a two-dimensional dynamical system which is well described by the model

$$\frac{dI}{dt} = 2I[AD - 1 - k(t)]$$

$$\frac{dD}{dt} = \gamma[1 - D(1 + I)]$$

The variables I and D are the laser intensity and population inversion respectively. Time t is measured in units of the cavity lifetime. A is the pump parameter and γ is the ratio of the population inversion rate to the cavity damping rate. $k(t)$ is the additional loss term containing the modulation and possibly feedback terms. The parameter $\gamma \approx 10^{-3}$ is small for any common class B laser which includes also semiconductor in addition to CO_2 and solid state lasers. By removing this factor from the right hand side of the second equation, one obtains equations for the deviations x and y from the zero-intensity steady-state $(I, D) = (I_0, D_0)$ where $I_0 = A - 1$ and $D_0 = 1/A$ and introducing new variables and parameters as defined in [Erneux *et al.*, 1995] eventually leads to the basic equations for the free-running class B laser

$$\frac{dx}{ds} = -y - \varepsilon x[1 + (A - 1)(1 + y)]$$

$$\frac{dy}{ds} = (1 + y)x$$

where s is the new time scale $s \equiv (2I_0\gamma)^{1/2}t$ and $\varepsilon \equiv \sqrt{2\gamma(A-1)}$.

In presence of loss modulation with an adimensional efficiency M and a delayed feedback with efficiency β, the second equation should be changed into

$$\frac{dy}{ds} = (1 + y)[x - \beta(y - y(s - \nu)) - M\cos\sigma s]$$

where ν is the time delay of the feedback loop and σ the reduced modulation frequency.

If the pump is modulated, e.g. by a two-tone signal as in the second half of this paper where

$$A = A_0(1 + r_1\cos\omega_1 t + r_2\cos(\omega_2 t + \varphi)).$$

The first equation should be altered to account for this modulation and reads then as

$$\frac{dx}{ds} = -y - \varepsilon x[1 + (A_0 - 1)(1 + y)] + \delta_1\cos\sigma_1 s + \delta_2\cos(\sigma_2 s + \varphi)$$

where δ_i and σ_i $(i = 1, 2)$ are the reduced modulation amplitude and frequency respectively for the two modulations. The phase φ is relevant only when σ_1/σ_2 is a rational number.

Suitable methods are developed in each case with the aim of determining the position of the first bifurcation, i.e. the value of the parameters for which the period 1 solution destabilizes. This gives the parameter range in which the control is efficient in stabilizing the period 1 orbit.

2. Analytical Analysis of the Delayed Feedback

For the delayed feedback, asymptotic analysis of the equations has been carried out using ε as a small parameter. The 0th order ($\varepsilon = \beta = 0$, $M \ll 1$) solution of the equations of the linear problem is a combination of 2π-periodic and $2\pi/\sigma$-periodic functions of the form

$$x = 2R\cos(s+\theta) + \frac{M}{1-\sigma^2}\cos\sigma s$$

$$y = 2R\sin(s+\theta) + \frac{M\sigma}{1-\sigma^2}\sin\sigma s$$

where R and θ are unknown amplitude and phase respectively. We wish to determine the bifurcation diagram of the $2\pi/\sigma$ and $4\pi/\sigma$ periodic solutions. Therefore we concentrate on $\sigma \approx 2$ and consider the above equation as our leading approximation. The bifurcation analysis consists of studying the amplitude $R = O(\varepsilon^{1/2})$ and phase $\theta = O(1)$ as functions of the slow time εs. They satisfy

$$\frac{dR}{ds} = -\left(\frac{1}{2}\varepsilon A + \beta\right)R + \frac{1}{6}MR\cos 2\theta$$

$$R\frac{d\theta}{ds} = \frac{1}{2}(2-\sigma)R - \frac{1}{6}MR\sin 2\theta - \frac{1}{6}R^3 .$$

Steady-state solutions correspond to periodic solutions of the original equations. Period 1 ($R = 0$, θ arbitrary) and period 2 solutions are determined and their linear stability analysis is performed. Let $M = M_L \equiv |3(2-\sigma)|$ be the limit point from which two distinct branches of steady-states $\theta = \theta_\pm(M)$ emerge. If $M < M_L$, there is no steady state for θ, which means that the laser is unlocked in phase.

The stability condition of the period 1 solution is

$$M_L < M < M^*$$

with

$$M^* = \left[M_L^2 + 36\left(\frac{1}{2}\varepsilon A + \beta\right)^2\right]^{1/2}$$

$$= 3[(\varepsilon A + 2\beta)^2 + (2-\sigma)^2]^{1/2} .$$

If $\beta > \beta_c \equiv -1/2\varepsilon A$, a stable period-doubling transition is observed at $M = M^*(\beta)$ where M^* is defined above. If $M < M^*$, the intensity of the laser is

$$I - I_0 \approx -\frac{2}{3}I_0 M\sin 2s$$

where $M = O(\varepsilon)$. If $M > M^*$, the leading approximation for the intensity is

$$I - I_0 \approx -2I_0 R\sin(s+\theta)$$

where $R = O((M-M^*)^{1/2})$.

If $\beta < \beta_c$, a period-doubling transition is still possible but all periodic solutions are unstable. Quasiperiodic oscillations are then expected.

The period 2 solution which corresponds to the $R \neq 0$ solution is stable when

$$R^2 > 3(2-\sigma) \quad \text{if} \quad \sigma < 2 .$$

This period 2 solution is subcritical ($M < M^*$) if $\sigma < 2$ which implies instability for small R. Similarly the period 2 solution is supercritical ($M > M^*$) if $\sigma > 2$ and is always stable because the above relation is always verified.

3. Numerical and Experimental Investigation of Delayed Feedback

The corresponding experiments were carried out on a CO_2 laser in presence of sinusoidal loss modulation. An electro-optic modulator inserted inside the laser cavity allows modulation of the cavity losses. The feedback may be easily applied by just adding the small correction signal to the main driving voltage applied to the modulator. The delay is realized thanks to an optical fiber delay line which is 600 meters long. The CO_2 laser intensity is detected by a photovoltaic detector and fed into a laser diode power supply. Part of the diode laser emission is directly detected and another part is sent into the fiber, allowing one to build a correction signal proportional to $I(t) - I(t-\tau)$. The balance between the two channels is obtained by inserting an attenuator in front of one detector and adjusting it so that the difference $I(t) - I(t-\tau)$ in presence of a $T(=\tau)$ periodically modulated signal is null.

Figure 1 shows the results of a typical experiment. The upper part is a bifurcation diagram of the modulated laser in the absence of feedback and is given as a reference. The lower part is the diagram obtained with the same laser parameters in presence of delayed feedback. This feedback stabilizes the period 1 solution by shifting the period-doubling bifurcation point. Measurements of the shift magnitude versus the feedback coefficient are reported on Fig. 2. The experiment compares well with the numerical and analytical predictions in two points: (i) the bifurcation point shifts continuously to larger modulation values as the feedback is increased from zero, and (ii) no period-doubling bifurcation is observed for negative values of the feedback. The analysis predicted a possible range of stabilization with negative feedback but it is too small to be observed here. The flat part of this curve in the region of small feedback is most probably due to discrepancies between the expected and the observed delays, which implies a loss of efficiency for low amplitude feedback.

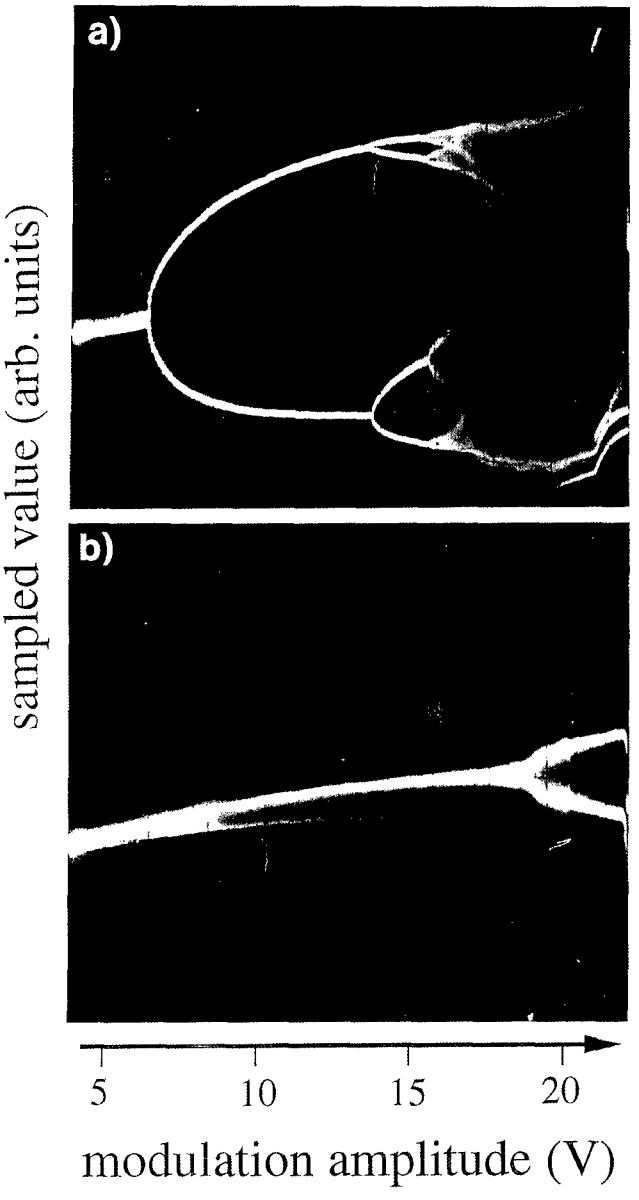

Fig. 1. Comparison of bifurcation diagrams (a) in the absence and (b) in the presence of delayed feedback for a CO_2 laser with modulated loss.

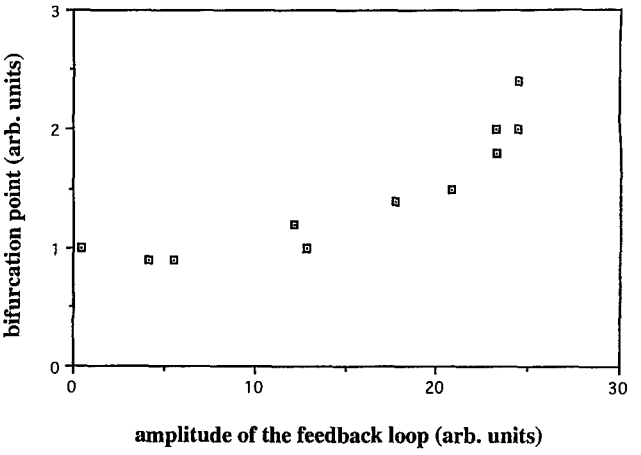

Fig. 2. Shift of the first period-doubling bifurcation versus amplitude of delayed feedback as observed on a modulated CO_2 laser with delayed feedback.

4. Control of Chaos by the Phase of Subharmonic Modulation. Analytic Results

For this system, Erneux *et al.* obtained a mapping by using a method based on matched asymptotic expansions and developed in [Newell *et al.*, 1997]. The pump modulated laser mapping relates the amplitude x_n and the time interval s_n between successive spikes. In the limit $\varepsilon \to 0$, the period $s_{n+1} - s_n$ and the change in amplitude $x_{n+1} - x_n$ are linked by

$$s_{n+1} - s_n = -2x_n + \frac{2\delta_1}{\omega_1}\sin(\omega_1 s_n) + \frac{2\delta_2}{\omega_2}\sin(\omega_2 s_n + \varphi)$$

$$x_{n+1} - x_n = -\frac{\delta_1}{\omega_1}[\sin(\omega_1 s_{n+1}) + \sin(\omega_1 s_n)] - \frac{\delta_2}{\omega_2}[\sin(\omega_2 s_n + \varphi) + \sin(\omega_2 s_n + \varphi)]$$

where the parameters describe the modulation of the pump parameter which writes in reduced units $\delta_1 \sin(\omega_1 s_n) + \delta_2 \sin(\omega_2 s_n + \varphi)$.

A fixed point analysis shows that if $\delta_2 = 0$, the period 1 solution undergoes a period-doubling bifurcation at $\delta_1 = 1$. Erneux *et al.* investigated the bifurcation diagram of the periodic states in the vicinity of this point and for small values of δ_2. They showed that if $\varphi \neq \pi/2$, the period 2 pitchfork bifurcation is destroyed and replaced by a smooth transition branch bounded by a fixed point. This limit point is located at

$$\delta_1 = 1 + \frac{1}{2}\left[6\delta_2 \sin\left(\varphi - \frac{\pi}{2}\right)\right]^{2/3}$$

In other words the standard bifurcation is then replaced by an imperfect bifurcation with two branches of solutions. For $\varphi = \pi/2$, the imperfection term disappears and the two-tone modulation problem reduces to the perfect bifurcation case. They also showed that when δ_2 is small, the period-doubling bifurcation is located approximately in $1 + \delta_2^2$.

5. Experimental and Numerical Investigations of Control by the Phase of Subharmonic Modulation

The influence of the phase φ of subharmonic modulation was investigated in two series of experiments on fiber lasers by Newell *et al.* [Newell *et al.*, 1997], Celet *et al.* [Dangoisse *et al.*, 1997] and one on a CO_2 laser by Chizhevsky *et al.* [1986]. The former concentrates on checking the predictions of the theory presented in the preceding paragraph, i.e. on the dynamics in the vicinity of the first period-doubling transition while Celet *et al.* aims at a global but less precise investigation of the effect of this phase φ, i.e. shift and/or change of nature of all bifurcation points versus the phase of the subharmonic modulation. Chizhevsky *et al.* carried out several investigations on the role of phase in a driven system subjected to harmonic and subharmonic modulations with special emphasis on the bistability induced by the second modulation in the presence of a swept parameter. In their study the nonadiabatic effects due to the sweeping of the control parameter strongly interefere with those due to subharmonic modulation. We concentrate here on experiments and theory in which these effects are made negligible as in [Newell *et al.*, 1997; Dangoisse *et al.*, 1997].

Both series of experiments have been carried out on Neodymium-doped fiber lasers pumped by diode lasers operating at 810 nm. Most experimental characteristics of the experimental set-ups are similar: fiber length 2.8 and 3.5 m, mirror reflecting coefficient 0.95, pump power 1.93 and 2 times above threshold respectively, making these two works quite complementary.

By probing the $\delta_2 - \varphi$ control space, Newell *et al.* could show that the response of the laser is drastically changed if $\varphi = 0$ and minimized when $\varphi = \pi/2$. The bifurcation diagrams they obtained are displayed on Fig. 3. In both sets the bifurcation diagram in presence of modulation is compared with a reference one obtained in absence of additional modulation ($\delta_2 = 0$). The existence of two branches when $\delta_2 \neq 0$ clearly shows that no true P1 orbit exists. The difference in the splitting of the branches of the bifurcation diagram [Figs. 3(a) and 3(b)] in the vicinity of the period-doubling bifurcation is clear and strongly dependent on the phase φ of subharmonic modulation in accordance with the predictions.

Examples of this effect together with the modifications of the other bifurcations are shown in Figs. 4 and 5. They show bifurcation diagrams obtained by numerical simulations with the cw part of the pump A_0 as the bifurcation parameter on the basis of a model of the fiber laser which proved very efficient in our previous studies of the dynamics of this kind of lasers [Derozier *et al.*, 1992]. In the following, experimental and numerical results have been obtained with a modulation of the form

$$A = A_0 + A_1 \cos\omega_1 t + A_2 \cos(\omega_2 t + \varphi)$$

for technical reasons. Extreme care has been taken to avoid any transient regime and slow passage effects in all simulations and experiments. In typical simulations we compare the bifurcation diagrams obtained with increasing and decreasing values of the control parameter to reveal the possible generalized bistability effects due to the coexistence of attractors, especially in the vicinity of boundary crises. These bistability effects are not studied in detail here and are partly discussed in a preceding paper [Dangoisse *et al.*, 1997].

Figure 4 shows the influence of a change in the amplitude of the additional modulation in the case of the fourth subhamonic modulation ($\omega_1 = 4\omega_2$). Figure 4(a) is a reference in presence of the main modulation only while Figs. 4(b) and 4(c) were obtained for relative modulation amplitudes of 5.10^{-4} and 5.10^{-3} respectively, the amplitude of the main modulation is 0.42 relative to the cw pump for all

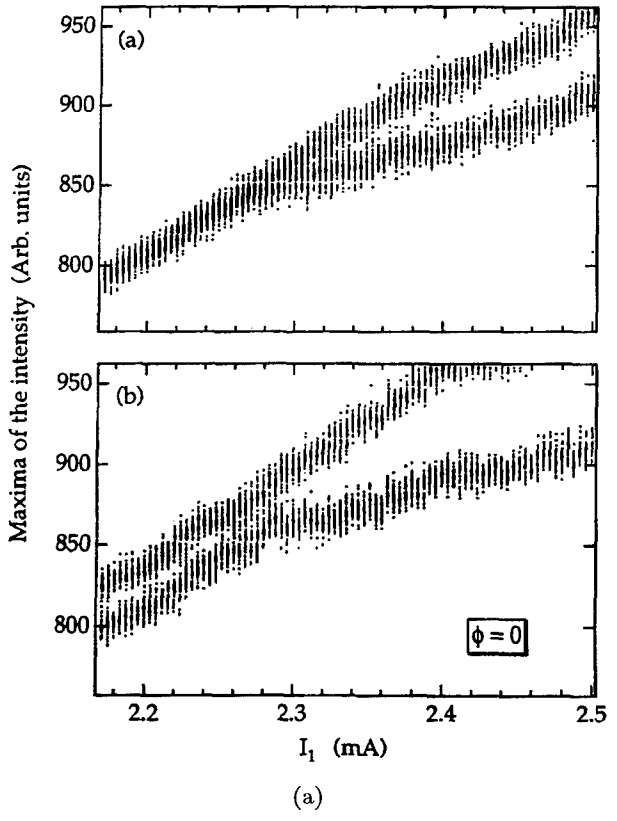

(a)

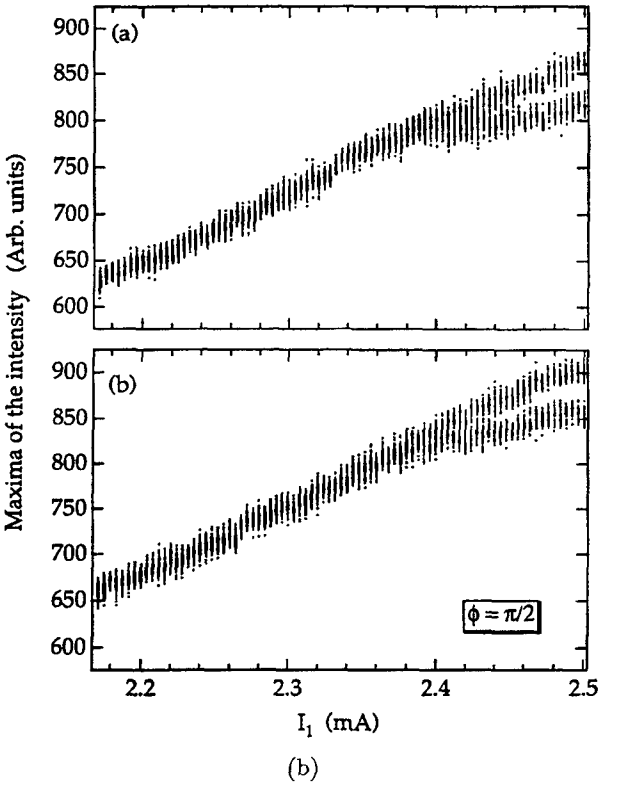

(b)

Fig. 3. Experimental demonstration of the influence of the phase φ of second subharmonic modulation on the first period-doubling bifurcation for a fiber laser. Diagrams at the top are references in absence of modulation, and those at the bottom correspond to additional (a) $\varphi = 0$, (b) $\varphi = \pi/2$ subharmonic modulation.

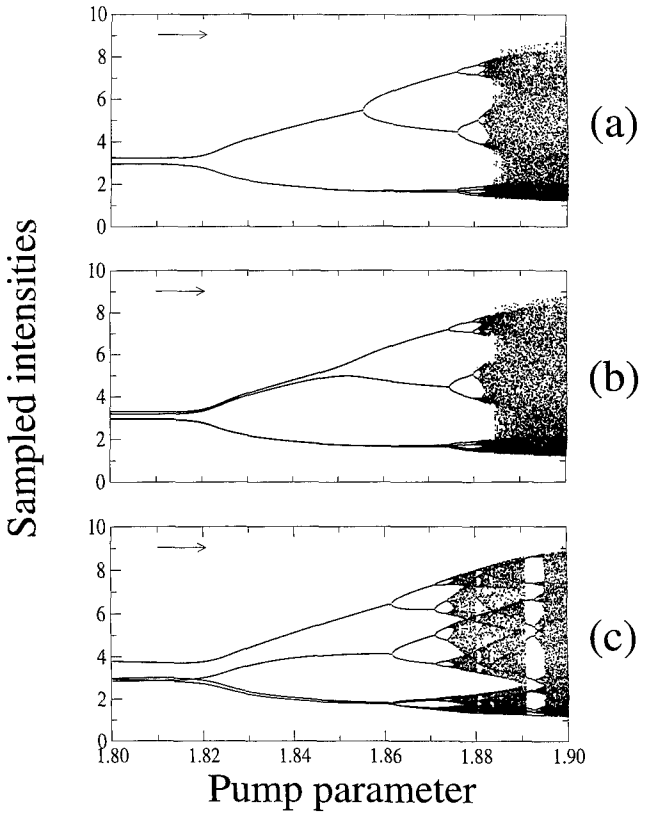

Fig. 4. Bifurcation diagrams versus amplitude of the subharmonic modulation for a model of the fiber laser (a) reference in absence of modulation $r_2 = 0$, (b) $r_2 = 5.10^{-4}$, (c) $r_2 = 5.10^{-3}$.

these recordings. Note that in all these simulations subharmonic modulations are much weaker than the main driving field. Other parameters and details about the model are given in [Dangoisse *et al.*, 1997]. The two branches of the original diagram in the domain $A = 1.80 - 1.855$ split into four branches as expected in the case of $n = 4$ subharmonic modulation and the $2T - 4T$ bifurcation becomes an imperfect bifurcation. The splitting of the $4T$ branches obviously increases with r_2, it is barely visible for $A = 1.80$ and $r_2 = 5.10^{-4}$ but becomes quite clear for $r_2 = 5.10^{-3}$. More interestingly, the whole bifurcation diagram shifts to lower pump values and chaos appears in a parameter domain where the system displays periodic response in absence of the second modulation and *vice-versa*. For instance, the one-tone modulated system is $4T$ periodic at $A_0 = 1.875$ and become $8T$ periodic and chaotic for $r_2 = 5.10^{-4}$ and 5.10^{-3} respectively.

The additional modulation also broadens the period-doubling cascade as demonstrated by the comparison of Figs. 4(a) and 4(c). More precisely, the cascade from the $4T$–$8T$ bifurcation to the

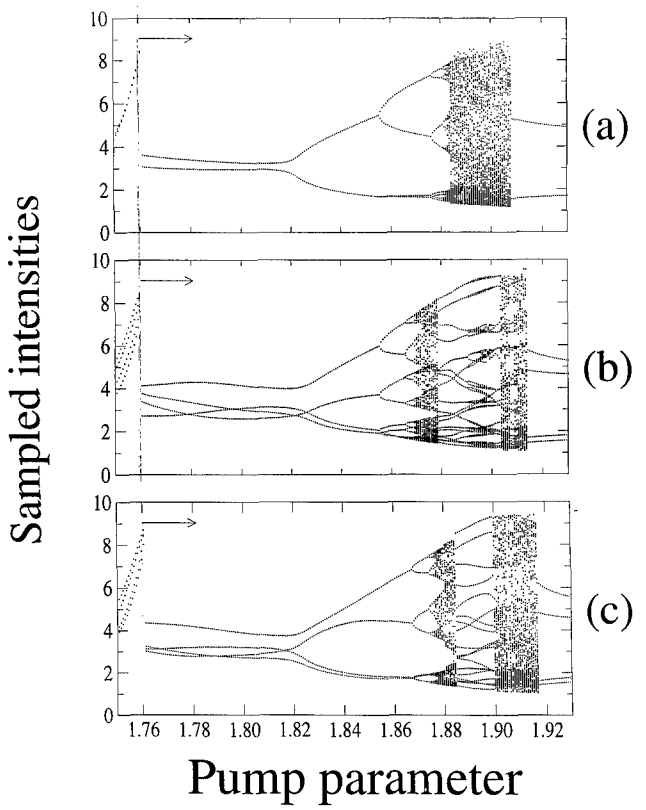

Fig. 5. Influence of the phase of subharmonic modulation on the bifurcation diagram for a model of the fiber laser (a) reference diagram in the absence of subharmonic modulation, (b) in the presence of in-phase ($\varphi = 0$), and (c) dephased ($\varphi = 2\pi/9$) fourth subharmonic modulation. Diagrams correspond to increasing pump parameters.

transition point to chaos extends on a range of A values which doubles in the presence of the second modulation, from $\Delta A \simeq 0.06$ in absence of modulation [Fig. 4(a)] to $\Delta A \simeq 0.12$ in the conditions of Fig. 4(c). As can be seen on Figs. 4(b) and 4(c), the second modulation also induces periodic windows in the parameter domain where the laser behavior was chaotic when $r_2 = 0$. For instance this is the case for the simulations reported on Fig. 4(c) in the domain $A = 1.891 - 1.894$ where the original system is chaotic but the perturbed one is periodic.

However the main information which can be extracted from these simulations is that both the shift of bifurcation points and the position of periodic windows strongly depend on the *phase* of the subharmonic with respect to the main modulation as shown on Fig. 5. This figure compares bifurcation diagrams obtained in absence of subharmonic modulation and with two different phases ($\varphi = 0$ and $2\pi/9$) for this modulation with respect to the main one. The reference diagram [Fig. 5(a)] displays a period-doubling cascade transition to chaos between $A = 1.76$ and 1.90 in absence of subharmonic modulation. Addition of a weak fourth subharmonic modulation leads to smaller A values for the bifurcation points but the magnitude of the shift towards lower A values depends on φ. Here the width of the chaotic region is reduced. Periodic windows and associated period-doubling cascades appear in the domain $A \sim 1.88 - 1.90$ where the unperturbed laser was chaotic. This definitely shows that the phase φ may be used to control the dynamics. This control is very efficient in two respects: (i) the subharmonic modulation may be much weaker than the main one — typically 10^2 to 10^3 times — and (ii) it allows control of almost all kinds of regimes, from periodic to chaotic and *vice versa*.

The diagrams presented in Figs. 5(b) and 5(c) also show that subharmonic modulation induces or shifts crises. The most obvious effect is the emergence of the periodic windows discussed in the preceding paragraph since these windows follow the disappearance of chaos in the boundary crises. In addition to that, more subtle effects show off at the end of the chaotic domain. In the absence of perturbation, the corresponding chaotic regime extends up to $A = 1.910$ where a period 2 attractor appears. The position of this crisis is perturbed by the subharmonic pertubation and here the chaotic domain is extended to larger A values. The period 4 regime which emerges at the crisis is simply due to the fact that in presence of $n = 4$ subharmonic modulation, a $4T$ cycle replaces the $2T$ attractor which was observed in this domain, as expected for low modulation amplitudes.

All the above bifurcation diagrams have been obtained with increasing values of the control parameter. Slightly different ones are sometimes obtained with decreasing A values, even when the slow passage effects are avoided because of the coexistence of attractors for the same values of the parameters. The corresponding bistability effects are particularly visible near the boundary crises as usually observed, e.g. in modulated loss CO_2 lasers. As expected the limits of these domains are regions of high sensitivity to additional modulation because the stability of the attractor which will disappear in the crisis is very low near these points. Note that crises also appear for lower A values and the scattered points obtained near $A = 1.76$ correspond to other periodic attractors which coexist in this parameter domain with the main one studied in this work. There is a small range of bistability between these two attractors as demonstrated by

bifurcation diagrams obtained with reverse (decreasing A) sweep [Dangoisse *et al.*, 1997].

Experiments carried out on a modulated fiber laser confirm the predictions of numerical simulations. Bifurcation diagrams have been recorded with the pump power as the bifurcation parameter and subharmonic ranks 2 and 4. In accordance with numerical simulations, they show that there is no strong dependence of the results on the subharmonic rank ω_2/ω_1. Experiments also confirm the predictions of numerical simulations in the following points (i) the additional modulation shifts and magnifies the whole bifurcation diagram, (ii) the phase of subharmonic modulation allows the control of dynamical regimes (iii) crises may be induced or suppressed by acting on the phase of subharmonic modulation. These are very common features which have been observed for a wide variety of parameters, some examples of which are given in [Dangoisse *et al.*, 1997] and will not be recalled here.

Control of chaos has also been observed in presence of transition to chaos via quasiperiodicity [Bergé *et al.*, 1984]. Period-doubling cascades are most easily observed for modulation frequencies equal to about half the relaxation frequency of the free running laser. Quasiperiodicity is obtained in the fiber laser when the external modulation frequency is detuned from this parametric resonance condition. We have considered the effect of subharmonic perturbation in these conditions. Contrary to the previous paragraphs, the effects are demonstrated here for fixed values of the laser parameters in the vicinity of quasiperiodic regimes. Dynamic regimes are identified by observation of the Poincaré section of the experimental attractor as indicated in [Derozier *et al.*, 1992]. Quasiperiodic regimes are identified by a closed curve in the Poincaré section, periodic ones by a discrete set of points and chaos by a strange attractor. As for the period-doubling cascade, the dynamics of the laser is altered by subharmonic modulation and it is possible to drive the laser in different regimes depending on the phase of this modulation. For instance in the conditions of Fig. 6 where the unperturbed ($r_1 = 0.438$, $r_2 = 0$) modulated laser is quasiperiodic [Fig. 6(a)], it becomes $8T$ periodic with in phase ($\varphi = 0$) modulation [Fig. 6(b)] while dephased ($\varphi = \pi/18$) second subharmonic modulation with $r_2 = 0.02$ induces a chaotic regime [Fig. 6(c)]. We have also observed situations in which an initially chaotic laser is controlled to periodic regimes by acting on the phase of a weak subharmonic modulation [Dangoisse *et al.*, 1997].

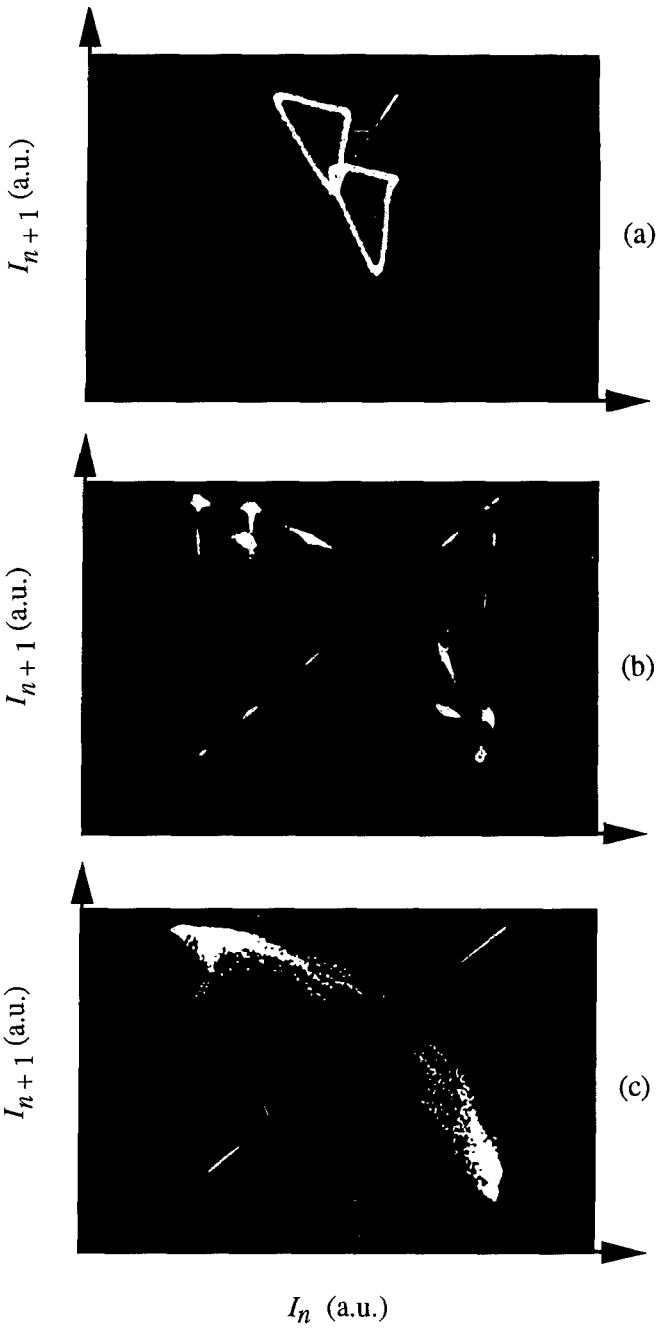

Fig. 6. Control of chaos in the case of quasiperiodicity route to chaos in a fiber laser (a) reference quasiperiodic state, (b) $\varphi = 0$ second subharmonic modulation induces period 8 regime, (c) $\varphi = \pi/18$ second subharmonic modulation induces a chaotic regime.

Experiments carried out on both period-doubling cascades and quasiperiodicity transitions to chaos have shown that these scenarios are in general globally preserved by the addition of a subharmonic modulation but that the dynamical regimes observed for given parameters may be qualitatively different. Moreover there may be some dramatic changes in the chaotic regimes such as the creation

of new attractors. All these effects are highly dependent on the phase of subharmonic perturbation and allow the control of the dynamics of nonlinear systems with a very small action like a simple phase shift of a modulation acting on this system. This control is very versatile in the sense that in well-selected parameter regions, it is possible to choose from a wide variety of regimes by just acting on the phase of the subharmonic modulation. The main drawback of this approach is that it applies only to externally nonautonomous systems.

6. Conclusion

The introduction of the concept of control of chaos was made on a very general model based on the local dynamics, i.e. on a linear approximation of the dynamics in the vicinity of the unstable period orbits. Here we have explored a different path which relies on a fully analytic description of the dynamics and showed that it is possible to obtain quantitative information on the control range, i.e. the parameter domain in which this control is efficient. These results have been supported by both numerical simulations and experiments on different lasers. Numerical simulations have allowed for the consideration of the bifurcations beyond the first period-doubling transition. They have demonstrated that control of chaos through the phase of a subharmonic modulation is extremely efficient and applies to various bifurcations including those of the quasiperiodic route to chaos. Experiments carried out on several lasers (YAG, fiber, CO_2) indicate that these methods are very general and consequently that this approach may be extended to other dynamical systems. In addition, the present work also provides an alternative explanation to the results obtained for the control of chaos by subharmonic modulation with extremely small detunings (near resonant perturbation) [Vohra *et al.*, 1995] since such detunings may be considered as a slowly drifting phase and extreme care should be taken to separate e.g. detunings as small as 0.1 Hz with a basic resonance frequency of 10 kHz from the effects discussed in the present paper.

Acknowledgments

The author is deeply indebted to T. Erneux with whom large parts of the work reported here were carried out. S. Bielawski, J. C. Celet, D. Dangoisse and D. Derozier also collaborated to parts of this work. A. Gavrielides, V. Kovanis, T. Newell, V. Chizhevsky, R. Corbalan and A. Pisarchik are gratefully thanked for sending preprints of their work prior to publication. The Centre d'Etudes et de Recherches sur les Lasers et leurs Applications is supported by the FEDER and the Région Nord-Pas de Calais.

References

Arecchi, F. T., Meucci, R., Puccioni, G. P. & Tredicce, J. R. [1982] "Experimental evidence of subharmonic bifurcations, multistability, and turbulence in a Q-switched gas laser," *Phys. Rev. Lett.* **49**, 1271–1274.

Bergé, P., Pomeau, Y. & Vidal, C. [1984] *L'Ordre dans le Chaos* (Hermann, Paris).

Bielawski, S., Derozier, D. & Glorieux, P. [1993] "Control of laser chaos," *Proc. SPIE* **2039**, 239–249 and references therein.

Bielawski, S., Derozier, D. & Glorieux, P. [1994] "Controlling unstable periodic orbits by a delayed continuous feedback," *Phys. Rev.* **E49**, R971–R974.

Biswas, D. J., Dev, V. & Chatterjee, V. K. [1987] "Experimental observation of oscillating instabilities and chaos in a gain-modulated single-mode cw CO_2 laser," *Phys. Rev.* **A35**, R456–R458.

Braiman, Y. & Goldhirsch, I. [1991] "Taming chaotic dynamics with weak perturbations," *Phys. Rev. Lett.* **66**, 2545–2548.

Bryant, P. & Wiesenfeld, K. [1986] "Suppression of period-doubling and nonlinear parametric effects in peridically perturbed systems," *Phys. Rev.* **A33**, 2525–2543.

Chen, Y. C., Winful, H. G. & Liu, J. M. [1985] "Subharmonic and irregular behaviour of modulated semiconductor lasers," *Appl. Phys. Lett.* **47**, 208–210.

Chizhevsky, V. N., Corbalan, R. & Pisarchik, A. N. [1996] "Experimental observation of pertubation induced intermittency in the dynamics of a loss-modulated CO_2 laser," *Phys. Rev.* **E54**, 4576–4579.

Chizhevsky, V. N., Corbalan, R. & Pisarchik, A. N. [1997] "Attractor splitting induced by resonant perturbations," *Phys. Rev.* **E56**, 1580–1584.

Ciofini, M., Meucci, R. & Arecchi, F. T. [1995] "Experimental control of chaos in a laser," *Phys. Rev.* **E52**, 94–97.

Colet, P. & Braiman, Y. [1996] "Control of chaos in multimode solid state lasers by the use of small periodic perturbations," *Phys. Rev.* **E53**, 200–206.

Dangoisse, D., Celet, J. C. & Glorieux, P. [1997] "Global investigation of the influence of the phase of subharmonic excitation of a driven system," *Phys. Rev.* **E56**, 1396–1406

Derozier, D., Bielawski, S. & Glorieux, P. [1992] "Antiphase dynamics and polarization effects in the Nd-doped fiber laser," *Phys. Rev.* **A46**, 2811–2822.

Erneux, T., Bielawski, S., Derozier, D. & Glorieux, P. [1995] "Stabilizing or destabilizing lasers by continuous delayed feedback," *Quant. Semiclass. Opt.* **7**, 951–963.

Gavrielides, A., Alsing, P. A., Kovanis, V. & Erneux, T. [1995] "Controlling chaos may induce new attractors in an optical device," *Opt. Commun.* **115**, 551–558.

Ivanov, D. V., Khanin, Ya. I., Matorin, I. I. & Pikovsky, A. S. [1982] *Phys. Lett.* **A89**, 229–230.

Khanin, Ya. I. [1995] *Principles of Laser Dynamics* (North-Holland, Amsterdam).

Meucci, R., Gadomski, W., Ciofini, M. & Arecchi, F. T. [1994] "Experimental control of chaos by means of small parametric perturbations," *Phys. Rev.* **E49**, R2528–R2531.

Midavaine, T., Dangoisse, D. & Glorieux, P. [1985] "Observation of chaos in a frequency-modulated CO_2 laser," *Phys. Rev. Lett.* **55**, 1989–1992.

Newell, T. C., Gavrielides, A., Kovanis, V., Sukow, D., Erneux, T. & Glasgow, S. A. [1997] "Unfolding of the period-two bifurcation in a fiber laser pumped with two-modulation tones," *Phys. Rev.* **E56**, 7223–7231.

Otsuka, K., Chern, J.-Y. & Lih, J.-S. [1997] "Experimental suppression of chaos in a modulated multimode laser," *Opt. Lett.* **22**, 292–294.

Ott, E., Grebogi, C. & Yorke, J. A. [1990] "Controlling chaos," *Phys. Rev. Lett.* **64**, 1196–1199.

Pyragas, K. [1992] "Continuous control of chaos by self-controlling feedback," *Phys. Lett.* **170A**, 421–428.

Pyragas, K. & Tamasevicius, A. [1993] "Experimental control of chaos by delayed self-controlling feedback," *Phys. Lett.* **180A**, 99–102.

Roy, R., Gills, Z. & Thornburg, K. S. [1994] "Controlling chaotic lasers," *Opt. Photon. News* **5**(5), 8–15 and references therein.

Tredicce, J. R., Arecchi, F. T., Puccioni, G. P., Poggi, A. & Gadomski, W. [1986] "Dynamic bahavior and onset of low-dimensional chaos in a modulated homogeneously broadened single-mode laser: Experiments and theory," *Phys. Rev.* **A34**, 2073–2081.

Vohra, S. T., Fabiny, F. & Bucholtz, F. [1995] "Suppressed and induced chaos by near resonant perturbation of bifurcations," *Phys. Rev. Lett.* **75**, 65–68.

International Journal of Bifurcation and Chaos, Vol. 8, No. 9 (1998) 1759–1768

EXPERIMENTAL TECHNIQUES FOR CONTROLLING CHAOS IN LASERS

R. MEUCCI, A. LABATE and M. CIOFINI
Istituto Nazionale di Ottica, L. E. Fermi, Florence, 50125 Italy

Received July 31, 1997; Revised November 28, 1997

This paper presents two control schemes for the chaotic dynamics of a CO_2 laser with feedback which can be applied after the recognition of a leading frequency of the motion in the power spectrum. The first one is realized by means of a selective feedback loop which rejects all the frequency components except that of the leading cycle to be stabilized. The second one consists in a resonant sinusoidal modulation of the control parameter.

1. Introduction

Lasers represent reliable systems to investigate nonlinear phenomena such as chaotic dynamics, both from an experimental and a theoretical point of view. In fact, it was demonstrated by Haken [1975] that the Maxwell–Bloch equations for the dynamics of a two-level laser are equivalent to the Lorenz model describing convective turbulence in fluid dynamics [Lorenz, 1963]. A recent aspect of nonlinear dynamics studies concerns the possibility of directing chaotic dynamics to periodic orbits or steady states by applying small external perturbations. Ott, Grebogi and Yorke [1990] proposed a general method to stabilize a given periodic orbit embedded in a chaotic attractor by means of small perturbations to a system parameter; such perturbations are proportional to the deviation of the system from the unstable fixed point, and this implies the presence of a suitable feedback loop (for reviews of the method and applications see [Shimbrot *et al.*, 1993; Ditto *et al.*, 1995; Petrov *et al.*, 1993]). In the field of laser physics, the "occasional proportional feedback" method (OPF) [Hunt, 1991], derived from the OGY scheme, has been applied to stabilize periodic orbits and steady states of a chaotic multimode Nd:YAG laser with a nonlinear intracavity KTP (potassium titanyl phospate) crystal [Roy *et al.*, 1992; Gills *et al.*, 1992; Colet *et al.*, 1994; Carr & Schwartz, 1995]. In such a case the stability regime has been extended over one order of magnitude with respect to the unperturbed system. The OPF has been also applied to control chaotic frequency emission in lead-salt diode lasers [Chin *et al.*, 1996]. Another variation of the OGY method, known as "minimal expected deviation" (MED), has been applied to stabilize periodic orbits of a NMR (nuclear magnetic resonance) laser [Reyl *et al.*, 1993]. Bielawsky *et al.* [1993] used a feedback scheme proportional to the derivative of the laser intensity to stabilize the chaotic regime of a Nd^{3+} doped fiber laser pumped by a single mode laser diode.

At the same time, other experimental [Meucci *et al.*, 1994; Liu *et al.*, 1994, 1995; Chizhevsky & Glorieux, 1995; Chizhevsky *et al.*, 1997] and theoretical [Liu & Rios Leite, 1994; Colet & Braiman, 1996; Vilaseca *et al.*, 1996] works on lasers deal with different control schemes not based on feedback loops, but still consisting of suitable small modulations of control parameters.

An alternative strategy to achieve control of chaos is based on modifications of state variables instead of control parameters. This technique has been first introduced by Pyragas [1992], which proposed a correction signal proportional to the difference between the values of a given variable at different times. The delay time is selected equal to

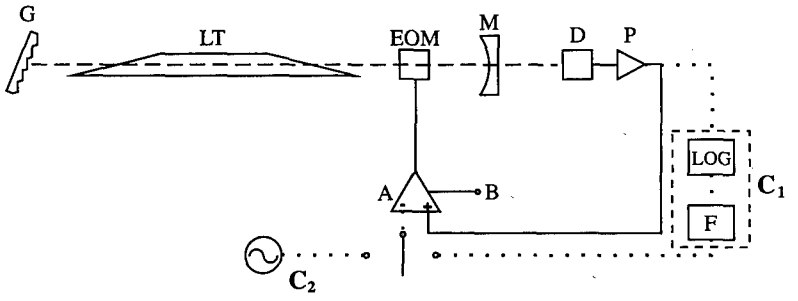

Fig. 1. Experimental setup. *G*: diffraction grating. *LT*: laser tube. *EOM*: electro-optic modulator. *M*: outcoupling mirror. *D*: HgCdTe detector. *P*: preamplifier. *A*: differential high-voltage amplifier amplifer. *B*: bias input. *LOG*: logarithmic converter. *F*: washout filter. The dotted lines represents the two control schemes: C_1: feedback loop control (subharmonic filtering). C_2: open loop control (resonant modulation).

the period of the unstable orbit to be stabilized. Bielawski *et al.* [1994] have successfully applied this method to a modulated CO_2 laser. Simmendinger and Hess [1996] used the Pyragas scheme in a semiconductor laser with optical feedback. In this work, we describe experimental testing of two methods for controlling chaotic dynamics in a CO_2 laser with electro-optic feedback, which is an autonomous system providing low-dimensional chaos. The first method involves a frequency domain approach by means of a filtering feedback loop where the only admitted frequency is that of the orbit to be stabilized [Genesio *et al.*, 1993; Meucci *et al.*, 1996; Ciofini *et al.*, 1997]. The second method is based on the introduction of a small modulation of the control parameter at a frequency suggested by the power spectrum.

The paper is organized as follows: In the second section, after a description of the experimental set up, we present the results obtained with the two methods. The third section is devoted to a presentation of the model and numerical simulations. Finally, we summarize the main results in the conclusions.

2. Experimental Results

The experimental setup is shown in Fig. 1. It consists of a single mode CO_2 laser with a feedback on the cavity losses, realized by means of an intracavity electro-optic modulator, driven by a signal proportional to the output intensity. The bias voltage B provided by the high-voltage amplifier is the control parameter of the system. The feedback voltage V obeys the following equation:

$$\dot{V} = -\beta\left(V - B + \frac{RI}{I + \alpha I}\right) \qquad (1)$$

where $\beta = 300$ kHz is the damping rate of the feedback loop, I is the adimensional laser intensity and $R = 6.6 * 10^{-10}$ is the total gain of the feedback loop. The term αI ($\alpha = 1.2 * 10^{-13}$) accounts for the nonlinearity of the detection apparatus, which consists of a HgCdTe detector. In this configuration, the laser undergoes a direct Hopf transition from a stationary to an oscillating regime beyond a critical bias value. For appropriate values of pump and feedback loop gain, the oscillating regime becomes chaotic through a sequence of subharmonic bifurcations. A three-dimensional reconstruction of the chaotic attractor, obtained for $B = 360$ V, is shown in Fig. 2. This reconstruction has been performed by an embedding technique of the laser intensity signal, using a delay time $\tau = 3$ μs. The delay time value has been chosen to

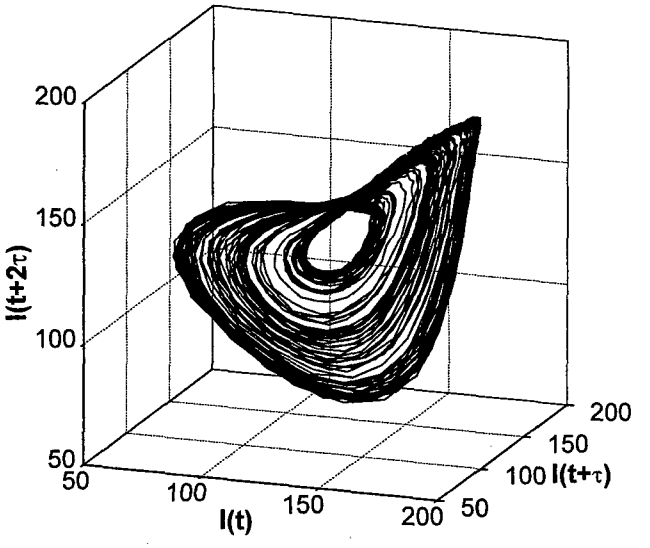

Fig. 2. Three-dimensional reconstruction of the chaotic attractor for $B = 360$ V, $\tau = 3$ μs.

closely reproduce the projection of the attractor in the two-dimensional phase space I–V [Meucci *et al.*, 1997]. We adopted a 3-D representation in Fig. 2 instead of a 2-D representation because it provides better insight into the stretching and folding mechanism which is necessary to maintain the chaotic orbit within a finite volume of phase space. Another useful method to represent the dynamical properties of a system is provided by Poincaré sections. In Fig. 3 we show the Poincaré map obtained by plotting an intensity maximum versus the previous one. The chaotic nature, namely the loss of information as time or iteration number increase, is related to the noninvertibility of the map $I(n+1) = f(I(n))$. In fact, due to this feature, it is always possible to estimate $I(n+1)$ from $I(n)$ (e.g. fitting the map of Fig. 3 with an appropriate polynomial expression), but there is ambiguity to retrieve $I(n)$ from $I(n+1)$. The fractal character of the attractor is confirmed by an evaluation of the correlation dimension $D_2 = 2.10 \pm 0.04$ [Grassberger & Procaccia, 1983]. Finally, an important feature related to our control schemes can be extracted from the chaotic power spectrum of the laser intensity (Fig. 4), that is, the peak at around $f_0 = 22$ KHz, which is the remnant of the Hopf bifurcation frequency.

The first control method has been realized by means of (Fig. 1). The transfer function of the filter, shown in Fig. 5, presents two zeroes: one corresponding to the peak of the unperturbed chaotic spectrum f_0, and the other at zero frequency. The maximum of the transfer function occurs at $f_0/2$,

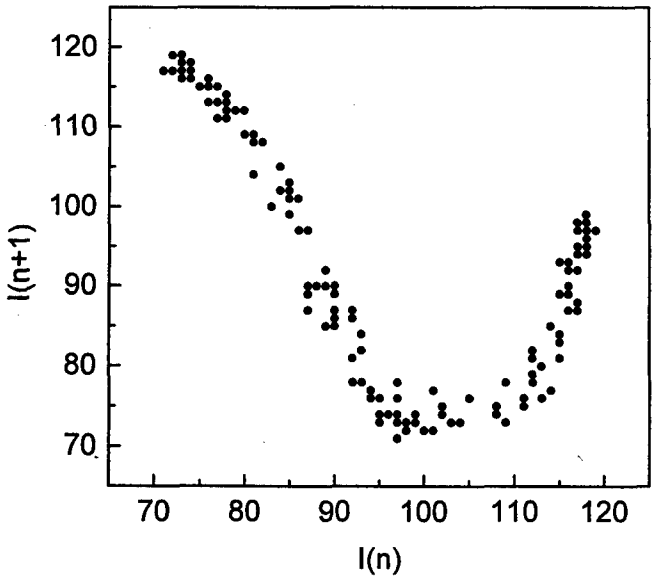

Fig. 3. Poincaré map, corresponding to the chaotic attractor of Fig. 2, obtained by plotting an intensity maximum versus the previous one.

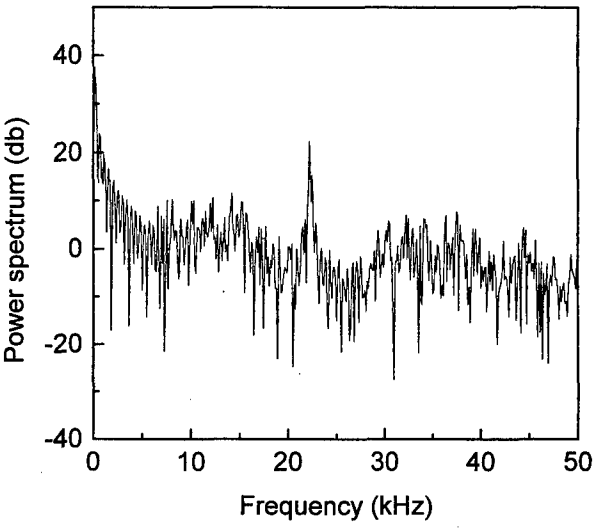

Fig. 4. Power spectrum corresponding to the chaotic attractor of Fig. 2.

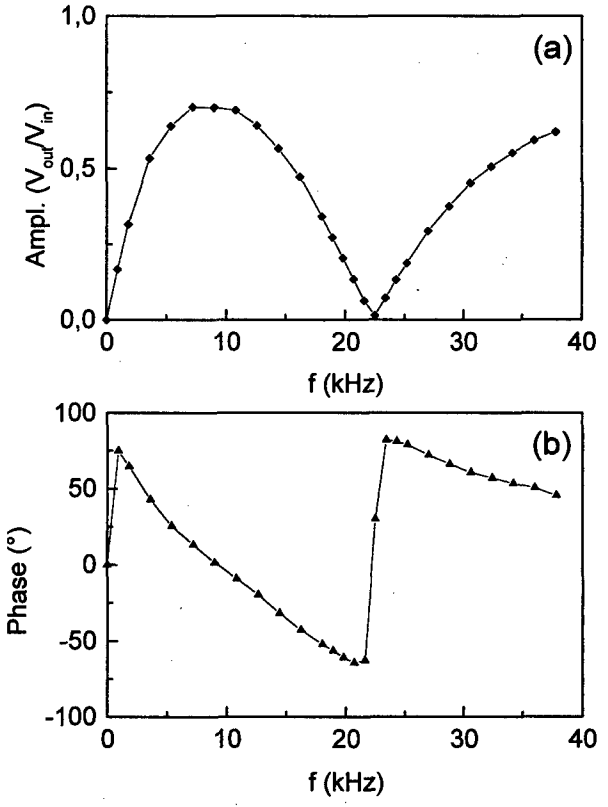

Fig. 5. Transfer function of the filter (a) Amplitude respones, (b) Phase response.

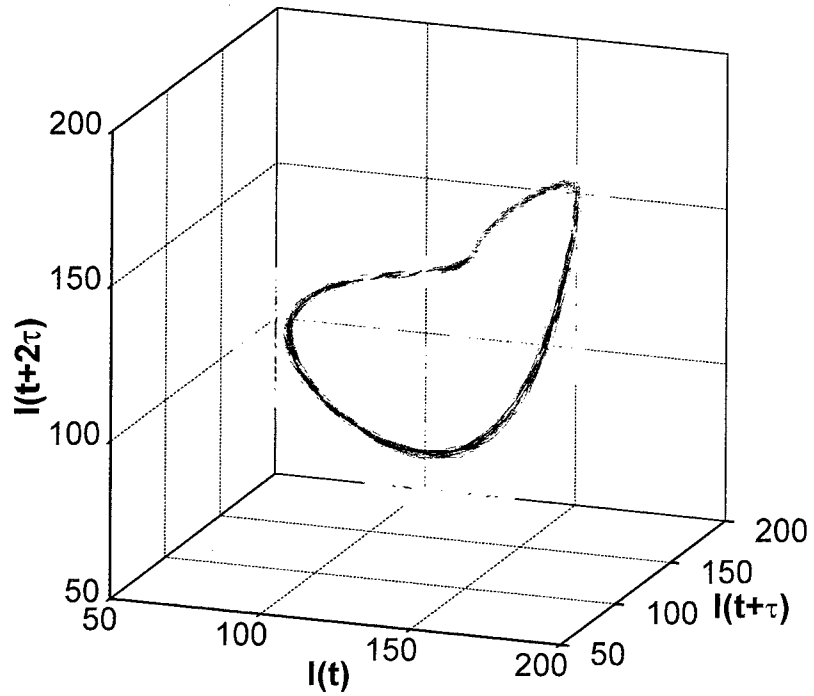

Fig. 6. Feedback control: period-1 stabilized orbit (blue) embedded in the chaotic attractor (yellow).

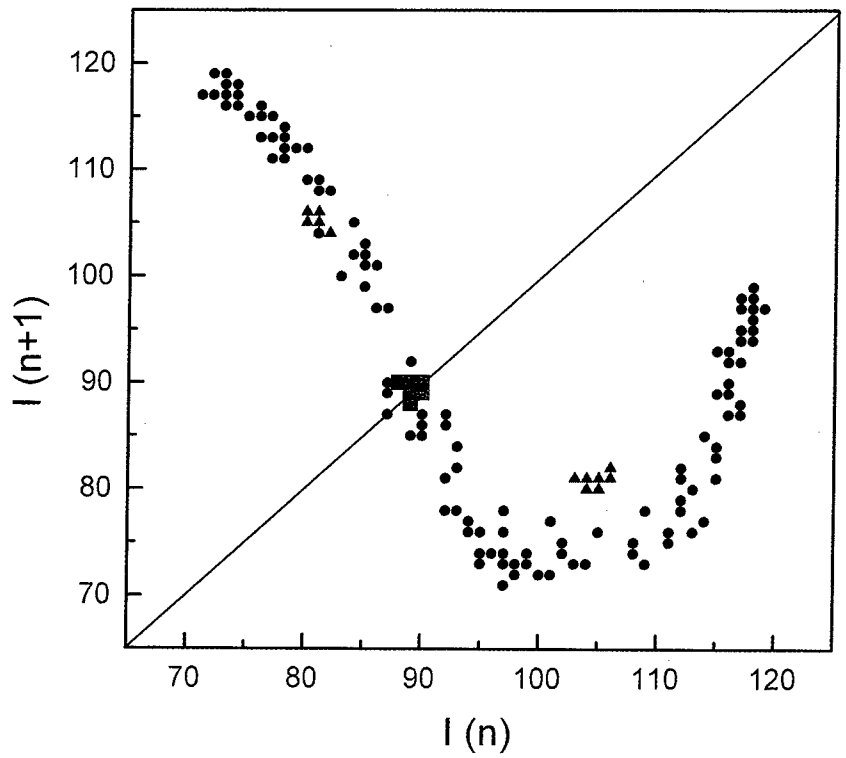

Fig. 7. Poincaré maps corresponding to Fig. 6 with period-2 stabilized orbit (black circles: chaos; green squares: period-1; red triangles: period-2).

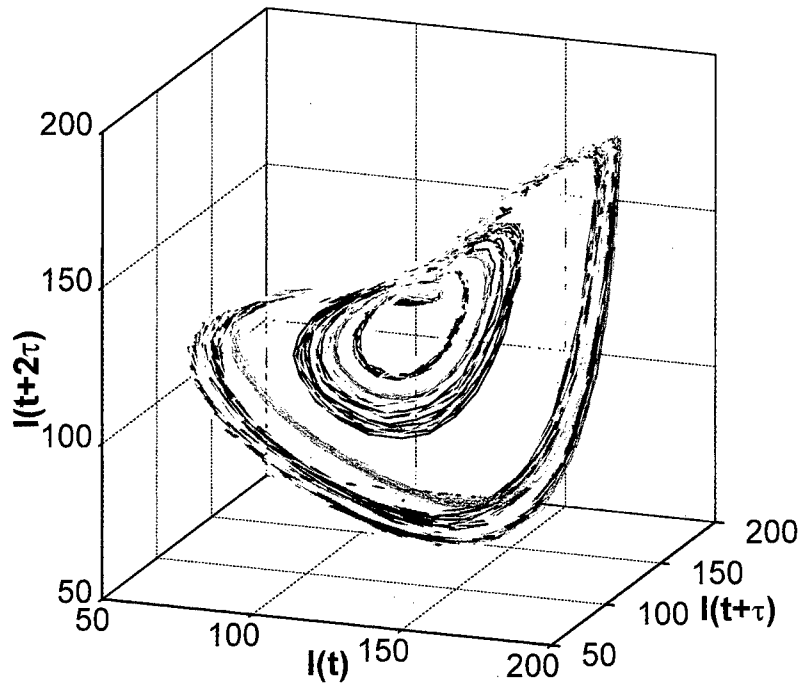

Fig. 8. Modulation control: stabilized period-4 (blue), period-2 (red) and period-1 (green) orbits superimposed on the chaotic attractor (yellow).

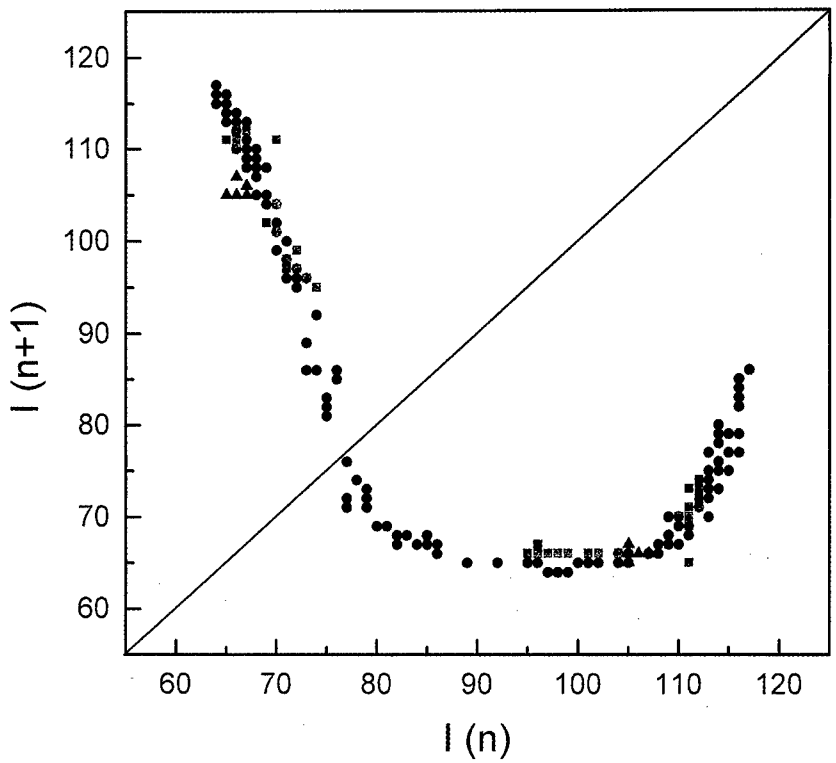

Fig. 9. Poincaré maps corresponding to the orbits of Fig. 8 (black circles: chaos; red triangles: period-2; green squares: period-4).

where the phase response crosses the zero. The effect of these characteristics, when the filter is inserted in the negative feedback loop of the laser intensity, is to stabilize the orbit corresponding to the only frequency component which is not fed back as a correction signal, that is the period-1 orbit with frequency f_0 embedded in the chaotic attractor (Fig. 6). In this case the relative perturbation amplitude is 7%. If the controller is modified by inserting a logarithmic amplifier to drive the filter, its performance increases, providing stabilization of the period-1 orbit with smaller values of the relative perturbation.

The Poincaré maps of the unperturbed chaotic attractor and of the period-1 stabilized orbit are shown superimposed in Fig. 7. This feedback method also allows stabilization of the period-2 orbit (Fig. 7). In this case however, the perturbation applied to the system is higher (12%) and, as a consequence, one of the points of the map does not lie exactly on the unperturbed map. Indeed, to optimize the control for the period-2 orbit (or for any other higher order subharmonics), one has to prepare a new filter with a zero at $f_0/2$ and a maximum at $f_0/4$ [Ciofini *et al.*, 1997].

The second control method we have implemented (Fig. 1) consists of introducing a small sinusoidal modulation of the control parameter $B(t) = B * (1 + m * \sin(\omega t))$ at a frequency close to that of the peak in the chaotic spectrum. Figure 8 shows, superimposed on the chaotic trajectory, the stabilized period-4, period-2 and period-1 orbits obtained by increasing the relative perturbation amplitude m (5%, 8% and 22%, respectively) at a frequency of 21.6 kHz where the system presents the maximum sensitivity. Note that stabilization of the period-1 orbit requires a large amount of modulation. As a consequence, the orbit is affected by large harmonic distortions, and it is not embedded in the chaotic attractor. It is important to observe that the fundamental frequencies of the stabilized attractors are locked to the perturbation frequency in agreement with the theory of periodic perturbations [Khalil, 1992]. The return maps of the stabilized cycles are shown in Fig. 9 superimposed on the unperturbed chaotic map. The differences between the chaotic maps of Figs. 7 and 9, which however maintain the same general features, are due to the slightly different values of B for which they have been recorded. The differences in the performances of the two control methods are summarized in Table 1.

Table 1. Relative perturbation amplitudes (experimental values) for the stabilization of period-1, period-2 and period-4 unstable orbits with the two different control schemes. The selective filter, optimized for period-1 stabilization, does not allow stabilization of the period-4 cycle.

	Period-1	Period-2	Period-4
Selective filter	7%	12%	—
Parametric mode.	22%	8%	5%

3. The Model

The behavior of a single mode CO_2 laser is quantitatively described by a set of five differential equations which, besides the radiative coupling between the resonant molecular transition (population inversion $N_2 - N_1$) and the field intensity, account also for the collisional transfer from the manifolds of the other rotational levels (population inversion $M_2 - M_1$). Considering the presence of the feedback [Eq. (1)], and a suitable rescaling of the variables, the model, also described in [Meucci *et al.*, 1997], is:

$$\begin{aligned}
\dot{w} &= \tilde{k}_0(x_2 - 1 - \tilde{k}_1 \sin^2(x_6)) \\
\dot{x}_2 &= -\Gamma_1 x_2 - 2\tilde{k}_0 x_2 e^w + \gamma x_3 + x_4 + P_0 \\
\dot{x}_3 &= -\Gamma_1 x_3 - x_5 + \gamma x_2 + P_0 \\
\dot{x}_4 &= -\Gamma_2 x_4 - \gamma x_5 + z x_2 + z P_0 \\
\dot{x}_5 &= -\Gamma_2 x_5 - z x_3 + \gamma x_4 + z P_0 \\
\dot{x}_6 &= -\tilde{\beta} x_6 + \tilde{\beta} B_0 - \tilde{\beta} f(e^w)
\end{aligned} \tag{2}$$

where $w = \log(x_1)$ (x_1 is the rescaled intensity), x_2 is proportional to the population difference $N_2 - N_1$, x_3 to $N_2 + N_1$, x_4 to $M_2 - M_1$, x_5 to $M_2 + M_1$ and x_6 to the feedback voltage V. The nonlinearity of the detector is contained in the function $f(x)$, while B_0 represents the rescaled control parameter. The other parameter values are: $\tilde{k}_0 = 28.57$, $\tilde{k}_1 = 4.56$, $\Gamma_1 = 10.06$, $\Gamma_2 = 1.06$, $\gamma = 0.05$, $P_0 = 1.6 * 10^{-2}$ and $\tilde{\beta} = 0.43$.

In the frequency domain, Eqs. (2) can be represented in the Lur'e form, shown in Fig. 10. $L(s)$, where $s = i\omega$, represents the transfer function of a linear dynamical block, corresponding to the second, third, fourth and fifth equations. The first and the last equations of (2) represent the feedback to the linear block. Note that the variable x_2 is not an accessible quantity in the experiment, while the variable w, neglecting the nonlinearity of

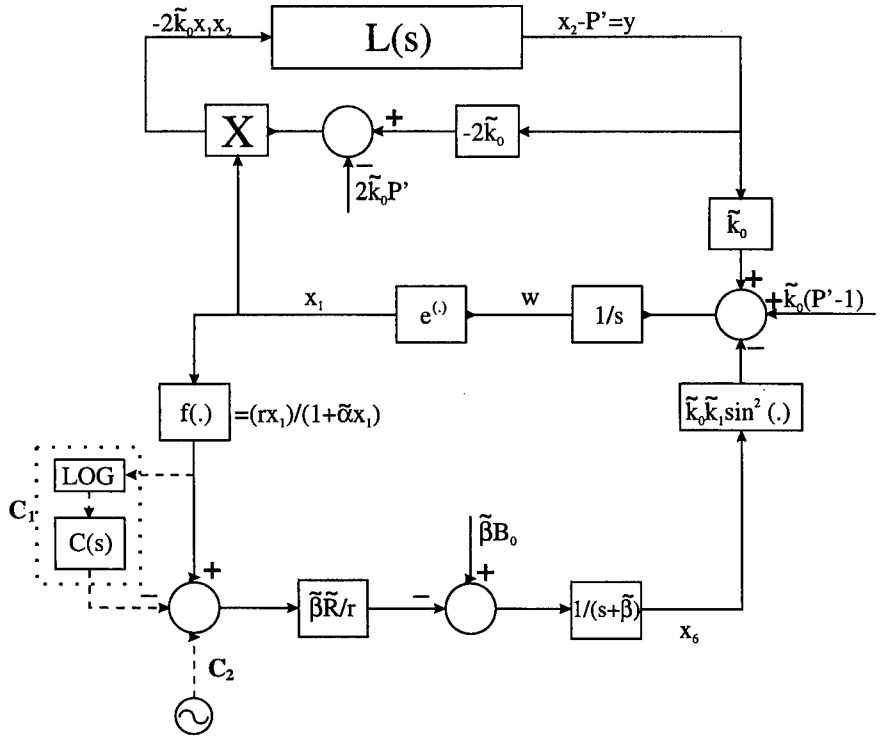

Fig. 10. Logical diagram corresponding to Eqs. (2) with the two control methods. C_1: feedback loop control (subharmonic filtering). C_2: open loop control (resonant modulation).

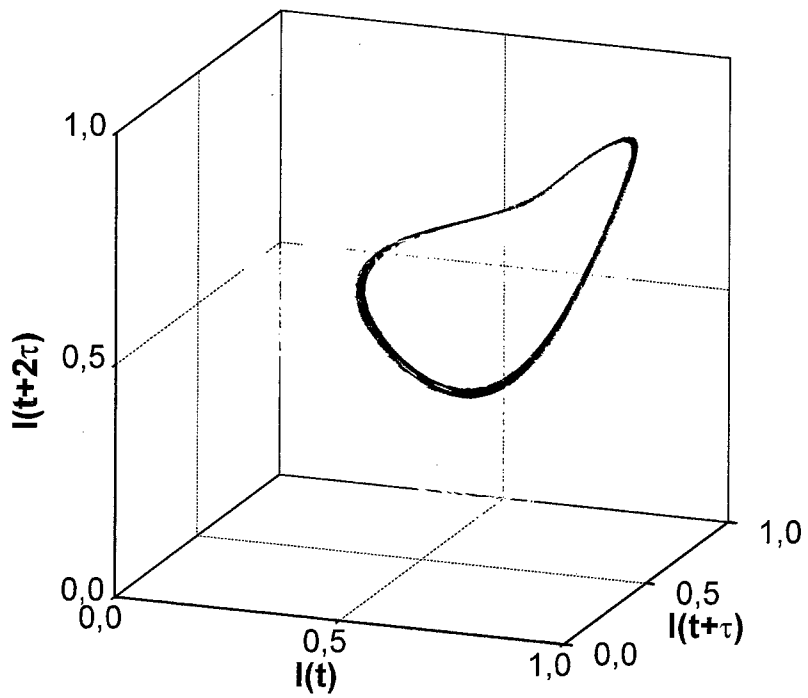

Fig. 11. Numerical simulations with control C_1. Unperturbed chaotic attractor (yellow) and stabilized orbit of period-1 (blue).

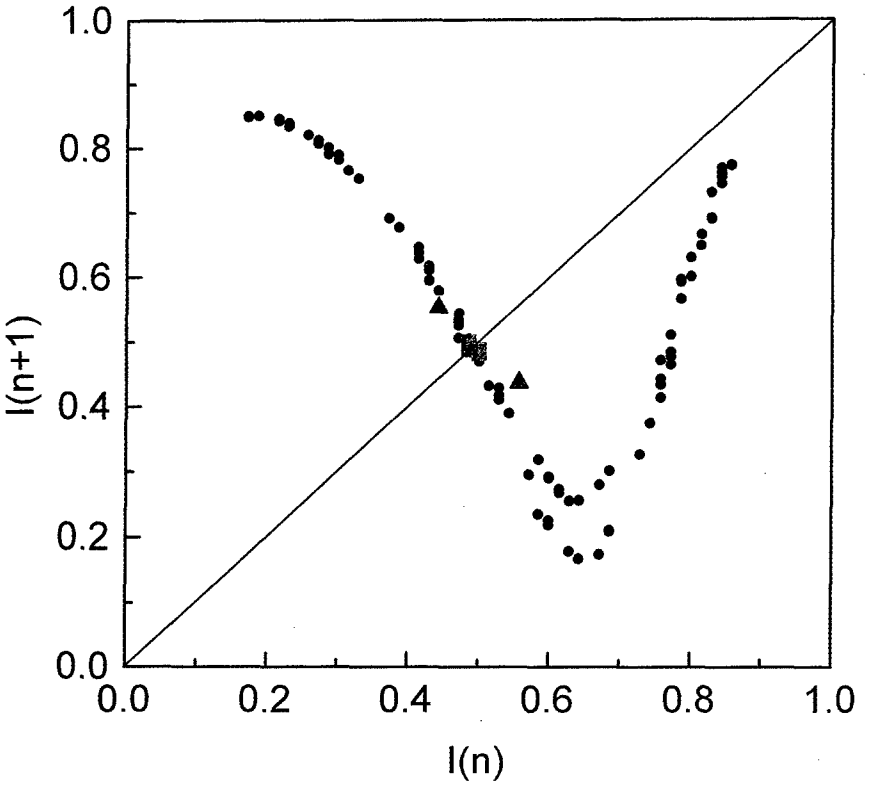

Fig. 12. Numerical simulations with control C_1. Poincaré maps corresponding to Fig. 11 together with period-2 orbit (black circles: chaos; green squares: period-1; red triangles: period-2).

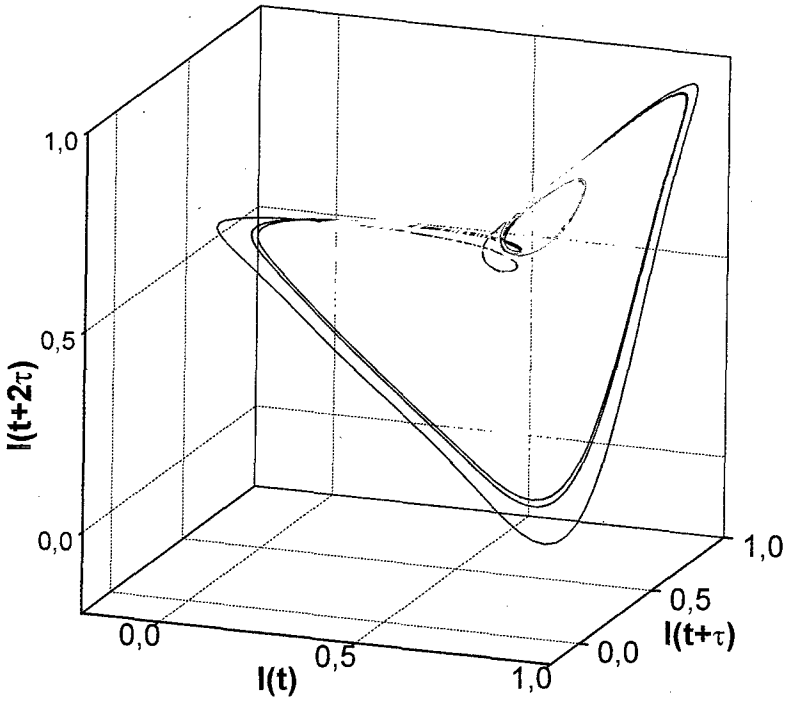

Fig. 13. Numerical simulations with control C_2. Unperturbed chaotic attractor (yellow) and stabilized orbit of period-2 (red) and period-4 (blue).

the detection process, can be obtained after a logarithmic amplification of the laser intensity. In this schematization, the total gain of the feedback loop $\tilde{R} = 133.9$ has been split in two parts; $r = 0.1339$ is the gain associated to the optical detector (in series with the preamplifier) and $\tilde{R}/r = 1000$ is the gain of the high-voltage differential amplifier.

The two control schemes are shown in Fig. 10. The first one (C_1) consists in the cascade of a logarithmic amplifier and a linear selective filter with transfer function $C(s)$. $C(s)$ fulfils the requirements given in the previous section, i.e. presents two zeroes at $f = 0$ and $f = f_0$, and a maximum at $f_0/2$. The analytical expression of $C(s)$ is ($\omega_0 = 2\pi f_0$):

$$C(s) = \frac{ks(s^2 + {\omega_0}^2)}{\left(s^2 + \zeta\omega_0 s + \frac{{\omega_0}^2}{4}\right)(s + \mu)}$$

The parameter values are: $\omega_0 = 0.2016$, $k = 3.5$, $\zeta = 0.7$ and $\mu = 0.8$.

The second controller (C_2) is simply a modulation signal applied to the summing point, which results in a sinusoidal modulation of the bias term B_0.

Figure 11 shows a three-dimensional reconstruction of the chaotic attractor of the unperturbed system obtained from numerical integration of Eqs. (2) ($B = 223$ V), with the superposition of the period-1 orbit stabilized with the selective filtering feedback C_1. In Fig. 12 we show the Poincaré maps corresponding to the unperturbed attractor and the period-1 ($k = 3.5$) and period-2 ($k = 2.9$) orbits. Finally, Fig. 13 shows the results obtained by applying the resonant modulation C_2 to the bias voltage. In this case, we observe that the stabilized period-2 and period-4 orbits also visit regions external to that of the chaotic attractor. This fact indicates some limitations of our model, which is able to satisfactorily reproduce the experimental results in the case of the filtering feedback control, but provides only a qualitative representation of the stabilized orbit in the case of the resonant modulation control.

4. Conclusions

In this paper we have shown that the chaotic dynamics of a CO_2 laser with feedback can be stabilized by using two different strategies, based on selective filtering and parametric modulation, respectively. From the results presented we summarize the main differences between the two proposed control schemes. On the one hand, the first method works correctly only for stabilization of period-1 cycle, and thus it seems less flexible than the second one, which provides stabilization of different periodic orbits only by changing the perturbation amplitude. On the other hand, the relative perturbation amplitude introduced by the second method to stabilize the period-1 orbit is very large, so that the controlled trajectory is quite different from that embedded in the chaotic dynamics.

As a final remark, it is important to compare the filtering feedback method with the time-delayed autosynchronization method proposed by Pyragas [1992]. In the frequency domain, the Pyragas scheme corresponds to performing a high-pass filtering without affecting the frequency component f_0 and its harmonics (all zeroes in the transfer function), thus ensuring that the stabilized orbit is exactly that embedded in the chaotic attractor. Anyway, at variance with our method, the presence of high frequency feedback makes the system sensitive to noise and reduces its robustness [Meucci *et al.*, 1997].

Acknowledgments

The authors wish to thank F. T. Arecchi and S. Boccaletti (Istituto Nazionale di Ottica), R. Genesio, A. Tesi and M. Basso (Dipartimento di Sistemi e Informatica of the University of Florence) for useful discussions, and F. Signorini for his contribution on performing the numerical simulations.

This work was partly supported by the EC Contract FMRX-CT96-0010 and by the coordinated project "Nonlinear dynamics in optical systems" of the Italian National Council of Research.

References

Bielawski, S., Bouazaoui, M., Derozier, D. & Glorieux, P. [1993] "Stabilization and characterization of unstable steady states in a laser," *Phys. Rev.* **A47**, 3276–3279.

Bielawski, S., Derozier, D. & Glorieux, P. [1994] "Controlling unstable periodic orbits by a delayed continuous feedback," *Phys. Rev.* **E49**, R971–R974.

Carr, T. W. & Schwartz, I. B. [1995] "Controlling the unstable steady state in a multimode laser," *Phys. Rev.* **E51**, 5109–5111.

Chin, G., Senesac, L. R., Blass, W. E. & Hillman, J. J. [1996] "Stabilizing lead-salt diode lasers:

Understanding and controlling chaotic frequency emission," *Science* **274**, 1498–1501.

Chizhevsky, V. N. & Glorieux, P. [1995] "Targeting unstable periodic orbits," *Phys. Rev.* **E51**, R2701–R2704.

Chizhevsky, V. N., Corbalan, R. & Pisarchik, A. N. [1997] "Attractor splitting induced by resonant perturbations," *Phys. Rev.* **E56**, 1580–1584.

Ciofini, M., Labate, A. & Meucci, R. [1997] "Tracking unstable periodic orbits in a modulated laser," *Phys. Lett.* **A227**, 31–36.

Colet, P., Roy, R. & Wiesenfield, K. [1996] "Controlling hyperchaos in a multimode laser model," *Phys. Rev.* **E50**, 3453–3457.

Colet, P. & Braiman, Y. "Control of chaos in multimode solid state lasers by the use of small periodic perturbations," *Phys. Rev.* **E53**, 200–206.

Ditto, W. L., Spano, M. L., Lindner, J. F. [1995] "Techniques for the control of chaos," *Physica* **D86**, 198–211.

Genesio, R., Tesi, A. & Villoresi, F. [1993] "A frequency approach for analyzing and controlling chaos in nonlinear circuits," *IEEE Trans. Circuits Syst. I: Fundamental Theor. Appl.* **40**, 819–828.

Gills, Z., Iwata, C., Roy, R., Schwartz, I. B. & Triandaf, I. [1992] "Tracking unstable steady states: expanding the stability regime of a multimode laser system," *Phys. Rev. Lett.* **69**, 3169–3172.

Grassberger, P. & Procaccia, I. [1983] "Characterization of strange attractors," *Phys. Rev. Lett.* **50**, 346–349.

Haken, H. [1975] "Analogy between higher instabilities in fluids and lasers," *Phys. Lett.* **A53**, 77–78.

Hunt, E. R. [1991] "Stabilizing high-period orbits in a chaotic system: The diode resonator," *Phys. Rev. Lett.* **67**, 1953–1955.

Khalil, H. K. [1992] *Nonlinear Systems* (MacMillan, Basingstoke, England), Chapter 7, pp. 408–411.

Liu, Y. & Rios Leite, J. R. [1994] "Control of Lorenz chaos," *Phys. Lett.* **A185**, 35–37.

Liu, Yun Ohtsubo, J. & Shoji, Y. [1994] "Accessing high-mode oscillations in a delayed optical bistable system," *Opt. Commun.* **105**, 193–198.

Liu, Yun Kikuchi, N. & Ohtsubo, J. [1995] "Controlling dynamical behavior of a semiconductor laser with external optical feedback," *Phys. Rev.* **E51**, R2697–R2700.

Lorenz, E. N. [1963] "Deterministic nonperiodic flows," *J. Atmos. Sci.* **20**, 130–141.

Meucci, R., Gadomski, W., Ciofini, M. & Arecchi, F. T. [1994] "Experimental control of chaos by means of weak parametric perturbations," *Phys. Rev.* **E49**, R2528–R2531.

Meucci, R., Ciofini, M. & Abbate, R. [1996] "Suppressing chaos in lasers by negative feedback," *Phys. Rev.* **E53**, R5537–R5540.

Meucci, R., Labate, A. & Ciofini, M. [1997] "Controlling chaos by negative feedback of subharmonic components," *Phys. Rev.* **E56**, 2829–2834.

Ott, E., Grebogi, C. & Yorke, J. A. [1990] "Controlling chaos," *Phys. Rev. Lett.* **64**, 1196–1199.

Petrov, V., Gaspar, V., Masere, J. & Showalter, K. [1993] "Controlling chaos in the Belousov–Zhabotinsky reaction," *Nature* **361**, 240–243.

Pyragas, K. [1992] "Continuous control of chaos by self-controlling feedback," *Phys. Lett.* **A170**, 421–428.

Reyl, C., Flepp, L., Badii, R. & Brun, E. [1993] "Control of NMR-laser chaos in high dimensional embedding space" *Phys. Rev.* **E47**, 267–272.

Roy, R., Murphy, T. W., Maier, T. D., Gills, Z. & Hunt, E. R. [1992] "Dynamical control of a chaotic laser: Experimental stabilization of a globally coupled system," *Phys. Rev. Lett.* **68**, 1259–1262.

Shimbrot, T., Grebogi, C., Ott, E. & Yorke, J. A. [1993] "Using small perturbations to control chaos," *Nature* **363**, 411–417.

Simmendinger, C. & Hess, O. [1996] "Controlling delay-induced chaotic behavior of a semiconductor laser with optical feedback," *Phys. Lett.* **A216**, 97–105.

Vilaseca, R., Kul'minskii, A. & Corbalan, R. [1996] "Tracking unstable steady states by large periodic-modulation of a control parameter in a nonlinear system," *Phys. Rev.* **E54**, 82–85.

International Journal of Bifurcation and Chaos, Vol. 8, No. 9 (1998) 1769–1775

INSTABILITIES AND TRACKING OF TRAVELLING WAVE PATTERNS IN A THREE-LEVEL LASER

WEIPING LU*, DEJIN YU and ROBERT G. HARRISON
Department of Physics, Heriot–Watt University, Riccarton, Edinburgh EH14 4AS, UK

Received July 31, 1997; Revised November 12, 1997

Based on our earlier theoretical work on tracking periodic patterns into spatiotemporal chaotic regimes in spatially extended systems, we present in this article a case study of a high-aspect-ratio three-level laser. Following a detailed investigation into travelling wave solutions of the laser system and their stability conditions, we discuss ways of stabilising these solutions by local feedback algorithms. In numerical simulations, we choose Pyragus continuous delayed feedback algorithm to be the local feedback form and demonstrate that stable travelling wave solutions of the spatially extended three-level laser can be greatly extended to unstable regions in the presence of this feedback.

1. Introduction

Spatiotemporal chaos occurs when different types of motion, excited in local regions in an extended system, interact to destroy the spatial coherence of the system concurrent with the onset of temporal chaos. This phenomenon in continuous physical systems is described by partial differential equations. While the transition from coherence to spatiotemporal chaos has yet to be characterised by global quantitative laws, certain normal mode equations have shown that such a chaotic state in a spatiotemporal context underlies different unstable coherent structures, which are sensitive to small perturbations. The possibility of controlling spatiotemporal dynamics by these perturbations has recently inspired considerable theoretical and experimental effort in many branches of nonlinear science [Sepulchre & Babloyantz, 1993; Hu & Qu, 1994; Auerbach, 1994; Qin *et al.*, 1994, Aranson *et al.*, 1994; Johnson *et al.*, 1995; Lourenco *et al.*, 1995; Petrov *et al.*, 1995; Poon & Grebogi, 1995; Hagberg *et al.*, 1996; Lu *et al.*, 1996; Bleich & Socolar, 1996; Martin *et al.*, 1996; Battogtokh & Mikhailov, 1996]. This offers an opportunity to stabilise, select and manipulate these systems for applications.

To control a spatially extended dynamical system, a feedback with spatial coupling is often applied to the system so that a desired state can be stabilised. Systems investigated are both one- and two-dimensional, continuous or discrete, in various disciplines. Based on these developments, control methodology has been further explored where emphasis has been given to algorithms which are simple and more readily implemented in experiments. In our recent work, it has been established that unstable periodic solutions of spatially extended two-dimensional systems, when weakly perturbed, can be stabilised by *local feedback* without spatial coupling [Lu *et al.*, 1997]. This is due to the fact that the evolution equations for weak perturbations to these periodic solutions can be reduced to ordinary differential equations, because of the

*E-mail: phywl@phy.hw.ac.uk

decoupling of the wave numbers in the perturbations to a first order small signal approximation. As a result, stable periodic solutions can be tracked to unstable and spatiotemporal chaotic regimes by simply utilising feedback control algorithms established for controlling temporal chaos in spatially constrained systems. In this article, we provide a case study of a high-aspect-ratio three-level laser in which a detailed investigation into the stability of travelling wave solutions of the laser system and ways to stabilise these solutions by local feedback are discussed. In numerical simulations, we choose the well-known Pyragus continuous delayed feedback algorithm to be the local feedback and demonstrate that stable travelling waves of the spatially extended laser system can be greatly extended to unstable regions in the presence of this feedback.

2. Theory for the Tracking Procedure

We first give a brief review of the theory for tracking procedure by using local feedback algorithms. We consider a general form of a distributed nonlinear optical system

$$\frac{\partial q}{\partial t} = N(q, \mu) + iD\nabla_{\perp}^2 q\,, \tag{1}$$

which admits a travelling wave solution of

$$q_0 = Ce^{i(\mathbf{k}\cdot\mathbf{r}-\omega t)}\,, \tag{2}$$

where q is the complex amplitude of the electromagnetic field, N the nonlinear function describing the local field-material interaction, $\nabla_{\perp}^2$ the transverse Laplacian in two-dimensional space $\mathbf{r}(x, y)$ and t the time. μ is the control parameter of the system and D a coefficient describing diffractive coupling in space. $\mathbf{k}$ and ω are the characteristic wave vector and frequency of the travelling waves while C is the amplitude. The stability of the travelling solution is determined by standard perturbation analysis which yields

$$\frac{\partial \delta q}{\partial t} = iD\nabla_{\perp}^2 \delta q + N'(q_0, \mu)\delta q + \frac{1}{2}N''(q_0, \mu)\delta q^2 + \mathcal{O}(\delta q^3)\,, \tag{3}$$

where δq is the perturbation strength and N' and N'' are the first and second derivatives of N with respect to q at $q = q_0$. We note that terms of δq^* should appear in the above equation if N comprises explicitly the variable q^*. In Fourier space, the perturbation is of the form

$$\delta q(\mathbf{r}, t) = e^{i(\mathbf{k}\cdot\mathbf{r}-\omega t)} \int_{-\infty}^{+\infty} \delta q_p e^{i\mathbf{p}\cdot\mathbf{r}} d\mathbf{p}\,, \tag{4}$$

where δq_p is the perturbation strength with wave vector $\mathbf{p}$. By substituting Eq. (4) into Eq. (3), we derive the evolution equation of perturbation for the specific $\mathbf{p}$

$$\frac{\partial \delta q_p}{\partial t} = i\omega\delta q_p - iD(\mathbf{k}+\mathbf{p})^2\delta q_p + N'\delta q_p + \frac{1}{2}N''e^{-i\omega t}\int_{-\infty}^{+\infty} \delta q_{p'}\delta q_{p-k-p'} d\mathbf{p}' + \mathcal{O}(\delta q_p^3)\,. \tag{5}$$

We note that since Eq. (2) is a solution of Eq. (1), $N'(q_0, \mu)$, the Jacobian which along with $\mathbf{k}$, $\mathbf{p}$ and ω determines the linear stability of the solution, is independent of the transverse coordinate $\mathbf{r}$.

When the perturbation against the travelling wave solution is weak, the stability of this solution is determined by the linearisation of Eq. (5) which is a wave vector decoupled ordinary differential equation. Control of such a solution, when unstable, can therefore be achieved by a feedback approach which is no more complicated than controlling an unstable periodic orbit in an ordinary differential equation; this is

$$\frac{\partial \delta q_p}{\partial t} = i\omega\delta q_p - iD(\mathbf{k}+\mathbf{p})^2\delta q_p + N'\delta q_p + f_p(t)\,, \tag{6}$$

where f_p is the feedback which depends only on the wave vector component $\mathbf{p}$ in the Fourier space. In $\mathbf{r}$ space the feedback is given as

$$F(\mathbf{r}, t) = e^{i(\mathbf{k}\cdot\mathbf{r}-\omega t)} \int_{-\infty}^{+\infty} f_p(t) e^{\mathbf{p}\cdot\mathbf{r}} d\mathbf{p} \tag{7}$$

which does not involve feedback coupling in different spatial regions. Thus, the feedback required for this case is local in the transverse space, in the sense that the signal at a given point depends on only its behaviour at that particular point, and not on that in the neighbouring and distant regions. It follows that when a state q is close enough to a targeted travelling wave solution of a distributed system as given by Eq. (1), this state can be stabilised to the solution by simply adopting the control algorithms developed for controlling temporal chaos in ordinary differential equations. In order to utilise

the linearised approach to stabilise a traveling pattern, we may take advantage of the tracking procedure [Gills *et al.*, 1992] which was first developed for extending a stable operating region of a low-dimensional laser system. In this procedure, the feedback to Eq. (1) is applied when the system is initially set in a region of a stable periodic pattern, and on varying a control parameter of the system, this stable solution can be extended to unstable and spatiotemporal chaotic regions in the presence of the feedback. Moreover, this tracking procedure can be adopted to manipulate a stabilised travelling wave pattern; the values of its frequency and wave vector can be altered, as can the orientation of the wave vector, by judiciously varying these parameters providing that they constitute one solution of the travelling wave family. The above analysis can be readily extended to stabilising more complex periodic patterns, such as square and hexagonal patterns, in a set of coupled equations.

3. Three-level Laser Model

We consider a coherently optically pumped three-level laser as a case for study. It has previously received considerable attention as a spatially constrained dynamical system in the investigation of temporal chaos [Moloney *et al.*, 1992; Forysiak *et al.*, 1991]. When the transverse space is broad, self-diffraction of the inter-cavity field plays an essential role. With inclusion of this transverse coupling the Maxwell–Bloch equations describing resonant single mode lasing are generalised to

$$
\begin{aligned}
\frac{\partial E}{\partial t} &= -\sigma E + gP_2 + ia\nabla_\perp^2 E\,,\\
\frac{\partial P_1}{\partial t} &= -P_1 + AN_1 - EP_3\,,\\
\frac{\partial P_2}{\partial t} &= -P_2 + EN_2 - AP_3^*\,,\\
\frac{\partial P_3}{\partial t} &= -P_3 + E^*P_1 + AP_2^*\,,\\
\frac{\partial N_1}{\partial t} &= -b(1+N_1) - 2A(P_1 + P_1^*)\\
&\quad - (E^*P_2 + EP_2^*)\,,\\
\frac{\partial N_2}{\partial t} &= -bN_2 - A(P_1 + P_1^*) - 2(E^*P_2 + EP_2^*)\,,
\end{aligned}
\tag{8}
$$

where E is the slowly varying electromagnetic field amplitude of the laser emission and P_1, P_2 and P_3 are the normalised off-diagonal density matrix elements of the polarisation. Due to the existence of transverse diffraction, these variables are complex even for the case of resonant pumping and laser emission, showing the important role of phase in optical pattern-forming phenomena. The other variables are N_1 and N_2, the diagonal density matrix elements describing the population differences between the common upper and lower levels of the pump and lasing transitions. Parameters of the system are σ, the cavity damping constant, g, the unsaturated gain of the laser medium, and a, the diffractive coefficient which can be set to unity by rescaling the transverse coordinates (x and y). Control parameters are A, the external pump strength, and b, the ratio of energy relaxation (γ) to dipole dephasing (Γ) rates of the medium. The laser system possesses translational symmetry and is invariant under the following transformation (E, P_1, P_2, P_3, N_1, N_2) $\Longrightarrow$ ($-E$, P_1, $-P_2$, $-P_3$, N_1, N_2), which give certain restrictions to the solutions of Eqs. (8).

3.1. *Travelling wave solutions*

Equations (8) admits a travelling wave solution

$$
\begin{aligned}
E &= E^0 e^{i(\mathbf{k}\cdot\mathbf{r}-\omega t)}, \quad & P_1 &= P_1^0\,,\\
P_2 &= P_2^0 e^{i(\mathbf{k}\cdot\mathbf{r}-\omega t)}, \quad & P_3 &= P_3^0 e^{-i(\mathbf{k}\cdot\mathbf{r}-\omega t)}\,,\\
N_1 &= N_1^0, & N_2 &= N_2^0\,,
\end{aligned}
\tag{9}
$$

where $\mathbf{k}$ and ω are the wave vector and frequency of the travelling wave solution on the transverse plane (x, y), and E^0, P_1^0, P_2^0, P_3^0, N_1^0 and N_2^0 are the amplitudes, of which E^0 can be assumed to be real. By using the transformation $E^0 = x_1$, $\omega = x_2$, $P_1^0 = x_3 + ix_4$, $P_2^0 = x_5 + ix_6$, $P_3^0 = x_7 + ix_8$, $N_1^0 = x_9$, $N_2^0 = x_{10}$ and substituting Eqs. (9) into Eqs. (8), we derive the following coupled equations for x_1, x_2, x_9 and x_{10} for a nontrivial solution,

$$
\begin{aligned}
&(1+x_1^2)[gx_{10} - \sigma - x_2(k^2 - x_2)]\\
&\quad - x_2[k^2 - (1+\sigma)x_2] - A^2(\sigma + gx_9) = 0\,,\\
&(1+x_1^2)[k^2 - (1+\sigma)x_2] + x_2[gx_{10} - \sigma\\
&\quad - x_2(k^2 - x_2)] + A^2(k^2 - x_2) = 0\,,\\
&2A^2x_9 + (b - 2x_1^2)x_{10}\\
&\quad + \frac{2}{g}x_1^2[3\sigma + x_2(k^2 - x_2)] = 0\,,\\
&b + (b + 4A^2)x_9 - 4x_1^2x_{10}\\
&\quad + \frac{2}{g}x_1^2[3\sigma + 2x_2(k^2 - x_2)] = 0\,,
\end{aligned}
\tag{10}
$$

while other variables are given by

$$
\begin{aligned}
x_3 &= Ax_9 - x_1x_7\,,\\
x_4 &= -x_1x_8\,,\\
x_5 &= \frac{\sigma}{g}x_1\,,\\
x_6 &= \frac{1}{g}(k^2 - x_2)x_1\,,\\
x_7 &= \frac{x_1}{Ag}[gx_{10} - \sigma - x_2(k^2 - x_2)]\,,\\
x_8 &= \frac{x_1}{Ag}[k^2 - (1+\sigma)x_2]\,.
\end{aligned}
\tag{11}
$$

Figure 1 shows a set of travelling wave solutions in three-dimensional space; the laser amplitude is the function of the pump strength A and the wave number k, with other parameters being held as $g = 52$, $b = 0.4$ and $\sigma = 1.3$. The curve for $k = 0$ corresponds to homogeneous steady state solutions, the laser branch ($E \neq 0$) of which exists only in a limited region of the pump strength due to the Rabi splitting effect of the laser gain profile. On increasing the value of k form a family of nontrival travelling wave solutions, which exist over an extended region of the pump strength but is limited only for small wave numbers.

3.2. *Stability of travelling wave solutions*

In general, the stability of the traveling solutions given by Eqs. (9) through Eqs. (10) and (11) depends on the control parameters of the laser system. To determine the stability conditions of these travelling waves, we perturb them with the following

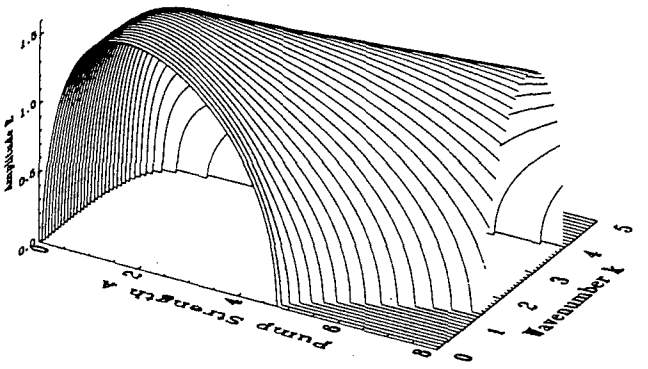

Fig. 1. Travelling wave solutions, E as a function of the pump strength A and wave number k for parameters $g = 52.0$, $b = 0.4$ and $\sigma = 1.3$.

trial solution

$$
\begin{aligned}
E &= \left[E^0 + \int_{-\infty}^{+\infty}\delta E_p e^{i\mathbf{p}\cdot\mathbf{r}}d\mathbf{p}\right]e^{i(\mathbf{k}\cdot\mathbf{r}-\omega t)}\,,\\
P_1 &= P_1^0 + \int_{-\infty}^{+\infty}\delta P_{1p}e^{i\mathbf{p}\cdot\mathbf{r}}d\mathbf{p}\,,\\
P_2 &= \left[P_2^0 + \int_{-\infty}^{+\infty}\delta P_{2p}e^{i\mathbf{p}\cdot\mathbf{r}}d\mathbf{p}\right]e^{i(\mathbf{k}\cdot\mathbf{r}-\omega t)},\\
P_3 &= \left[P_3^0 + \int_{-\infty}^{+\infty}\delta P_{3p}e^{i\mathbf{p}\cdot\mathbf{r}}d\mathbf{p}\right]e^{-i(\mathbf{k}\cdot\mathbf{r}-\omega t)}\,,\\
N_1 &= N_1^0 + \int_{-\infty}^{+\infty}\delta N_{1p}e^{i\mathbf{p}\cdot\mathbf{r}}d\mathbf{p}\,,\\
N_2 &= N_2^0 + \int_{-\infty}^{+\infty}\delta N_{2p}e^{i\mathbf{p}\cdot\mathbf{r}}d\mathbf{p}\,,
\end{aligned}
\tag{12}
$$

where the second terms on the right-hand side are perturbations integrated over all wave numbers. By substituting Eqs. (12) into Eqs. (8) and considering only to the first order small terms, we derive the following linearised evolution equation for the perturbation strength

$$
\begin{aligned}
\frac{\partial\delta E_p}{\partial t} &= i\omega\delta E_p - i(\mathbf{k}+\mathbf{p})^2\delta E_p - \sigma\delta E_p + g\delta P_{2p}\,,\\
\frac{\partial\delta P_{1p}}{\partial t} &= -\delta P_{1p} + A\delta N_{1p} - E^0\delta P_{3p} - P_3^0\delta E_p\,,\\
\frac{\partial\delta P_{2p}}{\partial t} &= i\omega\delta P_{2p} - \delta P_{2p} + E^0\delta N_{2p}\\
&\quad + N_2^0\delta E_p - A\delta P_{3p}^*\,,\\
\frac{\partial\delta P_{3p}}{\partial t} &= -i\omega\delta P_{3p} - \delta P_{3p} + E^0\delta P_{1p}\\
&\quad + P_1^0\delta E_p^* + A\delta P_{2p}^*\,,\\
\frac{\partial\delta N_{1p}}{\partial t} &= -b\delta N_{1p} - 2A(\delta P_{1p} + \delta P_{1p}^*) - (E^0\delta P_{2p}\\
&\quad + P_2^0\delta E_p + E^0\delta P_{2p}^* + P_2^{0*}\delta E_p),\\
\frac{\partial\delta N_{2p}}{\partial t} &= -b\delta N_{2p} - A(\delta P_{1p} + \delta P_{1p}^*) - 2(E^0\delta P_{2p}\\
&\quad + P_2^0\delta E_p + E^0\delta P_{2p}^* + P_2^{0*}\delta E_p)\,,
\end{aligned}
\tag{13}
$$

where $(\mathbf{k}+\mathbf{p})^2$ is equal to $(k+p)^2$ for the two vectors being parallel, corresponding to the Eckhaus instability, and to k^2+p^2 for the vectors being perpendicular, a case of Zig–zag instability. The eigenvalue equations for λ_p are obtained by substituting the relation $\partial\delta(\,)/\partial t = \lambda_p\delta(\,)$ into Eqs. (13), where

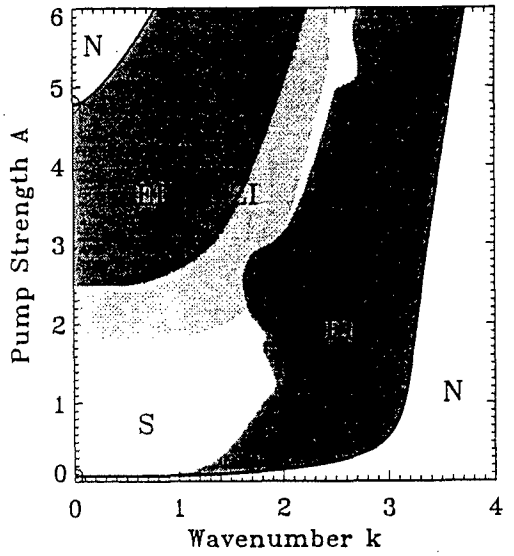

Fig. 2. (A, k) two-dimensional stability diagram for travelling wave solutions for parameters $g = 52.0$, $b = 0.4$ and $\sigma = 1.3$. The region surrounded by the solid curves comprises nontrival solutions in which domains marked by EI and ZI correspond to Eckhaus and Zig–zag instabilites. N and S stands for regions of trival solutions and stable solution respectively.

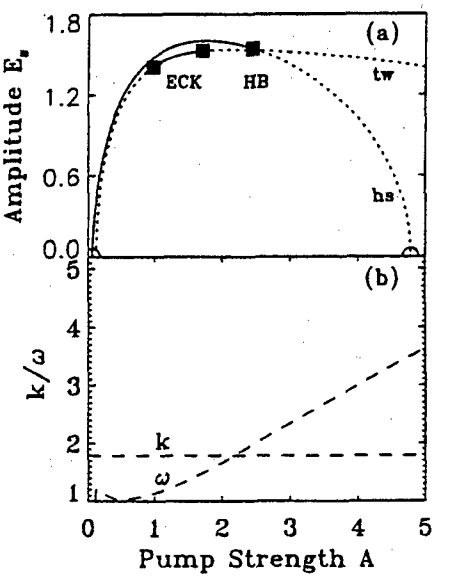

Fig. 3. (a) Travelling wave (tw) and homogeneous steady state (hs) solutions as a function of the pump strength for $g = 52.0$, $b = 0.4$, $\sigma = 1.3$ and $k = 1.78$. The solid and dash curves stand for stable and unstable solutions respectively, separated by the Hopf bifurcation (HB) points, which for the travelling wave is further referred to as the Eckhaus instability (ECK). (b) The corresponding wave numbers and frequencies of the travelling wave in trace(a), both as the function of the pump strength.

$\delta(\ )$ stands for the above perturbations. The travelling wave solutions are linearly stable if $\mathrm{Re}(\lambda) < 0$ and unstable if $\mathrm{Re}(\lambda) > 0$. Figure 2 shows a bifurcation diagram of the steady state and travelling wave solutions in (A, k) two-dimensional space, for parameters $g = 52.0$, $b = 0.4$ and $\sigma = 1.3$. The region surrounded by the solid curves is that of nontrival travelling solutions in which domains marked by EI correspond to the Eckhaus instabilites and the area under ZI is Zig–zag unstable. N stands for regions of trival solutions.

4. Tracking of Travelling Wave Solutions

In this section, we apply the general theory in Sec. 2 to the laser equations (8) to track the travelling wave solutions from a stable region into an unstable domain. As we discussed earlier, tracking of such unstable solutions can be realised by simply adopting the control approaches developed for controlling temporal chaos in ordinary differential equations. Well-known methods for control of temporal chaos, such as the Ott–Grebogi–Yorke algorithm (OGY) [Ott *et al.*, 1990], occasional proportional feedback (OPF) [Hunt, 1991] and continuous delayed feedback (CDF) [Pyragas, 1992], can therefore be used. Here we take the continuous delayed feedback as an example. For this case, the form of the feedback as discussed in Eq. (6) is $f_p \sim (\delta E_p(t - t_0) - \delta E_p(t))$. Using Eq. (7) the feedback in $\mathbf{r}$ space is given as

$$F(\mathbf{r}, t) = \alpha(E(\mathbf{r}, t - t_0) - E(\mathbf{r}, t)), \qquad (14)$$

which is now applied to the right-hand side of the first equation of Eqs. (8). In the above equation α is the proportionality constant defining the feedback strength and t_0 the period in time of the travelling wave solution to be stabilised.

We have simulated the tracking procedure by numerically integrating the three-level laser system in the presence of CDF control in the laser field equation. The numerical integration is based on the Fourier transformation method by using typically 60×60 grid points in a square in the transverse plane and is checked by 120×120 grid point simulations. The width of the square is chosen to be $32\pi/k_A$, where k_A is the spatial wave number corresponding to the largest growth rate of the unstable travelling wave solution. An example is shown in Fig. 3. The travelling wave solutions, the frequencies and wave numbers of which are given in trace (b), are stable only in a small pump region as depicted in trace (a). These solutions corresponds to the vertical line of $k = 1.78$ in Fig. 2 in which

the stable region is bounded by two points of the Eckhaus instability. To track this travelling wave branch, the feedback is first applied to each grid point, when the system is initially in the parameter region for stable travelling waves. The pump strength A is then increased from this region in small steps $\delta A = 0.1$ to extend to the unstable region. At each value of the pump strength, the initial conditions of the system are set to be the output of the system at its previous value, whereas the delay time t_0 in the feedback is chosen to be the period of the travelling wave at the current value of the pump strength. Numerical simulations have shown that the travelling wave can be stabilised along the dash curves of k and ω in Fig. 3(b), extending the periodic pattern into both the spiral and spatiotemporal chaos regions. For each value of the pump strength, there is a threshold of the coefficient α for a successful tracking, the values of which are less than 1.0. In the process of tracking, the stabilised travelling waves are found to be robust against external perturbations to the pump strength A. For $\alpha = 0.7$ and different values of A, the system is shown to be stable when A is perturbed by different levels of white noise signal (peak value) up to 20% of the signal. We further find that the feedback strength throughout the tracking process is small, demonstrating the noninvasive nature of the control. In these simulations it is limited to less than 2% of the laser output (peak to peak) due to the limited temporal and spatial resolution in the simulation scheme. We note that for stabilizing a state when it is far away from a targeted periodic pattern, the feedback by contrast requires both temporal and spatial coupling [Lu *et al.*, 1996].

The tracking procedure has also been tested numerically on travelling wave solutions of different sets of wave numbers k and frequencies ω. Moreover, such a tracking procedure can be applied to track a travelling wave solution using other control parameters of the system, for instance, the wave number k, while the pump strength is held constant. For this case, the wave number of a stabilised travelling wave can vary while the corresponding frequency is judiciously chosen so that these two parameters satisfy solutions of the travelling wave family. In such a way, the spectrum of the periodicity of the stabilised pattern can be extended. In summary, we have shown that, as an example of a spatially extended dynamical system, the high-aspect-ratio three-level laser is well within our general theoretical description for the use of the tracking procedure to extend its coherent pattern formations. The advantage of this tracking procedure lies in the use of local feedback in a spatially extended system. Such a simple control approach with no involvement of spatial coupling is more easily accessible to experiments. In optics, the CFD algorithm can be implemented using the interference technogue of theoutput beam with delayed itself.

Acknowledgments

This work is supported by EPSRC (UK) Grants No. GR/J73285 and No. GR/K23768.

References

Aranson, I., Levine, H. & Tsimring, L. [1994] "Controlling spatiotemporal chaos," *Phys. Rev. Lett.* **72**, 2561–2564.

Auerbach, D. [1994] "Controlling extended systems of chaotic elements," *Phys. Rev. Lett.* **72**, 1184–1187.

Battogtokh, D. & Mikhailov, A. [1996] "Controlling turbulence in the complex Ginzburg–Landau equation," *Physica* **D90**, 84–95.

Bleich, M. B. & Socolar, J. E. S [1996] "Controlling spatiotemporal dynamics with time-delay feedback," *Phys. Rev.* **E54**, R17–R20.

Forysiak, W., Moloney, J. V. & Harrison, R. G. [1991] "Bifurcation of an optically pumped 3-level laser model," *Physica* **D53**, 162–186, and references therein.

Gills, Z., Iwata, C., Roy, R., Schwartz, I. B. & Triandaf, I. [1992] "Tracking unstable steady-state — Extending the stability regime of a multimode laser system," *Phys. Rev. Lett.* **69**, 3169–3172

Hagberg, A., Meron, E., Rubinstein, I. & Zaltzman, B. [1996] "Controlling domain patterns far from equilibrium," *Phys. Rev. Lett.* **76**, 427–430.

Hu, G. & Qu, K. [1994] "Controlling spatiotemporal chaos in map lattice systems," *Phys. Rev. Lett.* **72**, 68–71.

Hunt, E. R. [1991] "Stabilizing high-period orbits in a chaotic system — The diode resonator," *Phys. Rev. Lett.* **67**, 1953–1955.

Johnson, G. A., Löcher, M. & Hunt, E. R. [1995] "Stabilised spatiotemporal waves in a convectively unstable open flow system — Coupled diode resonators," *Phys. Rev.* **E51**, R1625–1628.

Lourenco, C., Hougardy, M. & Babloyantz, A. [1995] "Control of low-dimensional spatiotemporal chaos in Fourier space," *Phys. Rev.* **E52**, 1528–1532.

Lu, W., Yu, D. & Harrison, R. G. [1996] "Control of patterns in spatiotemporal chaos in optics," *Phys. Rev. Lett.* **76**, 3316–3319.

Lu, W., Yu, D. & Harrison, R. G. [1997] "Tracking periodic patterns into spatiotemporal chaotic regimes," *Phys. Rev. Lett.* **78**, 4375–4378.

Martin, R., Scroggie, A. J., Oppo, G.-L. & Firth, W. J. [1996] "Stabilization, selection, and tracking of unstable patterns by Fourier space techniques," *Phys. Rev. Lett.* **77**, 4007–4010.

Moloney, J. V., Forysiak, W., Uppal, J. S. & Harrison, R. G. [1989] "Regular and chaotic dynamics of optically pumped molecular lasers," *Phys. Rev.* **A39**, 1277–1285.

Ott, E., Grebogi, C. & Yorke, J. A. [1990] "Controlling chaos," *Phys. Rev. Lett.* **64**, 1196–1199.

Petrov, V., Metens, S., Borckmans, P., Dewel, G. & Showalter, K. [1995] "Tracking unstable Turing patterns through mixed-mode spatiotemporal chaos," *Phys. Rev. Lett.* **75**, 2895–2898.

Poon, L. & Grebogi, C. [1995] "Controlling complexity," *Phy. Rev. Lett.* **75**, 4023–4026.

Pyragas, K. [1992] "Continuous control of chaos by self controlling feedback," *Phys. Lett.* **A170**, 421–428.

Qin, F., Wolf, E. E. & Chang, H. C. [1994] "Controlling spatiotemporal patterns on a catalytic wafer," *Phys. Rev. Lett.* **72**, 1459–1462.

Sepulchre, J. A. & Babloyantz, A. [1993] "Controlling chaos in a network of oscillations," *Phys. Rev.* **E48**, 945–950.

International Journal of Bifurcation and Chaos, Vol. 8, No. 9 (1998) 1777–1782

EXPERIMENTAL SWITCHINGS IN BISTABILITY DOMAINS INDUCED BY RESONANT PERTURBATIONS

V. N. CHIZHEVSKY*,†,‡, R. VILASECA* and R. CORBALAN†
*Departament de Fisica i Enginyeria Nuclear, Universitat Politecnica de Catalunya, Colom 11, E-08222 Terrassa, Spain
†Departament de Física, Universitat Autónoma de Barcelona, E-08193 Bellaterra, Barcelona, Spain
‡Stepanov Institute of Physics, Belarus Academy of Sciences, 220072 Minsk, Belarus

Received July 31, 1997; Revised October 28, 1997

We show that a combination of a resonant perturbation which induces bistability in the system with the targeting technique based on the action of a short-lived pulse perturbation makes the nonfeedback control of nonlinear systems (not only in a chaotic state) more flexible and even competitive with OGY's method in the sense of fast switching between controlled orbits belonging to coexisting attractors. For different initial states we present several experimental and numerical examples of such a type of control, which does not require feedback system.

1. Introduction

Controlling chaos and, more generally, controlling dynamics and complexity of nonlinear systems attracted much attention over the last years. For these purposes a diversity of approaches and methods has been proposed. Many of them have been successfully implemented experimentally in diverse systems ranging from physics, and optics to biology and chemistry and showed high efficiency and flexibility. The latter is especially true with regard to the method of chaos control proposed by Ott, Grebogi and Yorke [Ott *et al.*, 1990; Ditto *et al.*, 1995]. Among the different approaches there is the so-called nonfeedback method which is based on the adding of weak periodic resonant perturbations to the system under control [Lima & Petttini, 1990; Braiman & Goldhirsch, 1991]. Typically, resonant perturbations at a subharmonic frequency, depending on their amplitude and phase and on the initial state, may produce stabilizing or destabilizing effects on the nonlinear system. As it has been experimentally shown, they may suppress chaos [Azevedo & Rezende, 1991; Fronzoni *et al.*, 1991; Ding *et al.*, 1994; Meucci *et al.*, 1994], suppress periodic orbits, induce a chaotic behavior if the system is initially in a periodic state, and, finally, may induce crisis of strange attractors [Chizhevsky & Corbalan, 1996]. Up till now, most attention was paid to the question of how resonant perturbations modify the dynamics of nonlinear systems. Recently, it has been experimentally and numerically shown with a loss-modulated CO_2 laser that resonant perturbations globally change the phase space of the system, splitting the primary attractor into two new ones [Chizhevsky *et al.*, 1997a]. It has been demonstrated that by changing the amplitude and/or the phase of resonant perturbations, one can control the overlapping of different dynamical regimes associated with these two new attractors. From the practical point of view, for example, in engineering, a new problem arises here: How to switch the motion in the system from one dynamical regime to another one belonging to these new attractors? Recently, the technique of targeting periodic orbits has been proposed and

developed experimentally [Chizhevsky & Turovets, 1994; Chizhevsky & Glorieux, 1995], which allows one (i) to switch the phase of a periodic motion, (ii) to reach unstable orbits created either at a period-doubling or saddle-node bifurcation, and (iii) to perform switching between stable periodic orbits belonging to coexisting attractors. It is based on the action of a large-amplitude pulse perturbation to the system that is equivalent to a change of initial conditions. There exists the optimal timing and the optimal amplitude of a pulse perturbation which allow one to perform switchings practically without transients [Chizhevsky *et al.*, 1997b].

The main aim of this work is to show that a combination of the resonant perturbation, which induces bistability in the system, with the targeting technique makes the nonfeedback control of nonlinear systems (not only in a chaotic state) more flexible and even competitive with OGY's method in the sense of fast switching between controlled orbits belonging to coexisting attractors. For different initial states we demonstrate several experimental and numerical examples of such a type of control. This technique does not require any feedback system and might be experimentally implemented in diverse nonlinear systems.

2. Experimental Setup and Model

The experiments were carried out on a CO_2 laser with two acousto-optic modulators inserted in the laser cavity as described earlier [Chizhevsky & Corbalan, 1996]. Two electric signals were applied to the modulator providing the time-dependent cavity losses. The driving signal had the frequency $f_d = 100$ kHz and the amplitude V_d. The perturbation signal had the frequency $f_p = f_d/2 = 50$ kHz, the amplitude V_p and the phase φ. Laser parameters such as relaxation-oscillation frequency $f_{RO} \cong 50$ kHz and decay rate $\gamma_{RO} \cong 200$ kHz were estimated from the laser response due to short-lived loss perturbations (in the absence of the driving and perturbation signals) and were used then in numerical simulations. The laser responses were detected with a CdHgTe detector and a digital oscilloscope coupled with a PC. The technique of stroboscopic data recording with a sampling period T ($T = 1/f_d$) was used. Short-lived pulse loss perturbations were caused by absorption of the laser emission on nonequilibrium charge carriers which were excited by illuminating the semiconductor window of the laser tube by short pulses of a YAG-laser [Chizhevsky & Turovets, 1994; Chizhevsky & Glorieux, 1995]. Several clocks and devices were used in experiments to synchronize all control signals.

Numerical simulations were performed using a simple two-level rate-equation laser model [Tredicce *et al.*, 1986]:

$$\frac{du}{dt} = \tau^{-1}(y - k)u\,, \tag{1}$$

$$\frac{dy}{dt} = (y_0 - y)\gamma - uy\,, \tag{2}$$

where

$$k = k_0 + k_d \cos(2\pi f t) + k_p \cos(\pi f t + \varphi) + k_\delta(t - t_0) \tag{3}$$

Here u is proportional to the radiation density, y and y_0 are the gain and the unsaturated gain in the active medium, respectively, τ is half round-trip time of light in the cavity, γ is the gain decay rate, k is the total cavity losses, k_0 is the constant part of the losses, k_d is the driving amplitude, k_p is the perturbation amplitude, φ is the perturbation phase, $k_\delta(t - t_0)$ is the pulse loss perturbation, t_0 is the moment of time of the action of the pulse losses perturbation ($k_\delta(t - t_0) = 0$ for $t < t_0$ and $k_\delta(t - t_0) = k_\delta(\exp(-\alpha(t - t_0)) - \exp(-(\beta t - t_0)))$ for $t \geq t_0$,where $\alpha = 3 \times 10^7$ s^{-1} and $\beta = 10^8$ s^{-1}). In order to compare the numerical results with the experimental ones the values f_{RO} and γ_{RO} measured in experiments were used for finding some parameters appearing in Eqs. (1) and (2) using the following expressions: $\gamma_{RO} = \gamma + u_0$ (where u_0 is a stationary value of u) and $f_{RO} = 1/2\pi[(\tau^{-1}u_0y_0) - (\gamma_{RO}/2)^2]^{1/2}$ which can be obtained from Eqs. (1) and (2) by a standard linearization procedure. Throughout our calculations the following fixed parameters were used: $\tau = 3.5 \times 10^{-9}$ s, $\gamma = 1.978 \times 10^5$, $y_0 = 0.175$, $k_0 = 0.17303$. The other parameters were varied in the simulations. Because in the numerical simulation and the experiments the control parameter (k_d in the simulations and V_d in the experiments) is measured in different units, we put also to the figure captions the value of normalized control parameter μ defined as $\mu = k_d/k_{1/2} = V_d/V_{1/2}$, where $k_{1/2}$ and $V_{1/2}$ are the values of the first period doubling threshold in the simulations and experiments, respectively.

3. Results and Discussions

The appearance of bistability induced by resonant perturbation is shown in Fig. 1 where numerical

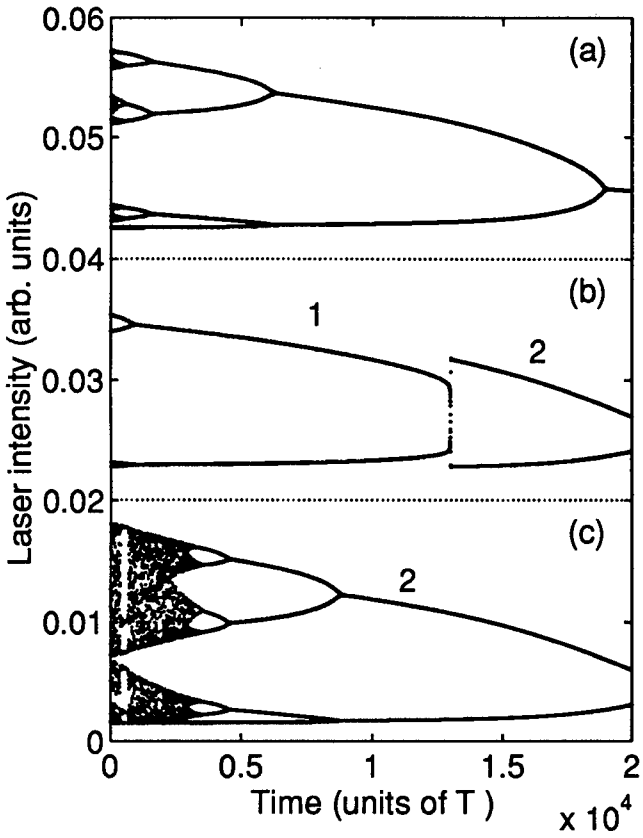

Fig. 1. Numerical bifurcation diagrams of a CO_2 laser showing the appearance of the bistability. (a) The laser response without the resonant perturbation, (b) and (c) the laser responses with the resonant perturbation. The parameters used in the computer simulation: $f_{RO} = 50$ kHz, $\gamma_{RO} = 200$ kHz, $f_d = 80$ kHz, k_d varied between 1.24×10^{-4} and 4.4×10^{-5}, (a) $k_p = 0$, (b) and (c) $k_p = 9 \times 10^{-6}$, $\varphi = 0$.

bifurcation diagrams of a CO_2 laser are presented. They were obtained with decreasing of the driving amplitude k_d by a linear law. Shown here are maximal peaks of the laser intensity versus time. Figure 1(a) shows the laser response without the resonant perturbation. Figures 1(b) and 1(c) correspond to two laser responses which appeared instead of the primary solution in the presence of the periodic perturbation. It is seen [Fig. 1(b)] that one solution (the solution-1) is suppressed. As the driving amplitude decreases, the system reaches the first bifurcation point shifted by the resonant perturbation and the solution-1 becomes unstable. Then the system jumps to the solution-2. This solution is entirely presented in Fig. 1(c) (for more details see [Chizhevsky *et al.*, 1997a]). By comparing Figs. 1(b) and 1(c) it is seen that for the given perturbation amplitude different dynamical regimes associated with solution-2 are overlapped with a $2T$ stable regime belonging to the solution-1 as the driving amplitude changes. The second effect which one can see from Fig. 1 is that the resonant perturbation shifts all bifurcation points on both coexisting attractors in an opposite direction so that one attractor is stabilized [Fig. 1(b), solution-1] while the second one is destabilized [Fig. 1(c), solution-2]. This means that by changing the perturbation amplitude we may also control at will the overlapping of different dynamical regimes associated with these new attractors. The third possibility to control overlapping is to change of the perturbation phase φ.

Experimental and numerical examples of switching between new coexisting attractors when the system was initially in a $2T$ state are shown in Figs. 2(a) and 2(b), respectively. For these experimental conditions only one attractor exists in the phase space. After switching on the resonant

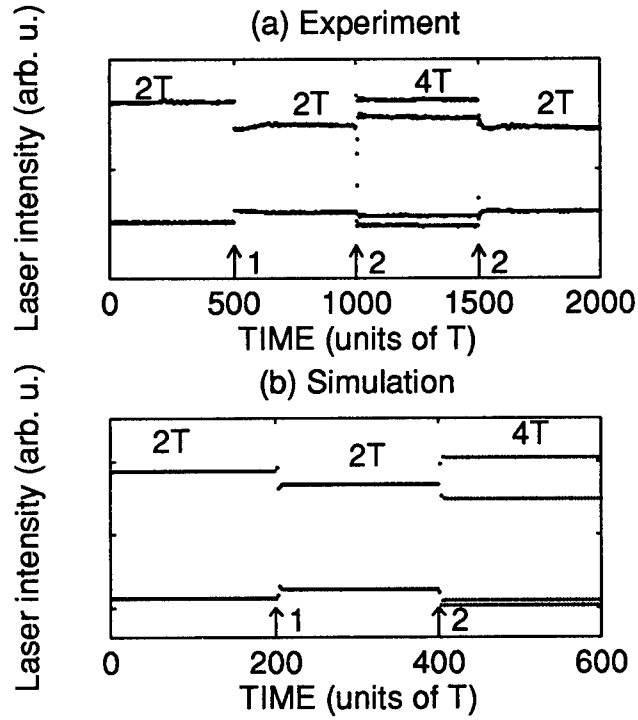

Fig. 2. Experimental (a) and numerical (b) stroboscopic CO_2 laser responses versus time (the laser intensity is sampled with the modulation period T). The unperturbed system (without the resonant perturbation) is initially in a $2T$ state. (a) The experimental parameters: $V_d = 3.35$ V ($\mu = 1.86$), $V_p = 3.64$ V, $\varphi \cong 30°$. (b) The parameters used in the computer simulation: $f_{RO} = 50$ kHz, $\gamma_{RO} = 200$ kHz, $f_d = 100$ kHz, $\mu = 2.1$, $\varphi \cong 30°$, $k_d = 1.25 \times 10^{-4}$, $k_p = 2.4 \times 10^{-5}$ ($k_p/k_d = 0.192$), $k_\delta = 2 \times 10^{-3}$ ($k_\delta/k_d = 16$); the point in time of turning on the resonant perturbation is shown by ↑1, the action of the pulse loss perturbation is shown by ↑2.

perturbation at $t = 500$ (units of the driving period T), the primary attractor splits into two ones. The system remains in the same $2T$ state but with a slightly suppressed amplitude. Simultaneously, there appears a new attractor which is in a $4T$ state. Acting by a single pulse perturbation (at $t = 1000$) the system was switched to the $4T$ state. The second pulse (at $t = 1500$) returned the system to the suppressed $2T$ state. Both switchings were performed practically without transients. It is worth noting that the duration of the transient after the action of the pulse perturbation strongly depends on its amplitude and can be reduced for large enough amplitudes to one or two periods of the driving modulation. Similar results were obtained in numerical simulations which are in a good agreement with experimental ones [Fig. 2(b)].

A more interesting case is shown in Fig. 3 when the system was initially in a $4T$ state [Fig. 3(a)]. No other attractors were observed for these experimental conditions. Depending on its phase, resonant perturbations with the same amplitude

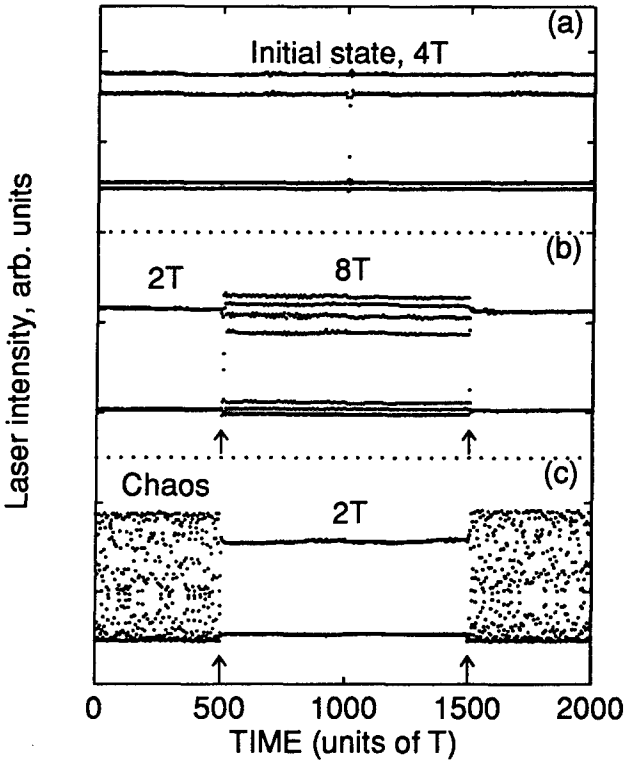

Fig. 3. Experimental stroboscopic CO_2 laser responses versus time (the laser intensity is sampled with the modulation period T). The unperturbed system is initially in a $4T$ state. The arrow shows the action of the pulse perturbation. The experimental parameters: $V_d = 4.11\,(\mu = 2.28)$, $V_p = 3.52$ V, (b) $\varphi \cong 65°$, (c) $\varphi \cong 215°$.

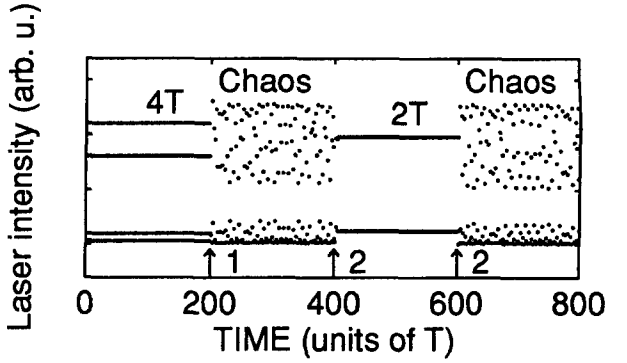

Fig. 4. Numerical stroboscopic CO_2 laser responses versus time (the laser intensity is sampled with the modulation period T). The unperturbed system is initially in a $4T$ state. The symbol $\uparrow 1$ shows switching on the resonant perturbation, the symbol $\uparrow 2$ shows the action of the pulse loss perturbation. The parameters used in the computer simulation: $f_{RO} = 50$ kHz, $\gamma_{RO} = 200$ kHz, $f_d = 100$ kHz, $\varphi \cong 30°$, $k_d = 1.55 \times 10^{-4}\,(\mu = 2.6271)$, $k_p = 2.5 \times 10^{-5}$ $(k_p/k_d = 0.1613)$, $k_\delta = 8 \times 10^{-3}$.

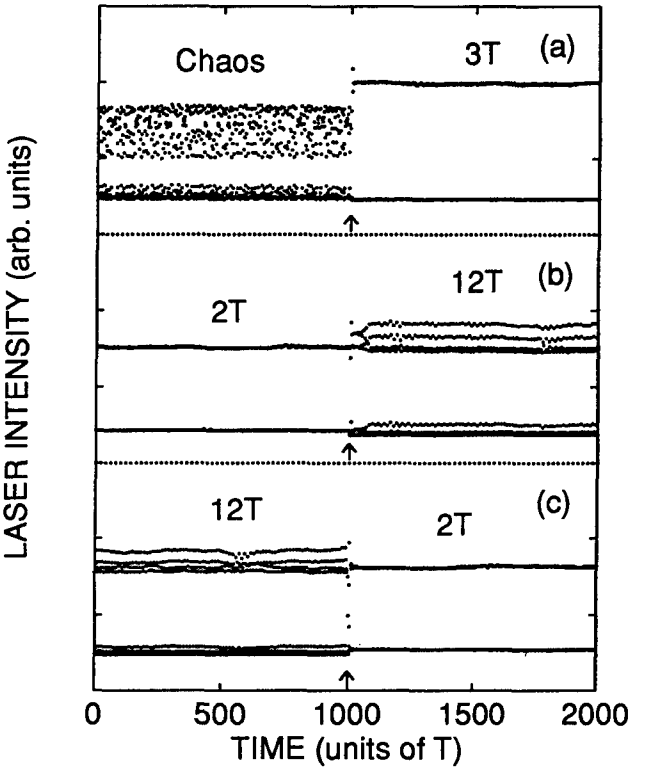

Fig. 5. Experimental stroboscopic CO_2 laser responses versus time (the laser intensity is sampled with the modulation period T). The unperturbed system is initially in chaos. The experimental parameters: $V_d = 4.84\,(\mu = 2.69)$; (a) $V_p = 0$ V, (b) and (c) $V_p = 3.64$ V, $\varphi \cong 205°$.

may suppress periodic orbits [Fig. 3(b)] or induce chaos [Fig. 3(c)]. At the same time there appears a new attractor. The final state after switching also strongly depends on the phase of the resonant

perturbation. One can see that the system can be very quickly sent from a stable $2T$ orbit to a stable $8T$ orbit [Fig. 3(b)], or from chaos to a stable $2T$ orbit [Fig. 3(c)] and vice versa. It should be noted that the latter case [Fig. 3(c)] is very interesting from the standpoint of a fast change of the state in the system between "chaos" and "order". The case represented in Fig. 3(c) was also simulated numerically and is shown in Fig. 4. It is seen to be in rather good agreement with the experimental results.

Now let us consider the effect of a resonant perturbation in the bistability domain inherent in the system. Figure 5(a) demonstrates a coexistence of period-1 and period-3 attractors. The latter appeared in the laser response after the action of the pulse perturbation. After switching on the periodic perturbation with the frequency $f_d/2$, chaos of the period-1 is converted to a $2T$ stable orbit, whereas the $3T$ stable orbit is transformed to the $12T$ stable orbit [Fig. 5(b)]. This means that the resonant perturbation exerts a different effect on both coexisting attractors so that the period-1 attractor is stabilized while the period-3 attractor is destabilized. A different effect of the resonant perturbation makes it possible to control the overlapping of diverse states associated with both coexisting attractors, and correspondingly to perform switchings between them. Similar results are obtained in the computer simulation shown in Fig. 6.

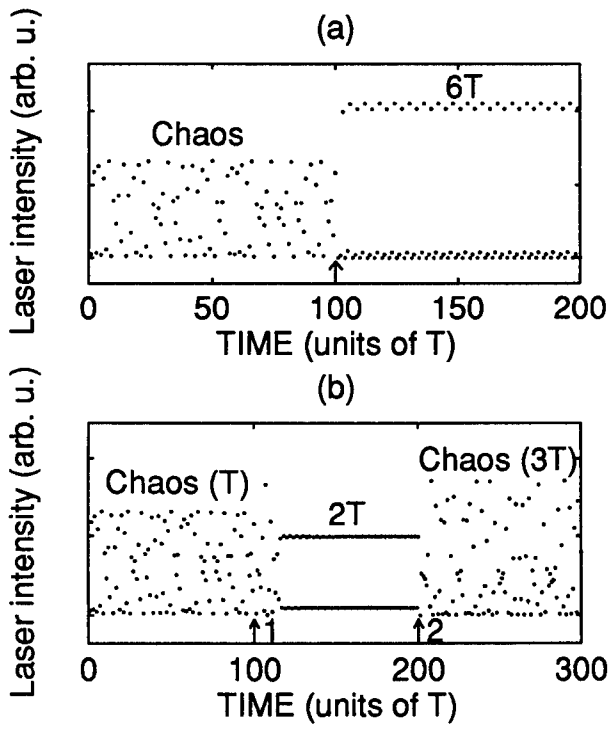

Fig. 6. Numerical stroboscopic CO_2 laser responses versus time (the laser intensity is sampled with the modulation period T). The parameters used in the computer simulation: $f_{RO} = 50$ kHz, $\gamma_{RO} = 200$ kHz, $f_d = 100$ kHz, $\varphi = 30°$, $k_d = 2.15 \times 10^{-4}$ ($\mu = 3.6441$), (b) $k_p = 2.5 \times 10^{-5}$ ($k_p/k_d = 0.11628$), $k_\delta = 7 \times 10^{-3}$.

4. Conclusions

To conclude, we have presented experimental and numerical results on the dynamics of a CO_2 laser with modulated losses which demonstrate that resonant perturbations at subharmonic frequency not only radically change the dynamics of the system but also globally change the phase space by splitting the primary attractor into two new ones. We have demonstrated the possibility to control at will the overlapping of different dynamical regimes associated with these new coexisting attractors by changing the amplitude and the phase of the resonant perturbations as well as the bifurcation parameter. We have also presented several examples showing that highly controllable switchings between these new attractors can easily be performed using the technique of short-lived large-amplitude pulse perturbations. Such a type of control of nonlinear systems could be of interest in the context of control of systems with a fast response because it does not require any feedback system. The splitting of attractors and the switching between new attractors might be observable in a number of nonlinear systems, both nonautonomous and autonomous, where the method of nonfeedback control of chaos has been implemented experimentally.

Acknowledgments

V. N. Chizhevsky acknowledges support from the Generalitat de Catalunya. Financial support from the DGICYT (Project No. PB95-0778-C02) is also acknowledged.

References

Azevedo, A. & Rezende, S. M. [1991] "Controlling chaos in spin-wave instabilities," *Phys. Rev. Lett.* **66**, 1342–1345.

Braiman, Y. & Goldhirsch, I. [1991] "Taming chaotic dynamics with weak periodic perturbations," *Phys. Rev. Lett.* **66**, 2545–2548.

Chizhevsky, V. N. & Turovets, S. I. [1994] "A loss-modulated CO_2 laser as an amplitude and phase multitrigger," *Phys. Rev.* **A50**, 1840–1843.

Chizhevsky, V. N. & Glorieux, P. [1995] "Targeting unstable periodic orbits," *Phys. Rev.* **E51**, R2701–2704.

Chizhevsky, V. N. & Corbalan, R. [1996] "Experimental observation of perturbation-induced intermittency in the dynamics of CO_2 laser," *Phys. Rev.* **E54**, 4576–4579.

Chizhevsky, V. N., Corbalan, R. & Pisarchik, A. N. [1997a] "Attractor splitting induced by resonant perturbations," *Phys. Rev.* **E56**, 1580–1584.

Chizhevsky, V. N., Grigorieva, E. V. & Kaschenko, S. A. [1997b] "Optimal timing for targeting periodic orbits in a loss-modulated CO_2 laser," *Opt. Commun.* **133**, 189–195.

Ding, W. X., She, H. Q., Huang, W. & Yu, C. X. [1994] "Controlling chaos in a discharge plasma," *Phys. Rev. Lett.* **72**, 96–99.

Ditto, W. L., Spano, M. L. & Lindner J. F. [1995] "Techniques for the control of chaos," *Physica* **D86**, 198–211.

Fronzoni, L., Giocondo M. & Pettini M. [1991] "Experimental evidence of suppression of chaos by resonant parametric perturbations," *Phys. Rev.* **A43**, 6483–6487.

Lima, R. & Petttini, M. [1990] "Suppression of chaos by resonant parametric perturbations," *Phys. Rev.* **A41**, 726–733.

Meucci, R., Gadomski, W., Ciofini, M. & Arecchi, F. T. [1994] "Experimental control of chaos by means of weak parametric perturbations," *Phys. Rev.* **E49**, R2528–2531.

Ott, E., Grebogi, C. & Yorke, J. A. [1990] "Controlling chaos," *Phys. Rev. Lett.* **64**, 1196–1999.

Tredicce, J. R., Arecchi, F. T., Puccioni, G. P., Poggi, A. & Gadomski, W. [1986] "Dynamic behavior and onset of low dimensional chaos in a modulated homogeneously broadened single-mode laser: Experiments and theory," *Phys. Rev.* **A34**, 2073–2081.

International Journal of Bifurcation and Chaos, Vol. 8, No. 9 (1998) 1783–1789

DYNAMIC STABILIZATION OF UNSTABLE PERIODIC ORBITS IN A CO_2 LASER BY SLOW MODULATION OF CAVITY DETUNING

A. N. PISARCHIK* and R. CORBALÁN
Departament de Física, Universitat Autònoma de Barcelona, E-08193 Bellaterra, Barcelona, Spain

V. N. CHIZHEVSKY* and R. VILASECA
Departament de Física i Enginyeria Nuclear, Universitat Politècnica de Catalunya, Colom 11, E-08222 Terrassa, Spain

B. F. KUNTSEVICH
Stepanov Institute of Physics, National Academy of Sciences of Belarus, Skaryna Pr. 70, 220072 Minsk, Belarus

Received July 31, 1997; Revised December 2, 1997

We demonstrate numerically and experimentally that a slow modulation of cavity detuning in a loss-modulated CO_2 laser can stabilize unstable periodic orbits even when the system remains in a particular dynamical regime for adiabatic changes of the detuning. When the parameter changes faster than the transient response of deformation of the original periodic attractor, the system can evolve toward an unstable periodic orbit.

1. Introduction

Recent trends in nonlinear dynamics are directed toward the development of effective methods of controlling chaos. A notable advance has been made by Ott *et al.* [1990] who proposed a feedback control technique based on stabilization of unstable periodic orbits embedded in a chaotic attractor. However, in some kinds of systems (particularly, in biological or chemical systems) a feedback loop is very difficult to realize. Lima and Pettini [1990] have shown that stabilization is possible without feedback. They suggested the creation of stable periodic orbits from a chaotic system using a weak resonant parametric perturbation. Both feedback and nonfeedback methods have been applied to many nonlinear systems including lasers (see e.g. [Roy *et al.*, 1992; Bielawski *et al.*, 1993; Meucci *et al.*, 1994]).

A simple nonfeedback and nonresonant control method which does not require prior knowledge of the system behavior has recently been proposed by Vilaseca *et al.* [1996]. They have shown numerically that accurate stabilization of an unstable steady state in an autonomous system can be achieved by large-amplitude slow periodical modulation of a control parameter. Earlier, Liu and Rios Leite [1994] demonstrated numerically that stabilization of unstable periodic orbits in the Lorenz system can be achieved by coupling periodic modulation to a control parameter. More recently, the main principles of the idea of Vilaseca *et al.* have been applied to a nonautonomous system and successfully realized in experiments with a loss-modulated CO_2 laser [Pisarchik *et al.*, 1997]. The physical mechanism underlying the stabilization effect is tracking

*Visiting from Stepanov Institute of Physics, Minsk, Belarus

unstable periodic orbits due to the delay of bifurcations when the control parameter is varied so that the system passes back and forth through an instability point [Mandel & Erneux, 1984; Kapral & Mandel, 1985]. A drawback of the method of Vilaseca *et al.* [1996] is the requirement for the amplitude of the control modulation to be large (the larger the amplitude, the better the stabilization). As a consequence, the system response carries a large-amplitude envelope at the control frequency.

In this work we present a method of stabilizing unstable orbits in a nonautonomous system which does not require very large amplitude modulation of a control parameter, as in previous studies with autonomous systems (see e.g. [Liu & Rios Leite, 1994]). This new technique is similar to that proposed by Vilaseca *et al.* [1996] but the physical principle underlying the stabilization is quite different. We show numerically and experimentally that stabilization of unstable periodic orbits can be performed by periodic modulation of a system parameter within some periodic or chaotic domain. In other words, to achieve the stabilizing effect it is not necessary for the system to pass back and forth through a bifurcation point.

2. Model and Experimental Arrangements

2.1. *Model*

For numerical simulations of the operation of a CO_2 laser with modulated losses we use a model based on the standard four-level scheme [Ciofini *et al.*, 1993]. Our modified model consists of eight differential equations for quasi-equilibrium and quasi-nonequilibrium populations of the upper and lower vibrational lasing levels, the global populations of the two manifolds of rotational levels, the population of the first excited level of N_2, and the equation for average radiation density inside the cavity.

The active medium of the CO_2 laser before switching on the electric discharge is a mixture of the gases CO_2, N_2 and He. For the sake of definiteness, we shall consider a single-mode lasing within a vibrational–rotational transition of the 00^01–10^00 channel of the CO_2 molecule. According to Kuntsevich and Churakov [1994], the CO_2 laser with modulated losses can be described by the following system of equations

$$\frac{dN_1}{dt} = \beta_1 n_e N_0 - W_{10} N_1 + W_{21} N_2 + B(\nu) u (n_2^j - n_1^j)\,, \tag{1}$$

$$\frac{dN_2}{dt} = \beta_2 n_e N_0 + W_{NC} N_N (N_0 M_1 - N_2 M_0) - W_{21} N_2 - B(\nu) u (n_2^j - n_1^j)\,, \tag{2}$$

$$\frac{dM_1}{dt} = \beta_3 n_e M_0 + W_{NC} N_C (N_2 M_0 - N_0 M_1)\,, \tag{3}$$

$$\frac{dn_1}{dt} = B(\nu) u (n_2^j - n_1^j) - V_1 (n_1 - N_1)\,, \tag{4}$$

$$\frac{dn_2}{dt} = B(\nu) u (n_2^j - n_1^j) - V_2 (n_2 - N_2)\,, \tag{5}$$

$$\frac{dn_1^j}{dt} = B(\nu) u (n_2^j - n_1^j) - V_R (n_1^j - F_1^j n_1) - V_1 (n_1^j - F_1^j N_1)\,, \tag{6}$$

$$\frac{dn_2^j}{dt} = B(\nu) u (n_2^j - n_1^j) - V_R (n_2^j - F_2^j n_2) - V_2 (n_2^j - F_2^j N_2)\,, \tag{7}$$

$$\frac{du}{dt} = c\mu [\kappa(\nu) y - k] u\,, \tag{8}$$

Here, N_0, N_1 and N_2 are the relative quasi-equilibrium populations of the vibrational 00^00, 10^00 and 00^01 levels of CO_2; M_0 and M_1 are the relative populations of the fundamental and first exited vibrational level of N_2; n_1 and n_2 are the relative quasi-nonequilibrium populations of the vibrational 10^00 and 00^01 levels of CO_2 [1]; n_1^j and n_2^j are the relative populations of lower and upper laser rotational sublevels[2]; n_e is the free electron density in active medium; W_{21} and W_{10} are the effective rates of collisional relaxation in 00^01–10^00 and 10^00-00^00 channels; V_R is the rotational relaxation rate; V_1 and V_2 are the vibrational relaxation rates that describe the relaxation of "instantaneous" populations n_1 and n_2 to their quasi-equilibrium values, N_1 and N_2; W_{NC} is the exchange rate of the vibrational excitation from N_2 to CO_2; β_1, β_2 and β_3 are the pumping rates of N_2 and the lower and upper levels of CO_2 in electric discharge; N_C and

[1]The introduction of the populations N_1, N_2, n_1, n_2 effectively allows us to take into account several important processes of intra- and intermode exchange in the active medium which are not included in Eqs. (1)–(3).

[2]For simplicity the rotational quantum number j is considered to be the same for both levels.

N_N are the volume density of CO_2 and N_2; k_0 and Δk are the constant and additive losses; F_1^j and F_2^j are the normalized Boltzmann functions determining the part of molecules in the corresponding rotational sublevels in thermodynamic equilibrium: $n_1^j = F_1^j n_1$, $n_2^j = F_2^j n_2$; $B(\nu)$ and $\kappa(\nu)$ are the Einstein coefficient and specific gain coefficient at the lasing frequency ν and both have a Lorentzian lineshape; l_m and l_a are the lengths of the loss modulator and active medium; c is the speed of light in the active medium; μ is the packing coefficient for the active medium in the cavity; u is the average radiation density; $y = n_2^j - n_1^j$ is the population inversion.

The cavity loss coefficient is expressed as follows

$$k = k_0 + \frac{1}{2}\Delta k[1 - \cos(2\pi f_0 t)], \qquad (9)$$

where k_0 is the constant losses without modulation, Δk and $f_0 = 1/T$ are the loss modulation (driving) depth and frequency, T is the period of the loss modulation. The expression for k is written in the form of (9) to satisfy the experimental situation, because the modulator of cavity losses used in our experiments always increases losses over their stationary value k_0, but does not decrease them. We define the cavity detuning as: $\delta = (\nu - \nu_0)/\gamma$, where ν_0 is the central frequency and γ is the halfwidth of the Lorentzian gain lineshape. We introduce the control modulation of cavity detuning in a form similar to (9)

$$\delta = \delta_0 + \frac{1}{2}\Delta\delta[1 - \cos(2\pi f_1 t)], \qquad (10)$$

where δ_0 is the initial cavity detuning from the center of gain contour, i.e. without the control modulation, $\Delta\delta$ and f_1 are the amplitude and frequency of the control modulation. The modulation of δ leads to the appropriate changes in the lasing frequency ν.

The numerical simulations are performed for the following set of parameters. The active medium consists of the gas mixture CO_2–N_2–He=1–1–8 at the total pressure of 15 torr. The CO_2 laser operates on a single mode at the 10P20 line. The cavity length is 2 m, the length of the active medium is 1.8 m, $k_0 = 6 \times 10^{-3}$ cm^{-1}, $f_0 = 110$ kHz. Other parameters (Δk, δ_0, $\Delta\delta$ and f_1) are varied in numerical simulations.

2.2. *Experimental setup*

The experimental setup is similar to that described in previous work [Pisarchik *et al.*, 1997]. The experiments have been performed on a single-mode CO_2 laser with modulated losses via an acousto-optic modulator. The driving electric signal, $V_0 = A_0 \sin(2\pi f_0 t)$, at frequency f_0 and amplitude A_0, is applied to the modulator providing the time-dependent cavity losses in accordance with Eq. (9). The control electric signal

$$V_1 = A_1^0 + \frac{1}{2}A_1[1 - \cos(2\pi f_1 t)] \qquad (11)$$

at frequency f_1 and amplitudes of the constant A_1^0 and alternative A_1 components, is utilized to tune the output mirror with the piezotranslator. This signal produces the appropriate changes in cavity detuning in accordance with Eq. (10). The frequency of relaxation oscillations at the center of the gain line estimated from averaged power spectra of the laser response to noise applied to the modulator is approximately 108 kHz. The frequency of the loss modulation, $f_0 = 105$ kHz, was chosen because it matches one of the acoustic resonances of the modulator. This is close to the frequency of relaxation oscillations at the center of the gain line but higher than the relaxation oscillation frequency in the region of significant detuning where the control is established. Other parameters are the same as those used in the numerical simulations.

3. Results and Analysis

3.1. *Diminution of periodicity*

Let us consider the effect of the modulation of cavity detuning when the CO_2 laser operates in a period-2 ($2T$) regime. Figure 1 shows diagrams with the cavity detuning, δ_0 for the numerical diagram [Fig. 1(a)] and the voltage A_1^0 applied to the piezotranslator for the experimental diagram [Fig. 1(b)], used as a control parameter at relatively small values of the driving amplitudes Δk and A_0. These diagrams are obtained without control modulation. Period-1 (T) and period-2 ($2T$) regimes are clearly seen on the bifurcation diagrams at certain detuning ranges. The windows of $2T$ behavior appear with detuning because the detuning moves the relaxation oscillation frequency of the laser into resonance with $1/2T$.

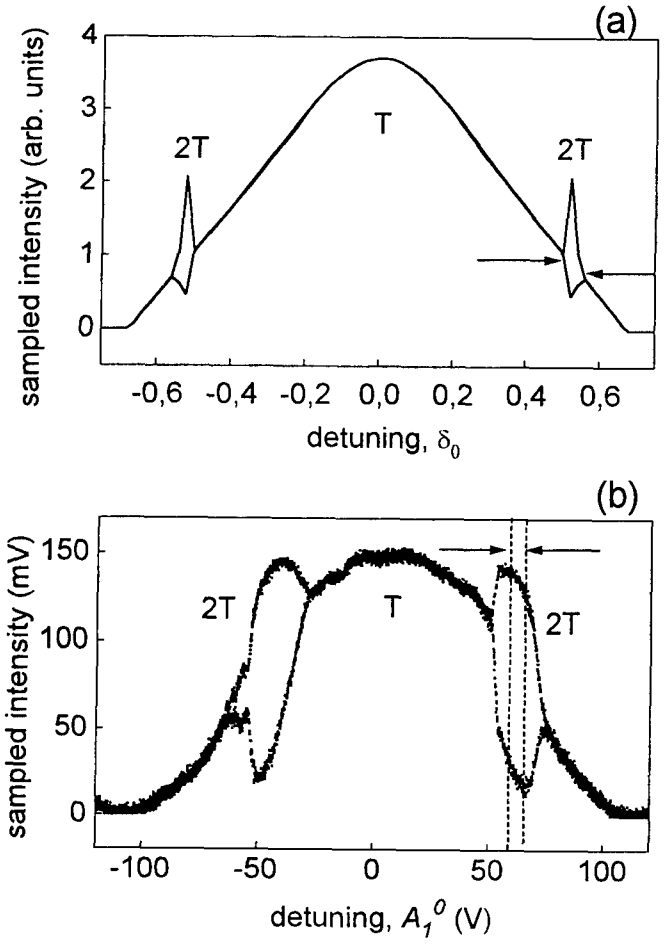

Fig. 1. (a) Numerical and (b) experimental bifurcation diagrams with cavity detuning as a control parameter. The arrows indicate the range of detuning alternation within which the control will be applied. (a) $\Delta k = 1.4 \times 10^{-5}$ cm^{-1}, $\Delta\delta = 0$, (b) $A_0 = 7$ V, $A_1 = 0$. On the Y axis are plotted values of the laser intensity sampled with the period T of the driving modulation.

For stabilization of the unstable period-1 orbit that exists in the domain of the $2T$ regime, first, we select an initial point on the gain curve corresponding to the $2T$ regime (right peaks on the curves in Fig. 1). Then, following Eq. (10) we apply a sinusoidal modulation to the cavity detuning so that the system remains inside the $2T$ domain. The ranges of the detuning variation are indicated in Fig. 1 by the arrows.

Numerical (left) and experimental (right) stroboscopic diagrams shown in Fig. 2 display the effect of the control modulation at different modulation frequencies. One can see that with increasing control frequency f_1, period 2 is progressively suppressed [Figs. 2(a)–2(c) and 2(e)–2(g)] and the unstable period 1 which is shown by dashed lines is stabilized as can be clearly seen in Figs. 2(d) and 2(h). Comparing experimental and numerical results one can see a good qualitative agreement. A difference in the shape of laser response between numerical and experimental curves is due to a distinction in the contours of the numerical and experimental gain lines (Fig. 1) as well as because of a difference in the ranges within which the detuning is varied.[3]

3.2. *Chaos suppression*

At high driving amplitude chaotic ranges appear in the bifurcation diagram at certain cavity detunings. To check the suitability of the method for the control of chaotic behavior of the laser, we choose a range of detuning modulation within one of the chaotic domains. Slow control modulation gives rise to the intervals of periodic behavior which alternate with chaotic ones at the control frequency [Figs. 3(a), 3(b) and 3(d), 3(e)] culminating with pulsed oscillations at the period 1 when f_1 further increases [Figs. 3(c)]. This effect is similar to that observed earlier in the experiments by Pisarchik *et al.* [1997] where the cavity detuning was larger and the system crossed T–$2T$ bifurcation point. Although a complete stabilization of periodic-1 orbit is not achieved in experiment [Fig. 3(f)] because of noise, these results clearly demonstrate the validity of the present approach for inhibition of chaos.

3.3. *Discussion*

A possible physical mechanism underlying the effect of dynamic stabilization can be associated with transient processes when the control parameter is changed. A detailed numerical and experimental study of transient processes occurring after fast change in the detuning within a period-2 domain allows us to reveal the following general features. (i) The duration of transient processes after forward and backward switching (with increasing and decreasing) the cavity detuning are different. When the cavity detuning increases, the transient processes are slower than when δ decreases. (ii) When δ is switched from smaller to higher value, the system falls on an unstable period-1 orbit at any phase

[3]In the experiments the detuning does not pass through the maximal intensity at the $2T$ range.

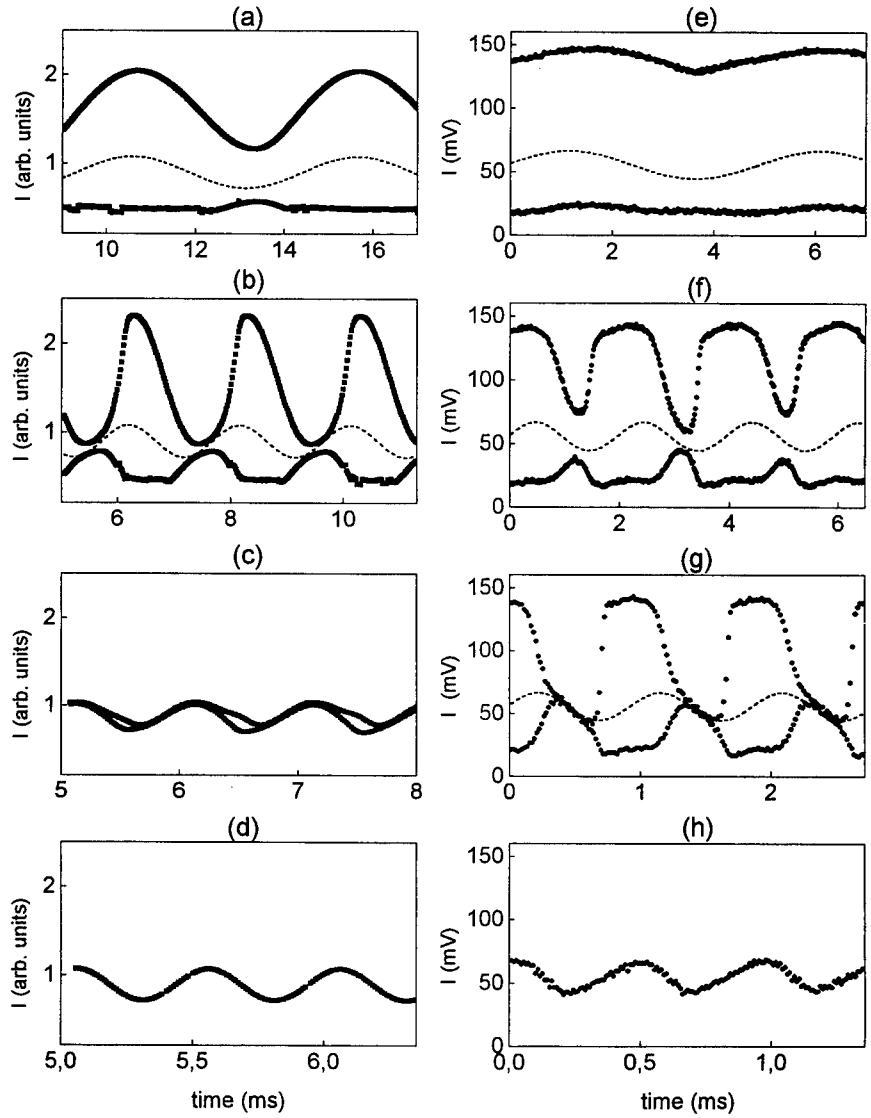

Fig. 2. Time evolution of (a)–(d) numerical and (e)–(h) experimental sampled intensities, I, with period T showing destabilization of period 2 and stabilization of period-1 orbit with increasing frequency f_1 of control modulation within ranges shown by arrows in Fig. 1. (a), (e) $f_1 = 200$ Hz; (b), (f) $f_1 = 500$ Hz; (c), (g) $f_1 = 1$ kHz; (d), (h) $f_1 = 2$ kHz. Numerical parameters are $\delta_0 = 0.525$, $\Delta\delta = 0.01$. Experimental parameters are $A_0 = 7$ V, $A_1 = 5$ V. Unstable period 1 is shown by dashed lines.

of switching with respect to the loss modulation, and then evolves towards a stable period 2 with the leading Lyapunov exponent $\lambda_1 = 7.7 \times 10^2$ s^{-1}. (iii) At the opposite switching (from higher to lower value), the system may also exhibit an unstable period-1 oscillation for a short time from which it later diverges with the leading Lyapunov exponent $\lambda_2 = 3.4 \times 10^3$ s^{-1}. The total duration of transient processes after switching essentially depends on the switching phase. (iv) The dynamic stabilization takes place only when the period of the control modulation is shorter than $1/\lambda_1$. This corresponds to the control frequency $f_1 \gtrsim 1$ kHz. These simple estimations are in a good agreement with our numerical and experimental results presented in Secs. 3.1 and 3.2.

All these features reveal a direct bearing of transient processes on the stabilization of unstable periodic orbits by periodic modulation of the detuning. The original periodic attractor is destabilized by the relatively fast change in the detuning. This suggests that the rate of change of the parameter requires a rate of change of the attractor that is greater than the negative Lyapunov exponent that governs the stability of the period-2 solution. Thus, the transition towards the unstable period-1 orbit

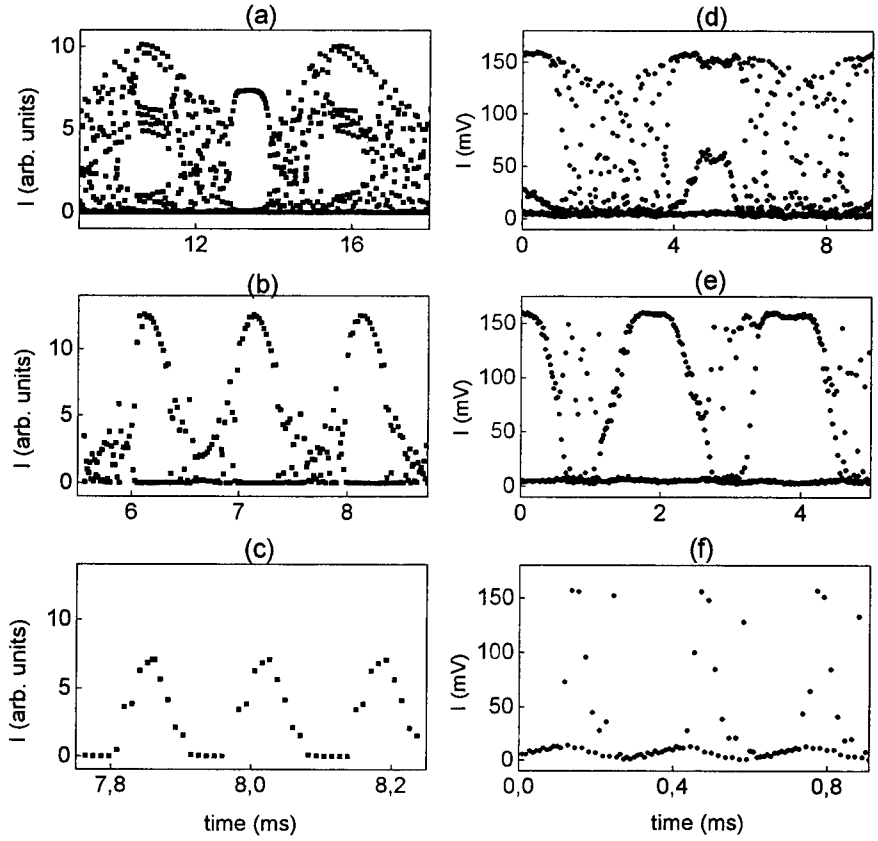

Fig. 3. (a)–(c) Numerical and (d)–(f) experimental stroboscopic (sampled with period T) diagrams showing inhibition of chaos with increasing control frequency f_1. (a) $f_1 = 200$ Hz, (b) $f_1 = 1$ kHz, (c) $f_1 = 6$ kHz, (d) $f_1 = 200$ Hz, (e) $f_1 = 500$ Hz, (f) $f_1 = 3$ kHz. Numerical parameters are $\delta_0 = 0.53$, $\Delta\delta = 0.02$. Experimental parameters are $A_0 = 10$ V, $A_1 = 5$ V.

can be achieved when the relatively fast change in the parameter is faster than the transient response of deformation of the period-2 solution.

4. Conclusions

We have shown that dynamic stabilization of unstable periodic orbits can be performed by a slow modulation of a control parameter even when the system does not pass through bifurcation points at adiabatic (quasi stationary) change of the parameter. This method has been demonstrated numerically and experimentally in a loss-modulated CO_2 laser whose cavity detuning was periodically modulated. We suggest that the physical mechanism underlying the dynamic stabilization is connected with transient processes in the laser when the detuning is varied. Numerical simulations using an improved model of a loss-modulated CO_2 laser are in a good agreement with experimental results. Although the method has been implemented in a laser, we think that this is quite general and can be applied to many nonlinear systems whose initial state is characterized as chaotic or regular.

Acknowledgments

A. N. Pisarchik acknowledges support from the Ministerio de Educación y Cultura (Spain) (project no. SAB95-0538). V. N. Chizhevsky is indebted to the Generalitat de Catalunya (Spain). We are grateful to the DGICYT (project no. PB95-0778) for financial support. A. N. Pisarchik thanks Professor F. T. Arecchi for useful discussions. The authors also thank the referee of this article for careful reading and very helpful suggestions.

References

Bielawski, S., Derozier, D. & Glorieux, P. [1994] "Experimental characterization of unstable periodic orbits by controlling chaos," *Phys. Rev.* **A47**(4), R2492–R2495.

Braiman, Y. & Goldhirsch, J. [1991] "Taming chaotic dynamics with weak periodic perturbations," *Phys. Rev. Lett.* **66**(20), 2545–2548.

Ciofini, M., Politi, A. & Meucci, R. [1995] "Effective two-dimensional model for CO_2 lasers," *Phys. Rev.* **A48**(1), 605–610.

Kapral, R. & Mandel, P. [1985] "Bifurcation structure of the nonautonomous quadratic map," *Phys. Rev.* **A32**(2), 1076–1081.

Kuntsevich, B. F. & Churakov, V. V. [1994] "Effect of lasing frequency detuning on the response of a CO_2 laser with modulated losses," *J. Appl. Spectrosc.* **60**(3–4), 213–218.

Lima, R. & Pettini, M. [1990] "Suppression of chaos by resonant parametric perturbations," *Phys. Rev.* **A41**(2), 726-733.

Liu, Y. & Rios Leite, J. R. [1994] "Control of Lorenz chaos," *Phys. Lett.* **A185**, 35–37.

Mandel, P. & Erneux, T. [1984] "Laser Lorenz equations with a time-dependent parameter," *Phys. Rev. Lett.* **53**(19), 1818–1820.

Meucci, R., Gadomski, W., Ciofini, M. & Arecchi, F. T. [1994] "Experimental control of chaos by mean of weak parametric perturbations," *Phys. Rev.* **E49**(4), R2528–R2531.

Ott, E., Grebogi, C. & Yorke, J. A. [1990] "Controlling chaos," *Phys. Rev. Lett.* **64**(11), 1196–1199.

Pisarchik, A. N., Chizhevsky, V. N., Corbalán, R. & Vilaseca, R. [1997] "Experimental control of nonlinear dynamics by slow parametric modulation," *Phys. Rev.* **E55**(3), 2455–2461.

Roy, R., Murphy, T. W., Jr., Maier, T. D. & Gills, Z. [1992] "Dynamical control of chaotic laser: Experimental stabilization of a globally coupled system," *Phys. Rev. Lett.* **68**(9), 1259–1262.

Vilaseca, R., Kul'minskii, A. & Corbalán, R. [1996] "Tracking unstable steady states by large periodic modulation of a control parameter in a nonlinear system," *Phys. Rev.* **E54**(1), 82–85.

International Journal of Bifurcation and Chaos, Vol. 8, No. 9 (1998) 1791–1799

CHAOS CONTROL IN EXTERNAL CAVITY LASER DIODES USING ELECTRONIC IMPULSIVE DELAYED FEEDBACK

A. V. NAUMENKO, N. A. LOIKO and S. I. TUROVETS
Institute of Physics, Academy of Sciences,
70 Skarina Ave., Minsk 220072, Belarus

P. S. SPENCER and K. A. SHORE
University of Wales, Bangor,
School of Electronic Engineering and Computer Systems,
Bangor, LL57 1UT, Wales, UK

Received July 31, 1997; Revised December 17, 1997

In this paper an examination is made of the performance characteristics of a scheme of chaos control using optimised impulsive delayed feedback. The scheme is applied in a model of external cavity laser diodes giving attention to the application of the feedback via modulation of the laser drive current taking into account practical constraints arising from technical delay and the frequency in application of the control signal. It is demonstrated that by use of a so-called ε-ball condition chaos control is achievable in the fully developed coherence collapse regime without preliminary targeting dynamics to an unstable orbit.

1. Introduction

Interest in developing practical applications for chaotic dynamics has been stimulated by the development of techniques for controlling chaotic dynamics. The chaos control technique published by Ott *et al.* (OGY) [1990] has been successfully applied to the control chaotic dynamics in a number of laser systems (see [Naumenko *et al.*, 1998] for appropriate references). In particular, the work includes attempts to control chaotic dynamics in external cavity laser diodes in the coherence collapse regime. Also mentioned is the use of occasionally proportional impulsive feedback (OPIF) [Gray *et al.*, 1993; Liu & Ohtsubo, 1994], external microwave modulation [Ryan *et al.*, 1994; Watanabe & Karaki, 1995; Liu *et al.*, 1995] and continuous Pyragas-like electronic feedback [Turovets *et al.*, 1996, 1997]. These approaches have achieved rather moderate success due to specific features of semiconductor lasers such as high levels of intrinsic noise and the need for extremely high sampling frequencies. Interest in controlling semiconductor laser dynamics has been stimulated, in particular, by the possibilities for achieving secure communication systems which exploit the properties of chaotic dynamical systems [Hayes *et al.*, 1993]. An efficient algorithm for improving the locking rate between the receiver and transmitter of such a system has been reported previously [Shore & Wright, 1994]. The feasibility of optical injection-locking techniques for reciprocal synchronization of two distant chaotic laser diodes has been considered recently [Mirasso *et al.*, 1996]. Another practical context where chaos control techniques may have an important role to play is in engineering immunity to coherence collapse caused by unintentional optical feedback which may arise in the hybrid integration and packaging of commercial laser diodes where rather expensive optical isolators must, in general be used to avoid the relevant

optical feedback. Reviews of that effect and further references thereon are given in [van Tartwijk & Lenstra, 1995; Petermann, 1995].

The scheme of control of chaos proposed in the present study allows the convenient manipulation of the regimes of operation in such configurations. Alternative methods involving continuous optoelectronic feedback studied recently [Turovets *et al.*, 1996, 1997] are not so flexible with respect to manipulating complex dynamics although they are possibly more advantageous in the context of engineering immunity to coherence collapse due to their modest requirements on the bandwidth of the electronic components in the feedback loop.

With a view to such potential applications, this paper reports an investigation of the potential of discrete chaos control schemes based on the original OGY method [Ott *et al.*, 1990] from its application to controlling the coherence collapse phenomenon in an external cavity laser diode. It is important to emphasize that the first attempts to control chaos in laser diode models were based on a oversimplified version of the OGY method like OPIF [Gray *et al.*, 1993]. The need to readjust numerous control scheme parameters did not permit effective optimization and lacked robustness to noise. For high operating frequencies the latter has had a rather discouraging impact on the perspectives of experimental implementation of such a scheme. In contrast, in earlier work [Naumenko *et al.*, 1998] attention has been focused on the optimization of parameters of control schemes with the aim to relax the requirements imposed by the basic features of laser diodes such as high levels of noise and fast dynamics. In particular, an examination has been made of several possible means of applying optimized discontinuous delayed feedback via different laser control parameters: the laser drive current, a laser field phase modulation in the external resonator and modulation of cavity losses. In this paper we test this scheme using corrections applied to the laser bias current as the control without preliminary targeting to the unstable orbit — which would require meeting the condition that two successive samples of laser intensity fall within a user-prescribed window: the so-called ε-ball condition.

2. Model

It is assumed that the laser operates in a single longitudinal mode and is subject to weak optical feedback from an external mirror. A rate equation treatment of this configuration has recently been developed on the basis of the Lang–Kobayashi model to take into account feedback effects in modulated external cavity laser diodes [Langley *et al.*, 1995; Langley & Shore, 1993]. The equations are as follows:

$$\frac{dS(t')}{dt'} = S(t')\left[G_n\{N(t')-N_0\}\Gamma\left\{\frac{1}{1+\varepsilon' S(t')}\right\}-\frac{1}{\tau_{\rm ph}}\right] + \frac{\gamma\Gamma N(t')}{\tau_{\rm sp}} + 2\frac{k_{\rm ext}}{\tau_L}\sqrt{S(t')}\sqrt{S(t'-\tau_{\rm ext})}\cos(\theta(t')) + F_s(t')\,, \tag{1}$$

$$\frac{dN(t)}{dt'} = \frac{I(t')}{eV} - \frac{N(t')}{\tau_{\rm sp}} - S(t')G_n\{N(t')-N_0\}\left\{\frac{1}{1+\varepsilon' S(t')}\right\} + F_n(t')\,, \tag{2}$$

$$\frac{d\Phi(t')}{dt'} = \frac{1}{2}\alpha G_n\{N(t')-N_{\rm th}\}\Gamma - \frac{k_{\rm ext}}{\tau_L}\frac{\sqrt{S(t'-\tau_{\rm ext})}}{\sqrt{S(t')}}\sin(\theta(t')) + F_\phi(t')\,, \tag{3}$$

where

$$\theta(t') = \Phi(t') - \Phi(t'-\tau_{\rm ext}) + \omega_{\rm th}\tau_{\rm ext}\,. \tag{4}$$

In the rate equations $N(t')$ is the carrier density, $S(t')$ is the photon density, $\Phi(t')$ is the electric field phase, $I(t')$ is the injection current and e is the electronic charge. Typical laser parameters for a DFB laser are used, where V is the active region volume (1.5×10^{-16} m^3), $\tau_{\rm sp}$ is the carrier lifetime (2 ns), G_n is the gain slope (2.125×10^{-12} m^{3}s^{-1}), $N_{\rm th}$ is the threshold carrier density (9.9×10^{23} m^{-3}), ε' is the saturation parameter (3×10^{-23} m^3), γ is the spontaneous emission factor (1×10^{-5}), $\tau_{\rm ph}$ is the photon lifetime (2 ps), Γ is the confinement factor (0.4), α' is the linewidth enhancement factor (5.5), N_0 is the transparency carrier density (4×10^{23} m^{-3}), $\omega_{\rm th}$

is the operating frequency ($\lambda = 1.55\ \mu$m), R_2 is the laser facet reflectivity (0.309), η is the laser to fibre coupling efficiency (0.4) and τ_L is the laser cavity round trip delay (9 ps). In the optical feedback terms, R_{ext} is the external reflector reflectivity and τ_{ext} is the external cavity round trip delay (0.2 ns, which corresponds to an external cavity of approximately 2 cm for the fibre refractive index 1.5). k_{ext} is the feedback coupling parameter, given by

$$k_{\text{ext}} = \frac{1 - R_2}{\sqrt{R_2}}\sqrt{R_{\text{ext}}}\eta\,.$$

The model can, in general, account for the effects of Langevin noise terms, but the calculations described below consider noise-free deterministic dynamics.

The introduction of new variables: $u = SG_n\tau_{\text{sp}}$, $n = NG_n\tau_{\text{ph}}$, $t = t'/\tau_{\text{sp}}$, leads to the following normalized equations which are more convenient for the subsequent analysis:

$$\dot{u} = \nu u(g(n, u)\Gamma - 1) + rn + 2k\sqrt{uu_\tau}\cos\theta\,, \quad (5)$$

$$\dot{n} = P_0 + K(t) - n - ug(n, u)\,, \quad (6)$$

$$\dot{\Phi} = \alpha(n - n_{\text{th}})\Gamma - k\sqrt{u_\tau/u}\sin\theta\,, \quad (7)$$

$$\theta = \Phi - \Phi_\tau + \omega\tau\,.$$

Here $g(n, u) = (n - n_0)(1 - \varepsilon u)$, $n_0 = N_0G_n\tau_{\text{ph}}$, $\varepsilon = \varepsilon'/G_n\tau_{\text{sp}}$, $\omega = \omega_{\text{th}}\tau_{\text{sp}}$, $r = \nu\gamma\Gamma$, $\nu = \tau_{\text{sp}}/\tau_{\text{ph}}$, $k = k_{\text{ext}}\tau_{\text{sp}}/\tau_L$, $\alpha = \alpha'\nu\Gamma/2$, $P_0 = IG_n\tau_{\text{ph}}\tau_{\text{sp}}/eV$, $\tau = \tau_{\text{ext}}/\tau_{\text{sp}}$.

The laser is taken to be biased by a DC injection current $I_{\text{DC}} = 2\ I_{\text{th}}$ where I_{th} is the threshold current so as to ensure that the operation conditions are typical of the coherence collapse regime. Since the external cavity is short (2 cm), a typical route to chaos is a Hopf instability of a single external cavity mode steady state at $R_{\text{ext}} \approx 6.25 \cdot 10^{-4}$ or $k \approx 2.5$ followed by a Feigenbaum period doubling sequence. The first period doubling bifurcation takes place at $k \approx 4.26$; full chaos is developed at $k \approx 4.79$. Referring to the classification scheme for regimes of operation of a laser diode with optical feedback (see e.g. [van Tartwijk & Lenstra, 1995] or [Petermann, 1995]), it is noted that due to the short external cavity the operating regimes II and III are mixed with the coherence collapse regime (IV) and the system enters regime IV directly from regime I.

The terms $K(t)$ in Eq. (6) describes an impulsive periodic control action applied to the driving current. The rate equations (1)–(3) are solved numerically using a fourth-order Runge–Kutta algorithm with a variable integration time step. Further technical details are provided in [Naumenko *et al.*, 1998].

3. Impulsive Optoelectronic Feedback

It is assumed that an impulsive electronic feedback signal is applied to the laser diode and that the amplitude of every sequential impulse in the chain is proportional to the difference between the laser optical output powers taken at discrete moments of time. Such an arrangement implies detection and sampling of the output intensity synchronized with the pulse train generator. Mathematically, the impulse optoelectronic feedback terms in the dimensionless equations are taken in the form:

$$K(t) = \beta\sum_i (u(\varphi + t_i) - u(\varphi + t_i - T_i))f(t - (\varphi + t_i + \tau_{\text{el}}))\,. \quad (8)$$

The factor β is associated with amplification in the electronic feedback loop. The tunable phases φ specify a phase shift between a chain of applied correction pulses and the reference signal which may be conveniently chosen as the laser output itself so as to measure phase with respect to a laser intensity maximum emitted at the discrete moments of time $t_i = \sum_{k=1}^{i} T_k$. We will refer to the quantities β, φ as the parameters of the control schemes which are to be optimized. Finally, T_i is assumed to be self-adjustable during the process of control time delay and equal to a time interval between successive laser intensity maxima. This means that the pulse generator triggering time and the interval of sampling are synchronized to the detected maximum intensity.

The term $K(t)$ is used to modify a selected control parameter of the laser diode slightly which, in the present case, is the driving current. Equation (8) essentially assumes that the electronic components of feedback $K(t)$ are fast enough to follow the laser output pulsations in real time, detect its maxima and trigger the pulse generator. In practice, of course, there will always be some frequency cut-off due to the finite bandwidth and also technical phase shift attributed in part to a finite speed of the electrical signal through the loop. This practical aspect is taken into account via an additional time delay τ_{el} in Eq. (8), which also includes a natural time shift by a half-width of the pulse applied. It is supposed, nevertheless, that the bandwidth is

wide enough to permit microwave spectra of amplitude fluctuations centered at the relaxation frequency (approximately 3 GHz for the parameters used here) to pass without significant distortion.

The motivation for choosing feedback in the specified form is as follows. First, to affect stabilization the feedback should be negative, secondly, the feedback is designed so that it has no effect on the state which is supposed to be stabilized (e.g. an unstable periodic orbit with period T). Every kick of the control scheme has a functional form given by $f(t)$. Its amplitude [see Eq. (8)] is proportional to the difference between the output powers that were emitted at instants of time $\varphi + t_i - \tau_{\rm el}$ and a previous time $\varphi + t_i - \tau_{\rm el} - T_l$. The functional form of the kicks was chosen to be super-Gaussian:

$$f(t) = M\,\exp(-at^{2m}), \quad a = (\Gamma(1/2m)/mw)^{2m}\,, \quad M = 1/w\,, \tag{9}$$

where $\Gamma(1/2m)$ is the special Γ-function [Abramowitz & Stegun, 1972].

The impulse function $f(t)$ is normalized in such a way that its integral area is a unity. When its effective width w tends to zero then it approaches a Dirac δ-function, whilst the exponent m regulates a specific shape of a kick. In particular, in the extreme case of $m \to \infty$ with a finite w, the pulses acquire a nearly square form.

4. Results

4.1. *Targeting and control of unstable T-periodic orbits*

General strategies of control of chaos often imply a preliminary targeting to an unstable orbit which is to be stabilized. For the present system, which exhibits a period-doubling route to chaos, one possible way of achieving this is to pull a system back from a regime of developed chaos into a period doubling regime. In this way, the aim is to target and control an unstable orbit and thence to track the stabilized system into the initial chaotic regime. Such an approach has been applied previously to low-dimensional dynamical systems such as modulated class B laser, and also to the external cavity laser diode configuration [Naumenko *et al.*, 1998]. Here we present further optimization of such an approach with the aim to test the effectiveness of activating the control scheme into the coherence collapse regime using an ε-ball condition.

First, the laser diode is assumed to be operating with such a level of optical feedback that its dynamics is set just after the first period doubling bifurcation ($k \approx 4.6$). The process of targeting consists of applying a single kick given by

$$K^{(\rm targ)}(t) = \beta_{\rm targ} f(t - \varphi_{\rm targ}) \tag{10}$$

and applied at the appropriate phase $\varphi_{\rm targ}$ and with an appropriate amplitude $\beta_{\rm targ}$, then after a short transient the system arrives in the vicinity of the unstable T-periodic orbit and finally, after staying a few periods on the unstable orbit the control scheme is activated. The difference signal $(u(\varphi + t_i) - u(\varphi + t_i - T_i))$ is constructed by sampling and storing the laser intensity at successive times and then a correction pulse is triggered and delivered to the driving current with a technical delay, $\tau_{\rm el}$.

In Figs. 1(a) and 1(b) the method is demonstrated. The first targeting impulse in this configuration is relatively large and is not shown here, but the moment of application of the targeting impulse is marked by a circle. It can be seen that the unstable orbit is stabilized and the control signal tends to zero. Of course, the kick strength at the first stage depends strongly on how accurately the system has been targeted to the unstable T-periodic cycle.

The effectiveness of the method is conveniently analyzed by computing domains of control and finding optimal conditions of control. In Figs. 2(a)–2(d) we present the domains of tracking the stabilized T orbit into the coherence collapse regime in the control parameter space defined by the optical feedback strength k and the feedback technical delay $\tau_{\rm el}$ for different electronic feedback strengths β and fixed sampling phase φ. Computationally, this has been obtained by a successive stepwise changing of the optical feedback strength k or the technical delay $\tau_{\rm el}$ without readjusting the control scheme parameters at nodes of a grid in this parameter space and calculating the time, $t_{\rm rel}$, needed to relax once again to the T orbit with a prescribed accuracy (here taken to be 10^{-4}) at every tracking step. Some small-scale details of the curves presented have been smoothed by spatial filtering. The external contour curve corresponds to $t_{\rm rel} = 300$ and for practical purposes defines the external boundaries of the control domain. Control is possible inside this domain and is not achievable outside of it. Along the inner curves in Fig. 2(a) $t_{\rm rel}$ is equal to 100, 50, 35, 25 and 15 in T units. The curves in Figs. 2(b)–2(d) have a similar meaning, except that the curves with the smallest $t_{\rm rel}$ are not shown. It can be seen that when an orbit has been stabilized one can vary the optical

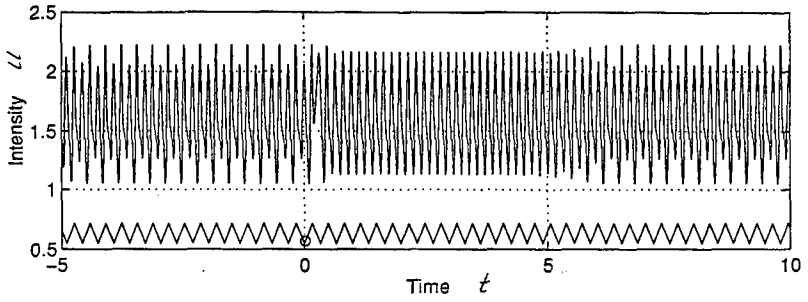

Fig. 1. Time domain demonstration of the processes of targeting and subsequent activation of the control scheme to stabilize the unstable T-cycle using finite width kick perturbations of a driving current. The parameters of the control scheme are: normalized pulse-width $w/T = 0.4$; electronic feedback strength $\beta = 0.2$; feedback phase $\varphi/T = 0.58$; form-factor of the superGaussian pulses $m = 3$. The parameters of the targeting pulse are $\varphi_{\text{targ}}/2T = 0.030825$, $\beta_{\text{targ}} = 0.1$. Time is normalized to τ_{sp}, the normalized laser parameters are as follows: $\nu = 1000$, $\Gamma = 0.4$, $r = 4 \cdot 10^{-3}$, $n_0 = 1.7$, $n_{\text{th}} = 4.2075$, $\alpha = 2500$, $\lambda_0 = 8.2$, $\omega\tau = 4.256$, $\varepsilon = 7.059 \cdot 10^{-3}$, $\tau = 0.1$, $k = 4.6$. (a) Laser intensity u versus time t. Having delivered the laser to the T-cycle by a targeting pulse [marked by the circle in Fig. 4(b)] the control scheme is activated [actually the first peak in Fig. 4(b)]. (b) Controlling kicks signal versus time. Kicks measured in the same units as the pump current and tend to zero when control is achieved.

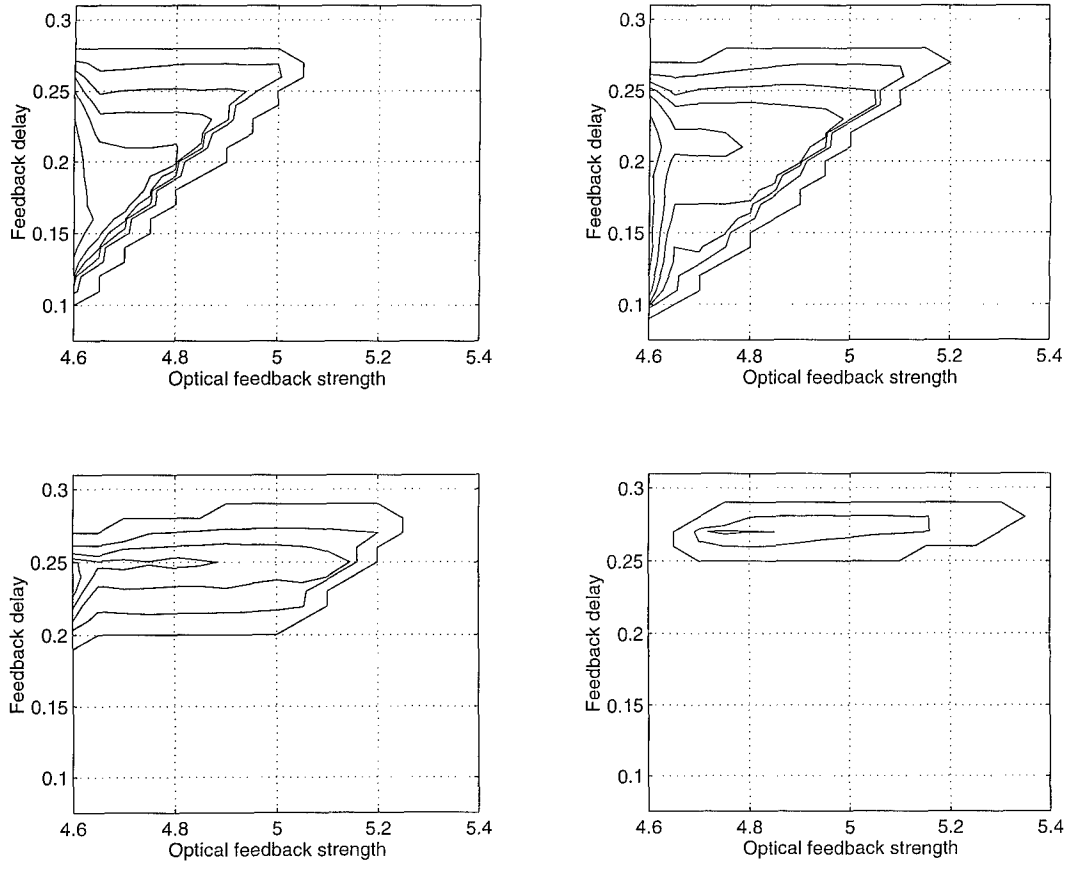

Fig. 2. Domains of control in the control parameter space for the stabilizing technique using finite width pulse perturbation of the pump current with feedback-monitored by the difference of intensities. The solitary laser parameters are the same as in Fig. 1. Contour plot of the relaxation time to the T-periodic unstable orbit in the phase space: optical feedback strength k, versus technical delay τ_{el}, the feedback phase $\varphi = 0$. The relaxation time t_{rel} is measured from the moment when the laser has been prepared near the T-cycle up to the moment when the system relaxes to T-cycle with an accuracy of 10^{-4}. The time is normalized to the period T. External curve corresponds to the $t_{\text{rel}} = 300$ and gives, in practice, the external boundaries of the control domain. The inner curves are for $t_{\text{rel}} = 100$, 50, 35, 25 and 15, respectively. The fixed electronic feedback strength $\beta = 0.2$ (a), 0.3 (b), 0.4 (c), 0.5 (d).

feedback strength without modifying the parameters of the electronic feedback system and advance into the developed coherence collapse regime. It is noted that the relaxation times correspond to the reciprocal of the dominant Lyapunov exponent describing the laser dynamics and hence the contour plots given in Fig. 2 provide an indication of the salient features of the dynamics. Moreover, the construction of these diagrams actually involves the optimization of a particular control scheme, because the bottom of the landscape represents the control with fastest relaxation to an unstable orbit (and thus the state of the closed feedback loop with the largest negative Lyapunov exponent). In particular, it can be seen that there exists an optimal technical delay value centred around 0.25. This means that the unstable manifold of the stabilized orbit is oriented at these instants of time in such a way that a projection of the kick on it reaches the maximal value and so the result of control is the largest. It is worth emphasizing here that for optical feedback levels $k \sim 5.9$ the first large periodic window occurs in the bifurcation diagram of the system, so that the results presented in Fig. 2(b) show the possibility of tracking the unstable T-periodic orbit through the entire first chaotic region. When the strength of electronic feedback is fixed at higher levels, it is possible to track the system even deeper into the coherence collapse regime [Fig. 2(d)], however at such levels of electronic feedback the scheme is already unable to stabilize the T-orbit at $k = 4.6$. This implies that in order to track through the whole domain accessible by changing k it is also necessary to monitor and change some parameters of the feedback scheme (β or φ). It is noted that, in accordance with its definition, the phase φ of the applied correction kick is varied from 0 to 1 in units of T, i.e. the correction kick is applied every period. If, for example, the phase φ is more than 1 (but less that 2), then the laser intensity is sampled and the correction pulse is applied to the driving current of every other period. Such a scheme, although still being formally described by Eq. (8), has different stability properties. In particular, the unstable T-cycle in the Poincare section taken every other period has real positive Floquet multipliers (in contrast with the negative ones for the Poincare section taken every period) and the impulse control scheme described by Eq. (8) is not able to stabilize it. But the scheme is stable when the frequency of sampling is higher than the frequency of kicks application. So, the model presents the worse-case

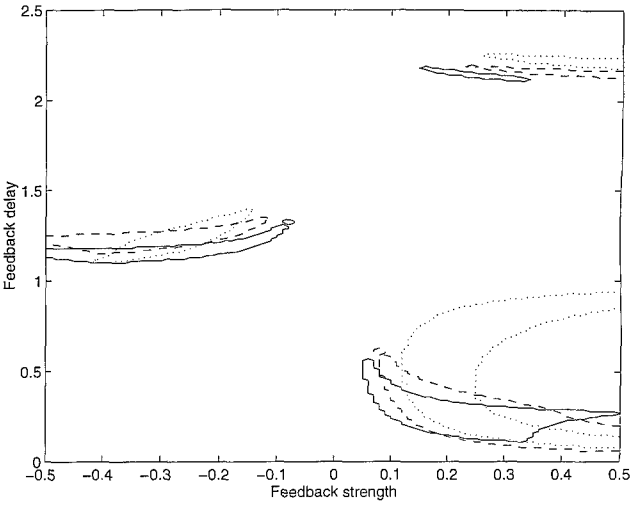

Fig. 3. Domains of control in the control parameter space the feedback strength β, versus technical delay τ_{el}, the feedback phase $\varphi = 0$. The solitary laser parameters are the same as in Fig. 1. The normalized pulse-width $w/T = 0.8$ (b). The kicks applied every $2T$ periods (solid lines), $3T$ periods (dashed lines) and $4T$ periods (dotted lines).

situation in the sense of the required speed of sampling of the laser intensity and applying the correction kicks. In fact, provided that the unstable trajectory is subject to preliminary targeting and the optimal parameters of the control scheme are chosen, impulsive corrections can be applied less frequently (e.g. every second, third or fourth period).

The effects of width and the application frequency of correcting pulses are demonstrated in Fig. 3 where the normalized pulse-width $w/T = 0.8$. Domains of control are shown in the control parameter space of the feedback strength, β, versus the technical delay, τ_{el}, at the fixed feedback phase $\varphi = 0$. The kicks are applied every $2T$ periods (solid lines), $3T$ periods (dashed lines) and $4T$ periods (dotted lines). The sampling of the laser intensity is undertaken every period. It is seen that the domains of control basically retain their location and size, although their form is distorted as the frequency of application of the correction pulsing is decreased. The stabilizing effect of increasing the correction pulse width is also clearly seen. Finally, the effect of alteration of the control domains with the period T (or recurrence with the period $2T$) with increasing the technical delay τ_{el} may be also observed (see also [Naumenko *et al.*, 1998] where this effect is described and explained in more detail). It is expected that in the centres (optima) of the control domains the scheme also

offers the maximum robustness to noise. The results presented thus clearly show that such complex nonlinear dynamic regimes as coherence collapse can be controlled with proper optimization.

4.2. *Control of unstable orbits using an ε-ball condition*

Attention is now given to the situation in which optimization of the control scheme, as identified in Sec. 4.1, has been made. In that situation it is possible to activate the control directly in the coherence collapse regime without preliminary targeting but by using a user prescribed window in which successive intensity maxima should fall — the so-called ε-ball condition. Events of falling into the ε-ball surrounding the unstable T-periodic orbit are guaranteed by the ergodicity of chaotic motion. This means that a chaotic trajectory must inevitably visit some neighborhood of any point embedded in the chaotic attractor. Of course, such events are stochastic by the definition and the time

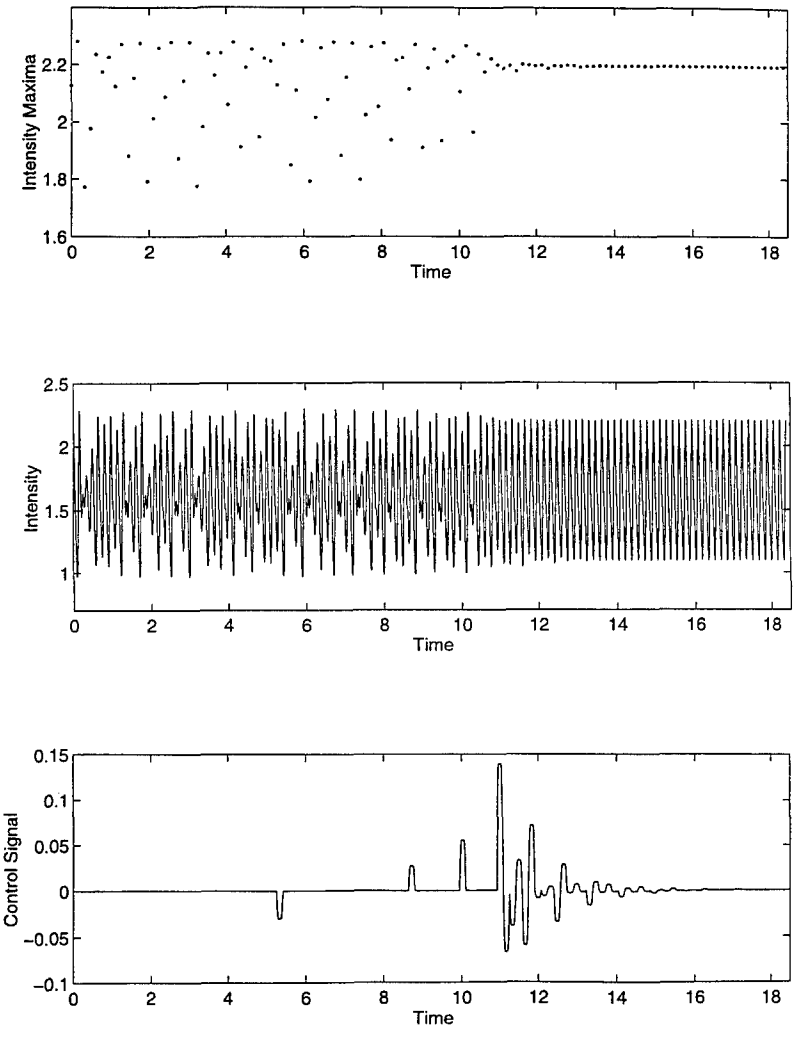

Fig. 4. Time domain demonstration of the process of activation of the control scheme to stabilize the unstable T-cycle embedded in chaos area using the ε-ball condition. The parameters of the control scheme are: the normalized pulse-width $w/T = 0.8$; the electronic feedback strength $\beta = 0.4$; the feedback phase $\varphi/T = 0$, the formfactor of the superGaussian pulses $m = 3$ and the technical delay $\tau_{el}/T = 0.25$. The parameters of laser diode are chosen in the coherence collapse zone, i.e. optical feedback strength $k = 5$ and the rest of parameters is as in Fig. 1. Time is normalized to τ_{sp}. (a) Maxima of laser intensity u versus time t. The control scheme is activated at time $t = 0$. After some chaotic transient the laser system finds itself in the vicinity of the unstable T-cycle satisfying to the ε-ball condition, i.e. $|u(t_i) - u(t_{i-1})| < \varepsilon = 0.05$ followed by the short relaxation transient to the T periodic orbit stabilized. (b) Laser intensity u versus time t. (c) Control signal versus time. Measured in the same units as the pump current and tends to zero when control is achieved.

which elapses between activating the control scheme and achieving control depends strongly on the initial conditions and should be treated statistically.

In Figs. 4(a)–4(c) show how the scheme works in this case. The stroboscopic view (a), the laser intensity (b) and the control signal (c) are plotted as functions of time. Consideration is given here to the behavior of the laser after cessation of turn-on transient in the fully developed coherence collapse regime (with optical feedback strength $k = 5.0$). The control scheme was activated at time, $t = 0$, but the scheme was in fact in a waiting regime ($\beta = 0$) until the ε-ball condition has been satisfied, i.e. $\beta \neq 0$ whenever $|u(\varphi+t_i)-u(\varphi+t_i-T_i)| \leq \varepsilon$ and $\beta = 0$ otherwise. The first such event takes place at $t \cong 5.5$, but the very first kick of the control knocks out the system of the ε-ball and the scheme is effectively switched off until the system next falls into the ε-ball. After three such trials control is finally reached at $t > 11$. It is noted that the ε-ball condition applied for control in Fig. 4 does not require a knowledge of the T-cycle at all. Thus, any occasional coincidence of two successive maxima turns on the control scheme. But it is still not guaranteed that this event takes place near a T-cycle, so some "false" alarms of the control scheme are possible as is shown in Fig. 4(c) (the first three kicks). We have also investigated a modification of this ε-ball condition taken as $|u(t_i) - u_0| < \varepsilon = 0.05$, where u_0 is the maximum intensity of the T-cycle. It is found in this case that only one "false" alarm takes place at $t \cong 1.5$ and then at $t > 3$ control is successfully achieved. For this case it is found that on average the stochastic transients in this case are shorter than those shown in Fig. 4. Finally, we observe that it is not required that u_0 be known *a priori* — rather it can be considered as a parameter of the control scheme.

5. Conclusion

In conclusion, a demonstration has been made of the opportunity for effecting control of the dynamics of external cavity laser diodes operating in the coherence collapse regime by the use of impulsive delayed feedback applied via the laser drive current. Account has been taken of practical constraints in the application of the feedback signal and control has been shown to be possible both with and without a preliminary targeting process. The effectiveness of the control scheme has been characterized via the computation of domains of control and by demonstrating the existence of optimal conditions of control. Such an optimized control configuration provides a significant advantage in practical application in comparison to previous chaos control schemes which have been compromised by the noise properties of laser diodes. Moreover it has been shown to be possible to relax requirements in respect to the frequency of the application of the control corrections. From the viewpoint of practical implementation this adds further to the attractiveness of the present scheme by removing requirements for very high frequency electronic circuitry for the application of the control.

Acknowledgments

A. V. Naumenko, N. A. Loiko and S. I. Turovets acknowledge financial support from the Royal Society, London, UK, which permitted visits to the University of Wales, Bangor where a part of this work was carried out. They were also supported in part by The Belorussian Foundation for Fundamental Research. The work of P. S. Spencer and K. A. Shore was supported by the UK EPSRC.

References

Abramowitz, M. & Stegun, I. [1972] *Handbook on Mathematical Functions, Applied Mathematics Series 55*, 10th Printing (National Bureau of Standards, Washington).

Gray, G. R., Ryan, A. T., Agrawal, G. P. & Gage, E. C. [1993] "Optical-feedback-induced chaos and its control in semiconductor lasers," in *Chaos in Optics*, ed. Roy, R., SPIE Proc. Vol. 2039, pp. 45–57.

Hayes, S., Greboggi, C. & Ott, E. [1993] "Communicating with chaos," *Phys. Rev. Lett.* **70**, 3031–3034.

Langley, L. N. & Shore, K. A. [1993] "The effect of external optical feedback on timing jitter in modulated laser diodes," *IEEE J. Lightwave Technol.* **11**, 434–441.

Langley, L. N., Turovets, S. I. & Shore, K. A. [1995] "Targetting periodic dynamics of external cavity semiconductor laser," *Opt. Lett.* **20**, 725–727.

Liu, Y. & Ohtsubo, J. [1994] "Experimental control of chaos in a laser diode interferometer with delayed feedback," *Opt. Lett.* **19**(7), 448–450.

Liu, Y., Kikuchi, N. & Ohtsubo, J. [1995] "Controlling dynamical behavior of a semiconductor laser with external optical feedback," *Phys. Rev.* **E51**, R2697–R2700.

Mirasso, C. R., Colet, P. & Garcia-Fernandez, P. [1996] "Synchronization of chaotic semiconductor lasers:

Application to encoded communications," *IEEE Photonics Tech. Lett.* **8**, 299.

Naumenko, A. V., Loiko, N. A., Turovets, S. I., Spencer, P. S. & Shore, K. A. [1998] "Controlling dynamics in external cavity laser diodes with electronic impulsive delayed feedback," *J. Opt. Soc Am. B*, accepted for publication.

Ott, E., Greboggi, C. & Yorke, J. A. [1990] "Controlling chaos," *Phys. Rev. Lett.* **64**, 1196–1199.

Petermann, K. [1995] "External optical feedback phenomena in semiconductor lasers," *IEEE J. Selected Topics in Quantum Electronics*, Vol. 1, pp. 480–489.

Ryan, A. T., Agrawal, G. P., Gray, G. R. & Gage, E. C. [1994] "Optical-feedback-induced chaos and its control in semiconductor lasers," *IEEE J. Quantum Electron.* **30**, 668–679.

Shore, K. A. & Wright, D. T. [1994] "Improved synchronization algorithm for secure communications systems using chaotic encryption," *Electron. Lett* **30**, 1203–1204.

Turovets, S. I., Dellunde, J. & Shore, K. A. [1996] "Selective excitation of periodic dynamics in external-cavity laser diodes," *Electron. Lett.* **32**, 42–43.

Turovets, S. I., Dellunde, J. & Shore, K. A. [1997] "Nonlinear dynamics of a laser diode subjected to both optical and electronic feedback," *J. Opt. Soc. Am. B — Opt. Phys.* **14**, 200–208.

Turovets, S. I., Valle, A. & Shore, K. A. [1997] "Effects of noise on the turn-on dynamics of a modulated class-B laser in the generalised multistability domain," *Phys. Rev.* **A55**, 2426–2434.

van Tartwijk, G. H. M. & Lenstra, D. [1995] "Semiconductor lasers with optical injection and feedback," *Quantum Semiclass. Opt.* **7**, 87–143.

Watanabe, N. & Karaki, K. [1995] "Inducing periodic oscillations from chaotic oscillations of a compound-cavity laser diode with sinusoidally modulated drive," *Opt. Lett.* **20**, 725–727.

International Journal of Bifurcation and Chaos, Vol. 8, No. 9 (1998) 1801–1809

SELF-PULSING AND CHAOS IN AN EXTENDED-CAVITY DIODE LASER WITH INTRACAVITY ATOMIC ABSORBER

F. DI TEODORO*, E. CERBONESCHI, D. HENNEQUIN† and E. ARIMONDO
INFM, Dipartimento di Fisica, Università di Pisa,
Piazza Torricelli, 2, I-56126 Pisa, Italy

Received July 31, 1997; Revised January 12, 1998

An experimental investigation of the temporal dynamics of a diode laser subject to optical feedback from an external cavity containing a cell filled with cesium vapor has been performed. Peculiar dynamic regimes, such as self-pulsing, low-dimensional, and high-dimensional chaos, characterized by a new time scale, much longer than the time scales of all instabilities taking place in diode lasers under standard feedback conditions, have been identified.

1. Introduction

Diode lasers exposed to optical feedback from an external cavity containing an atomic absorber are systems of great interest in the fields of spectroscopy, atomic physics and quantum optics, as they provide stable sources, with very narrow linewidth, on resonance with atomic transition frequencies. In recent years, these systems were widely investigated, mainly for the purpose of improving the spectral performance of the lasers and achieving an absolute frequency stabilization [Cuneo *et al.*, 1994; Kitching *et al.*, 1994; Liu *et al.*, 1994]. On the contrary, there was no knowledge about the nonlinear dynamics and chaotic properties of these systems. In this paper, we provide a description of such properties and identify distinctive features of the dynamics related to the presence of the absorber.

We report on experimental investigations performed on an extended-cavity diode laser containing a cell filled with cesium vapor, in a saturation spectroscopy configuration [Schmidt *et al.*, 1994]. We focus on the temporal dynamics of the system, showing that the presence of the atomic absorber inside the feedback cavity produces characteristic dynamic regimes, which take place on a peculiar time scale, much longer than the time scales typical of the dynamics of laser diodes under standard feedback conditions. Starting from a stable operating regime characterized by self-locking of the laser frequency to the central Lamb dip of the saturated absorption spectrum of the Cs D_2 line, we have observed, with increasing detuning from the atomic resonance, a self-pulsing regime of the laser output in the form of a sequence of intensity dropouts and, eventually, a chaotic regime. Taking advantage of the fact that the dynamics of the system takes place on different time scales, spaced at least by three–four orders of magnitude, we have separated the slow dynamics induced by the absorber. Due to its long time scale, this dynamics is very easily accessible experimentally. The experimental time series have been analyzed with the time-delay method so as to reconstruct embedding portraits

*Current address: Physics Department, Bryn Mawr College, Bryn Mawr, PA 19010-2899 USA.
†Permanent address: Laboratoire de Spectroscopie Hertzienne, Unité associée au CNRS, Université des Sciences et Technologies de Lille, 59655 Villeneuve d'Ascq Cedex, France.

and recurrence plots. The attractors in the phase space of the laser system have been characterized quantitatively by computing the Lyapunov exponent spectrum and the correlation dimension. From this analysis, it turns out that the signal observed for large detuning from the atomic resonance shows high dimensional chaos, characterized by two positive Lyapunov exponents. This feature could either pertain to the hyperchaos [Rössler, 1979] or to the coexistence of different chaotic attractors. The dynamics, either periodic or chaotic, observed out of the locking range, within a certain range of detuning from the atomic resonance, is characterized by the long time scale mentioned above. This time scale is absent in the dynamics of laser diodes in the standard feedback set-up, and therefore, it identifies, among the operation regimes of the extended-cavity laser, those which are determined by the presence of the atomic absorber.

Extended-cavity diode lasers with intracavity atomic absorber have never been studied previously from the point of view of nonlinear dynamics. In [di Teodoro *et al.*, 1997], we discussed the spectral features of this system, pointing out that the presence of the absorber substantially modifies the mode pattern in the phase space of the extended-cavity laser. We also developed a rate equation model suitable for the interpretation of the spectral phenomena, which could not provide, however, a description of the global dynamics. In the absence of a comprehensive theoretical model for the system considered, the analysis performed here makes it possible to infer general information on the dynamics in the phase space from the measured time dependence of the laser emission.

This paper is organized as follows: In Sec. 2 we describe the experimental apparatus and the measurements performed. In Sec. 3 we illustrate the observed dynamic evolution of the laser emission and discuss the results of the time-series analysis. Conclusions and final remarks are presented in Sec. 4.

2. Experimental

The experimental setup is shown schematically in Fig. 1. The observations were performed using a Spectra Diode Laser SDL-5400. The laser was optically coupled, through an antireflection coated collimating objective, to an external cavity terminated by a diffraction grating, placed 46 cm from the laser. A 4 cm long cell containing Cs vapor at the equilibrium density at room temperature was inserted within the external cavity. A fraction of the laser intensity was extracted from the external cavity by means of a beam splitter with less than 10% reflectivity and used for the detection. To avoid unwanted feedback from optical surfaces in the measuring equipment, a magneto-optical isolator providing 40 dB of attenuation for counterpropagating light was placed on the path of the extracted beam. A scanning confocal Fabry–Perot spectrum analyzer, model 240 by Coherent, was used to detect the optical spectrum of the laser emission. Absolute optical frequency measurements were performed by comparing, with the spectrum analyzer, the laser frequency and the frequency of a reference diode laser. The reference laser was locked, through a standard technique of hybrid optical and electronic feedback, to the transition $F = 4 \rightarrow F' = 5$ of the Cs D_2 line. The temporal evolution of the output laser intensity was detected, simultaneously with the spectral measurements, by means of an avalanche photodiode with 1.2 GHz cutoff frequency. The photodiode signal was monitored with a Tektronix TDS540 digital oscilloscope, with 500 MHz bandwidth.

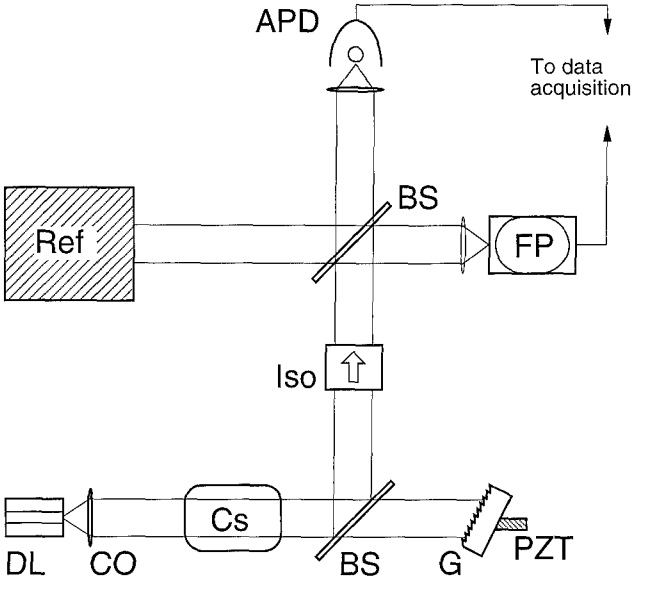

Fig. 1. Scheme of the experimental set-up. DL, diode laser; CO, collimating objective; Cs, cesium cell; BS, beam splitters; G, diffraction grating; PZT, piezoelectric transducer; Iso, magneto-optical isolator; Ref, reference diode laser; FP, scanning confocal Fabry–Perot spectrum analyzer; APD, avalanche photodiode.

The diffraction grating terminating the external cavity was mounted on a piezoelectric transducer, fixed to a mirror mounting. A continuous tuning of the laser wavelength within a range of tens of nanometers was achieved by combining the rotation of the grating and the variation of the cavity length through the piezoelectric transducer. For laser frequencies far from the Doppler-broadened absorption line of the atoms, the feedback power ratio was estimated, including losses at the optical surfaces within the external cavity, as about 30%.

In the feedback scheme considered, the light field emitted from the output facet of the diode laser, tuned to the D_2 line, passes through the atomic vapor cell as a pump field and, after being attenuated by the vapor, is retroreflected and used as a counterpropagating probe field, which is fed back into the laser cavity. At the center of any hyperfine transition of the D_2 absorption line, the pump beam bleaches a hole in the absorption spectrum of the weaker probe beam. Therefore, the probe transmission, and hence the optical feedback intensity, is resonantly enhanced when the laser frequency matches one of the principal transition or crossover lines [Schmidt *et al.*, 1994]. The saturated medium also modifies, due to its dispersive properties, the feedback phase. As an effect of the frequency-dependent changes produced by the intracavity absorber on the feedback parameters, we observed single-mode emission with frequency locking to an atomic resonance, as well as multi-mode operation with each oscillation frequency locked to a different sub-Doppler feature of the atomic absorption spectrum. This is a clear evidence of the influence of the atomic absorber on the laser operation. An extensive analysis of the results of the spectral measurements performed on this system is reported in [di Teodoro *et al.*, 1997], where a discussion of the absorption and dispersion properties of the atomic vapor under saturation spectroscopy conditions is included.

3. Temporal Dynamics and Time-Series Analysis

Mono-mode self-locked operation was obtained within a locking range of ~160 MHz around the frequency of the hyperfine transition $F = 4 \rightarrow F' = 5$. The corresponding laser emission had a stable intensity, with a low noise level. Out of the locking range, in the low-frequency direction, unstable regimes in the emitted intensity were observed. The time dependence of the laser output was detected while varying, as a control parameter, the free spectral range (FSR) of the external cavity by means of the piezoelectric transducer. Here we indicate the relative difference of external-cavity FSR with respect to the case of self-locked operation as $\Delta\nu$.

Figure 2(a) illustrates a portion of the time series of the laser output intensity $i(t)$ recorded for $\Delta\nu = 120$ MHz. The laser output experiences dropouts which decrease the absolute intensity by about 30%. The dropout pattern appears to be periodic with a time scale of about 0.1 ms. The power spectrum of the signal, calculated by fast Fourier transform (FFT), and shown in Fig. 2(b), is characterized by a few, well separated dominant features. This is consistent with the picture of a periodic signal. The observed period of the dropouts might be qualitatively associated with characteristic time scales of optical pumping processes within the absorber. For instance, the mean time for diffusion of Cs atoms at room temperature through the laser beam cross-section is of the order of tenths of millisecond [Schmidt *et al.*, 1994]. We should also notice that all documented intensity instabilities occurring in diode lasers subject to mere optical feedback from an external reflector take place on a much faster time scale. For example, in the regime of feedback intensity adopted in our experiment, extended-cavity diode lasers without absorber typically exhibit dropouts of the output intensity, called low-frequency fluctuations (LFF), characterized by a mean repetition rate of hundreds of MHz [Cerboneschi *et al.*, 1993]. The intensity dropouts in Fig. 2(a) resemble, in shape, the LFF dropouts. However, in addiction to the difference in time scale, a clear distinction of the self-pulsing phenomenon detected in our system with respect to LFF is the periodicity. In fact, LFF appear as intensity fluctuations irregularly spaced in time and their phase-space dynamics is very complex and described in terms of chaotic itinerancy [Sano, 1994]. Sub-nanosecond dynamics, which is not detectable with our measuring equipment, is also involved in the low-frequency fluctuation regime [Fischer *et al.*, 1996].

The time series of the output laser intensity have been processed with the time-delay method [Packard *et al.*, 1980]. Let $i(t)$ be the time dependent laser intensity, measured at equal sampling

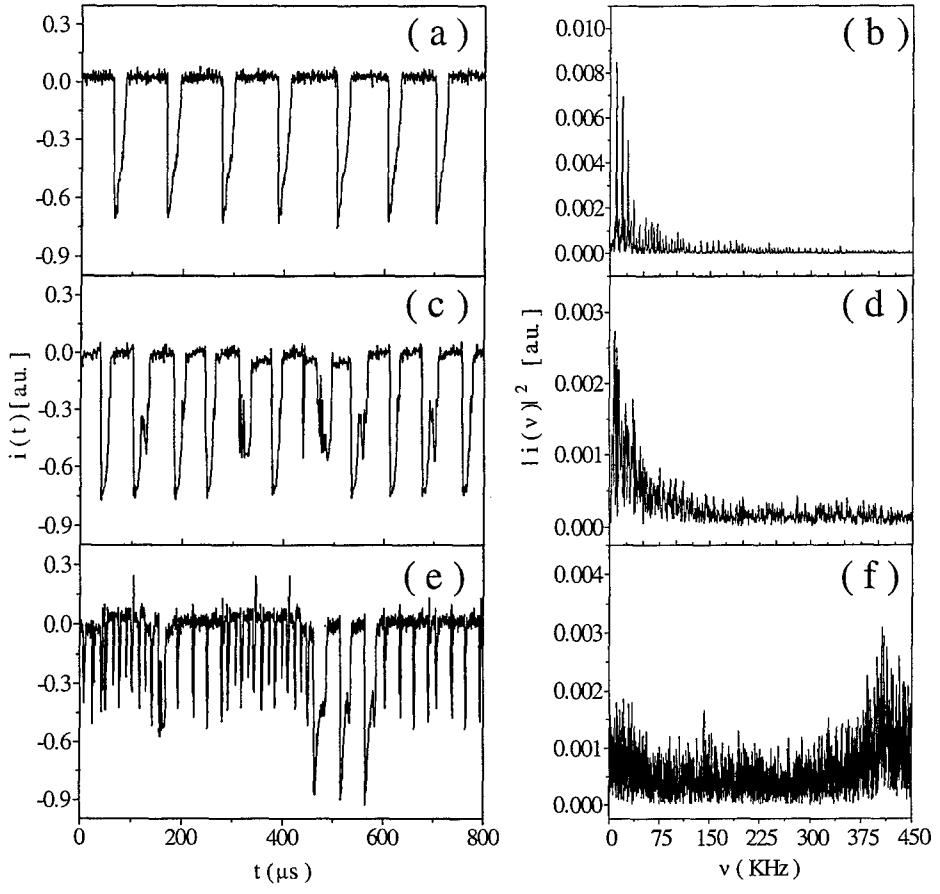

Fig. 2. Laser intensity time-series (left-hand column) and corresponding power spectra (right-hand column): (a) and (b) $\Delta\nu = 120$ MHz, (c) and (d) $\Delta\nu = 140$ MHz, (e) and (f) $\Delta\nu = 200$ MHz.

intervals δ in the temporal window $(0, \tau)$, where, for the signals recorded in our experiment, $\delta = 2\ \mu$s and $\tau = 32$ ms. A portrait of the phase trajectory of the system is represented by the set of m-dimensional embedding vectors $\mathbf{I}_n^T$, defined as

$$\mathbf{I}_n^T = \{i(n\delta),\ i(n\delta + T), \ldots,\ i[n\delta + (m-1)T]\}, \qquad n = 0, \ldots, S, \tag{1}$$

where the lag parameter T is an integral multiple of the sampling interval δ and $S = [\tau - (m-1)T]/\delta$. In order to extract, from the time-delay portrait, both qualitative and quantitative information about the physics underlying the time series, a proper choice of m and T is needed. The algorithms applied in our analysis allowed us to test several values of m and verify the convergence of the calculated quantities for $m > 3$. The choice of parameter T was based upon the computation of the average displacement, according to the method outlined by Albano *et al.* [1988], Casdagli *et al.* [1991], and Rosenstein *et al.* [1994]. The time-delay reconstruction was utilized to calculate recurrence plots, as introduced by Eckmann *et al.* [1987]. These plots are obtained, after choosing an embedding dimension m and a suitable radius r, as a square grid of $S \times S$ elements, in which a dot is displayed at coordinate (k, n) whenever $\|\mathbf{I}_k^T - \mathbf{I}_n^T\| < r$. The embedding portrait corresponding to the time series in Fig. 2(a) is depicted in Fig. 3(a) and suggests that the dynamics of the laser intensity, in this regime, may be properly described by a limit cycle. Consistently, the recurrence plot in Fig. 3(b) belongs to the so-called periodic typology [Eckmann *et al.*, 1987], since its large-scale pattern is dominated by long lines parallel to the main diagonal, which would be the only feature in the recurrence plot of a purely oscillatory signal, superimposed to an array of regular blocks emerging from stochastic fluctuations of the characteristic frequencies.

A quantitative analysis of the time series has been performed by evaluating the largest Lyapunov

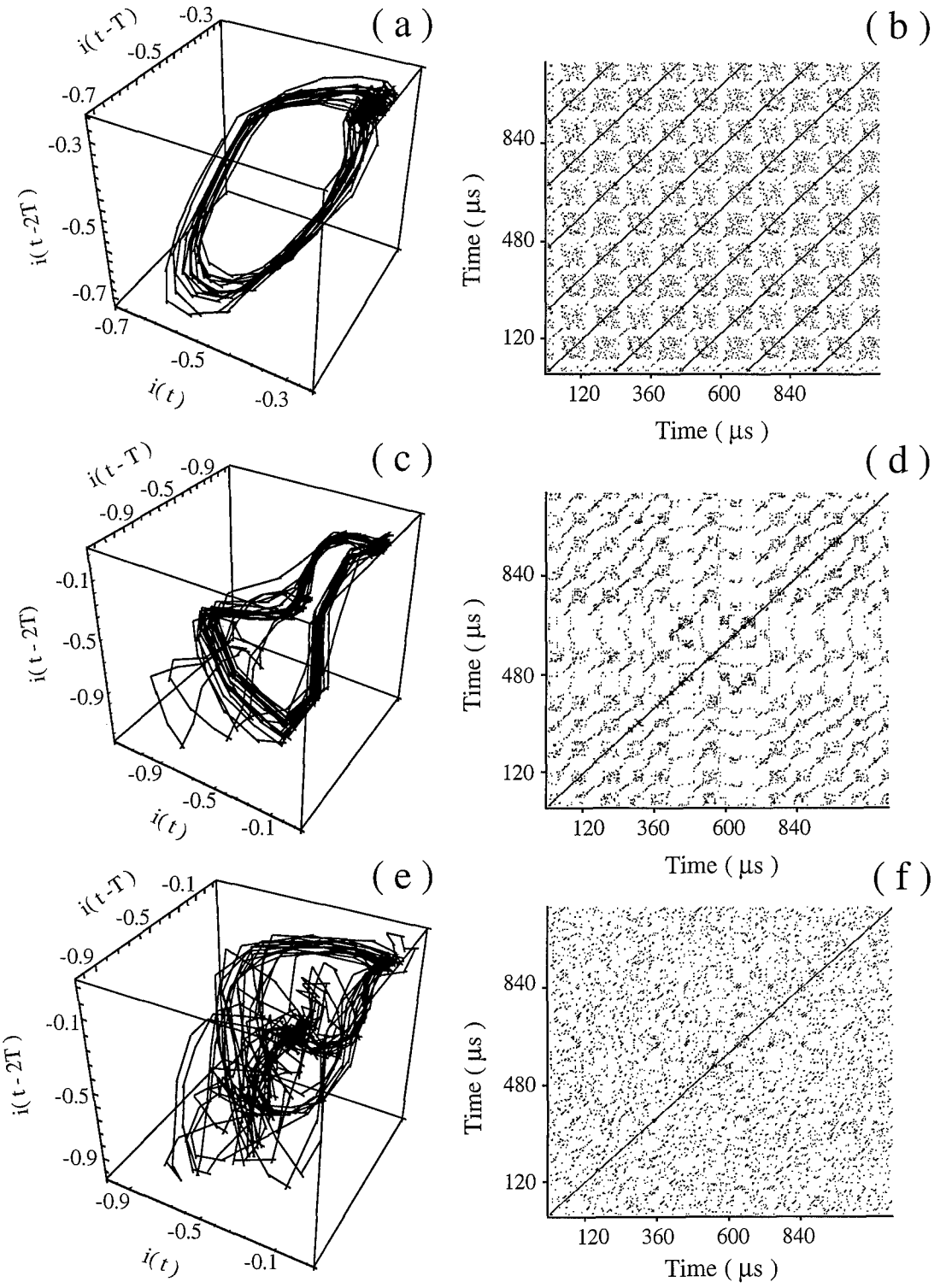

Fig. 3. Phase portraits for embedding dimension $m = 3$ (left-hand column) and recurrence plots for $m = 10$ (right-hand column) extracted from the experimental time-series: (a) and (b) $\Delta\nu = 120$ MHz, (c) and (d) $\Delta\nu = 140$ MHz, (e) and (f) $\Delta\nu = 200$ MHz. The time lag used for the phase-portraits is $T = 32$, 24, and 16 μs in (a), (c) and (e), respectively.

exponent, according to the method introduced by Rosenstein *et al.* [1993]. For the signal in Fig. 2(a), the largest Lyapunov exponent, calculated for different embedding dimensions m, is nearly equal to zero, as expected for an asymptotically stable limit cycle [Parker & Chua, 1989].

In addition, the correlation dimension D_{corr} [Grassberger & Procaccia, 1983] has been extracted

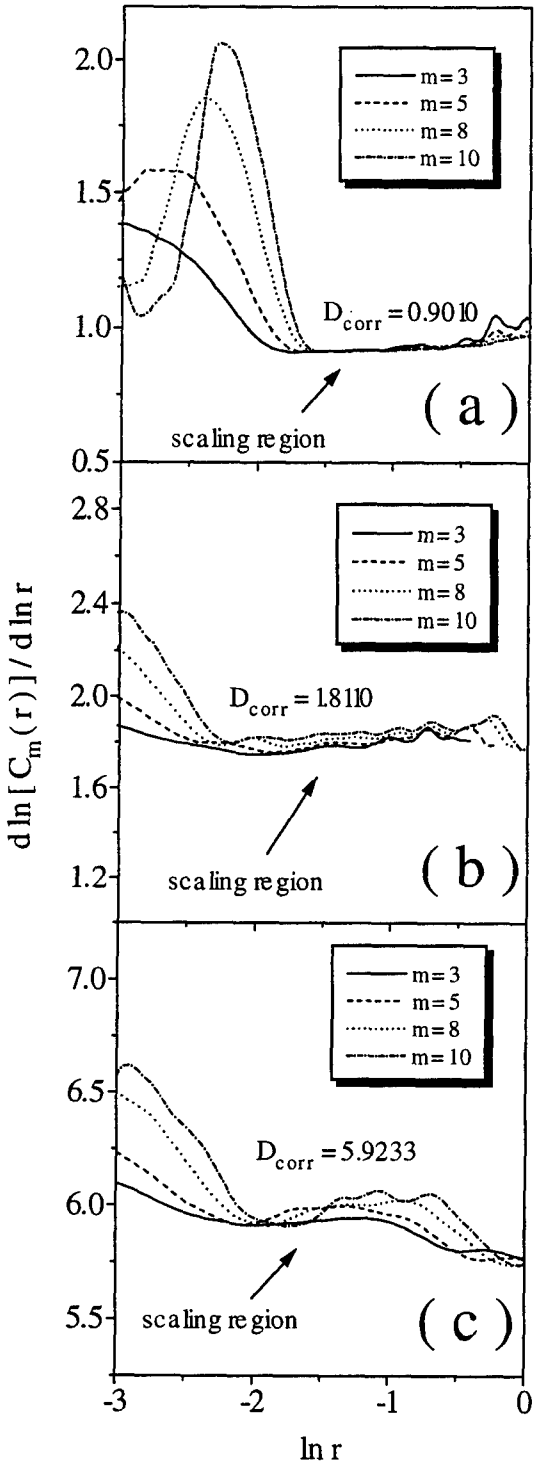

Fig. 4. Logarithmic slope of the correlation sum $C_m(r)$ as a function of $\ln r$, for several values of the embedding dimension m: (a) $\Delta\nu = 120$ MHz, (b) $\Delta\nu = 140$ MHz, (c) $\Delta\nu = 200$ MHz. The height of the plateaux indicates the value of the correlation dimension $D_{\rm corr}$.

from the experimental signals as

$$D_{\rm corr} = \lim_{m\to\infty} \lim_{r\to 0} \frac{d\ln C_m(r)}{d\ln r}. \qquad (2)$$

Here, the correlation sum $C_m(r)$ is given by

$$C_m(r) \equiv \frac{2}{S(S-1)} \sum_{\{n,k\}} \Theta(r - \|\mathbf{I}_k^T - \mathbf{I}_n^T\|), \qquad (3)$$

where Θ is the Heavyside step-function and $\{n, k\}$ is a set of indices such that $|k-n| > t_{\rm co}/\delta$, $t_{\rm co}$ being a suitable cutoff time introduced to avoid artificial correlations arising from too closely spaced embedding vectors which may result from measurements taken nearly at the same time. In our analysis, $t_{\rm co}$ was chosen as the inverse of the mean frequency of the power spectrum of the signal, obtained by FFT. The limit $r \to 0$ is, actually, unreliable, because small values of r are blurred by noise and limitations on experimental accuracy. In practice, a plateau referred to as scaling region should appear in the plot of $d\ln C_m(r)/d\ln r$ versus $\ln r$. In Fig. 4(a), such a plot is shown, for the time series in Fig. 2(a), for several values of m and the scaling region is clearly visible. The height of the plateau represents the estimated value of the correlation dimension $D_{\rm corr}$. The result obtained, $D_{\rm corr} \simeq 1$, definitely confirms that the dynamics is described by a limit cycle.

In Fig. 2(c), part of the time series acquired for $\Delta\nu = 140$ MHz is shown. In this case, the period fades in an irregular pattern of dropouts and the spectrum in Fig. 2(d) shows a broad-band structure. Although broad-band spectra may be associated with either stochastic or nonlinear deterministic processes, the exponential decay of the spectral intensity at high-frequencies indicates chaotic dynamics [Brandstater & Swinney, 1987]. The distortion of the phase portrait in Fig. 3(c) and the sharp change in the pattern of the recurrence plot in Fig. 3(d) support this interpretation. In particular, in the recurrence plot, the long lines parallel to the main diagonal appearing in Fig. 3(b) are now fragmented in shorter segments, the length of which has been proven to be inversely proportional to the largest Lyapunov exponent [Zbilut & Webber, 1992]. A more striking evidence of chaotic behavior is provided by the largest Lyapunov exponent, which is now positive [see Fig. 5(a)] and by the value of $D_{\rm corr}$ which is about 1.8 [see Fig. 4(b)].

The time series shown in Fig. 2(e) has been recorded for $\Delta\nu = 200$ MHz. The signal shows no apparent regularity and the power spectrum in Fig. 2(f) has a broad structure which also includes additional high-frequency components. The

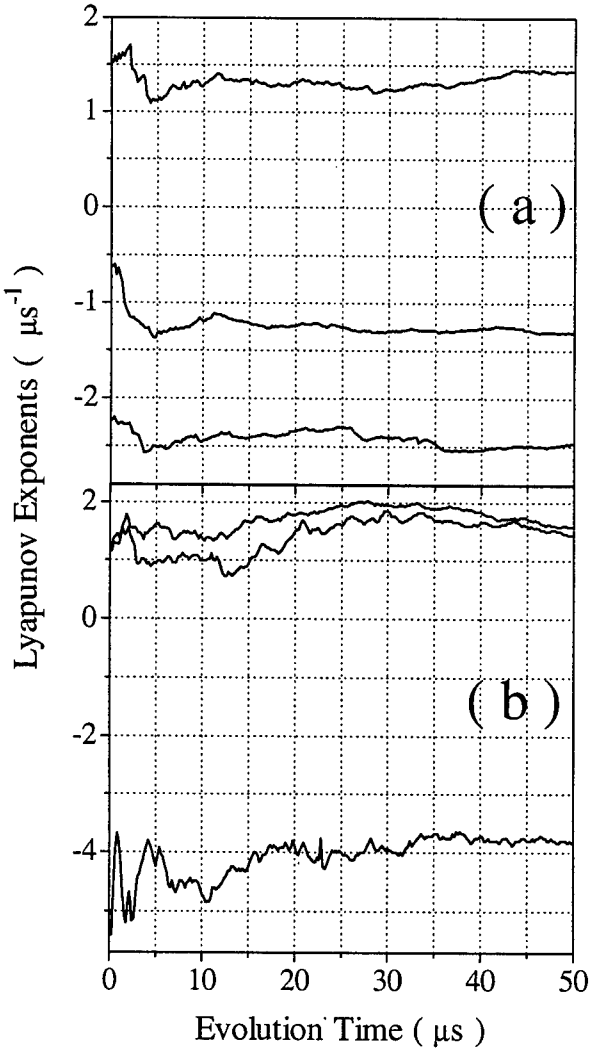

Fig. 5. Spectrum of Lyapunov exponents extracted from the time-series for $m = 3$: (a) $\Delta\nu = 140$ MHz, (b) $\Delta\nu = 200$ MHz.

phase portrait in Fig. 3(e) is markedly different from the previous ones and the trajectory explodes in a blurred and folded geometry indicating that the embedding dimension $m = 3$ used for the portrait is too low to provide reliable topological information about the laser intensity dynamics. The recurrence plot in Fig. 3(f) belongs to the homogeneous typology [Eckmann *et al.*, 1987] and any small-scale texture is hardly visible. Again, a positive largest Lyapunov exponent is found [see Fig. 5(b)] and the calculated value of D_{corr} is about 6 [see Fig. 4(c)].

The characterization of the chaotic regimes has been completed with the computation of the entire spectrum of Lyapunov exponents. For this purpose, the algorithm introduced by Darbshyre and Broomhead [1996] has been implemented in a revised and noise-robust version described by Banbrook *et al.* [1997]. The procedure has been iterated in order to obtain the evolution of the Lyapunov exponents within a certain time interval and verify their convergence. The results are shown in Fig. 5, for an embedding dimension $m = 3$. Two positive exponents have been found for $\Delta\nu = 200$ MHz and only one for $\Delta\nu = 140$ MHz. The calculation has been repeated for values of m up to 10, producing no substantial difference. Indeed, all additional Lyapunov exponents are negative in both cases.

4. Summary and Conclusions

The temporal evolution of the light emitted by a diode laser subject to feedback from an external cavity containing a cell of Cs vapor in a saturation spectroscopy configuration has been investigated experimentally. Frequency locking to the central Lamb dip of the saturated absorption spectrum of the D_2 line, accompanied by a stable laser emission has been observed. With increasing detuning $\Delta\nu$ from the atomic resonance, within the range $0 < \Delta\nu < 140$ MHz, where the laser operation appears to be strongly influenced by the presence of the atomic absorber, the output intensity displays self-pulsing and low-dimensional chaos, which take place on a time scale much longer than the time scales typical of the dynamics of a diode laser coupled to an external cavity with no absorber. For larger values of $\Delta\nu$, the laser emission shows high-dimensional chaos, characterized by two positive Lyapunov exponents. Although the presence of two positive exponents is commonly associated with hyperchaos [Rössler, 1979], it might be explained, here, in terms of coexistence of different attractors. The coexistence of attractors has been demonstrated theoretically also for diode lasers under usual feedback conditions [Masoller, 1994].

In the range of feedback strengths used in our experiment, high-dimensional chaos has been proven to underlie the dynamics of extended-cavity diode lasers with no absorber [Sano, 1994; Mirasso *et al.*, 1997]. On the other hand, our analysis suggests that a low-dimensional attractor emerges when, for relatively small detuning, the laser operation is dominated by the absorber. An interplay between different chaotic attractors might explain why no clear route to chaos has been observed. In diode lasers coupled to an external cavity with no

absorber, low-dimensional chaos, reached through definite routes, has been identified in several works, as, for instance, [Mørk *et al.*, 1992; Ye *et al.*, 1993].

The time-, frequency-, and optical frequency-domain analyses performed in this paper clearly detect the same aspects of the phenomena investigated and their mutual consistency has been regarded as a significant test. The variety of dynamic regimes identified in a range of laser frequencies close to the atomic resonance, along with the ease of the experimental access to the slow absorber-induced dynamics, makes this system an interesting subject for further experimental and theoretical investigations, which would be required for a full understanding of the nonlinear and chaotic properties described here. For instance, it would be needed to explain how the characteristic time scale induced by the absorber emerges from the destabilization of the regime of self-locking.

Acknowledgments

The work of D. Hennequin at the University of Pisa was within the framework of a collaboration between the CNR of Italy and the CNRS of France.

References

Albano, A. M., Muench, J., Schwartz, C., Mees, A. I. & Rapp, P. E. [1988] "Singular-value decomposition and the Grassberger–Procaccia algorithm," *Phys. Rev.* **A38**(6), 3017–3026.

Banbrook, M., Ushaw, G. & McLaughlin, S. [1997] "How to extract Lyapunov exponents from short and noisy time series," *IEEE Trans. Signal Process.* **45**(5), 1378–1382.

Brandstater, A. & Swinney, H. L. [1987] "Strange attractors in weakly turbulent Couette–Taylor flow," *Phys. Rev.* **A35**(5), 2207–2220.

Casdagli, M., Eubank, S., Farmer, J. D. & Gibson, J. [1991] "State space reconstruction in the presence of noise," *Physica* **D51**(1–3), 52–98.

Cerboneschi, E., de Tomasi, F. & Arimondo, E. [1993] "Low frequency fluctuation instabilities in diode lasers with optical feedback," in *Nonlinear Dynamics in Lasers and Optical Systems*, ed. Mel'nikov, L. A., SPIE, Vol. 2099, pp. 183–192.

Cuneo, C. J., Maki, J. J. & McIntyre, D. H. [1994] "Optically stabilized diode laser using high-contrast saturated absorption," *Appl. Phys. Lett.* **64**(20), 2625–2627.

Darbshyre, A. G. & Broomhead, D. S. [1996] "Robust estimation of tangent maps and Lyapunov spectra," *Physica* **D89**(3, 4), 287–305.

di Teodoro, F., Cerboneschi, E., Hennequin, D. & Arimondo, E. [1997] "Multi-stability for an extended-cavity diode laser with intracavity atomic absorber," *Quantum Semicl. Opt.* **9**(5), 867–878.

Eckmann, J.-P., Oliffson Kamphorst, S. & Ruelle, D. [1987] "Recurrence plots of dynamic systems," *Europhys. Lett.* **4**(9), 973–977.

Fischer, I., van Tartwijk, G. H. M., Levine, A. M., Elsässer, W., Göbel, E. & Lenstra, D. [1996] "Fast pulsing and chaotic itinerancy with a drift in the coherence collapse of semiconductor lasers," *Phys. Rev. Lett.* **76**(2), 220–223.

Grassberger, P. & Procaccia, I. [1983] "Characterization of strange attractors," *Phys. Rev. Lett.* **50**(5), 346–349.

Kitching, J., Boyd, R., Yariv, A. & Shevy, Y. [1994] "Amplitude noise reduction in semiconductor lasers with weak, dispersive optical feedback," *Opt. Lett.* **19**(17), 1331–1333.

Liu, Z. D., Bloch, D. & Ducloy, M. [1994] "Absolute active frequency locking of a diode laser with optical feedback generated by Doppler-free collinear polarization spectroscopy," *Appl. Phys. Lett.* **65**(3), 274–276.

Masoller, C. [1994] "Coexistence of attractors in a laser diode with optical feedback from a large external cavity," *Phys. Rev.* **A50**(3), 2569–2578.

Mirasso, C. R., Mulder, M., Spoelder, H. J. W. & Lenstra, D. [1997] "Visualization of the 'Sisyphus' attractor," *Comput. Phys.* **11**(3), 282–286.

Mørk, J., Tromborg, B. & Mark, J. [1992] "Chaos in semiconductor lasers with optical feedback: Theory and experiment," *IEEE J. Quantum Electron.* **28**(1), 93–108.

Packard, N. H., Crutchfield, J. P., Farmer, J. D. & Shaw, R. S. [1980] "Geometry from a time series," *Phys. Rev. Lett.* **45**(9), 712–716.

Parker, T. A. & Chua, L. O. [1989] *Practical Numerical Algorithms for Chaotic Systems* (Springer-Verlag, Berlin) Chapter 3, p. 70.

Rosenstein, M. T., Collins, J. J. & De Luca, C. J. [1993] "A practical model for calculating largest Lyapunov exponents from small data sets," *Physica* **D65**(1, 2), 117–134.

Rosenstein, M. T., Collins, J. J. & De Luca, C. J. [1994] "Reconstruction expansion as a geometry-based framework for choosing proper delay times," *Physica* **D73**(1, 2), 82–98.

Rössler, O. E. [1979] "An equation for hyperchaos," *Phys. Lett.* **A71**(2, 3), 155–157.

Sano, T. [1994] "Antimode dynamics and chaotic itinerancy in the coherence collapse of semiconductor lasers with optical feedback," *Phys. Rev.* **A50**(3), 2719–2726.

Schmidt, O., Knaak, K.-M., Wynands, R. & Meschede, D. [1994] "Cesium saturation spectroscopy revisited:

How to reverse peaks and observe narrow resonances," *Appl. Phys.* **B59**(2), 167–178.

Ye, J., Li, H. & McInerney, J. G. [1993] "Period-doubling route to chaos in a semiconductor laser with weak optical feedback," *Phys. Rev.* **A47**(3), 2249–2252.

Zbilut, J. P. & Webber, C. L. [1992] "Embeddings and delays as derived from quantification of recurrence plots," *Phys. Lett.* **A171**(3, 4), 199–203.

International Journal of Bifurcation and Chaos, Vol. 8, No. 9 (1998) 1811–1819

CONTROL OF TURN-ON IN CLASS B LASERS

P. A. PORTA, L. M. HOFFER, H. GRASSI and G. L. LIPPI*
Institut Non Linéaire de Nice, UMR 6618 CNRS, Université de Nice-Sophia Antipolis, 1361 Route des Lucioles, F-06560 Valbonne, France

Received July 31, 1997; Revised January 8, 1998

A very simple technique, which uses a succession of two different but constant levels in the pump parameter, is shown to be quite effective in controlling the turn-on transient of a class B laser. In particular, a drastic reduction in the delay time, as well as a lowering of the intensity overshoot under suitable conditions, has been observed both in numerical simulations and in experiments on a CO_2 laser. Such a straightforward, nonfeedback technique may have very promising applications in the realm of communications.

1. Introduction

Lasers, like many other optical systems, have attracted considerable attention for their nonlinear response to parameter variations and to perturbations. Their behavior, both regular and chaotic, was extensively investigated during the 1980's [Abraham *et al.*, 1985; Bandy *et al.*, 1988]. The theoretical prediction that unstable periodic orbits in a developed chaotic regime could be stabilized with small perturbations [Ott *et al.*, 1990] sparked investigations in many different systems. Since then, much work has been done to control unstable periodic orbits (e.g. [Hunt, 1991]) and in lasers several different schemes for the control of such orbits have been devised (e.g. [Roy *et al.*, 1992; Bielawski *et al.*, 1994]). More recently, interest has focused on reaching the desired periodic orbit in a minimum time, and many questions related to the targeting of particular states [Shinbrot *et al.*, 1993; Boccaletti *et al.*, 1997] have been examined. The application of optimal targeting to loss-modulated lasers has been very recently proposed in a few theoretical papers [Kotomtseva *et al.*, 1997; Turovets *et al.*, 1997]. What is being stabilized in all these cases, however, is asymptotic behavior. Very recently, this field has expanded to address the characteristics of the *transition* between two states of a dynamical system and its control. A solution to the general problem of "customizing" a transient has been pioneered by Petrov and Showalter, who used a nonlinear control method on a model for a nonlinear chemical reaction, with excellent results [Petrov & Showalter, 1996].

In this short communication, we present a simple and effective way of controlling the transient evolution of a class B laser [Tredicce *et al.*, 1985] between two states: below threshold (which becomes unstable after the laser is switched on) and above threshold (final *stable* steady state). Although the control of laser turn-on may sound quite simple, class B[1] systems show nontrivial dynamical behavior due to the coupling of variables which respond at very different rates. Since a large part of all lasers sold for commercial applications (from high power to communications) belong to this class, a *simple* means of controlling their turn-on behavior could have very important and useful applications. With the help of a simple model that captures the essential dynamical properties of class B lasers, we discuss the basic physical features of these

*Corresponding author
[1]The main elements of this class are solid state lasers (in particular Nd:YAG), semiconductor lasers, and CO_2 lasers.

systems when they are turned on by a sudden switch of the pump parameter. We then show the result of measurements obtained with a CO_2 laser and compare it to the predictions of a model that takes into account the specific molecular features of this laser. Finally we interpret physically the observations and, in the conclusions, comment on possible applications.

Extensive studies of the response of class A lasers (e.g. He-Ne, Ar^+, and most lasers emitting in the visible part of the spectrum) have conclusively shown that their turn-on is controlled solely by the amount of spontaneous emission present at the switch-on time. The stochastic delay time with which these lasers respond by converting spontaneous emission into a stimulated one closely mirrors the statistics of the initial photons [Arecchi & Degiorgio, 1972; Arecchi *et al.*, 1982] (below threshold). The response to noise at turn-on of class B lasers, which are modeled by two dynamical variables (instead of only one variable as in class A systems), has instead shown more complex features [Ciofini *et al.*, 1992; Balestri *et al.*, 1991; Balle *et al.*, 1994; Grassi *et al.*, 1994; Lippi *et al.*, 1997]. In this case, when the laser is turned on by abruptly increasing the pump value (which is what happens when a laser's electrical switch is turned on), the system's evolution is not just the result of a single variable, the intensity, that builds up from noise. Here the slow variable — the population inversion — is strongly coupled to the intensity and plays an important role in determining the system's response, profoundly affecting its characteristics (cf. Sec. V in [Lippi *et al.*, 1997]).

The more complex response to noise in class B lasers is an indication of their intrinsic dynamical richness, which we exploit for the control of the turn-on transient. We are primarily interested in controlling the system's switch-on *on average*, and so in the experiment we performed averages over many repetitions of the laser turn-on. In the theoretical discussion, we do not specifically include the influence of noise and instead explain our results using the deterministic elements of the model. Figure 1 shows the intensity of a CO_2 laser (lower trace) in response to a rapid variation of its pumping current (upper trace) from below to above threshold. Note the macroscopic delay time (≈ 185 μs) between the abrupt current commutation and the rise of the laser intensity out of noise. The overshoot in the intensity (past the final steady state value) is characteristic of these systems, as are the relaxation oscillations which follow.

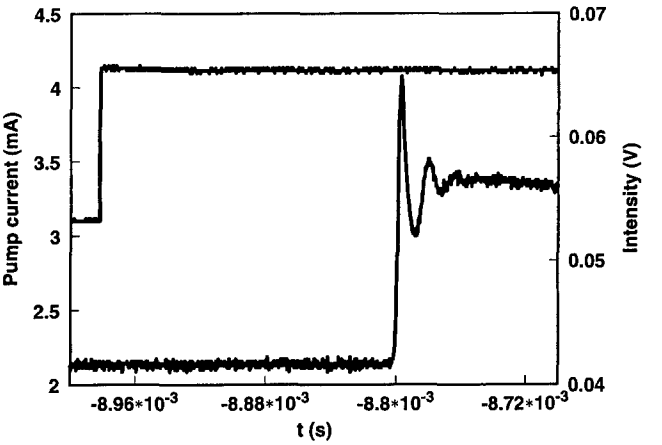

Fig. 1. Turn-on of a CO_2 laser by a sudden commutation of the pump parameter from below to above threshold. Upper trace: Time behavior of the current flowing through the laser, which excites the molecules — initial current value: below threshold; final current value: above threshold. Lower trace: laser power. Note the delay time (≈ 185 μs) between the switch-up of the pump current and the actual laser's turn-on, and the peak overshoot followed by strongly damped relaxation oscillations.

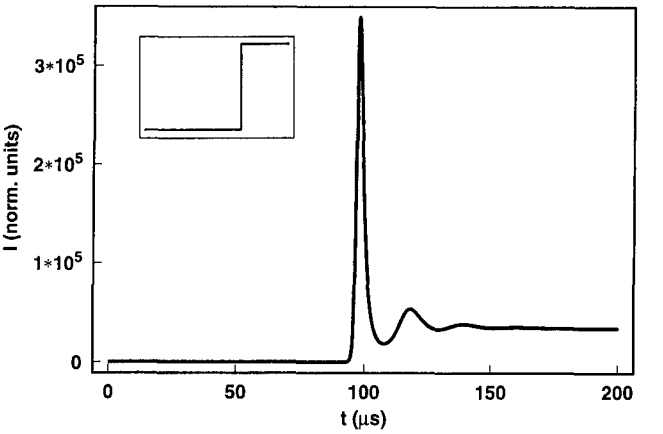

Fig. 2. Numerical integration of a five-dimensional model for a CO_2 laser, showing the intensity as a function of time after the application of an abrupt jump in the pump parameter (see inset) at time $t = 0$.

Figure 2 shows the result of integrating a complete five-dimensional model for a CO_2 laser [Meucci *et al.*, 1992; Ciofini *et al.*, 1993] for parameters close to those of Fig. 1. This model, the best presently available, correctly reproduces most of the laser's features: delay time, frequency and amplitude of the relaxation oscillations. Indeed, it was developed to account specifically for these features [Meucci *et al.*, 1992] in the transient regime

and is therefore much more appropriate to the simulation of the laser turn-on than equivalent reduced models (with two or three variables, e.g. [Oppo *et al.*, 1989]). The improved agreement, also compared to earlier five equations models (e.g. [Arimondo *et al.*, 1983]), is achieved using the relaxation rates of the upper and the lower levels as fitting parameters. Although this procedure may seem somewhat arbitrary, it is justified by the fact that no simple dynamical model can take into account all of the laser's features, especially in the transient regime (cf. [Meucci *et al.*, 1992] for details). Our preference for this model comes from the fact that it predicts realistic delay times, while in the reduced models the delay is always largely underestimated (for reasonable parameter values). We remark that the time delay in the experiment (cf. Fig. 1) has an additional component of about 100 μs, which comes from the time required to transfer the pump pulse to the lasing levels [Witteman, 1987] and which is never taken into account in dynamical models. Therefore, the comparison has to be drawn after subtraction of this additional time lag. In spite of its considerable advantages, one should not expect a quantitative agreement on the peak amplitudes from this model, either. Indeed, even in this case the amplitude of the peak overshoot is higher than in the real system.

Although useful for the comparison between experiment and theory, the five-dimensional model is too complex for a simple analytical treatment, from which we would gain a physical understanding of the mechanisms involved in the transient. We will therefore discuss a reduced two-dimensional (rate equation) model [Siegman, 1986], which captures the main topological features of the phase space:

$$\frac{dI}{dt} = -K(1-D)I\,, \tag{1a}$$

$$\frac{dD}{dt} = -\gamma_{\|}[D(1+I) - P(t)]\,, \tag{1b}$$

where I and D are the e.m. field intensity and population inversion variables, respectively, K and $\gamma_{\|}$ are their respective relaxation constants, and $P(t)$ is the pump parameter, which is switched here at time $t = 0$ from below (P_{off}) to above threshold (P_{on}).

A numerical integration of these two equations is given in Fig. 3. In Fig. 3(a), the intensity response of the laser after the switch-on at time $t = 0$ shows the effects of the reduced phase space in the increased number of relaxation oscillations present. The corresponding time evolution of the population inversion is shown in Fig. 3(b) where the horizontal dashed line at 1 represents the threshold value. The joint phase space portrait is given in Fig. 3(c).

Since this model is purely deterministic, the below-threshold condition corresponds to the steady state ($I_{s,i} = 0$, $D_{s,i} = P_{\text{off}}$). Thus, the population inversion D, as described by Eq. (1b), initially undergoes an exponential growth and in the absence of laser intensity would asymptotically saturate at P_{on}. The evolution of D closely follows this functional dependence as long as I is negligibly small: certainly whenever its growth rate [Eq. (1a)] is negative, and in part even beyond that. As soon as threshold is reached, the sign of the prefactor of I in Eq. (1a) changes [$(1 - D)$ becomes negative] and the intensity begins to feel the nonlinear (bilinear) coupling between itself and the population inversion. Thus, although the intrinsic growth rate of the intensity is much larger than that of the population inversion ($K \gg \gamma_{\|}$), its actual growth depends on the evolution of D. In particular, we observe that the population inversion, D, must be larger than 1 [i.e. than the final steady state value ($I_{s,f} = P_{\text{on}}$, $D_{s,f} = 1$)] for the intensity to grow, and that the field intensity's growth is proportional to the distance in phase space between the instantaneous population inversion and its equilibrium value.

Since the initial value of I is negligibly small[2] (the spontaneous emission power is typically at least seven orders of magnitude smaller than the final laser power), there will be a certain time lag between the moment when $(1 - D)$ becomes negative and when I assumes values that are non-negligible [compared to 1, cf. Eq. (1b)]. During this time D continues to grow [Fig. 3(b)], albeit at a slower rate [due to the term $-\gamma_{\|}DI$, Eq. (1b)]. The instantaneous value of D, above $D_{s,f}$, causes the intensity I to overshoot and then to exhibit the characteristic damped, ringing behavior [Tredicce *et al.*, 1985] well illustrated by the phase space plot [Fig. 3(c)] which clearly shows the various stages of the evolution of the transient.

[2]For the numerical integration we add a very small constant to I to allow the code to move away from the unstable fixed point.

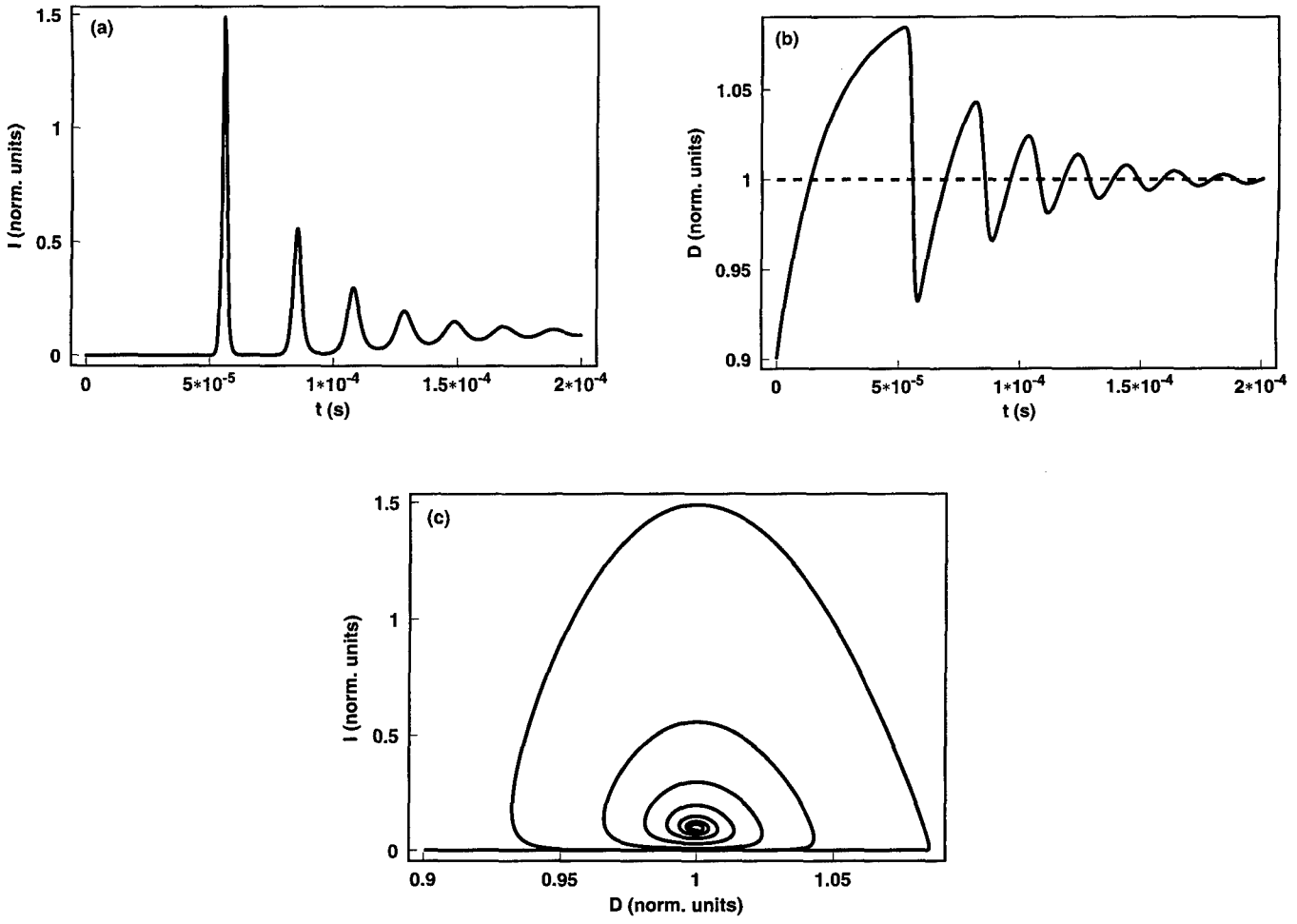

Fig. 3. Results of the numerical simulation of the laser rate equations under conditions comparable to those in Fig. 2. (a) Shows the laser intensity as a function of time after an abrupt commutation of the pump parameter at $t = 0$ (see inset of previous figure). (b) Shows the corresponding behavior of the population inversion. (c) Shows the phase space portrait.

From the above discussion we extract the following important points:

1. There exists a deterministic component of the delay time at turn-on due to the slow response of the population inversion, which has to attain threshold before the intensity may grow.
2. The field intensity cannot grow away from its initial value until the population inversion is *larger* than 1 (in these normalized units).
3. Due to the lack of a "macroscopic" intensity during the additional delay time, the population keeps growing further and further away from threshold under the steady action of the pump. (This "dead time" for the field is due to its rapid, *but not instantaneous* growth out of noise after the population is inverted.)

If we want to influence the delay time with which the laser turns on, and, possibly also the height of the overshoot, we need to modify the evolution of the population. Since its relaxation constant $\gamma_{\|}$ cannot be changed, we must act on the pump parameter directly.

The simplest way of achieving our goal is that of adding to the pump pattern shown in the inset of Fig. 2 an intermediate control step (Fig. 4), whose height and duration can be chosen to suit our purposes. The addition of this intermediate step, of height P_c (higher than the final level at P_{on}) and duration t_c, serves a double purpose: (1) increasing the speed at which the population inversion grows — since its saturation value, P_c, will be higher during this step — and (2) providing a better initial condition for the evolution of the field intensity (this point will be clarified in the physical discussion).

Figure 5 compares the results obtained using the five-dimensional CO_2 laser model [Meucci *et al.*, 1992] for various values of the height, P_c,

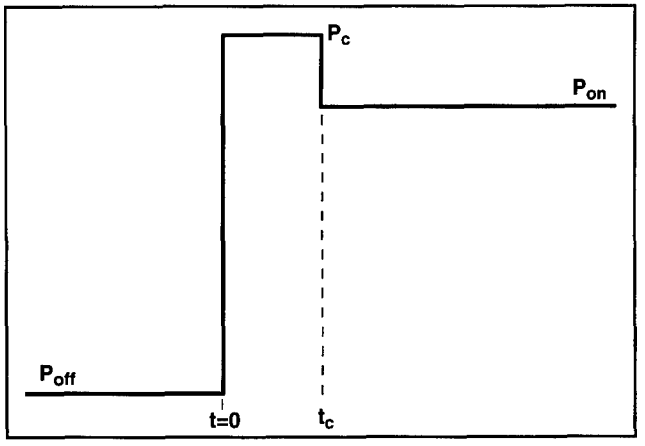

Fig. 4. Two-step control pattern for laser turn-on. The pump parameter is switched up from its initial value, P_{off} at time $t = 0$, towards a control level of height P_c, larger than P_{on}, and duration t_c. P_c and t_c can be varied to optimize the turn-on behavior. P_{on} is the desired final pump level.

of the control step. The effect of inserting this step is clear: The population inversion [Fig. 5(a)] increases more rapidly during the time interval during which the laser is pumped harder (between $t = 0$ and $t = t_c = 20$ μs). As a result [Fig. 5(b)], the laser turns on sooner, i.e. the delay time at turn-on is reduced (mainly) by the faster growth of the population inversion from its initial value up to threshold.[3] A nontrival additional result, clearly visible in Fig. 5(b), is that there is an optimal height of the intermediate pump value for which we simultaneously reduce the turn-on delay time *and* the peak intensity.

The effect of the control step is summarized in Fig. 6, which shows the peak amplitude [Fig. 6(a)] and the delay time [Fig. 6(b)] as a function of control step height. A strong deviation from a linear relationship (marked by the solid line in Fig. 6(b), obtained by interpolation between the leftmost two points) appears only after the minimum in the peak height has been passed [cf. Fig. 6(a)]. Near the minimum the deviation from linearity is recognized to be approximately 8%.

The experimental application of the pump pattern in Fig. 4 to a CO_2 laser (cf. [Grassi *et al.*, 1994] for details about the setup), confirms the existence of both effects: The reduction in delay time and

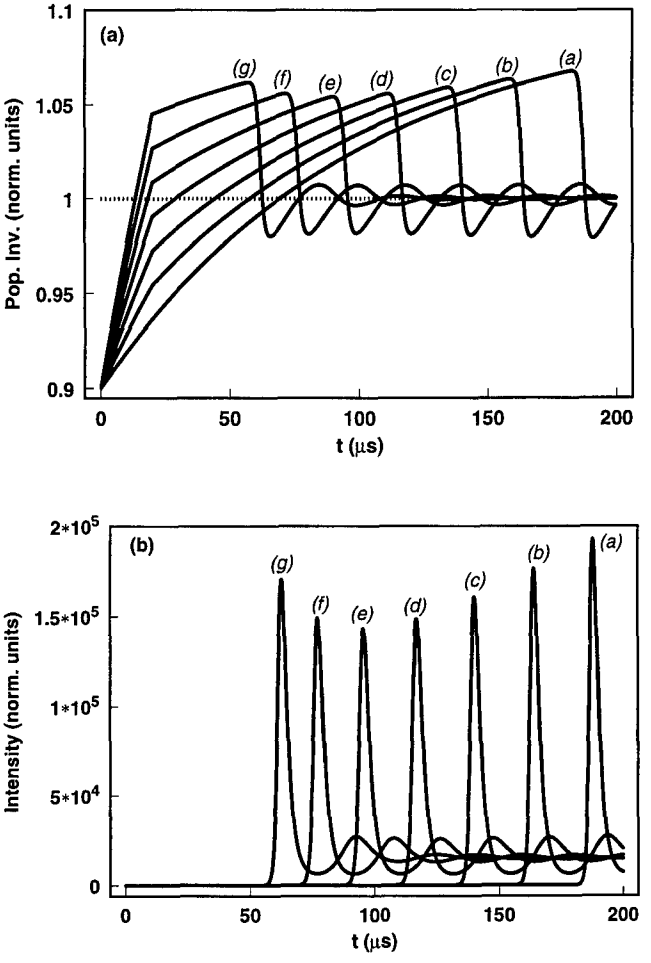

Fig. 5. Numerical integration of a five-dimensional model for a CO_2 laser. (a) Temporal evolution of the population inversion for (*a*) $\lambda_c = \lambda_{\text{on}} = 0.1$, (*b*) $\lambda_c = 0.2$, (*c*) $\lambda_c = 0.3$, (*d*) $\lambda_c = 0.4$, (*e*) $\lambda_c = 0.5$, (*f*) $\lambda_c = 0.6$ and (*g*) $\lambda_c = 0.7$. The other parameters are $t_c = 20$ μs, $P_{\text{off}} = 0.9$, $P_{\text{on}} = 1.1$, and the relaxation constants of the model $k = 2 \times 10^7 \text{s}^{-1}$, $\gamma_1 = 8 \times 10^4 \text{s}^{-1}$, $\gamma_2 = 1 \times 10^4 \text{s}^{-1}$, $\gamma_R = 7 \times 10^5 \text{s}^{-1}$, $z = 16$. The horizontal dotted line (at 1) marks the lasing threshold. Notice that the duration of the control step corresponds to the time at which the population inversion curves (*b–g*) show a discontinuity given by the abrupt change in pump level. (b) Temporal evolution for the correspondent field intensity. The minimum in the intensity occurs between curves (*d*) and (*e*), i.e. for a population inversion level at time t_c very close to threshold (as predicted by the simplified model).

the presence of a minimum overshoot height. In Fig. 7, we show the average values of peak height as a function of the average delay time for different amplitudes of P_c (the values of the pump parameter are estimated under the assumption of a linear

[3]The discontinuity appearing in Fig. 5(a) is not a numerical artefact, but reflects the sudden variation of the pump parameter onto the population inversion growth. We have extensively checked both the integration routine and the time step, in the framework of this and of another investigation [Lippi *et al.*, 1997], to ensure that the sudden change in the control parameter does not affect the quality of the numerical prediction.

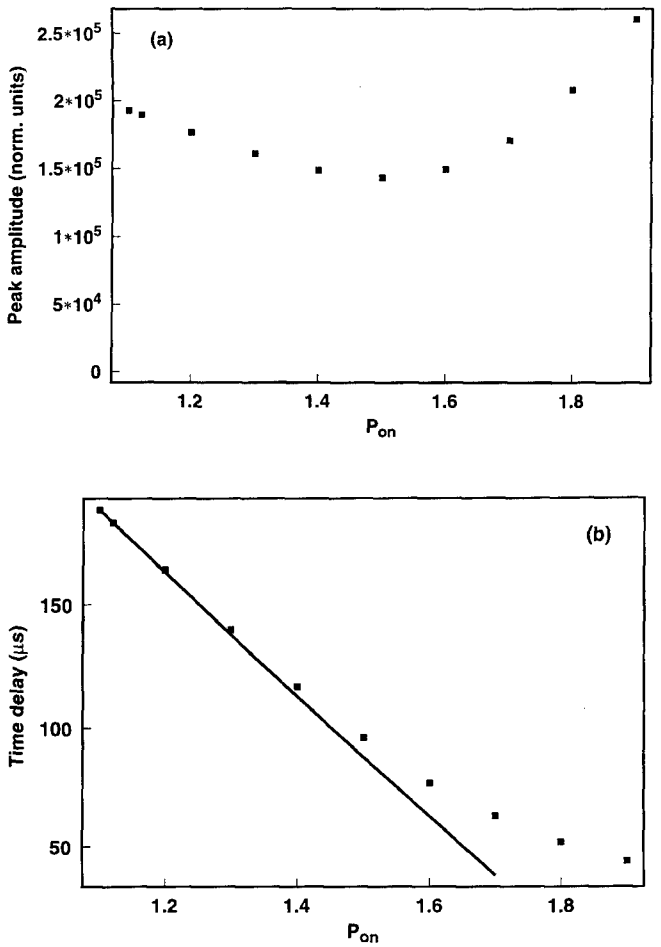

Fig. 6. (a) Height of the peak overshoot as a function of the control step; (b) time delay as a function of the control step; the straight line marks the extrapolated linear dependence of the delay, estimated from the two leftmost points. All parameters as in the previous figure (more λ_c levels are calculated here).

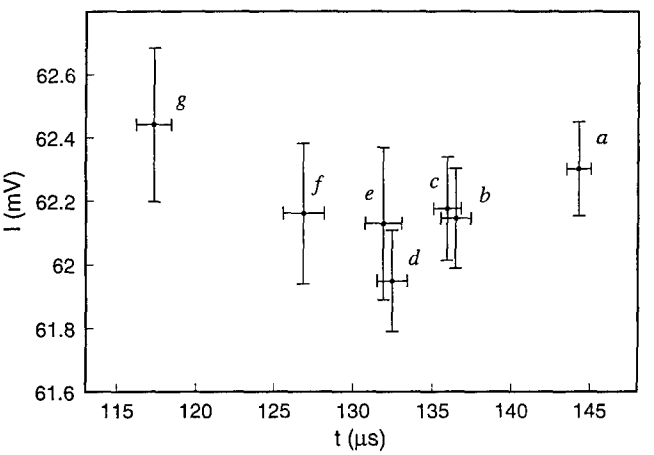

Fig. 7. Average peak intensity (weighted averages) as a function of average delay time (weighted averages) for different values of the height of the control peak. Duration of the control $t_c = 20$ μs. Estimated amplitudes of the control step: (a) $P_c \approx 1.25$ (uncontrolled turn-on); (b) $P_c \approx 1.27$; (c) $P_c \approx 1.28$; (d) $P_c \approx 1.3$; (e) $P_c \approx 1.34$; (f) $P_c \approx 1.43$; (g) $P_c \approx 1.61$. $P_{\rm off} \approx 0.9$, $P_{\rm on} \approx 1.25$. The intensity values are given without subtracting the detector's offset, ≈ 42 mV.

relationship between excitation current and effective pump). The averages are taken over 50 successive turn-ons. Three sequences, of 50 events each, are averaged together (for each value of the parameters) to provide the weighted averages with weighted standard deviations (cf. [Worthing & Geffner, 1943] for details), that we show in the figure. The first measurement, far right point, marked as *a*, corresponds to $P_c = P_{\rm on}$ — i.e. turn-on without control (simple one-step commutation, as in Fig. 1). By gradually increasing the intermediate step height, we see that the average amplitude of the overshoot peak, plotted as a function of the average delay time, decreases down to a minimum ($\approx 2.5\%$ reduction). If we continue increasing this amplitude beyond the optimal value, then the delay time is further reduced, but the overshoot amplitude increases. We first provide an approximate analytical explanation for the occurrence of this minimum and then interpret all results physically.

We start from the equations of the simplified model already considered [Eqs. (1)]. For an analytical treatment we use the approximation of [Balle *et al.*, 1991] where we neglect the intensity during the time period when it is very small. In this regime,[4] we can neglect the intensity term in Eq. (1b) and integrate the resulting expression for the population inversion as a function of time. Using the equilibrium value of the population inversion $D_{s,i}$ as the initial condition, we obtain the value of the population at the end of the control step:

$$D_c = D(t_c) = D_{\rm off} e^{-\varepsilon t_c} + P_c(1 - e^{-\varepsilon t_c}), \qquad (2)$$

where $\varepsilon = \sqrt{(\gamma_\parallel / K)}$, and t_c is the time at which the control step ends. Using the latter expression [Eq. (2)] as a new initial condition, we integrate Eq. (1b) again, with pump value $P_{\rm on}$, to obtain the

[4] As can be seen from Fig. 5 the minimum in the peak overshoot occurs when the pump is brought from P_c to $P_{\rm on}$ before the field intensity becomes macroscopic (a fact that will be clear later). Hence, the approximation we are presenting applies to the whole of the control step and beyond.

growth of the population inversion as a function of time after the control step. The approximate expression that we obtain in this way is valid up to a time t^*, which corresponds to the time for which the e.m. field intensity reaches a threshold value I^*, which we can freely choose. Beyond this value, the intensity cannot be considered to be negligible anymore. We can write the value of the population inversion at time t^* as a function of all other parameters:

$$D^* = D(t^*) = D_{\text{off}}(1 - \varepsilon t^*) + \varepsilon[(1 + \lambda_{\text{on}})t^* + (\lambda_c - \lambda_{\text{on}})t_c], \quad (3)$$

where

$$P_c = 1 + \lambda_c, \quad (4)$$

$$P_{\text{on}} = 1 + \lambda_{\text{on}}, \quad (5)$$

for convenience, and where we have expanded all exponentials to first order in εt.

After time t^*, the full, coupled nonlinear system [Eqs. (1)] describes the dynamics. However, if we are only interested in determining the peak amplitude of the laser, we can once again solve the system of equations in an approximate form. In the region where the intensity is at its highest, the contribution of the population inversion can, in comparison, be neglected [Balle *et al.*, 1991]. Following the solution technique outlined in [Balle *et al.*, 1991], we obtain for the peak intensity the expression:

$$I_p = I^* + \frac{D^* - D_p}{\varepsilon^2} + \frac{\log D_p - \log D^*}{\varepsilon^2}, \quad (6)$$

where I^* and D^* are the value of the intensity and of the population inversion at time t^*, respectively, and I_p and D_p their corresponding values at the maximum of the intensity overshoot. If we now search for the existence of a minimum in the amplitude of this peak as a function of P_c (or equivalently, λ_c), we find that this occurs if and only if

$$D_c = 1 - \lambda_{\text{on}}\varepsilon(\bar{t} - t_c), \quad (7)$$

which, because of the smallness of ε, is very close to the laser threshold value ($\bar{t}$ is the time at which the population inversion reaches threshold during its growth). This is equivalent to saying that the minimum value of the overshoot is reached when the population inversion is brought very close to threshold by the control step. We note that the expression, Eq. (7), is independent of the "macroscopic threshold" that we have chosen for the field intensity, I^*. Looking back at the simulations in Fig. 5, we remark that the minimum in the intensity overshoot indeed occurs near the condition in Eq. (7).

This result can also be understood intuitively. As already mentioned, the decrease in delay time is mainly due to the faster growth of the population inversion during the control step. However, if the control step is kept beyond the time for which the threshold is passed, the population inversion grows at a faster rate in the time interval where the field intensity grows. Hence, corresponding to the further reduction in delay time that is brought about by the longer control duration is a higher excess of population inversion when the field intensity reaches macroscopic levels, and hence a higher overshoot. This explains the increase of the peak amplitude when the optimal value for the minimum is passed. The existence of the minimum itself can be understood in the following way. The amount of spontaneous emission present at all times determines the instantaneous value of the field intensity. Once the population inversion crosses the lasing threshold, the intensity starts growing from the instantaneous value that it has acquired at the time of crossing. A faster growth of the population inversion, below threshold, implies a faster growth of the spontaneous emission, and hence an initial condition for the intensity somewhat closer to the final steady state value $I_{s,f}$. Hence, provided that the control step does not continue above threshold — but that it actually stops just before reaching threshold [cf. Eq. (7)] — the faster growth of the population brings the intensity closer to the final operating condition, thereby reducing the time intervening between the crossing of threshold and the occurrence of the peak. The consequence of this is a (small) reduction of the overshoot height, accompanied by a small contribution in the reduction of the delay time.

Before concluding, we remark that the optimal value for the control to obtain the minimum overshoot can also be found by keeping the control height, P_c, constant and varying its duration t_c. Indeed, if we approximate Eq. (2) to first order in εt_c and equate it to the expression for the optimal value of D_c, Eq. (7), under the further assumption that the laser is initially very close to threshold ($D_{\text{off}} \approx 1$), we obtain an approximate "area law" of

the form:

$$\lambda_c t_c = \frac{1 - D_{\text{off}}}{\varepsilon} - \lambda_{\text{on}}(\bar{t} - t_c)\,, \qquad (8)$$

whose validity, however, is limited to short times (because of the approximation of the exponential time dependencies). This "area law" can be numerically verified to an acceptable degree even with the five-dimensional CO_2 laser model, but the equivalence between the time duration and the step height in the control exists only under very restrictive conditions. In general, a better degree of control is obtained by changing the step height, as we have found both numerically and experimentally.

In conclusion, we have seen that a very simple control technique, based on the introduction of an intermediate flat level in the pump parameter, is quite effective in reducing the class B laser's delay time at turn-on and, under suitable conditions, even in lowering the height of the intensity overshoot. The advantage of such a simple nonfeedback technique is that it could be implemented on very fast systems — e.g. semiconductor lasers — where, at present, any other technique of influencing transients is unrealizable. In spite of the potential technological difficulties that can be encountered in the implementation of even such a simple method, its applications could be rather far reaching. For instance, used to reduce the delay time at turn-on, it would permit faster modulation and higher bit transmission rates in VCSELs.

We are grateful to I. Boscolo for the collaboration and to C. Green and J. R. Tredicce for earlier developments and discussions. P. A. Porta has been a recipient of an Erasmus scholarship of the European Union.

References

Abraham, N. B., Lugiato, L. A. & Narducci, L. M. (eds.) [1985] "Instabilities in active optical media," Special Issue of the *J. Opt. Soc. Am.* **B2**(1), 5–264.

Arecchi, F. T. & Degiorgio, V. [1972] "Measurement of the statistical properties of optical fields," in *Laser Handbook*, eds. Arecchi, F. T. & Schulz-Dubois, E. O. (North Holland, Amsterdam), pp. 191–264.

Arecchi, F. T., Politi, A. & Ulivi, L. [1982] "Stochastic-time description of transitions in unstable and multistable systems," *Nuovo Cimento* **71B**, 119–154.

Arimondo, E., Casagrande, F., Lugiato, L. A. & Glorieux, P. [1983] "Repetitive passive Q-switching and bistability in lasers with saturable absorbers," *Appl. Phys.* **B30**, 57–77.

Balestri, S., Ciofini, M., Meucci, R., Arecchi, F. T., Colet, P., San Miguel, M. & Balle, S. [1991] "CO_2 laser with swept pump parameter: The nonlinear regime," *Phys. Rev.* **A44**, 5894–5897.

Balle, S., Colet, P. & San Miguel, M. [1991] "Statistics for the transient response of single-mode semiconductor laser gain switching," *Phys. Rev.* **A43**, 498–506.

Balle, S., San Miguel, M., Abraham, N. B., Tredicce, J. R., Alvarez, R., D'Angelo, E. J., Gambhir, A., Thornburg, K. S. & Roy, R. [1994] "Transients in multivariable dynamical systems depend on which parameter is switched as illustrated in lasers," *Phys. Rev. Lett.* **72**, 3510–3513.

Bandy, D. K., Oraevski, A. N. & Tredicce, J. R. (eds.) [1988] "Nonlinear dynamics of lasers," Special Issue of the *J. Opt. Soc. Am.* **B5**(5), 879–1215.

Bielawski, S., Derozier, D. & Glorieux, P. [1994] "Controlling unstable periodic orbits by a delayed continuous feedback," *Phys. Rev.* **E49**, R971–R974.

Boccaletti, S., Farini, A., Kostelich, E. J. & Arecchi, F. T. [1997] "Adaptive targeting of chaos," *Phys. Rev.* **E55**, R4845–R4848.

Ciofini, M., Lapucci, A., Meucci, R., Wang, P.-Y. & Arecchi, F. T. [1992] "Two-peak passage-time distributions in transient CO_2 lasers near threshold," *Phys. Rev.* **A46**, 5874–5878.

Ciofini, M., Politi, A. & Meucci, R. [1993] "Effective two-dimensional model for CO_2 lasers," *Phys. Rev.* **A48**, 605–610.

Grassi, H., Green, C., Hoffer, L. M., Lippi, G. L. & Tredicce, J. R. [1994] "Experimental study of the turn-on statistics of class-B lasers under the influence of additive noise," *Phys. Rev.* **A50**, 805–812.

Hunt, E. R. [1991] "Stabilizing high-period orbits in a chaotic system: The diode resonator," *Phys. Rev. Lett.* **67**, 1953–1956.

Kotomtseva, L. A., Naumenko, A. V., Samson, A. M. & Turovets, S. I. [1997] "Targeting unstable orbits and steady states in class-B lasers by using simple off/on manipulations," *Opt. Commun.* **136**, 335–349.

Lippi, G. L., Hoffer, L. M. & Puccioni, G. P. [1997] "Noise at the turn-on of a class-B laser," *Phys. Rev.* **A56**, 2361–2372.

Meucci, R., Ciofini, M. & Wang, P.-Y. [1992] "Analysis of the dynamical behavior of a Q-switched CO_2 laser: The linear and nonlinear regime," *Opt. Commun.* **91**, 444–452.

Oppo, G.-L., Tredicce, J. R. & Narducci, L. M. [1989] "Dynamics of vibro-rotational CO_2 laser transitions in a two-dimensional phase space," *Opt. Commun.* **69**, 393–397.

Ott, E., Grebogi, C. & Yorke, J. A. [1990] "Controlling chaos," *Phys. Rev. Lett.* **64**, 1996–1999.

Ott, E. & Spano, M. [1995] "Controlling chaos," *Phys. Today* **48**(5), 34–40.

Petrov, V. & Showalter, K. [1996] "Nonlinear control of

dynamical systems from time series," *Phys. Rev. Lett.* **76**, 3312–3315.

Roy, R., Murphy Jr., T. W., Maier, T. D., Gills, Z. & Hunt, E. R. [1992] "Dynamical control of a chaotic laser: Experimental stabilization of a globally coupled system," *Phys. Rev. Lett.* **68**, 1259–1262.

Shinbrot, T., Grebogi, C., Ott, E. & Yorke, J. A. [1993] "Using small perturbations to control chaos," *Nature* **363**, 411–417.

Siegman, A. E. [1986] *Lasers* (University Science Books, Mills Valley, CA), Chapter 13, pp. 505–511.

Tredicce, J. R., Arecchi, F. T., Lippi, G. L. & Puccioni, G. P. "Instabilities in lasers with an injected signal," *J. Opt. Soc. Am.* **B2**, 173–183.

Turovets, S. I., Valle, A. & Shore, K. A. [1997] "Effects of noise on the turn-on dynamics of a modulated class-B laser in the generalized multistability domain," *Phys. Rev.* **A55**, 2426–2434.

Witteman, W. J. [1987] *The CO_2 laser*, ed. Shimoda, K., Springer Series in Optical Sciences, Vol. 53, (Springer, Berlin).

Worthing, A. G. & Geffner, J. [1943] *Treatment of Experimental Data* (Wiley, NY).

International Journal of Bifurcation and Chaos, Vol. 8, No. 9 (1998) 1821–1830

SYNCHRONIZATION OF A NETWORK OF CHAOTIC NEURONS USING ADAPTIVE CONTROL IN NOISY ENVIRONMENTS

BERNARD CAZELLES*
CNRS URA 258, Université Pierre et Marie Curie,
7 quai Saint Bernard, Case 237, 75252 Paris, France
and
UFR de Biologie, Université Paris 7-Denis Diderot

Received July 31, 1997; Revised November 28, 1997

The synchronization of chaotic systems have received an increasing interest in the last few years. In an attempt to understand some of the possible mechanisms of synchronization of neurons in a noisy environment, the present study extends a control method which is based on the Kalman filter. This adaptive control mechanism is able to modulate the frequency and the clustering behavior of a network of neurons and can thus make the network switch dynamically to different rhythmic activity, leading to different coding possibility.

1. Introduction

Individual neurons often exhibit temporal chaotic behavior as observed in the characteristics of intracellular voltage measurements [Aihara & Matsumoto, 1986; Mpitsos *et al.*, 1988; Hayashi & Ishizuka, 1992; Abarbanel *et al.*, 1996]. Individual neurons generate chaotic oscillations but groups of coupled neurons can display quasiperiodic synchronous rhythmic activity. Such dynamics are typical for many neurons in cortex and small neural systems like central pattern generators that control the rhythmic motor behavior of animals [Eckhorn *et al.*, 1988; Singer, 1993; Fujii *et al.*, 1996]. Physiological studies have accumulated evidence indicating the existence of synchronous rhythmic activity in different areas of the brain of some animals [Gray *et al.*, 1989; Engel *et al.*, 1990; Bressler *et al.*, 1993; Whittington *et al.*, 1995; Neuenschwander & Singer, 1996] and in some other small neural system [Dickinson *et al.*, 1990; Meyrand *et al.*, 1991; Wu *et al.*, 1994]. For instance, based on *in vitro* experiments on the stomastogastric nervous system of a crustacea, Meyrand *et al.* [1991] have reported that under an identified neuromodulatory stimulus, neurons operating independently as members of differents networks may be reconfigured into a new pattern-generating network that oscillates coherently but differently from the original networks. Moreover, it is commonly assumed that every cognitive action is mediated by the coherent activity of neuron groups at multiple locations and it has been suggested [Eckhorn *et al.*, 1988; Singer, 1993; Gray & McCormick, 1996; Fujii *et al.*, 1996; MacLeod & Laurent, 1996] that this synchronous activity may have a role in solving the so-called binding problem.

So some coordination or synchronization of these chaotic individual activities must be arranged for a directed functional behavior that

*Address for correspondence: CNRS URA 258, Université Pierre et Marie Curie, 7 quai Saint Bernard, Bât. A, 7ème étage, Case 237, F-75252 Paris Cedex 05, France.
E-mail: bcazelle@snv.jussieu.fr

have cooperative properties related to the function performed. The cooperative behavior of these coupled neurons can be much richer and much more organized than the activity of the individual neurons forming network. A fundamental question that remains open is how such assemblies are transiently self-synchronized for each specific task. In this view recent findings in the field of nonlinear dynamical systems are very promising, opening the possibility of controlling [Ott *et al.*, 1990; Shinbrot *et al.*, 1993; Chen & Dong, 1993] and synchonizing [Pecora & Carroll, 1990; Rulkov *et al.*, 1995] chaotic dynamics. It has been shown that two identical chaotic systems can be synchronized by applying small temporal perturbations (parameter or variable perturbations) to one of them [Pyragas, 1992; Lai & Grebogi, 1993; Cazelles *et al.*, 1995].

There has been some work on applying control techniques to networks of model neurons. Sepulchre and Babloyantz [1993] have used the Ott–Grebogi–Yorke control technique in a high dimensional network of coupled neurons and shown that higher dimensional control is possible. Lourenço and Babloyantz [1994] have used the Pyragas method to stabilize the unstable periodic orbits of the chaotic dynamics of network neurons of moderate size. A pulse control scheme that requires less knowledge of the system than an Ott–Grebogi–Yorke control technique is used by Carroll [1995a, 1995b] to control and synchronize the dynamics of a network of four neurons described by a modified version of the FitzHugh–Nagumo equations. Carroll [1995b] has shown that for some coupling configuration the group of neurons are only partially synchronized even though all groups share a common drive. Güémez and Matias [1996] have studied different coupling of small groups of simple chaotic neuron models which are synchronized by applying proportional perturbations to the dynamical variables of the system. Their method suppresses chaos in each neuron, yielding to a particular periodic or quasiperiodic dynamics. Abarbanel and his group [Abarbanel *et al.*, 1996; Huerta *et al.*, 1997] investigate the variation of the rhythmic activity produced by two coupled chaotic Hindmarsh–Rose neurons. They showed that sufficiently strong inhibitory coupling between chaotic neurons organizes regular out-of-phase rhythmic behavior and that the change of the strength of the inhibitory coupling is responsible for the variations in the number of spikes in each burst.

The purpose of the present work is to extend a previous work [Cazelles *et al.*, 1997] to the case of a network of model neurons. These previous works have pointed out that adaptive control even in noisy environment can provide a mechanism that permits a network of chaotic elements to modify or stabilize its clustering behavior and can be necessary to maintain a network at a desired ordered state. These control mechanisms can also induce transition from high dimensional disordered motion to coherent synchronized pattern via feedback parameter perturbations. The adaptative control method [Cazelles *et al.*, 1995] is based on the Extended Kalman Filter (EKF). This method progressively adapts the system parameters and/or the system variables to tune the dynamics towards a target behavior, taking into account uncertainties both in the system behavior and in the goal behavior.

Depending on the parameters of the model network, different types of clustering behaviors from synchronized to completely desynchronized and different types of dynamics from quasiperiodic to chaotic can be observed from a single network of neurons. In response to a certain external stimulus the network could modify its clustering behavior and the firing frequencies of the neurons. The modification of the rhythmic activity of the network is obtained by applying the EKF to force the neurons of the network to imitate a target dynamics, which could be the dynamics of a pacemaker cell which would want to impose its behavior on the network. Maintenance of an "optimal" functioning of these neural systems depends on their capacities of extracting pertinent information which is embedded in large noise. The key feature of this approach is to cope with this kind of noise to permit synchronization (for example) in spite of environmental changes and in the presence of large noise in the dynamics of the pacemaker.

This article is organized as follows. In Sec. 2 the models used are presented and the EKF approach as a parametric adaptive control method is summarized. In the first part of Sec. 3 the dynamics of individual neurons are reported as the dynamics and the clustering behavior of the network. The second part of Sec. 3, after providing the conditions required to apply the control method, reports on how the degree of synchronization or the degree of chaos is modified as the parameters of the neurons are controlled. Finally, the last section is devoted to some concluding remarks.

2. Methods

2.1. *Models*

Actual neurons are quite complicated and for many years, simple approximate models of neurons have been used to understand their basic function. It has been shown in many cases that simple models can adequately reproduce some of the basic features behind the firing dynamics of neurons (see e.g. [Hoppensteadt, 1986]). The aim of the present work is to modify the synchronized dynamics of a network of neurons and also the firing frequency by adaptive control. So a simple model that reproduces the basic features should be sufficient and in this present work, I used the Chialvo model [Chialvo & Apkarian, 1993; Chialvo, 1995] which has a neuron like dynamics and was found to agree qualitatively with experiments reported in previous works [Aihara & Matsumoto, 1986]. The model is a two-dimensional map written in the form:

$$\begin{aligned} x(t+1) &= x(t)^2 \cdot \exp(y(t) - x(t)) + k \\ y(t+1) &= a \cdot y(t) - b \cdot x(t) + c \end{aligned} \tag{1}$$

where the x variable is related to an instantaneous membrane potential of the neuron and the y variable is equivalent to a recovery current. This model has four parameters, a determines the time constant of reactivation, b the activation dependence of the recovery process and c the maximum amplitude of the recovery current. The parameter k can be viewed either as a constant bias or as a time-dependent external stimulation.

To simulate a network of neurons, each individual neuron is connected through a global coupling by the membrane potentials. One obtains globally coupled maps which are a dynamics of N individual cells evolving according to local mappings and a "mean-field" interaction, the global information influencing each individual cell. These maps are analogous to a "mean-field" version of coupled map lattices [Kaneko, 1989] in which the short-range coupling (nearest-neighbor diffusion) is replaced by a long-range coupling resulting from a feedback from the "mean-field" [Kaneko, 1992]. The model of the network of neurons is written as:

$$\begin{aligned} \bar{x}(t) &= (1-\varepsilon) \cdot x_i(t) + \frac{\varepsilon}{N} \cdot \sum_{j=1}^{j=N} x_j(t) \\ x_i(t+1) &= \bar{x}(t)^2 \cdot \exp(y_i(t) - \bar{x}(t)) + k \\ y_i(t+1) &= a \cdot y_i(t) - b \cdot x_i(t) + c \end{aligned} \tag{2}$$

where t is a time index, i a neuron index, N the number of neurons in the network, and ε the coupling strength between neurons.

2.2. *The extended Kalman filter as an adaptive control method*

The basic idea of our control algorithm is to apply perturbations in the accessible system parameters to bring the system back to a desired state [Cazelles *et al.*, 1995]. The adaptive control applies recursively to the system, an external force based on the difference between the actual output and a target behavior. This external force takes into account the correspondence between parameter values and behavior types, the goal parameter value corresponds to the dynamics of the goal behavior. This control method thus synchronizes the system dynamics with a target behavior. Various methods can be used for this task but the Kalman filter makes it possible to account for noise (uncertainties) both in the model and in the target dynamics.

The evolution of the discrete nonlinear system (network of neurons in this study) is given by:

$$\mathbf{X}(t+1) = f(\mathbf{X}(t), \mu) + \xi(t) + \text{External Force} \tag{3}$$

$\mathbf{X}(t)$ is the n-vector of state variables, μ is the j-vector of model parameters subject to control, f is a nonlinear map defined in (2) and $\xi(t)$ the system noise (Gaussian noise with zero mean and variance matrix $\mathbf{Q}$). The external force is computed by the Kalman control procedure.

The target dynamics are produced by a reference model, a pacemaker cell that has the same dynamics as the individual neurons (1) but with constant parameter goal value μ_g. The underlying model of the target behavior is unknown for the system and only observations of the target behavior are available. An observation equation is defined:

$$\mathbf{Y}(t+1) = h(\mathbf{X}(t), \mu_g) + \eta(t) \tag{4}$$

where $\mathbf{Y}(t)$ is the m-vector of observations, h the function which defines the relation between state variables ($\mathbf{X}$) and observations ($\mathbf{Y}$) and $\eta(t)$ the observation noise (Gaussian noise with zero mean and variance matrix $\mathbf{R}$) which can be interpreted as an error caused by a noisy environment.

In (3) the accessible system parameter μ operates as the control input driving the system to its target regime defined by noisy observations $\mathbf{Y}(t)$.

The change of the parameter vector μ is defined according to:

$$\mu(t+1) = \mu(t) + \xi(t) \tag{5}$$

with $\xi(t)$ being the parameter noise.

The state equation (3) is increased by the expression (5) for the parameter dynamics and can be easily incorporated into a state-space framework as follows:

$$\mathbf{X}_a(t+1) = f(\mathbf{X}_a(t)) + \xi(t) \tag{6a}$$

$$\mathbf{Y}(t) = h(\mathbf{X}_a(t), \mu_g) + \eta(t) \tag{6b}$$

where the increased state-parameter vector $\mathbf{X}_a$ is defined as: $\mathbf{X}_a^{\mathrm{T}} = [\mathbf{X}_a^{\mathrm{T}}, \mu^{\mathrm{T}}]$.

Originally, the Kalman filter is conceived for linear models and for nonlinear models a linearized system using the first order Taylor series expansion led to the "extended Kalman filter" (EKF) [Anderson & Moore, 1979]. EKF makes incremental corrections of the state-parameter vector at time t to guide the system towards the target observation vector of state-variables. For more biological realism, as in the work of Carroll [1995a, 1995b] only a pulse control has been performed. The corrections have been computed only when there is a spike in the target observations. The recursive form of the algorithm can be written as the following scheme:

- Prediction of the states' mean and variance:

$$\mathbf{X}_a(t+1|t) = f(\mathbf{X}_a(t|t))\,, \tag{7}$$

$$\mathbf{P}(t+1|t) = \Phi(t+1|t) \cdot \mathbf{P}(t|t) \cdot \Phi(t+1|t)^{\mathrm{T}} + \mathbf{Q}\,. \tag{8}$$

- Correction of the states' mean and variance, only if there is a spike in the target dynamics:

$$\mathbf{X}_a(t+1|t+1) = \mathbf{X}_a(t+1|t) + \mathbf{K} \cdot [\mathbf{Y}(t+1) - h(\mathbf{X}_a(t+1|t))]\,, \tag{9}$$

$$\mathbf{P}(t+1|t+1) = [\mathbf{I} - \mathbf{K} \cdot \mathbf{H}(t)] \cdot \mathbf{P}(t+1|t) \cdot [\mathbf{I} - \mathbf{K} \cdot \mathbf{H}(t)]^{\mathrm{T}} + \mathbf{K} \cdot \mathbf{R} \cdot \mathbf{K}^{\mathrm{T}}\,. \tag{10}$$

In the above equations, the notation $(t|t)$ indicates an estimation at time t conditionally to all of the observations up to and including those available at t; and superscript "T" denotes matrix transpose; $\mathbf{P}$ is the variance matrix of the state-parameter estimation errors; $\mathbf{Q}$ is the variance matrix of the state-parameter noises; $\mathbf{R}$ the variance matrix associated with the noise of the target behavior, Φ and $\mathbf{H}$ are the jacobian matrices associated with the linearized form of the maps f and h; the term $\mathbf{K} \cdot [\mathbf{Y}(t+1) - h(\mathbf{X}_a(t+1|t))]$ represents the *External Force* (3) with $\mathbf{K}$ the Kalman gain matrix:

$$\mathbf{K} = \mathbf{P}(t+1|t) \cdot \mathbf{H}^{\mathrm{T}}(t+1) \cdot [\mathbf{H}(t+1) \cdot \mathbf{P}(t+1|t) \cdot \mathbf{H}^{\mathrm{T}}(t+1) + \mathbf{R}]^{-1} \tag{11}$$

3. Results and Discussion

3.1. *Neuron and network dynamics*

The individual neuron model used exhibits a rich dynamics, for example modifying the parameter b, one obtains either fixed point, periodic,

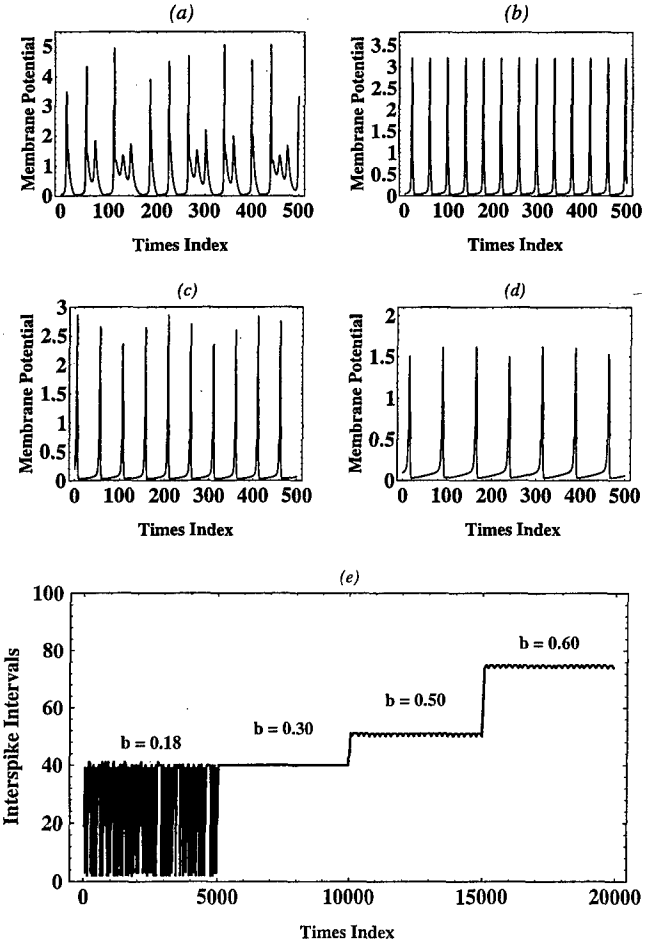

Fig. 1. Dynamics of the Chialvo model. Time evolution of the membrane potential with (a) $b = 0.18$, (b) $b = 0.30$, (c) $b = 0.50$ and (d) $b = 0.60$. Time series of the interspike intervals (e) obtained with different b values.

quasiperiodic or chaotic dynamics [Figs. 1(a)–1(d)] [Chialvo, 1995; Güémez & Matias, 1996]. But more interesting from a neurophysiological point of view, when modifying the dynamics of the model the interspike interval is also modified; with b egal 0.18 one has interspike interval chaotic time series and with higher values one has fixed interspike intervals. But increasing the parameter b, the interspike intervals are increased, decreasing the firing frequency of the neuron [Fig. 1(e)]. It is particularly interesting because some neurobiologist conjectures that the firing frequency of a neuron acts as neural coding [Fujii *et al.*, 1996; MacLeod & Laurent, 1996].

Chaotic globally coupled maps, as our network model, are known to have two conflicting trends: destruction of coherence due to the chaotic divergences of individual oscillator and a synchronization force through global averaging. In a globally coupled chaotic system, the following clustering phases can appear [Kaneko, 1992]: (i) a coherent phase where all oscillators are synchronized; (ii) an ordered phase with few clusters in which each oscillator is synchronized; (iii) a partially ordered phase with many coexisting clusters and (iv) a turbulent phase where all oscillators have their own dynamics. Figure 2 displays an overview of the clustering behavior and of the temporal dynamics of a network with 50 neurons (with 100 neurons quite similar results are observed). The clustering behavior diagram [Fig. 2(a)] is obtained by counting the numbers of different x values (membrane potential) for final attractor when 10000 points have been discharged. On one randomly chosen neuron, the temporal dynamics [Fig. 2(b)] is approximate by counting the number of different spikes for the last 5000 iterations. In function of the coupling strength, ε, and of the parameter, b, the behavior of the network varies from a phase of completely incoherent chaotic behavior, through phases of partial synchronization to a global synchronization phase whereas the temporal dynamics can be chaotic, quasiperiodic or regular.

Thus modifying the activation dependence of the recovery process, b, or the coupling strength, ε, by adaptive control, one can induce different clustering behavior and different firing frequencies of the network thus modifying and arranging the coding possibilities of the network.

3.2. *Modification of the clustering behavior of the network*

Different types of clustering behaviors from synchronized to completely desynchronized and different types of dynamics from quasiperiodic to chaotic can be obtained from a single network of neurons (Fig. 2). This opens the possibility of controlling the degree of chaos or the degree of synchronization of a network, by modifying either the parameters of each individual neuron or the coupling strength among neurons. In this work, I focus on modifying the activation dependence of the recovery process, b, by applying the Kalman control process described above. To use the EKF procedure, one must specify the target dynamics and matrices $\mathbf{Q}$ and $\mathbf{R}$: (i) An external signal, the dynamics of a pacemaker cell which would want to impose its behavior on the network is used for observations (the target behavior); (ii) the variance matrix $\mathbf{Q}$ of the state-parameter noises will take on values between 5% and 10% of the mean of the network dynamic; (iii) the variance matrix of the observation error $\mathbf{R}$ will take on the same values as $\mathbf{Q}$, in the absence of noise; if observations (the target behavior) are corrupted by noise, the variance of the additive noise will be assigned to $\mathbf{R}$.

At one time, I chose to synchronize an initially chaotic and turbulent network of 50 identical neurons ($b = 0.18$) with low coupling strength ($\varepsilon = 0.02$) to the dynamics of a pacemaker characterized by a quasiperiodic behavior ($b_g = 0.25$). Figure 3 illustrates this example: Fig. 3(a) displays the parameter adaptation; Fig. 3(b) shows the dynamics of the 50 neurons and Fig. 3(c) the decimal logarithm of the difference between the membrane potential of one randomly chosen neuron and the membrane potential of the pacemaker cell. The network and the pacemaker cell dynamics originally behaved quite differently. As soon as the control action is switched on at time index egal 100, the parameter value b starts converging towards the goal value b_g [Fig. 3(a)] and the trajectories become fully synchronized [Fig. 3(b)], the difference between the two signals (network and pacemaker) decreased dramatically [Fig. 3(c)]. At time index 400 the target behavior is modified, the new driven pacemaker cell have a quasiperiodic behavior with low firing frequency ($b_g = 0.50$). Once again the network is quickly resynchronized to the new rhythmic activity by the adaptive controller.

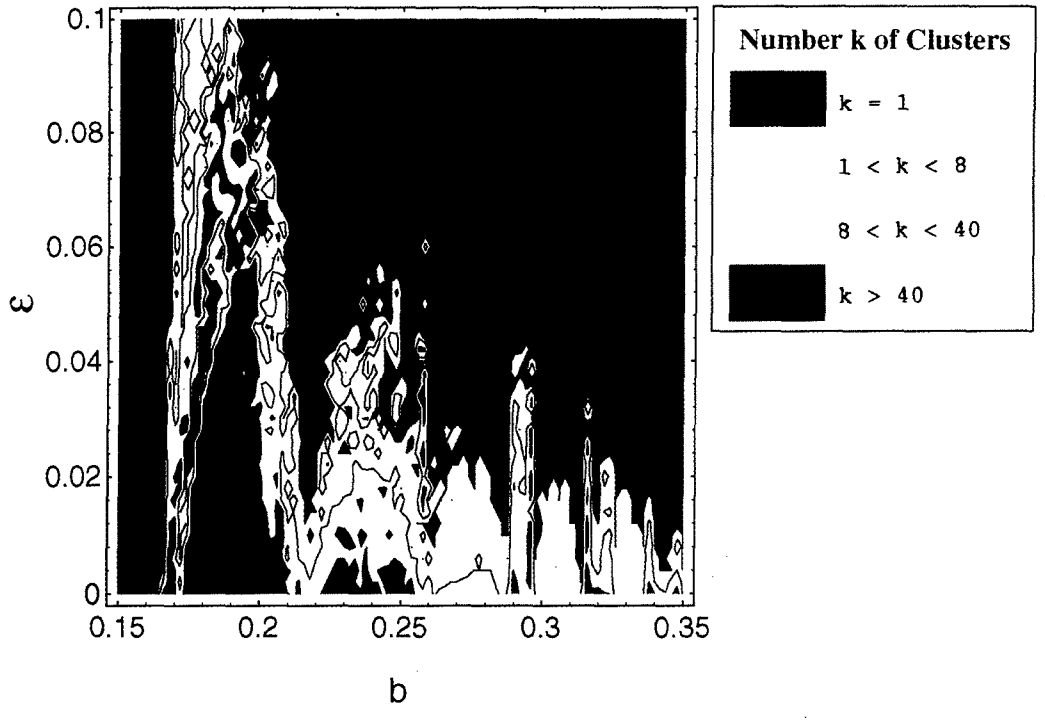

(a)

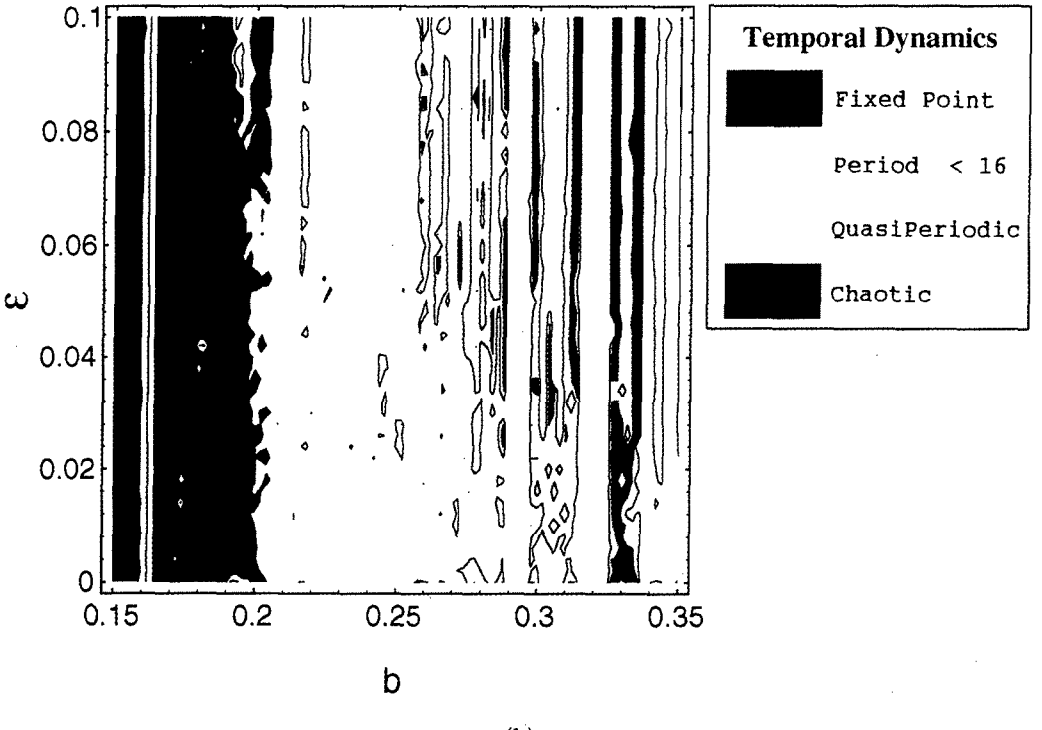

(b)

Fig. 2. Phase diagram for a network of 50 neurons. Part (a) shows the clustering behavior and part (b) the temporal dynamics of the network. The numbers of clusters, k, have been obtained by counting for the final attractor the numbers of different x values (membrane potential) when 10000 points have been discharged. Temporal dynamics of the network have been approximated by counting on one randomly chosen neuron the number of different spikes for the last 5000 iterations. All calculus were carried out by incrementing the parameters b and ε by 0.001.

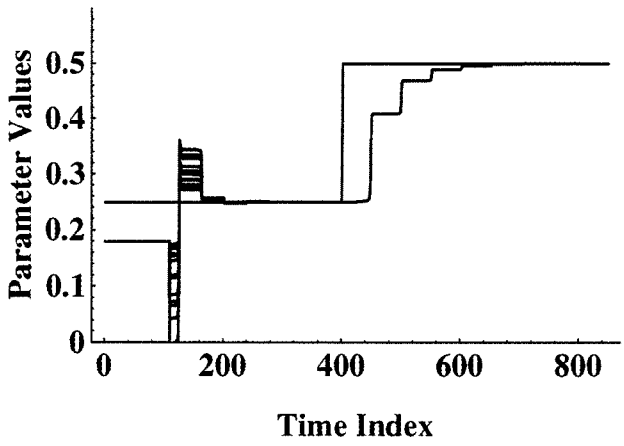

(a)

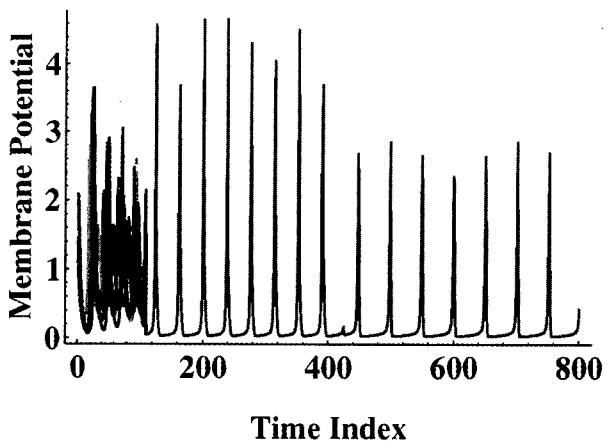

(b)

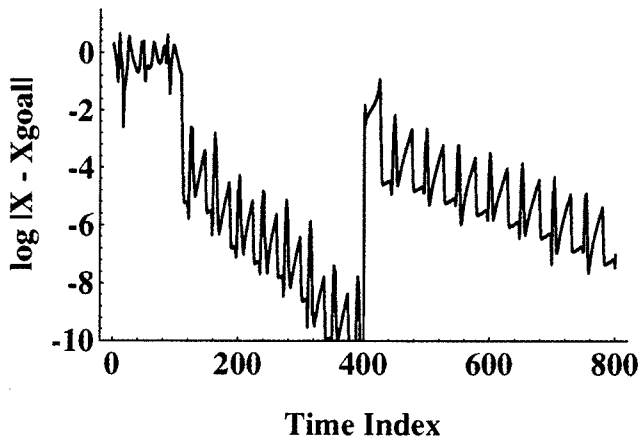

(c)

Fig. 3. Synchronization of a chaotic turbulent network of identical neurons ($N = 50$, $b = 0.18$ and $\varepsilon = 0.02$) to the dynamics of a pacemaker cell characterized by a quasiperiodic behavior ($b_g = 0.25$ and $b_g = 0.50$). The control is active at time index 100 and at time index 400 the dynamics of the pacemaker cell is modified. (a) Parameter adaptation (blue lines: parameter of each neuron; red line: parameter of the pacemaker cell which defined the target dynamics). (b) Time series of the 50 neurons. (c) Time evolution of the log of the absolute value of the difference between the membrane potential (X) of one randomly chosen neuron and the membrane potential (X_{goal}) of the pacemaker cell.

At each time, after 3 or 4 pacemaker spikes the parameter convergence is complete and the dynamics of the network is fully synchronized to the rhythmic activity of the pacemaker cell.

The robustness of the method used when noise is added to the target behavior have been tested. The noise intensity is characterized by the signal to noise ratio (SNR) which is the standard-deviation of the reference dynamics (noise-free target behavior) divided by the standard-deviation of noise. Figure 4 displays the parameter adaptation and the behavior of an initially chaotic and turbulent network ($b = 0.18$, $\varepsilon = 0.02$) that is control to a target behavior with a quasiperiodic synchronized behavior ($b_g = 0.25$). For each neuron of the network, the dynamics of the pacemaker cell is spoiled by large additive noise (SNR = 5.00). As in the previous noiseless example, despite the large noise, the control successfully drives the parameter b towards the goal value b_g and the network presents a synchronous rhythmic activity [Fig. 4(c)]. Figure 4(a) displays the parameter adaptation, Figs. 4(b) and 4(c) show the networks' behavior before and after controlling.

Similar results (not showed) are obtained with other values of the coupling strength (ε) or the activation dependence parameter (b), for example with chaotic synchronized or with two-cluster

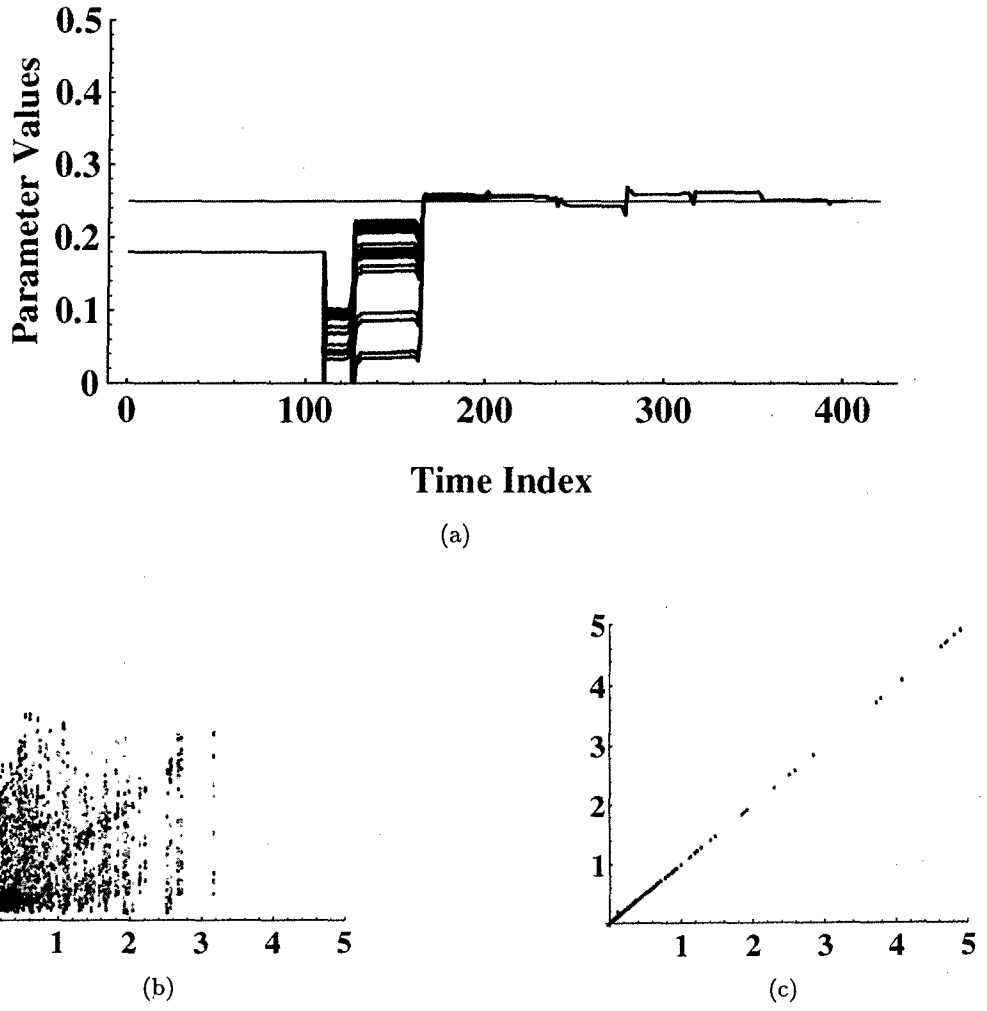

Fig. 4. Synchronization of a chaotic turbulent network of identical neurons ($N = 50$, $b = 0.18$ and $\varepsilon = 0.02$) to the dynamics of a pacemaker cell characterized by a quasiperiodic behavior ($b_g = 0.25$). For each neuron, the target behavior is spoiled by a large additive white noise characterized by SNR = 5.00 (7.0 dB). The control is active at time index 100. (a) Parameter adaptation (blue lines: parameter of each neuron; red line: parameter of the pacemaker cell). (b) Plot of the evolution of the first neuron of the network versus the 49 others before activation of the adaptive control. (c) Plot of the evolution of the first neuron of the network versus the 49 others after activation of the adaptive control (simulations were run over 400 iterations and the last 200 points are shown).

periodic target behavior. The parameter fluctuations produced by the adaptive controller stabilize the network momentarily into a coherent state with a given firing frequency, more appropriate for a specific information task. This behavior may explain short episodes of synchronization of the assembly of neurons at different firing frequency even when the external signal is embedded by large noise. At each time, synchronizations arise only from the action of an adaptive controller driven by an external input, the pacemaker cell. These synchronizations occur in sufficient short time scales that it may be reasonable to think that they could be explained by electrophysiological mechanisms.

4. Conclusion

Neuronal sensory systems of living organisms are capable of dealing with noisy signals. An important issue in neurosciences is the study of the ability of neuronal systems to cope with uncertainty and the lack of precision which arises from different sources of perturbations. Temporal coherence or synchronous firing, postulated as a mechanism for functional organization of the assembly of neurons and as a potential neural code.

In an attempt to understand some of the possible mechanisms of synchronization of neurons in a noisy environment, this paper reports on an

adaptive control mechanism which is able to modulate the frequency and the clustering behavior of an assembly of neurons. The adaptive control method used is analogous to a learning process: by comparing the system dynamics with a target behavior and by correcting its dynamics, the system learns to adapt itself in so as to recover the target dynamics, which could be the dynamics of a pacemaker cell. Adaptive control of coupled neurons may be an analogous mechanism to mediate the general process which is responsible for dynamical "linking" and "unlinking" of neurons into varying coherent groups. This controller can thus make the assembly of neurons switch dynamically to different rhythmic activity (e.g. from noncoherent to synchronized, from chaotic to periodic), leading to different coding possibility.

The framework of control and synchronization of chaos seems promising for the treatment for the description of rapid changes in the dynamics of neuronal networks. If the assembly of neurons could be viewed as a network with spatiotemporal chaotic activity then rapid transition between states of different synchronized activity could be a framework that enables us to propose a mechanism for understanding some aspects of neural dynamics and recent works go along these lines [Lourenço & Babloyantz, 1994; Caroll, 1995a, 1995b; Güémez & Matias, 1996; Abarbanel *et al.*, 1996; Huerta *et al.*, 1997].

References

Abarbanel, H. D. L., Huerta, R., Rabinovich, M. I., Rulkov, N. F., Rowat, P. F. & Selverston, M. [1996] "Synchronized action of synaptically coupled chaotic model neurons," *Neural Comput.* **8**, 1567–1602.

Aihara, K. & Matsumoto, G. [1986] "Chaotic oscillations and bifurcations in squid giant axons," in *Chaos*, ed. Holden, A. R. (Manchester University Press, Manchester), pp. 257–269.

Anderson, B. D. O. & Moore, J. B. [1979] *Optimal Filtering* (Prentice-Hall, Englewoods Cliffs).

Bressler, S. L., Coppola, R. & Nakamura, R. [1993] "Episodic multiregional cortical coherence at multiple frequencies during visual task performance," *Nature* **366**, 153–156.

Carroll, T. L. [1995a] "Synchronization and complex dynamics in pulse-coupled circuits models of neurons," *Biol. Cybern.* **73**, 553–559.

Carroll, T. L. [1995b] "Controlling a chaotic array of pulse-coupled circuits," *Phys. Rev.* **E52**, 5817–5824.

Cazelles, B., Boudjema, G. & Chau, N. P. [1995] "Adaptive control of chaotic systems in a noisy environment," *Phys. Lett.* **A196**, 326–330.

Cazelles, B., Boudjema, G. & Chau, N. P. [1997] "Adaptive synchronization of globally coupled chaotic oscillators using control in noisy environments," *Physica* **D103**, 452–465.

Chen, G. & Dong, X. [1993] "From chaos to order — Perspectives and methodologies in controlling chaotic nonlinear dynamical systems," *Int. J. Bifurcation and Chaos* **3**, 1363–1409.

Chialvo, D. R. & Apkarian, A. V. [1993] "Modulated noisy biological dynamics: Three examples," *J. Stat. Phys.* **70**, 375–391.

Chialvo, D. R. [1995] "Generic excitable dynamics on a two-dimensional map," *Chaos, Solitons and Fractals* **5**, 461–479.

Dickinson, P. S., Mecsas, C. & Marder, E. [1990] "Neuropeptide fusion of two motor-pattern generator circuits," *Nature* **344**, 155–158.

Eckhorn, R., Bauer, R., Jordan, W., Brosch, M., Kruse, W., Munk, M. & Reitboeck, H. J. [1988] "Coherent oscillations: A mechanism for feature linking in the visual cortex? Multiple electrode and correlation analyses in the cat," *Biol. Cybern.* **60**, 121–130.

Engel, A. K., König, P., Gray, C. M. & Singer, W. [1990] "Stimulus-dependant neuronal oscillations in cat visual cortex: Inter-columnal interaction as determinated by cross-correlation analysis," *Eur. J. Neurosci.* **2**, 588–606.

Fujii, H., Ito, H., Aidhara, K., Ichinose, N. & Tsukada, M. [1996] "Dynamical cell assembly hypothesis-theoretical possibility of spatio-temporal coding in the cortex," *Neural Networks* **9**, 1303–1350.

Gray, C. M., Koenig, P., Engel, A. K. & Singer, W. [1989] "Oscillatory responses in cat visual cortex exhibit inter-columnar synchronization which reflects global stimuls properties," *Nature* **338**, 334–337.

Gray, C. M. & McCormick, D. A. [1996] "Chattering cells: Superficial pyramidal neurons contributing to the generation of synchronous oscillations in the visual cortex," *Science* **274**, 109–113.

Güémez, J. & Matias, M. A. [1996] "Synchronous oscillatory activity in assemblies of chaotic model neurons," *Physica* **D96**, 334–343.

Hayashi, H. & Ishizuka, S. [1992] "Chaotic nature of bursting discharges in the Onchidium pacemaker neuron," *J. Theor. Biol.* **156**, 269–291.

Hoppensteadt, F. C. [1986] *An Introduction to the Mathematics of Neurons* (Cambridge University Press, Cambridge).

Huerta, R., Rabinovich, M. I., Abarbanel, H. D. L. & Bazhenov, M. [1997] "Spike-train bifurcation scaling in two coupled chaotic neurons," *Phys. Rev.* **E55**, R2108–R2110.

Kaneko, K. [1989] "Pattern dynamics in spatiotemporal chaos," *Physica* **D34**, 1–41.

Kaneko, K. [1992] "Mean field fluctuation of a network of chaotic elements," *Physica* **D55**, 368–384.

Lai, Y. C. & Grebogi, C. [1993] "Synchronization of chaotic trajectories using control," *Phys. Rev.* **E47**, 2357–2360.

Lourenço, C. & Babloyantz A. [1994] "Control of chaos in networks with delay: A model of synchronization of cortical tissue," *Neural Comput.* **6**, 1141–1154.

MacLeod, K. & Laurent, G. [1996] "Distinct mechanisms for synchronization and temporal patterning of odor-encoding neural assemblies," *Science* **274**, 976–979.

Meyrand, P., Simmers, J. & Moulins, M. [1991] "Construction of a pattern-generating circuit of different networks," *Nature* **351**, 60–63.

Mpitsos, G. J., Burton, R. M., Creech, H. C. & Soinla, S. S. [1988] "Evidence for chaos in spike trains of neurons that generate rhythmic motor patterns," *Brain Res. Bull.* **21**, 529–538.

Neuenschwander, S. & Singer, W. [1996] "Long-range synchronization of oscillatory light responses in the cat retina and lateral geniculate nucleus," *Nature* **379**, 728–733.

Ott, E., Grebogi, C. & Yorke, J. A. [1990] "Controlling chaos," *Phys. Rev. Lett.* **64**, 1196–1199.

Pecora, L. & Carroll, T. L. [1990] "Synchronization in chaotic systems," *Phys. Rev. Lett.* **64**, 821–824.

Pyragas, K. [1992] "Continuous control of chaos by self-controlling feedback," *Phys. Lett.* **A170**, 421–428.

Rulkov, N. F., Sushchik, M. M., Tsimring, L. S. & Abarbanel, H. D. I. [1995] "Generalized synchronization of chaos in directionally coupled chaotic systems," *Phys. Rev.* **E51**, 980–994.

Sepulchre, J. A. & Babloyantz, A. [1993] "Controlling chaos in a network of oscillators," *Phys. Rev.* **E48**, 945–950.

Shinbrot, T., Grebogi, C., Ott, E. & Yorke, J. A. [1993] "Using small perturbations to control chaos," *Nature* **363**, 411–417.

Singer, W. [1993] "Synchronization of cortical activity and its putative role in the information processing and learning," *Annu. Rev. Physiol.* **55**, 349–374.

Whittington, M. A., Traub, R. D. & Jefferys, J. G. R. [1995] "Synchronized oscillations in interneurons networks driven by metabotropic glutamate receptor activation," *Nature* **373**, 612–615.

Wu, J. Y., Cohen, L. B. & Falk, C. X. [1994] "Neuronal activity during different behaviors in Aplysia: A distributed organization," *Science* **263**, 820–823.

International Journal of Bifurcation and Chaos, Vol. 8, No. 9 (1998) 1831–1838

NONLINEARITY TESTS USING THE EXTREMA OF A TIME SERIES

A. DI GARBO*, R. BALOCCHI† and S. CHILLEMI*
*Istituto di Biofisica CNR, Via S. Lorenzo 26, 56127 Pisa, Italy
†Istituto di Fisiologia Clinica CNR, Via Trieste 41, 56127 Pisa, Italy

Received July 31, 1997; Revised December 2, 1997

The analytical properties of the solution of a system of ODEs in the complex time plane influence its dynamical behavior on the real time axis. In particular, the extrema of the real time solution can be associated to the singularities of the complex solution falling close to the real time axis. Moreover for a twice differentiable stochastic process, the expected value of the number of extrema for unit time can be determined. These two results are used here as the starting point to introduce two new algorithms to test for time series nonlinearity. They do not require the phase space reconstruction protocol and seem to work well also for short data sets.

1. Introduction

The nonlinear analysis of time series is based on the theory of dynamical systems: It is assumed that the signal under examination is generated by a deterministic law. When experimental data are used, the analysis of time series becomes more difficult for the presence of noise. However it is generally assumed that the stochastic component in the signal is small and that it does not destroy completely the original properties of the bare (without stochastic perturbation) dynamical system. Since a nonlinear system can exhibit deterministic chaos a first step, in the analysis of an irregular signal, is to check whether its values are characterized by nonlinear time correlations. Understanding the nature of the dynamical processes responsible for the observed data is one of the most challenging and important problems in nonlinear time series analysis and several methods have been proposed to this aim [Abarbanel *et al.*, 1993]. Here we suggest the use of two new algorithms to detect nonlinearity in a stationary time series (that is to check whether nonlinear time correlations are present among the time series values) both based on the analysis of the extrema (local maxima and minima). Two theoretical considerations justify these algorithms. The first is connected to the theoretical and numerical results obtained in the study of systems of ordinary differential equations (ODEs). It has been shown that the dynamical behavior of the real time solution of an ODE is strongly connected to its analytic properties in the complex time plane, and in particular to the distribution of the singularities nearest to the real axis [Ramani *et al.*, 1989]. The second consideration arises from a general property of a stochastic process which states that given a mean-square differentiable stochastic process $x(t)$ the expected number of its extrema for unit time is contained in the joint density function of $x(t)$, $\dot{x}(t)$ and $\ddot{x}(t)$ [Soong, 1973]. These theoretical and numerical results suggest that the sequence of the extrema of a time series contains dynamical information on the

process responsible for its generation. The method of surrogate data was used to test if a suitable statistic evaluated on a sequence of extrema could be accounted for by a Gaussian linear stochastic process [Theiler *et al.*, 1992].

2. The Algorithms

2.1. *PSC algorithm*

The problem of establishing whether a system of ODEs is integrable or chaotic is generally difficult. During the last two decades some important theoretical results have been obtained: Of particular interest, a strong connection between the dynamical properties of the real time solution of an ODE and the analytical ones in the complex time plane, has been shown to exist [Ramani *et al.*, 1989]. The solutions of the Lorenz equations in the complex time plane, for different dynamical regimes, were studied both analytically and numerically [Tabor & Weiss, 1981]. It was found that the distribution of the singularities in the complex time plane is critical in determining the behavior of the real time solution. In particular, from the function theory of complex variables, it follows that the main contributions to the real time solution come from the nearest singularities to the real time axis. This last fact is justified by the Cauchy's integral formula for a function of complex variable $f(z)$ analytic and single-valued in a simply connected domain D: $\oint_\Gamma f(z)/(z-z_0)dz = 2\pi\imath f(z_0)$ where $\Gamma \in D$ and z_0 is enclosed whithin Γ. For a better clarification we just consider the example of the Duffing equation $\ddot{x} + a\dot{x} + x^3 = b\cos(t) + c$ where a, b, c are real constants. Let us consider initially the very simple case $a = b = c = 0$: $\ddot{x} + x^3 = 0$; we search for a solution of this equation over the complex time plane. It is easy to prove that a particular solution of this equation can be expressed by means of an elliptic function: $x_p(z) = \mathrm{cn}(z, 1/2)$, where $z = t + \imath\tau$; $x_p(z)$ is a double periodic function of z. In general the function $\mathrm{cn}(z, q)$, $q^2 < 1$, is analytic over the complex time plane except for the set of points $A = \{z_{m,n} = 2mK + \imath(2n+1)K' : m, n \in Z\}$ where polar singularities are present; K and K' are, respectively, the complete elliptic integral and its complementary (constants for a fixed q). From the definition of the set A it follows that the nearest singularities corresponding to the real time axis are those for which $n = 0$ and $n = -1$: This sequence of poles is regularly distributed on the complex time plane. Furthermore it can be shown that a polar singularity corresponds to each local maximum (or minimum) of the real time solution $x_p(t)$. Such regular distribution of singularities reflects the corresponding periodic behavior of the real time solution. What happens to the distribution of the singularities when the parameters a, b, c of the Duffing equation are not zero? If these parameters are chosen such that the behavior of its solution $x(z)$ on the real time axis is chaotic, then the corresponding sequence of singularities in the complex time plane associated to the local extrema becomes very irregular. A complete study on the properties of the solutions of the Duffing equation on the complex time plane can be found in [Konno & Tateno, 1984]. Other numerical investigations were performed also on the Lorenz equations [Tabor & Weiss, 1981]. In the case of the periodic regime of the Lorenz equations (limit cycle) the arrangement of singularities (poles) reflects, as for the Duffing equation, the corresponding periodicity of the real time solution. As the dynamical regime goes toward the chaotic one the corresponding arrangement of singularities becomes very irregular. Moreover, as for the Duffing equation, it was numerically shown that a singularity (the nearest to the real time axis) can be associated to each position t on the real time axis where a local maximum (or minimum) of the real time solution occurs. It was shown that the distances of these singularities from the real time axis are related to the real values of the solution [Tabor & Weiss, 1981; Konno & Tateno, 1984]. In other words, let be $\tau = Imz$ the imaginary part of the position $z = t + \epsilon + \imath\tau$ $(0 \leq |\epsilon| \ll 1)$ of the singularity corresponding to a local maximum (or minimum) of $f(t)$, then as $|\tau|$ decreases the value of $|f(t)|$ increases (and viceversa). From these last remarks it follows that the sequence of points $\{t_j, f(t_j)\}$, each associated to a local maximum (or minimum) of the function $f(t)$, can be thought of as a representation of the sequence of singularities of $f(z)$ nearest to the real time axis. A point to be stressed is that for a system of ODEs the position of the singularities (if they exist) is deterministically defined [Ramani *et al.*, 1989]. In other words the pattern of singularities in the complex time plane is directly determined by the properties of the system of ODEs. For example, as seen before, for the ODE $\ddot{x} + x^3 = 0$ the set of singularities is well defined: These are poles and are disposed in a regular lattice on the complex time plane. These theoretical

and numerical results suggest the first algorithm, whose protocol is the following:

(a) Given the time series $s(t)$ let us consider the set of couples $\{(t_j, s(t_j) : j = 1, n)\}$ where $s(t_j)$ are the local maxima (or indifferently the local minima);
(b) define the quantity

$$L = \sqrt{\sum_{j=1}^{n-1} [t_{j+1} - t_j]^2 + [s(t_{j+1}) - s(t_j)]^2} \quad (1)$$

that represents the length of the broken line joining the points $\{t_j, s(t_j) : j = 1, n\}$;
(c) test if the value of L can be statistically accounted for by a linear Gaussian stochastic process obtained from the original time series $s(t)$ by using Fourier Shuffled surrogate data. It is worth recalling that Fourier Shuffled surrogates preserve the histogram of amplitudes and, approximately, the linear time correlations of the original data. More details on the surrogate data properties can be found in [Theiler *et al.*, 1992]. In what follows the above algorithm will be denoted as PSC (**P**attern of **S**ingularities in the **C**omplex time plane).

2.2. *NET algorithm*

Several arguments support the correctness of a statistical description of a chaotic dynamical system $\dot{\mathbf{x}} = \mathbf{F}(\mathbf{x}), \mathbf{x} \in R^n$ that, as it is well known, exhibits sensitivity to the initial conditions [Eckmann & Ruelle, 1985]. Among them the most important is that in nature the measurement process, by which the observer interacts with a physical system, is characterized by a finite precision. Consequently, the state of the system at time t is not represented by a point in phase space but, rather, by a small region whose size reflects the finite precision of the measurement. Other sources of delocalization of the state are the incomplete specification of the initial conditions or the roundoff errors in numerical calculations. For a chaotic dynamical system, represented by $\dot{\mathbf{x}} = \mathbf{F}(\mathbf{x})$, the probability density function $\rho(\mathbf{x}, t)$ of a given system state $\mathbf{x}$ can be determined by solving the Liouville equation which is a particular case of the differential Chapman–Kolmogorov equation describing Markov processes [Gardiner, 1983; Nicolis, 1995; Soong, 1973]. If we have at our disposal only a time series, the probability density can be evaluated numerically [Abarbanel *et al.*, 1993]. Given a scalar time series $s(t) = M(\mathbf{x})$, where $\dot{\mathbf{x}} = \mathbf{F}(\mathbf{x})$ and M represents the measurement function, the reconstruction theorem [Takens, 1981] ensures that for a sufficiently high embedding dimension E the dynamical properties of the original system are equivalently described by $\dot{\mathbf{y}} = \mathbf{G}(\mathbf{y})$, where $\mathbf{y} = [s(t), ds(t)/dt, \ldots, d^{E-1}s(t)/d^{E-1}t]$, $\mathbf{y} \in R^E$, $E \geq 2m + 1$ (m is the box-counting dimension of the attractor). We can therefore concentrate our attention on the dynamical system $\dot{\mathbf{y}} = \mathbf{G}(\mathbf{y})$, $\mathbf{y} \in R^E$. In principle the probability density function $\rho(\mathbf{y}, t)$ can be determined and, from it [Soong, 1973], the joint probability density $p(s, \dot{s}, \ddot{s}, t)$ can be obtained (here we are supposing $E \geq 3$). Now, according to [Soong, 1973] the expected number of extrema for unit time of the time series is given by

$$q(t) = \int_{-\infty}^{+\infty} d\ddot{s} \int_{-\infty}^{+\infty} p(s, 0, \ddot{s}, t) ds \,. \quad (2)$$

In the particular case of a stationary process, $q(t)$ is independent of t. For example, if the probability density is Gaussian with zero mean it can be easily shown that

$$q(t) = q_0 = \frac{1}{\pi} \frac{\sigma(\ddot{s})}{\sigma(\dot{s})} \quad (3)$$

where $\sigma(\ddot{s})$ and $\sigma(\dot{s})$ are, respectively, the standard deviation of $\ddot{s}$ and $\dot{s}$. By assuming that the dynamical system is ergodic we can estimate $q(t)$ from the experimental time series without knowing $p(s, \dot{s}, \ddot{s}, t)$. We remark that in Eq. (2) $p(s, 0, \ddot{s}, t) ds d\ddot{s}$ represents the probability to find the intersection of the trajectory, described by $\mathbf{y}$, within the rectangle of sides $s + ds$ and $\ddot{s} + d\ddot{s}$ in the plane $(s, \ddot{s})$ of the Poincaré section defined by $\dot{s} = 0$. If the evolution law of $\mathbf{y}$ is characterized only by linear time correlations we expect that the statistic $q(t)$, computed using surrogata data preserving linear time correlations, will be not statistically different from that obtained with the original data.

Consequently the idea is to test whether the number of extrema for unit time of an experimental time series $s(t)$ can be accounted for by a linear Gaussian stochastic process. If this does not happen then we have an indication that the generating process responsible for the observed $s(t)$ is nonlinear [Theiler *et al.*, 1992]. This suggests that the probability density function $p(s, \dot{s}, \ddot{s}, t)$ cannot

be associated to a linear stochastic process. The recipe of the algorithm is the following:

(a) The number of extrema for unit time ν_0 of the given time series $s(t_j)\,(j = 1, \ldots, N)$ is determined and used as discriminating statistic;
(b) from the time series $s(t_j)\,(j = 1, \ldots, N)$ a set of n surrogate time series $s_{s,j}(t)$ is generated;
(c) the average number of extrema for unit time of the surrogate time series $\nu_s = \frac{1}{n}\sum_{j=1}^{n} \nu_{s,j}$ is computed
(d) by using the standard deviation σ_ν of the set $\nu_{s,j}\,(j = 1, 2, \ldots, n)$, ν_0 and ν_s are compared to test if they are statistically different [Theiler *et al.*, 1992]. Hereupon to indicate this algorithm we will use the abbreviation NET (**N**umber of **E**xtrema for unit **T**ime).

3. Numerical Results

A number of time series, from well-known models, were generated to test the PSC and NET algorithms and to find their possible limitations. In the previous section we considered only continuous time dynamical system. A naturally arising question is whether the NET and PSC algorithms work also for maps. There is not a clear answer to this question from the theoretical point of view. Therefore we decided to investigate numerically the performance of both algorithms also on the well-known Henon map.

The Lorenz equations,

$$\begin{aligned} \dot{x} &= \sigma(y - x) \\ \dot{y} &= \rho x - y - xy + \epsilon\xi(t) \\ \dot{z} &= -\beta z + xy \end{aligned} \tag{4}$$

with parameters $\sigma = 10$, $\rho = 28$, $\beta = 8/3$ corresponding to the chaotic regime, were integrated numerically; in Eq. (4) $\xi(t)$ is the Gaussian white noise of unit standard deviation. Two time series were obtained for the case $\epsilon = 0$ and $\epsilon \neq 0$, respectively. Two other time series were generated by using the Henon map: one without noise and the other with additive noise. Two time series, representing Gaussian white noise and colored noise, were also generated. Finally the last two time series were obtained from the signal $s(t) = \sin(\omega t) + \epsilon\xi(t)$ in the cases $\epsilon = 0$ and $\epsilon \neq 0$. The occurrence of a local maximum (or minimum) in the time series $s(t)$ was determined from the change of sign of the first difference series. In Fig. 1 the results obtained using the NET algorithm are plotted in terms of the significance $S = |\nu_0 - \nu_s|/\sigma_\nu$ [Theiler *et al.*, 1992]. For the left panel $N = 1000$ points were used and $N = 2000$ for the right one. For both panels 10 phase randomized surrogate data were used for each time series. According to [Theiler *et al.*, 1992] for S values ≥ 2 the null hypothesis that the data came from a linear Gaussian stochastic process can be rejected with a probability greater or equal to 95%. In Fig. 1

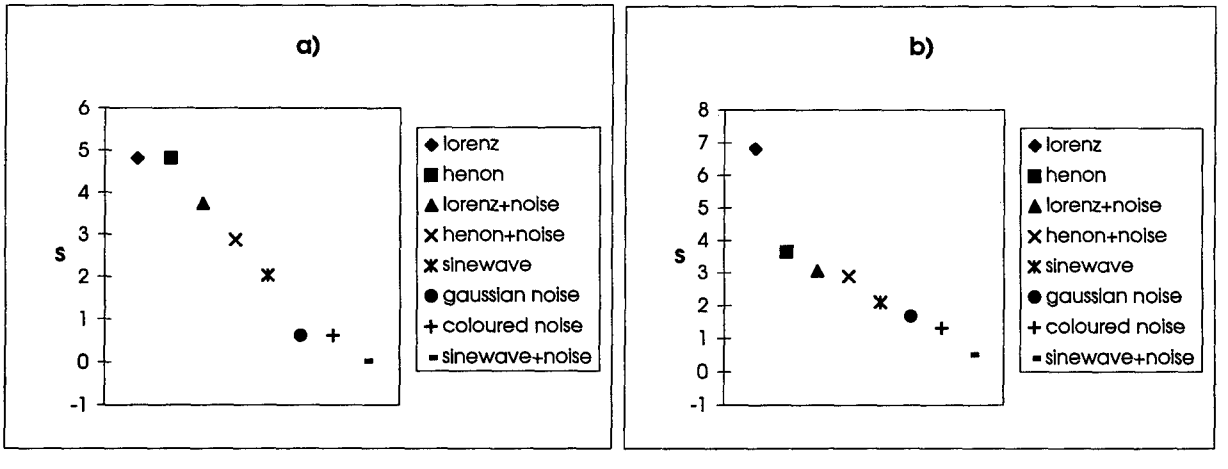

Fig. 1. NET algorithm: Significance $S = |\nu_0 - \nu_s|/\sigma_\nu$ for the model time series. In what follows $\xi(t)$ is Gaussian white noise of unit standard deviation. The noisy Lorenz time series was obtained with $\epsilon = 0.2$; for the sinus wave $\sin(\omega t)$ is $\omega = 0.1$; for the sinus wave plus noise $\sin(\omega t) + \epsilon\xi(t)$ is $\omega = 0.1$ and $\epsilon = 0.3$; the colored noise was obtained from $x(t+1) = ax(t) + \epsilon\xi(t)$ with $a = 0.85$ and $\epsilon = 0.2$; the amplitude of the additive noise in the Henon map was $\epsilon = 0.36$. The sampling time for the Lorenz equation is $\Delta t = 0.025$. $(n = 10)$, (a) $N = 1000$, (b) $N = 2000$.

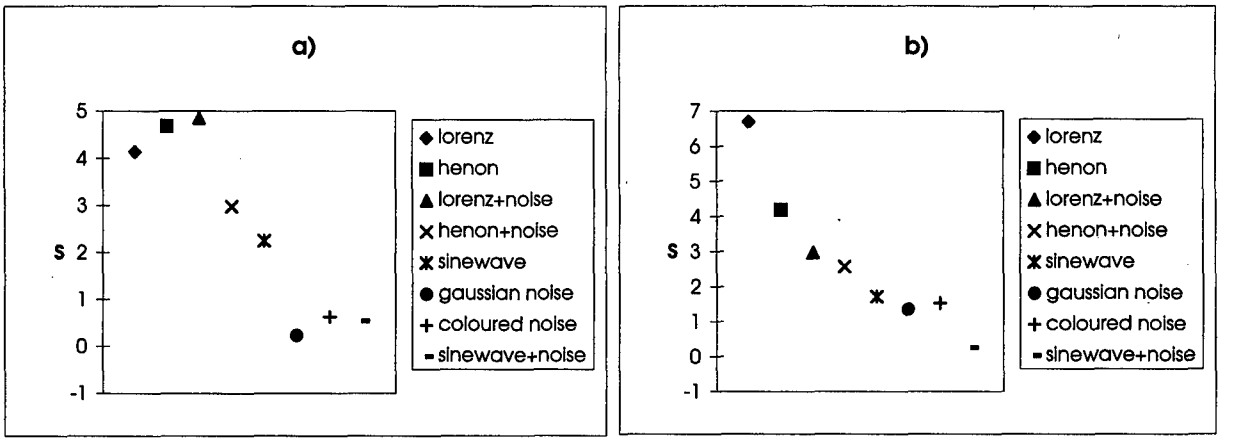

Fig. 2. As in Fig. 1 but using $n = 20$ surrogates for each time series. (a) $N = 1000$, (b) $N = 2000$.

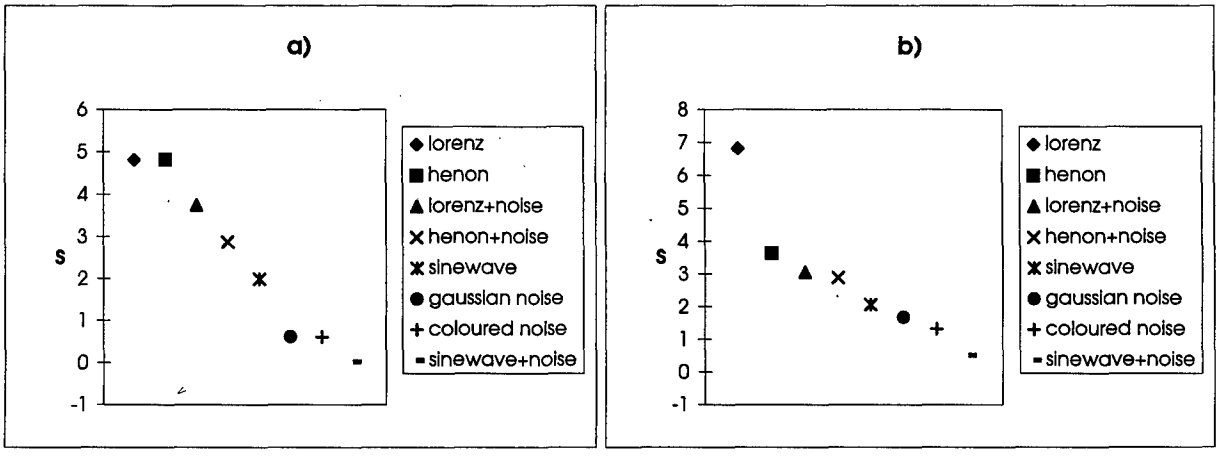

Fig. 3. As in Fig. 1, but using Fourier Shuffled surrogate time series ($n = 10$), (a) $N = 1000$ (b) $N = 2000$.

each symbol identifies a model time series as Qspecified in the legend (this correspondence will be maintained). The test gives a clear indication of nonlinearity only for the time series Lorenz, Lorenz plus noise, Henon map and Henon map plus noise that are known to be nonlinear dynamical systems. The case of the sinus wave is more problematic: The S value is slightly above 2 for both panels and this disagrees with the fact that the time series is linear. However, as will be shown in the following, this anomalous behavior is corrected when the PSC algorithm is applied. In Fig. 2 the results obtained with the NET algorithm, and using 20 surrogate data for each time series, are plotted (the number of points used for each time series are as in Fig. 1). The results are qualitatively similar to those in Fig. 1. However, from the left panel of Fig. 2 the noisy Lorenz time series seems to be more nonlinear than the corresponding noise-free one. But, as the number of points is increased (from 1000 to 2000) this discrepancy disappears (right panel). The analysis was repeated using 10 sets of Fourier Shuffled surrogate data for each model time series and the corresponding results are plotted in Fig. 3. These last results are very similar to those obtained with the phase randomized surrogate data; this means that the computed statistic is insensitive to slight changes in the distribution of the amplitudes of the time series. Next the PSC algorithm was applied to the same model time series. The PSC algorithm requires the calculation of the length L, defined in Eq. (1), on the original time series and the statistical evaluation of its difference from $L_s = \frac{1}{n}\sum_{j=1}^{n} L_j$ (L_j is calculated on the jth surrogate time series). To identify the local extrema (maxima in this case) we used the

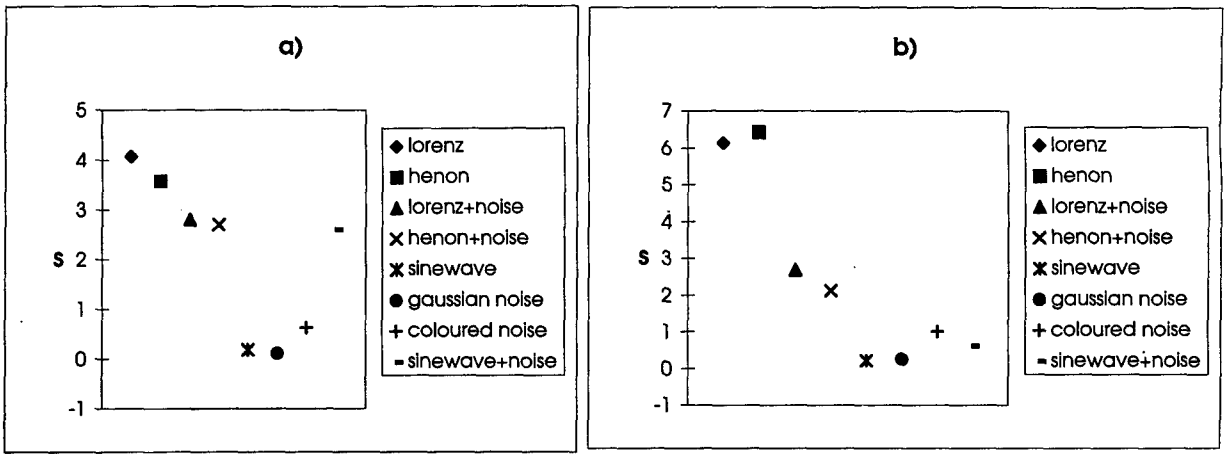

Fig. 4. PSC algorithm using local maxima ($n = 10$), (a) $N = 1000$, (b) $N = 2000$, $S = |L - L_s|/\sigma_L$. Fourier Shuffled surrogata data are used.

same protocol as for the NET algorithm. In Fig. 4 the values of the significance $S = |L - L_s|/\sigma_L$ obtained using the PSC algorithm are plotted (σ_L is the standard deviation of the set $\{L_j\}$). The number of points in the left panel is $N = 1000$ and $N = 2000$ in the right one. The time series corresponding to the sinus wave plus noise seems to show a nonlinear character (left panel). However, as the number of points increases this apparent nonlinearity disappears (right panel). Figure 5 shows the results obtained with the PSC algorithm by using the local minima instead of maxima.

The results obtained in the Henon map, Henon map plus noise and Gaussian white noise increasing the series length up to $N = 4000$ points are reported in Table 1. Similar results were also obtained for the other time series (data not shown). The conclusion arising from these numerical experiments is that increasing the length of the time series does not produce results contrasting with those obtained using shorter sequences of data. Furthermore in presence of nonlinearity (S values ≥ 2) the value of S improves (statistically) as the length of the time series increases.

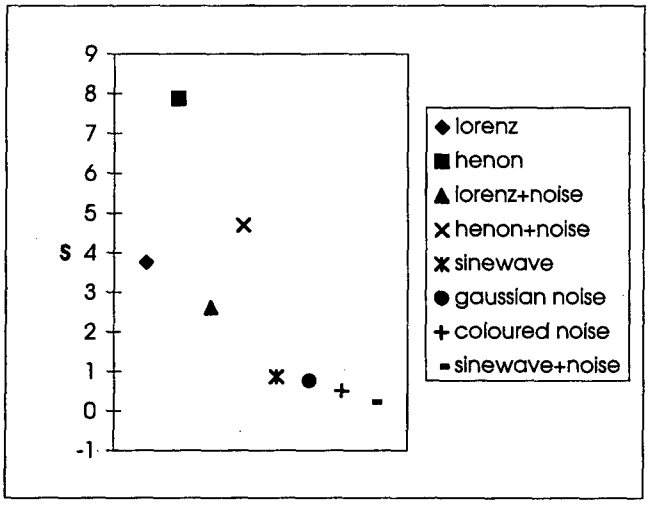

Fig. 5. PSC algorithm: The local minima are used ($n = 10$), $N = 2000$, $S = |L - L_s|/\sigma_L$. Fourier Shuffled surrogata data are used.

Another important point that we faced is whether the PSC and NET algorithms were able to detect nonlinear correlations in time series coming from a high dimensional chaotic attractor. Some preliminary considerations are needed before showing the numerical results obtained with both methods. As shown in the previous section the PSC algorithm requires the computation of L defined by Eq. (1). The set of points $\{(t_j, s(t_j) : j = 1, n)\}$, where $s(t_j)$ are the local maxima (or minima) of the time series $s(t)$, is a bidimensional Poincaré section [Hegger & Kantz, 1997; Kantz & Schreiber, 1997] defined by $\dot{s}(t) = 0$, $\ddot{s}(t) < 0$ (or $\dot{s}(t) = 0$, $\ddot{s}(t) > 0$ for the minima). For high dimensional attractors (dimension ≥ 3) the Poincaré section can mimic the one due to a stochastic process [Kantz & Schreiber, 1997]. Similar considerations are also valid for the NET algorithm. Therefore it is expected that both PSC and NET algorithms can have problems with time series from a high dimensional attractor. We performed numerical experiments by using time series generated with the Mackey–Glass

$$\dot{x}(t) = \frac{ax(t-\tau)}{1 + x(t-\tau)^c} - bx(t) \qquad (5)$$

Table 1. Values of significance S obtained with the PSC and NET algorithms against the number of points N of the time series.

Number of points	Henon Map		Henon Map + Noise		Gaussian White Noise	
N	PSC	NET	PSC	NET	PSC	NET
1000	3.6	4.8	2.7	2.86	0.7	1.01
2000	6.4	3.6	2.1	2.87	0.1	1.1
3000	6.6	6	2.9	3.95	0.08	0.46
4000	13.4	9.5	4.3	4.7	0.49	0.09

time-delay differential equation [Mackey & Glass, 1977]. In this study we set $a = 0.2, b = 0.1, c = 10$. Two time series of $N = 4000$ points corresponding to $\tau = 30$ and $\tau = 100$ were generated; the sampling time was $\Delta t = 10$. The corresponding correlation dimension of the attractor is $\simeq 3$ (for $\tau = 30$) and $\simeq 7.1$ (for $\tau = 100$). The values of the significance S computed for these two time series are the following: (a) ($\tau = 30$): PSC algorithm $S = 0.04$, NET algorithm $S = 2$; (b) ($\tau = 100$): PSC algorithm $S = 0.02$, ET algorithm $S = 0.6$. The above results show that both algorithms have problems to detect nonlinear correlations in time series from high dimensional attractors. The NET algorithm, however, seems to be less sensitive to the high dimensional dynamics than the PSC one.

4. Concluding Remarks

The time series corresponding to chaotic dynamics (time series: Lorenz, Lorenz plus noise, Henon map and Henon map plus noise) exhibit the expected nonlinear character for both algorithms ($S \geq 2$). Similarly the time series corresponding to Gaussian white noise and colored noise present values of the significance S below 2 for both algorithms. This means that the null hypothesis that they are generated by a linear stochastic process cannot be rejected with a probability higher than 95%. The time series corresponding to the sinus wave, as seen in Figs. 1–3, exhibits an unexpected nonlinear behavior using the NET algorithm. This behavior disappears for the sinus wave and appears for the sinus wave plus noise (left panel of Fig. 4) when the PSC algorithm is used. However, as the number of points is increased (right panel of Fig. 4) this effect for the sinus wave plus noise disappears. We studied the dependence of the values of the significance S from the length of the time series. The results were that the growth of the number of points N of the sequence produces values of S coherent with those obtained using shorter data sets; furthermore in the presence of nonlinear correlations in the time series (S values ≥ 2) the value of S improves statistically as N increases.

We checked also the performance of both algorithms to detect nonlinear correlations in time series from a high dimensional attractor. The result was that both algorithms fail in such a case; furthermore it seems that the NET algorithm is less sensitive than the PSC one to the growth of the dimension of the attractor. We remark that, using the classical algorithm to estimate the correlation dimension from time series, the high dimensional dynamics of the Mackey–Glass system is detected, using large amount of data points ($\gg$4000), correctly [Ding *et al.*, 1993]. It is presently under investigation to assess whether some change in the protocols of both algorithms can improve their perdormance on time series from a high dimensional attractor.

All the above results lead to the following remarks: (a) For low dimensional chaotic dynamics the nonlinear property ($S \geq 2$) is detected by both algorithms; (b) for colored noise or Gaussian white noise significance values $S < 2$ are obtained with both algorithms; (c) when the signal power spectrum exhibits a strong sharp peak the two algorithms give contrasting results. This can be partially explained by the fact that the use of surrogate data for periodic signals with long coherence time can lead to ambiguous results that need to be interpreted very carefully [Theiler *et al.*, 1992]. These preliminary results suggest that the two methods used together are able to discriminate between low dimensional chaotic dynamics and noise. The last remark is that the NET and PSC algorithms do not require the reconstruction protocol of the phase space as it happens for many of the current tools for the nonlinear analysis of time series (Lyapunov exponents, dimension calculations, nonlinear

prediction methods, etc.) [Abarbanel *et al.*, 1993]; consequently we do not need to determine the embedding dimension E and the lag-time τ. Moreover these more complex tools to study time series are not trivial to be implemented using numerical codes. On the contrary the NET and PSC algorithms are very simple to implement and they do not require large amount of data in order to check the presence of nonlinear correlations in time series from low dimensional attractor. Therefore the NET and PSC algorithms can be used as a first test before using the aforementioned more complex tools.

References

Abarbanel, H. D. I., Brown, R., Sidorowich, J. J. & Tsimring, L. S. [1993] "The analysis of observed chaotic data in physical systems," *Rev. Mod. Phys.* **65**, 1331–1392.

Ding, M., Grebogi, C., Ott, E., Sauer, T. & Yorke, J. A. [1993] "Estimating correlation dimension from a chaotic time series: When does plateau onset occur?" *Physica* **D69**, 404–424.

Eckmann, J. P. & Ruelle, D. [1985] "Ergodic theory of chaos and strange attractors," *Rev. Mod. Phys.* **57**, 617–656.

Gardiner, C. W. [1983] *Handbook of Stochastic Methods* (Springer-Verlag).

Hegger, R. & Kantz, H. [1997] "Embedding of sequences of time intervals," *Europhys. Lett.* **38**, 267–272.

Kantz, H. & Schreiber, T. [1997] *Nonlinear Time Series Analysis* (Cambridge University Press).

Konno, K. & Tateno, H. [1984] "Duffing's equation in complex time and chaos," *Prog. Theor. Phys.* **72**, 1047–1049.

Mackey, M. C. & Glass, L. [1977] "Oscillations and chaos in physiological control systems," *Science* **197**, 287–289.

Nicolis, G. [1995] *Introduction to Nonlinear Science* (Cambridge University Press).

Ramani, A., Grammaticos, B. & Bountis, T. [1989] "The Painlevé property and singularity analysis of integrable and non-integrable systems," *Phys. Rep.* **180** 161–245.

Soong, T. T. [1973] *Random Differential Equations in Science and Engineering*, ed. Bellman, R. (Academic Press).

Tabor, M. & Weiss, J. [1981] "Analytic structure of the Lorenz system," *Phys. Rev.* **A24**, 2157–2167.

Takens, F. [1981] "Detecting strange attractors in turbulence," *Lectures Notes in Mathematics*, Vol. 898, pp. 366–381.

Theiler, J., Eubank, S., Longtin, A., Galdrikian, B. & Farmer, D. [1992] "Testing for nonlinearity in time series: The method of surrogate data," *Physica* **D58**, 77–94.

International Journal of Bifurcation and Chaos, Vol. 8, No. 9 (1998) 1839–1842

TRANSMISSION OF SIGNALS VIA SYNCHRONIZATION OF CHAOTIC TIME-DELAY SYSTEMS

K. PYRAGAS
Semiconductor Physics Institute, 11 A. Goštauto, LT-2600 Vilnius, Lithuania

Received July 31, 1997; Revised December 1, 1997

Secure communication via chaotic synchronization is demonstrated using dynamical systems governed by delay deferential equations. Strange attractors of such systems can have an arbitrarily large number of positive Lyapunov exponents giving rise to very complex time signals. This feature can provide high security of masked messages.

1. Introduction

Synchronization of chaotic systems has aroused much interest in recent years, particularly in light of potential application of this phenomenon in secure communication. Different approaches for constructing synchronized chaotic systems are proposed. Among them is the approach of Pecora and Carroll [1990] who show that when a state variable from a chaotically evolving system is transmitted as an input to a replica of part of the original system, the replica subsystem (receiver) can synchronize to the original system (sender). To use this phenomenon for masking messages one can transmit to the receiver a summary signal consisting of a chaotic signal generated by sender and a small information signal containing a message [Kocarev *et al.*, 1992]. Then the message can be recovered by synchronizing the receiver with the scalar signal which is transmitted from the sender. The shortcoming of this approach is that the information signal violates the synchrony between sender and receiver giving rise to reconstruction errors in the recovered information.

Recently, Kocarev and Parlitz [1995] have proposed a generalization of the Pecora and Carroll [1990] method, which extends the capabilities for constructing synchronized chaotic systems. This new approach enables the information signal to be integrated in the sender as a driving signal. The scalar signal which is transmitted from the sender to the receiver is a function of the sender state variables and the information signal. At ideal conditions the information signal can be recovered exactly, without the reconstruction errors.

Most theoretical as well as experimental studies of secure communication reported so far concern low-dimensional systems with one positive Lyapunov exponent. Perez and Cerdeira [1995] have shown that messages masked by such simple chaotic processes, once intercepted, can be sometimes readily extracted. To improve security it is desirable to use high-dimensional systems with multiple positive Lyapunov exponents (hyperchaotic systems) which take advantage of the increased randomness and unpredictability. Recently, Peng *et al.* [1996] have demonstrated the possibility of synchronizing hyperchaotic systems by transmitting just a single scalar variable composed of a linear combination of state variables of the sender. Another way of synthesizing synchronized hyperchaotic systems using a series of low-dimensional subsystems as building blocks has been proposed by Kocarev and Parlitz [1995]. These methods have many advantages, but they have been applied only to finite-dimensional systems described by ordinary differential equations

(ODE's). The number of positive Lyapunov exponents of such systems is limited by dimension of the state space.

An alternative efficient approach of constructing synchronized hyperchaotic systems can be based on delay differential equations (DDE's). Systems governed by DDE's have an infinite-dimensional state space and can produce hyperchaos with an arbitrarily large number of positive Lyapunov exponents. A typical example of these is the Mackey and Glass (MG)[1977] system:

$$\dot{x} = f[x(t-\tau), \alpha] - cx\,, \tag{1}$$

where $f[x(t-\tau), \alpha] = ax(t-\tau)/[1 + x^b(t-\tau)]$ and $\alpha \equiv \{a, b\}$ denotes a set of parameters of the function f. All parameters a, b, c, and τ are supposed to be positive. We choose this model for our studies since it has been thoroughly investigated in the literature (e.g. [Farmer, 1982]) and is easily implementable electronically [Namajūnas *et al.*, 1995]. The number of positive Lyapunov exponents as well as dimension of strange attractor of this system can easily be controlled by varying the delay time τ. For fixed values of the parameters a, b, and c, both these quantities increase linearly with the increase of τ [Farmer, 1982].

Below we demonstrate secure communication with two types of senders based on a single MG system and using a set of coupled MG systems.

2. Communication Based on a Single MG System

Let us consider the communication system with the equations of the sender, the transmitted signal, and the receiver given by

$$\dot{x} = f[x(t-\tau) + i(t), \alpha] - \mathrm{cx} \qquad \text{sender}\,, \tag{2}$$

$$s(t) = x(t-\tau) + i(t) \qquad \text{transmitted signal}\,, \tag{3}$$

$$\dot{y} = f[s(t), \alpha] - \mathrm{cy} \qquad \text{receiver}\,, \tag{4}$$

where $i(t)$ is the information signal. The sender (2) is an infinite-dimensional system described by nonlinear DDE, while the receiver (4) is presented by a simple linear ODE driven (through a nonlinear function f) by transmitted signal $s(t)$. Subtracting Eq. (4) from Eq. (2) we obtain for the difference $e = x - y$ a simple linear ODE $\dot{e} = -ce$. This equation possesses an unique globally stable fixed point $e = 0$. Thus the synchronized state $x = y$ is globally stable, i.e., the receiver synchronizes to the sender independently on initial conditions. The characteristic time of synchronization is given by $1/c$. At the receiver the information i_R can be recovered as

$$i_R = s(t) - y(t-\tau)\,. \tag{5}$$

Figure 1 illustrates secure communication for the parameter values of the MG system $a = 0.2$, $b = 10$, $c = 0.1$, and $\tau = 100$. Here and below we perform numerical integration of the underlying DDE's by a second order Runge–Kutta method taking an integration step $h = 0.1$. Without the information signal, $i(t) = 0$, the sender [Eq. (2)] has five positive Lyapunov exponents. The eleven largest exponents multiplied by factor 10^3 are {3.53, 2.88, 2.09, 1.28, 0.46, 0.00, −0.54, −1.49, −2.63, −3.83, −4.98}. This corresponds to information dimension [Kaplan & Yorke, 1979] of the strange attractor equal to $d_\lambda \approx 10.35$.

Figure 1(a) shows the transmitted signal $s(t)$ in the case of a sine information signal $i(t)$ with the period $T = 80$ and amplitude $A = 0.1$ switched on at the moment $t = 200$ and switched off at $t = 800$. The recovered information signal $i_R(t)$ is presented in Fig. 1(b). It coincides with the original information signal $i(t)$, to within the error of numerical integration.

In a real experiment, the parameters of sender and receiver are not exactly the same. This factor and additional noise in a transmission channel will

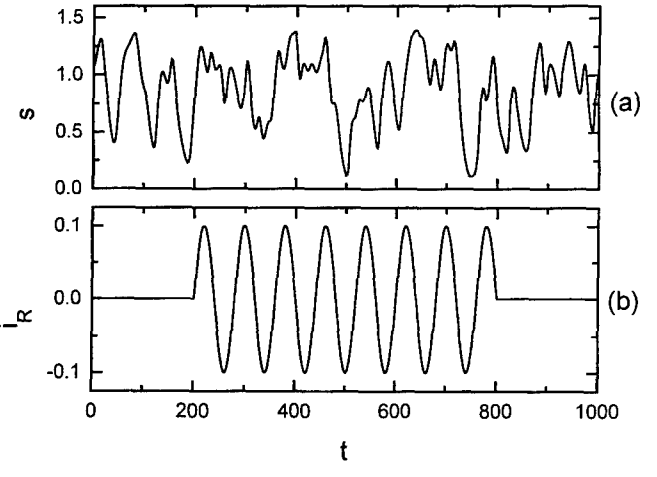

Fig. 1. Numerical simulation of a communication scheme based on a single MG system in the case of sine information signal $i = 0.1\sin[2\pi(t-200)/80]$ switched on at the moment $t = 200$ and switched off at $t = 800$. The parameter values of the MG system are $a = 0.2$, $b = 10$, $c = 0.1$, and $\tau = 100$. (a) Transmitted signal s. (b) Recovered information signal i_R.

result in reconstruction errors. However, due to the global stability of the synchronized state $x = y$, the system is robust with respect to these factors. Suppose that the parameters of the driving and the response systems are different, say α and α', respectively. If the difference $\delta\alpha = \alpha - \alpha'$ is small, the difference $e = x - y$ is governed by a linear nonhomogenous differential equation

$$\dot{e} = \delta\alpha \frac{\partial f}{\partial \alpha} - ce\,.$$

Clearly the difference e is proportional to the parameter mismatch $\delta\alpha$, $e \propto \delta\alpha$. The same is valid for the difference between the original and the reconstructed information signal, $i - i_R \propto \delta\alpha$, which defines the reconstruction errors. The information signal can be properly recovered if the difference $\delta\alpha$ is small compared to the amplitude of information signal. The influence of the mismatch between parameters to the reconstruction errors is numerically illustrated in Fig. 2(a). The parameter a is taken to have different values at the sender and the receiver, a and a', respectively. We measure the reconstruction errors by the r.m.s. deviation $\sigma = \sqrt{\langle (i - i_R)^2 \rangle}$, where $\langle \cdot \rangle$ denotes the time average. As is seen from the figure, the reconstruction errors decrease linearly with the decrease of the difference $\delta a = a - a'$. Similar results are observed in the presence of noise. To model an influence of noise in the transmission channel, we add (at every step of numerical integration) random numbers uniformly distributed in the interval $[-a_n/2, a_n/2]$ to the transmitted signal $s(t)$. Figure 2(b) shows that for small noise the reconstruction errors are proportional to the noise amplitude a_n.

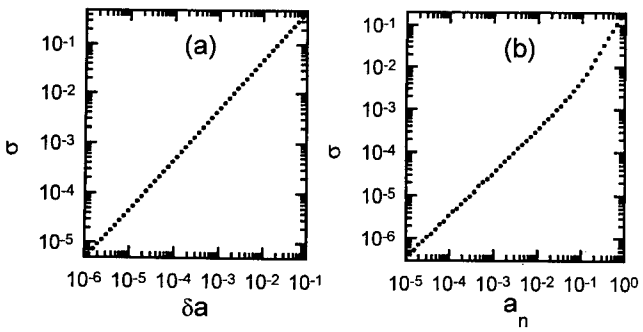

Fig. 2. Dependence of the r.m.s. deviation $\sigma = \sqrt{\langle (i - i_R)^2 \rangle}$ on (a) parameter mismatch δa and (b) noise amplitude a_n. The parameters of the MG system are the same as in Fig. 1. The information signal represents the sine wave $i = 0.1 \sin(2\pi t/80)$.

Although the MG system allows us to generate very complex signals, it is still described by a very simple DDE. In the absence of information signal, $i(t) = 0$, such simple DDE can be reconstructed from transmitted signal $s(t)$ using, for example, the method proposed by Bünner *et al.* [1996]. Certainly, the presence of information signal ($i \neq 0$) considerably complicates the possibility of such reconstruction, since the sender becomes a nonautonomous system. To make the communication system even more secure one can increase the complexity of the sender by using a set of coupled MG systems.

3. Communication Based on a Set of Coupled MG Systems

To illustrate the possibility of more complex constructions of a communication system we consider the specific example with the equations of the sender, the transmitted signal, and the receiver given by

$$\left.\begin{aligned} \dot{x}_1 &= f[x_1(t-\tau_1) + i(t), \alpha_1] - c_1 x_1 \\ s_{\rm aux}(t) &= x_1(t-\tau_1) + i(t) \\ \dot{x}_2 &= f[x_2(t-\tau_2) + k s_{\rm aux}(t), \alpha_2] - c_2 x_2 \end{aligned}\right\} \text{sender}\,, \tag{6}$$

$$s(t) = x_2(t-\tau_2) + k s_{\rm aux}(t) \text{ transmitted signal}\,. \tag{7}$$

$$\left.\begin{aligned} \dot{y}_2 &= f[s(t), \alpha_2] - c_2 y_2 \\ \tilde{s}_{\rm aux}(t) &= [s(t) - y_2(t-\tau_2)]/k \\ \dot{y}_1 &= f[\tilde{s}_{\rm aux}(t), \alpha_1] - c_1 y_1 \end{aligned}\right\} \text{receiver}\,. \tag{8}$$

The idea [Kocarev & Parlitz, 1995] behind this construction is based on successive transmission of information signal through different building blocks (here they represent the MG systems) of the sender and then successive recover of the transmitted signal at the different blocks of the receiver. Here we consider the construction with only two building blocks. The generalization for an arbitrary number of building blocks is straightforward.

This construction as well as previous examples provides the global stability of the synchronized state $x_1 = y_1$, $x_2 = y_2$. Indeed, the difference $e_2 = x_2 - y_2$ is governed by the linear equation $\dot{e}_2 = -c_2 e_2$ possessing the globally stable fixed point $e_2 = 0$. This guarantees the global stability of the state $x_2 = y_2$. Taking into account the last equality we obtain $\tilde{s}_{\rm aux}(t) = s_{\rm aux}(t)$, and the

equation for the difference $e_1 = x_1 - y_1$ takes the form $\dot{e}_1 = -c_1 e_1$. Thus the state $x_1 = y_1$ is also globally stable. At the receiver the information i_R can be recovered as

$$i_R = [s(t) - y_2(t - \tau_2)]/k - y_1(t - \tau_1)\,. \quad (9)$$

Figure 3(a) shows the amplitude spectrum of the transmitted signal in the case of sine information signal $i(t) = 0.1\sin(2\pi t/40)$. The amplitude spectrum of the recovered information signal i_R is shown in Fig. 3(b). The information signal is practically invisible in the spectrum of the transmitted signal.

4. Conclusions

We have demonstrated an efficient way of constructing secure communication systems using delay differential equations. The sender of such systems has an infinite-dimensional state space and can produce chaotic carrier signals with an easily controllable number of positive Lyapunov exponents. The receiver is constructed as a linear low-dimensional system. The synchronization with the sender is achieved by transmitting only single scalar signal. An important advantage of this construction is the global stability of the synchronized state. As a result these communication systems are insensitive to small noise levels and mismatching between parameters.

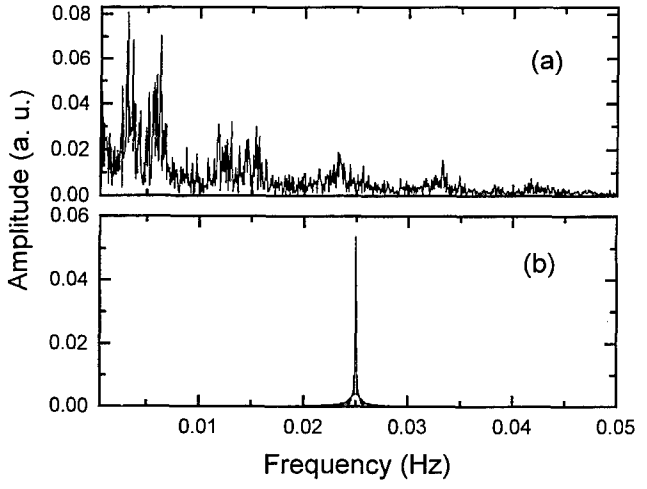

Fig. 3. Numerical simulation of a communication scheme based on a set of coupled MG systems in the case of sine information signal $i = 0.1\sin(2\pi t/40)$. The parameter values of the MG systems are $a_1 = 0.22$, $b_1 = 12$, $c_1 = 0.1$, $\tau_1 = 110$, $a_2 = 0.2$, $b_2 = 10$, $c_2 = 0.1$, $\tau_2 = 100$, and $k = 0.1$. (a) Amplitude spectrum of the transmitted signal s. (b) Amplitude spectrum of the recovered sine signal i_R.

References

Bünner, M. J., Popp, M., Meyer, Th., Kittel, A. & Parisi, J. [1996] "Tool to recover scalar time-delay systems from experimental time series," *Phys. Rev.* **E54**, R3082–3085.

Farmer, J. D. [1982] "Chaotic attractors of infinite-dimensional dynamical systems," *Physica* **D4**, 366–393.

Kaplan, J. L. & Yorke J. A. [1979] "Chaotic behavior of multi-dimensional differential equations," in *Functional Differential Equations and Approximations of Fixed Points*, eds. Peitgen, H. O. & Walther, H. O. (Springer-Verlag, Berlin), pp. 228–237.

Kocarev, L., Halle, K. S., Eckert, K., Parlitz, U. & Chua, L. O. [1992] "Experimental demonstration of secure communication via chaotic synchronization," *Int. J. Bifurcation and Chaos* **2**(3), 709–713.

Kocarev, L. & Parlitz, U. [1995] "General approach for chaotic synchronization with applications to communication," *Phys. Rev. Lett.* **74**(25), 5028–5031.

Mackey, M. C. & Glass, L. [1977] "Oscillations and chaos in physiological control systems," *Science* **197**, 287–289.

Namajūnas, A., Pyragas, K. & Tamaševičius, A. [1995] "An electronic analog of the Mackey–Glass system," *Phys. Lett.* **A201**, 42–46.

Pecora, L. M. & Carrol, T. L. [1990] "Synchronization in chaotic systems," *Phys. Rev. Lett.* **64**, 821–823.

Peng, J. H., Ding, E. J., Ding, M. & Yang, W. [1996] "Synchronizing hyperchaos with a scalar transmitted signal," *Phys. Rev. Lett.* **76**, 904–907.

Perez, G. & Cerdeira, H. A. [1995] "Extracting messages masked by chaos," *Phys. Rev. Lett.* **74**, 1970–1973.

International Journal of Bifurcation and Chaos, Vol. 8, No. 9 (1998) 1843–1848

CONTROL OF AMPLITUDE TURBULENCE IN DELAYED DYNAMICAL SYSTEMS

D. MAZA*, H. MANCINI*, S. BOCCALETTI*,†,
R. GENESIO‡ and F. T. ARECCHI†
*Department of Physics and Applied Mathematics,
Universidad de Navarra, Pamplona, Spain
†Istituto Nazionale di Ottica, I50125 Florence, Italy
Department of Physics, University of Florence, I50125 Florence, Italy
‡Department of Sistemi e Informatica,
University of Florence, I50139 Florence, Italy

Received July 31, 1997; Revised December 11, 1997

An experiment on Bénard–Marangoni time-dependent convection shows evidence of an amplitude turbulent regime in the temperature signal which is modeled by a delayed dynamical system. Application of a control procedure, which perturbs the value of the delay time, leads to the control of such dynamical regime, by suppression of phase defects and stabilization of the regular oscillations. The control technique is robust against the presence of large amounts of noise.

1. Introduction

The original idea of Ott, Grebogi and Yorke [Ott *et al.*, 1990] on chaos control has generated many different theoretical schemes and experimental applications facing the problem of controlling unstable periodic orbits (UPO's) in chaotic concentrated systems (CS), that is in systems modeled by ordinary differential equations.

Controlling spatially extended systems (ES), i.e. systems ruled by partial differential equations whose order parameter y is a m-dimensional vector ($m \geq 1$) in phase space, with k components ($k \geq 1$) in real space, is still an open problem. Even though some proposals have been put forward for the case $k = 2$ [Lu *et al.*, 1996], experimentally implementable tools have not yet been introduced for the control of unstable periodic patterns (UPP) in extended systems.

The link between CS and ES is provided by delayed dynamical systems (DS), i.e. systems ruled by

$$\dot{y} = \mathcal{F}(y, y_d)\,, \tag{1}$$

$y = y(t)$, dot denotes temporal derivative, $\mathcal{F}$ is a nonlinear function, $y_d \equiv y(t - T)$, and T is a time delay.

The evidence of the analogy between DS and ES was given experimentally for a CO_2 laser with delayed feedback [Arecchi *et al.*, 1992] and supported by a theoretical model [Giacomelli & Politi, 1996].

The DS to ES conversion is based on a two variable time representation, defined by $t = \sigma + \theta T$, where $0 \leq \sigma \leq T$ is a continuous space-like variable and θ is a discrete temporal variable [Arecchi *et al.*, 1992]. In this framework, the long range interactions introduced by the delay can be reinterpreted as short range interactions along the θ direction ($y_d \equiv y(\sigma, \theta - 1)$) and the formation and propagation of *space-time* structures, as defects and/or spatiotemporal intermittency can be identified [Arecchi *et al.*, 1992; Giacomelli & Politi, 1996].

For delays T larger than the period of oscillation of the system, the behavior of a DS is analogous to that of an ES with $k = 1$. Namely, DS may display phase defects, i.e. points where the phase suddenly changes its value and the amplitude goes to zero. In this paper we show evidence of these phase defects in a recent experiment on Bénard–Marangoni convection [Mancini & Maza, 1997], and we propose a control technique to suppress them. The control restores regular patterns within an amplitude turbulent regime, which implies the presence of a large number of defects. The control efficiency persists even in presence of a large amount of noise.

2. The Experiment and The Delayed Dynamical Model

The experimental setup is depicted in Fig. 1. A cylindrical cell (diameter 128 mm) confines a fluid layer of silicon oil (Pr $\simeq$ 3000) with the free surface open to the atmosphere and heated from the bottom. The heater does not cover the whole of the container giving open boundaries for the heating. A convective instability driven by buoyancy and temperature dependent surface tension (80% and 20%, respectively), takes place as the heating is increased giving rise to a stationary planform [Fig. 1(a)]. This pattern is composed of four convective cells located on the heater region, but the flow is developed over all the container size.

Following an imaginary drop of fluid traveling with the flow in one of these cells, the drop is heated while traveling near the bottom over the heater, rises up to the centre, travels out near the surface until it becomes cold and then falls down near the lateral boundaries. Finally, the drop is fed back to the heater region completing a round trip in a mean time T [Fig. 1(b)].

If the heating is further increased a time-dependent regime arises, generating spatio-temporal modulations of the stationary velocity and temperature fields. The origin of this behavior is related with a thermal boundary layer instability which give rise to *thermals* or "hot plumes" which are dragged by the flow along the cell. This behavior can be seen in the space-time image of Fig. 1(c). An experimental measurement of the temperature at the center of the cell shows modulated oscillations which have a power spectrum composed by two frequencies clearly differentiated (plus their nonlinear combinations terms). One of these frequencies corresponds to a relaxation oscillation inside the thermal boundary layer, the other one corresponds to the characteristic time necessary for

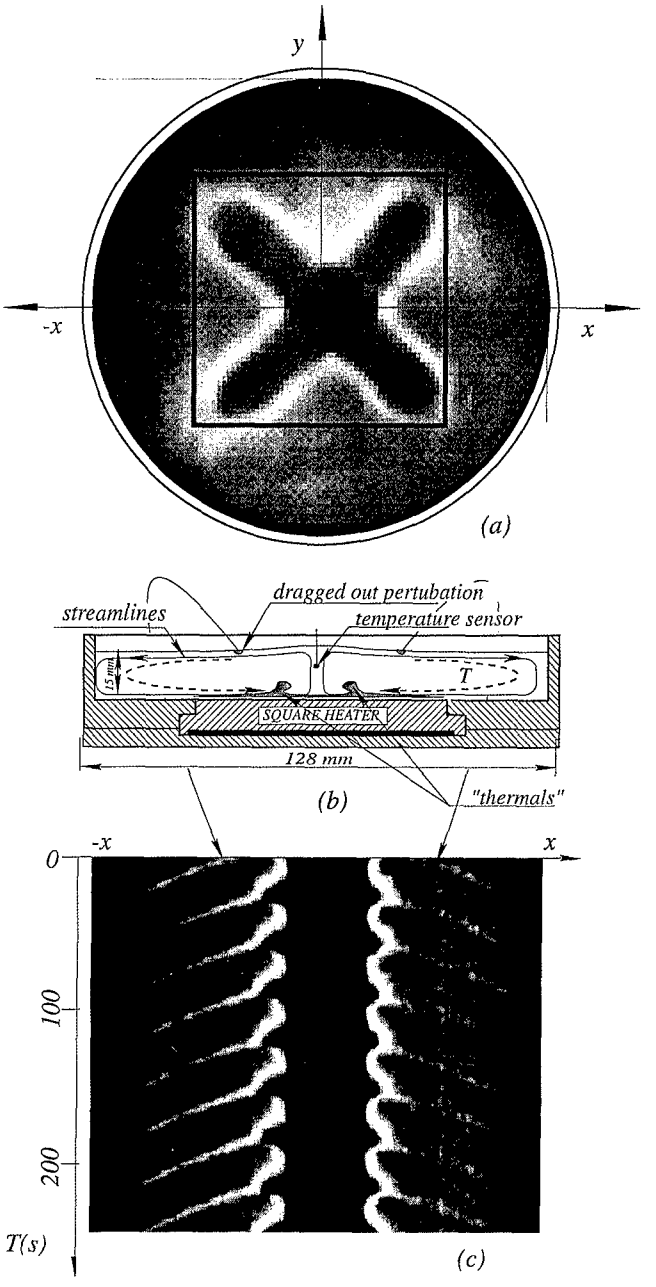

Fig. 1. (a) Image of the stationary planform below the time-dependent regime. (b) Cross-section of the experimental setup. Above the time-dependent threshold, the thermals coming from the thermal boundary layer generate hot drops which are dragged by the flow along the convective cells in a mean time T. (c) Time-dependent regime observed from the planform. The white traces in the spatiotemporal diagram correspond to the effect of the hot drop traveling near the surface in the x-axis direction. See [Mancini & Maza, 1997] for futher details.

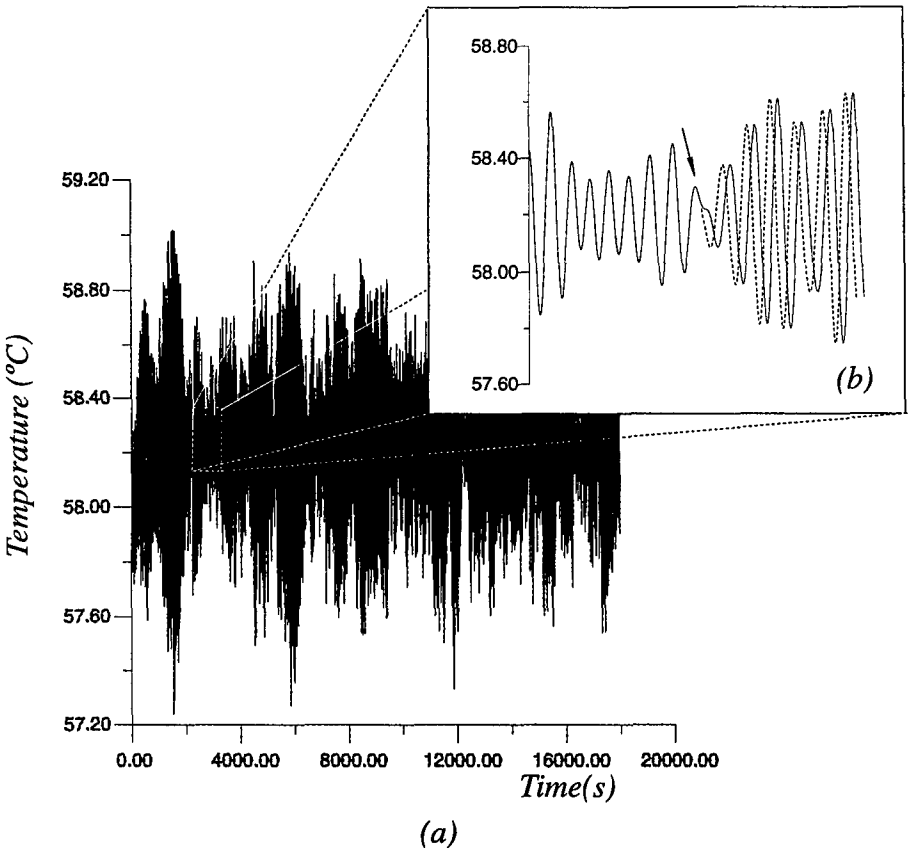

Fig. 2. (a) Experimental time behavior of the temperature signal. Vertical axis reports the temperature at the center of the cell near the bottom and horizontal axis reports the time in seconds ($T \simeq 330$ sec.). (b) Expanded view of the signal within the box which exhibits a phase jump (indicated by the arrow).

a round trip of a thermal along the convective cell. Further details on the experiment and a detailed discusion of this mechanism can be found in [Mancini & Maza, 1997].

If the temperature of the heater is further increased, a chaotic regime is reached. In this regime, an experimental measurement of the temperature at the center of the cell yields the data in Fig. 2. The signal shows trains of modulated oscillations, interrupted by localized events (phase defects), wherein the phase changes suddenly and the amplitude decreases to zero. Figure 2(b) highlights the presence of a phase defect within the data.

The experimental configuration provides a natural delayed interaction between thermals and thermal boundary layer since it reiterates at each position the local value of the order parameter after a *time delay* T, which equals the time lag necessary for the trip of the cell. Moreover, it involves a pertubated state far from the time dependent convection threshold. We propose a nonlinear model for the experimental temperature signal:

$$\dot{A} = \varepsilon A + \beta_1 \left(\int_0^\infty A^2(t-t') f(t') dt' \right) A + \beta_2 \left(\int_0^\infty A^4(t-t') f(t') dt' \right) A , \qquad (2)$$

$$\dot{\varepsilon} = \mu \left(S - \frac{\mu_1}{\mu} \varepsilon - k A^2 \right) . \qquad (3)$$

Here, all quantities are real. A represents the temperature, ε is a time dependent control parameter, β_1, β_2, μ_1, k are suitable fixed parameters, μ is a measure of the ratio between the characteristic time scales for A and ε, and S is a measure of the power provided to the system.

The relaxation oscillations of the temperature in Fig. 1(b) are represented by the normal form of a Hopf bifurcation [Eq. (2)], in which the saturating terms include a delayed function modulated by $f(t')$ to account the delayed action of the thermal inside the convective cell. Equation (3) models the slow evolution ($\mu < 1$) of the linear gain ε,

which is enhanced by the external heating (S) and depressed by the convective motion ($-kA^2$) which tends to uniformize top and bottom temperatures. In general $f(t')$ is a Gaussian-type function which expresses the lateral heat diffusion of the thermal to the main flow. However, we will consider the case of a perfectly localized pulse using a Dirac delta function located a $t' = T$. The model can be written as:

$$\dot{A} = \varepsilon A + \beta_1 A^2(t-T)A + \beta_2 A^4(t-T)A\,, \quad (4)$$

$$\dot{\varepsilon} = \mu\left(S - \frac{\mu_1}{\mu}\varepsilon - kA^2\right)\,. \quad (5)$$

Even though Eqs. (4) and (5) have been here introduced for modeling a specific experimental situation (a chaotic transition associated with quasiperiodicity), they are in fact rather general. When $T = 0$, $S < 0$, $\beta_1 > 0$, $\beta_2 < 0$, $\mu > 0$, $\mu_1 > 0$, $k > 0$, they model an excitable system, producing the so-called *Leontovitch* bifurcation, evidence of which has been shown experimentally on a CO_2 laser with intracavity saturable absorber [Plaza *et al.*, 1997]. For $T \neq 0$, they are similar to the models already introduced to describe self-sustained oscillations of confined jets [Villermaux & Hopfinger, 1994], or memory induced low frequency oscillations in closed convection boxes [Villermaux, 1995], or even the pulsed dynamics of a fountain [Villermaux, 1994].

Adjusting pump and delay parameters (S and T) in Eqs. (4) and (5), the system enters the chaotic region. This region, in fact, is split into two different regimes. For low T values, chaos is due to a local chaotic evolution of the phase, whereas no appreciable amplitude fluctuations are observed. This regime is called *phase turbulence* (PT). By increasing T, a transition toward *amplitude turbulence* (AT) is observed. In AT, the dynamics is dominated by the amplitude fluctuations, and a large number of defects is present. Both PT and AT have counterparts in a one-dimensional complex Ginzburg–Landau equation, for which the parameter space shows a transition from a regime of stable plane waves toward PT (Benjamin–Fair instability), followed by another transition to AT with evidence of space-time defects [Montagne *et al.*, 1996] .

3. The Control

The aim of the present paper is to control AT by an adaptive technique recently introduced for chaos recognition [Arecchi *et al.*, 1994], and applied to chaos control on CS [Boccaletti & Arecchi, 1995], chaos synchronization [Boccaletti *et al.*, 1997], targeting of chaos [Boccaletti *et al.*, 1997] and filtering of noise from chaotic data sets [Boccaletti *et al.*, 1997]. A direct application of such a technique to Eqs. (4) and (5) has been already provided in [Boccaletti *et al.*, 1997]. In that case, a small continuous perturbation $U(t)$ of the local value of the temperature leads to the suppression of the phase defects, and restores the regular Hopf oscillations. Here we show an alternative strategy for the control of AT, whereby tiny continuous modifications of the parameter T lead to a local control of the phase of the signal. In order to prove the efficacy of our method we use the system in Eqs. (4) and (5) in the AT regime. Here, the time delay is proportional to the spatial extension of the system. We will show that very small perturbations of the time delay are sufficient for the control of phase defects.

Let us, therefore, consider the modified system

$$\dot{A} = \varepsilon A + \beta_1 A^2(t-(T+U(t)))A + \beta_2 A^4(t-(T+U(t)))A\,, \quad (6)$$

$$\dot{\varepsilon} = \mu\left(S - \frac{\mu_1}{\mu}\varepsilon - kA^2\right)\,. \quad (7)$$

The control algorithm which selects $U(T)$ can be summarized as follows. At time $t_{n+1} = t_n + \tau_n$ (τ_n being an adaptive observation time interval to be later specified), the observer defines the variation $A(t_{n+1} - T_H) - A(t_{n+1})$ between the actual and the delayed values of A (T_H being the Hopf period). The corresponding variation rate

$$\lambda_{n+1} = \frac{1}{\tau_n}\log\left|\frac{A(t_{n+1}-T_H) - A(t_{n+1})}{A(t_n - T_H) - A(t_n)}\right| \quad (8)$$

allows to select a new time interval

$$\tau_{n+1} = \tau_n(1 - \mathrm{tgh}(g\lambda_{n+1})), \quad g > 0 \quad (9)$$

and consequently a new observation at the time $t_{n+2} = t_{n+1} + \tau_{n+1}$. In the following we perturb T by adding iteratively to it a controlling term given by

$$U(t) = \frac{1}{\tau_{n+1}}(A(t-T_H) - A(t))\,. \quad (10)$$

The details of the algorithm have been given in [Arecchi *et al.*, 1994; Boccaletti *et al.*, 1997]. For relatively small perturbations, the following approximation holds. Let $\langle\tau\rangle$ denote the average of the $\{\tau_n\}$ set, then Eq. (9) can be written as

$$\tau_{n+1} \simeq \langle\tau\rangle(1 - g\lambda_{n+1}) \quad (11)$$

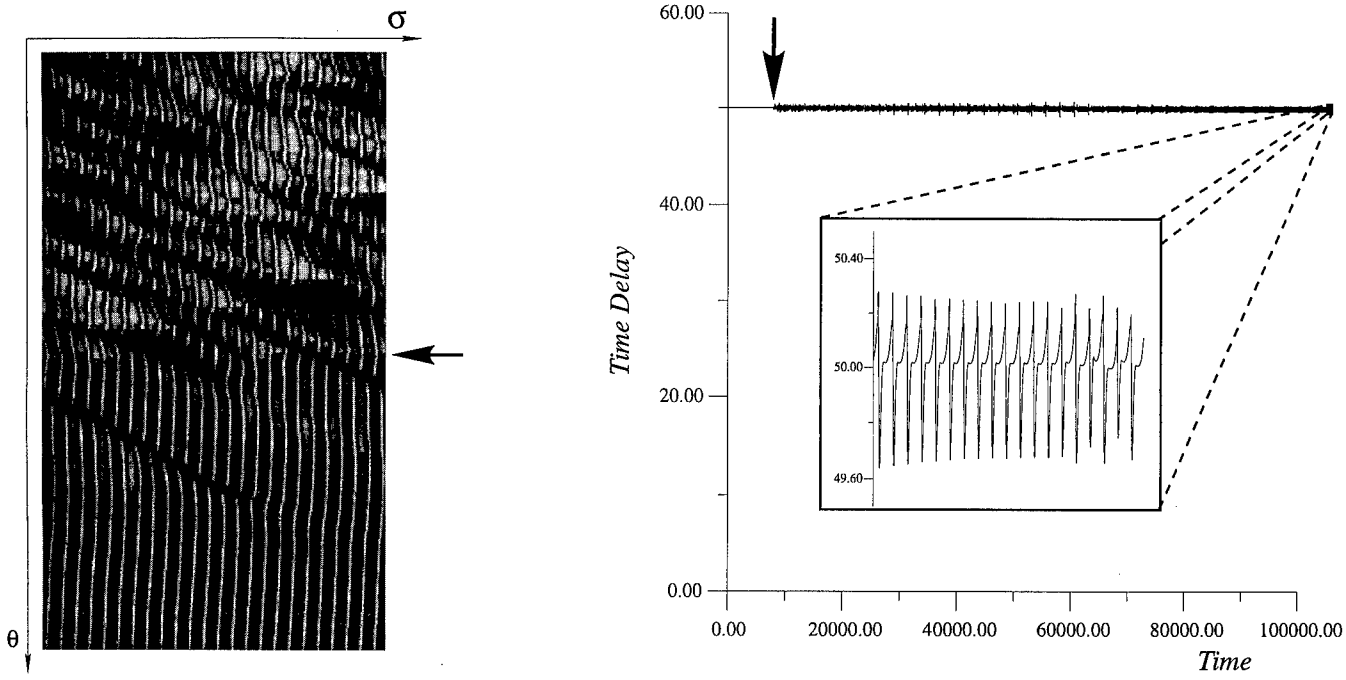

(a) (b)

Fig. 3. (a) Space(σ)-time(θ) representation of the controlling process for Eqs. (6) and (7). $\beta_1 = 1$, $\beta_2 = -1/16$, $\mu = 0.8$, $\mu_1 = 0.8$, $k = 11$, $S = 7$, $T_H = 1.95$. $T = 50$, AT regime. The dynamics is dominated by amplitude fluctuations, with the presence of defects. Phase defects appear as dislocations in such a representation. The algorithm ($K_1 = 0.3$, $K_2 = 0.07$) suppresses the defects and restores the regular oscillation. Arrow indicates the instant at which control is switched on. (b) The behavior of the time delay $T + U(t)$.

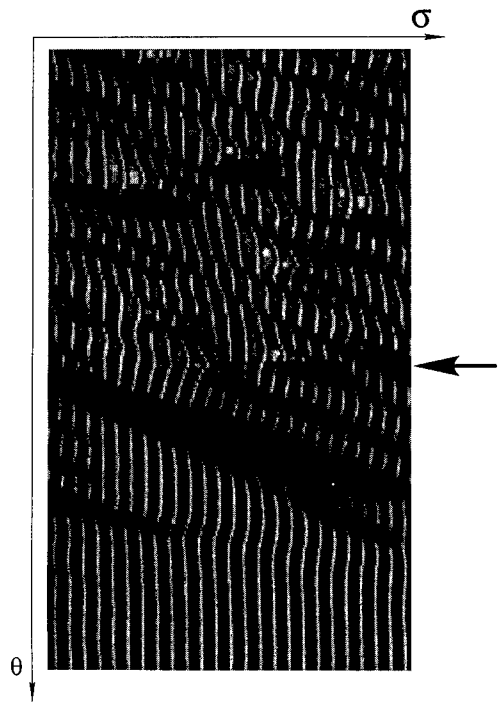

Fig. 4. $T = 50$, AT with 10% noise. Control with $K_1 = 0.3$, $K_2 = 0.07$. Same stipulations and parameters as in the caption of Fig. 2. Arrows indicate the instant at which control is switched on.

where (i) τ_n has been replaced with its ensemble average, and (ii) the tgh function has been linearized. In the same way, Eq. (8) can also be linearized as

$$\lambda(t) \simeq \frac{1}{\langle\tau\rangle} \frac{\dot{A}(t) - \dot{A}(t - T_H)}{A(t) - A(t - T_H)} \tag{12}$$

where the discretized stroboscopic observations have been approximated with a continuous inspection. Combining Eqs. (11) and (12) into Eq. (10), this reduces to

$$U(t) = K_1(A(t - T_H) - A(t)) + K_2(\dot{A}(t - T_H) - \dot{A}(t)) \tag{13}$$

with $K_1 = 1/\langle\tau\rangle$ and $K_2 = g/\langle\tau\rangle^2$. The consequences of this approximation are relevant. First of all, for $K_2 = 0$ one recovers the Pyragas control method [Pyragas, 1992]. However, in our case, K_1 and K_2 can be independently selected, and this introduces an extra degree of freedom with respect to [Pyragas, 1992].

In Fig. 3 we report the application of our method to Eqs. (6) and (7). The desired oscillation, which in the space-time representation gives rise to

a roll set, is controlled in AT [Fig. 2(a)]. Figure 2(b) reports the behavior of $U(t)$, which is vanishing up to the instant at which control is switched on.

Let us now discuss the robustness of our procedure against external noise. For this purpose, we add white noise to the measured A values before the onset of the adaptive feedback control. In such a case, the noise does not act additively, since it affects the calculation of $U(t)$, hence the local value of the time delay. As a consequence, the noise acts dynamically on the evolution of the system. A relevant result is that our method is robust against large amounts of noise, as it can be appreciated in Fig. 4 where the control is achieved within AT for 10% noise.

4. Conclusion

We show that is possible to control delayed dynamical systems applying small perturbations on the time delay variable. The control algorithm is easily implementable. The robustness of this method against noise has been verified. The proposed procedure would imply an experimental setup wherein the control is achieved by modifying the cell length.

Acknowledgments

Work was partly supported by Ministerio de Educacion y Ciencia, Spain (Grant n. PB95-0578), Universidad de Navarra, Spain (PIUNA) and Research Project MURST 40% "Dynamical Systems and Control". H. Mancini also thanks Human Capital and Mobility Network "Complexity and Chaos" (CXRX-CT-94-0546).

References

Arecchi, F. T., Giacomelli, G., Lapucci, A. & Heucci, R. [1992] "Two-dimensional representation of a delayed dynamical system," *Phys. Rev.* **A45**, R4225–R4228.

Arecchi, F. T., Basti, G., Boccaletti, S. & Perrone, A. L. [1994] "Adaptive recognition of a chaotic dynamics," *Europhys. Lett.* **26**, 327–332.

Boccaletti, S. & Arecchi, F. T. [1995] "Adaptive control of chaos," *Europhys. Lett.* **31**, 127–132.

Boccaletti, S., Farini, A., Kostelich, E. J. & Arecchi, F. T. [1997] "Adaptive targeting of chaos," *Phys. Rev.* **E55**, R4845–R4848.

Boccaletti, S., Farini, A. & Arecchi, F. T. [1997] "Adaptive synchronization of chaos for secure communication," *Phys. Rev.* **E55**, 4979–4981.

Boccaletti, S., Giaquinta, A. & Arecchi, F. T. [1997] "Adaptive recognition and filtering of noise using wavelets," *Phys. Rev.* **E55**, 5393–5398.

Boccaletti, S., Maza, D., Mancini, H., Genesio, R. & Arecchi, F. T., "Control of defects and space-like structures in delayed dynamical systems," *Phys. Rev. Lett.*, to appear.

Giacomelli, G. & Politi, A. [1996] "Relationship between delayed and spatially extended dynamical systems," *Phys. Rev. Lett.* **76**, 2686–2689.

Lu, W., Yu, D. & Harrison, R. G. [1996] "Control of patterns in spatiotemporal chaos in optics," *Phys. Rev. Lett.* **76**, 3316–3319.

Mancini, H. & Maza, D. [1997] "Bénard Marangoni thermal oscillators: An experimental study," *Phys. Rev.* **E55**, 2757–2768.

Montagne, R., Hernández-Garcia, E. & San Miguel, M. [1996] "Winding number instability in the phase turbulence regime of the complex Ginzburg–Landau equation," *Phys. Rev. Lett.* **77**, 267–270.

Ott, E., Grebogi, C. & Yorke, J. A. [1990] "Controlling chaos," *Phys. Rev. Lett.* **64**, 1196–1199.

Plaza, F., Velarde, M. G., Arecchi, F. T., Boccaletti, S., Ciofini, M. & Meucci, R. [1997] "Excitability following an avalanche collapse process," *Europhys. Lett.* **38**, 85–90.

Pyragas, K. [1992] "Continuous control of chaos by self controlling feedback," *Phys. Lett.* **A170**, 421–425.

Villermaux, E. & Hopfinger, E. J. [1994] "Self sustained oscillations of a confined jet: A case study for the nonlinear delayed saturation model," *Physica* **72D**, 230–238.

Villermaux, E. [1994] "The pulsed dynamics of a fountain," *Nature* **371**, 24–26.

Villermaux, E. [1995] "Memory induced low-frequency oscillations in closed convection boxes," *Phys. Rev. Lett.* **75**, 4618–4621.

International Journal of Bifurcation and Chaos, Vol. 8, No. 9 (1998) 1849–1856

DIFFUSION PARAMETER CONTROL OF SPATIOTEMPORAL CHAOS

RAUL MONTAGNE*
Instituto de Física, Facultad de Ciencias & Facultad de Ingeniería,
T. Narvaja 1674, C. P. 11200,
Universidad de la República, Montevideo, Uruguay
Departament de Física, Universitat de les Illes Balears,
E-07071 Palma de Mallorca, Spain

PERE COLET†
Instituto Mediterráneo de Estudios Avanzados, IMEDEA (CSIC-UIB),
E-07071 Palma de Mallorca, Spain

Received July 31, 1997; Revised December 2, 1997

The stabilization of periodic solutions in the regime of spatiotemporal chaos through a diffusion parameter control is studied. We show that unstable plane waves in the Complex Ginzburg–Landau equation can be effectively stabilized in chaotic regimes such as phase turbulence and spatiotemporal intermittency or defect turbulence.

1. Introduction

There has been recently a considerable experimental and theoretical effort to characterize Spatiotemporal Chaos (STC) [Cross & Hohenberg, 1994; Gollub, 1994]. Weak STC seems to be an ubiquitous phenomenon in large nonequilibrium systems. In some cases STC arise in the proximity of threshold and can be described within the context of weakly nonlinear theories. These theories are well developed in the form of the so-called complex Ginzburg–Landau equations (CGLE) [Cross & Hohenberg, 1993]. The CGLE is a prototypical equation for a complex field A that exhibit STC [Chaté, 1995]. It accounts for the slow modulations, in space and time of the oscillatory state in a physical system which undergoes a Hopf bifurcation [van Saarloos & Hohenberg, 1992].

The control of spatiotemporal chaos is a complicated problem, and so, there is a wide variety of methods intended to control such chaotic behavior. There have been several attempts to achieve such control in the CGLE [Aranson *et al.*, 1994; Bleich & Socolar, 1996; Mertens *et al.*, 1994; Battogtokh & Mikhailov, 1996; Montagne & Colet, 1997]. The most common approach is adding time-delayed feedback terms to the CGLE. The feedback can be either local [Bleich & Socolar, 1996] (at each spatial point, the field at the same point at previous times is fed back) or global [Mertens *et al.*, 1994; Battogtokh & Mikhailov, 1996] (at each spatial point a term proportional to the integral of the field over the spatial variable is fed back). Feedback has also been used for control in a nonlinear drift-wave equation driven by a sinusoidal wave [Gang,

*Present address: Supercomputa Computations Research Institute, Florida State University, Tallahassee, FL 32306-4052, USA.
E-mail: montagne@fisica.edu.uy, WWW http://www.imedea.uib.es/~montagne
†E-mail: pere@hp1.uib.es, WWW http://www.imedea.uib.es/~pere

1993]. And, in conjunction with a spatial filter, it has been applied to stabilize rolls and hexagonal structures in a model for a transversally extended three level laser [Lu *et al.*, 1996] and to control filamentation in a model for wide aperture semiconductor lasers based on the Swift–Hohenberg equation [Bleich *et al.*, 1997].

A different approach using nonlinear diffusion effects has been introduced recently in [Montagne & Colet, 1997]. It was shown that an imaginary nonlinear diffusion term was able to stabilize unstable plane waves in several regimes of STC. Here we generalize this study considering the case of having both, real and imaginary nonlinear diffusion terms in the CGLE. One of the main advantages of this generalization is the possibility of controlling plane waves outside the region where control works using only an imaginary nonlinear diffusion term. In particular, in that case it was practically impossible to stabilize plane waves with a large wavevector, whereas this can be easily achieved in the case shown here. Also, in situations where control was already possible, this extension allows to achieve the stabilization of plane waves using a control parameter with smaller absolute value. As it happens with most of the control techniques, stabilization is possible only when starting from an initial state close to the unstable orbit. If the initial condition is an arbitrary chaotic state, the system will explore the different regions in phase space of the chaotic attractor and eventually may approach the unstable orbit one wishes to stabilize, although this can take an extremely long time. If the system goes close enough to the unstable orbit then the control technique shown here should work. Although we are not exploring in detail how close to the unstable orbit the system has to be to achieve stabilization, we show numerically that our scheme is robust to finite size perturbations of the initial condition.

In Sec. 2 we briefly describe the parameter regions for which different chaotic behaviors have been found for the CGLE and we introduce the modified equation. Section 3 is devoted to the linear stability analysis of the plane wave solutions. We calculate for which parameter values the added term is able to stabilize plane waves in the STC regions of the CGLE. In Sec. 4 we show, integrating the equations numerically, that the region of stability of the plane waves when finite size perturbations are applied is in excellent agreement with the analytical prediction of the linear stability analysis. Finally we give some concluding remarks in Sec. 5.

2. Model

The one-dimensional CGLE [Cross & Hohenberg, 1993; van Saarloos & Hohenberg, 1992; van Saarloos, 1995; Newell *et al.*, 1993] for a complex field $A(x, t)$, describes the slow dynamics of spatially extended systems close to a Hopf bifurcation,

$$\partial_t A = A + (1 + ic_1)\partial_x^2 A - (1 + ic_2)|A|^2 A\,. \quad (1)$$

We will assume periodic boundary conditions throughout the paper. This equation admits among other exact solutions, plane waves of the form

$$A_{pw}(x, t) = A_0 e^{i(kx-\omega t)}\,, \quad (2)$$

with amplitude $A_0 = \sqrt{1-k^2}$, $|k| < 1$ and frequency $\omega = c_2 + (c_1 - c_2)k^2$.

For $1 + c_1c_2 > 0$ plane wave solutions are linearly stable for wave numbers smaller than a limit value $|k| \leq k_E$ given by

$$k_E^2 = \frac{1 + c_1c_2}{3 + c_1c_2 + 2c_2^2}\,. \quad (3)$$

For $|k| > k_E$, plane waves are unstable to phase perturbations (Eckhaus instability [Eckhaus, 1965]). The stability range vanishes at $1+c_1c_2 = 0$, the Benjamin–Feir–Newell (BFN) line, and there are no stable plane wave solutions for $1 + c_1c_2 < 0$.

Numerical work for large system size [Shraiman *et al.*, 1992; Chaté, 1994, 1995] has identified regions of the parameter space displaying different kinds of regular and spatiotemporal chaotic behavior, leading to a "phase diagram" for the CGLE in the plane c_1–c_2. The five different regions, each leading to a different asymptotic phase, are shown in Fig. 1. Two of these regions are in the BFN stable zone and the other three in the BFN unstable one. In this paper we will concentrate in the regimes with a chaotic behavior, namely SpatioTemporal Intermittency, Phase Turbulence and Defect Turbulence. A detailed description can be found in [Chaté, 1995].

We modify the CGLE by changing a parameter of the system dynamically and proportionally to the deviation of the system from the state to be stabilized. We will show that the stabilization of plane waves can be achieved by replacing the coefficient c_1 by $c_1 + \gamma(|A|^2/|A_{pw}|^2 - 1)$ where $\gamma = \gamma_r + i\gamma_i$ is a complex constant and $|A_{pw}| = A_0$ is the modulus of the plane wave to be stabilized. Notice that

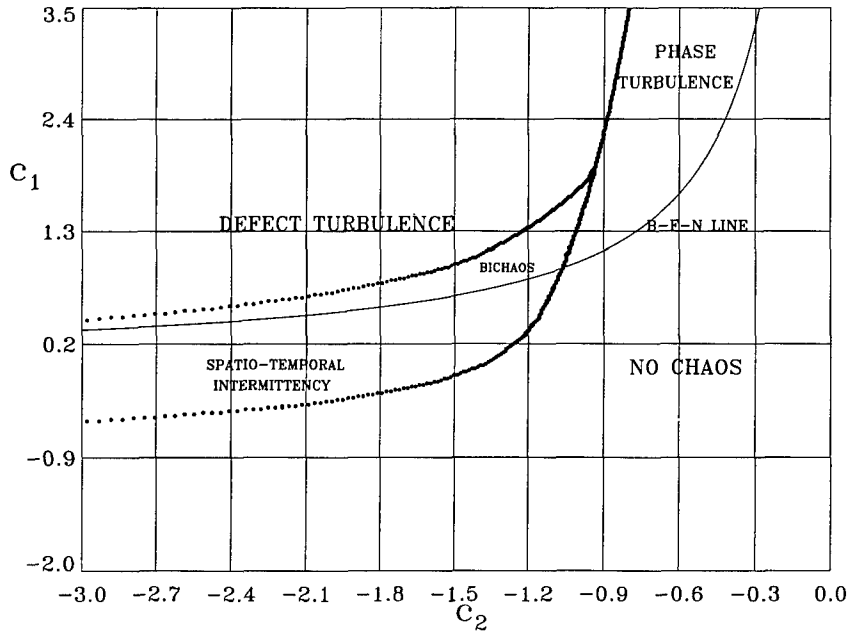

Fig. 1. Regions of the parameter space $c_1 - c_2$ for which the $d = 1$ CGLE displaying different kinds of regular and chaotic behavior. The Benjamin–Feir–Newell line (BFN line) is also shown.

as the added term $\gamma(|A|^2/A_0^2 - 1)$ vanishes identically for $A = A_0$, any plane wave A_0 that is a solution of (1) is also a solution of the modified equation. We are not changing the solution but we will change its stability. The added term also preserves the phase invariance of the solution of the original CGLE, $A \to Ae^{i\psi}$, with ψ being an arbitrary phase. The modified CGLE is then explicitly given by,

$$\partial_t A = A + [1 + ic_1 + \gamma(|A|^2/A_0^2 - 1)]\partial_x^2 A - (1 + ic_2)|A|^2 A\,. \tag{4}$$

3. Stability Analysis

We use a standard linearization procedure for studying the stability of the plane wave solutions (2) in Eq. (4). Consider the time evolution of small perturbations in the amplitude and phase,

$$A(x, t) = (A_0 + \varepsilon r(x, t))e^{i(kx - \omega t + \varepsilon\phi(x,t))}\,, \tag{5}$$

where $r(x, t)$ and $\phi(x, t)$ are real perturbations in the amplitude and phase, respectively and ε is a formal parameter to keep track of small numbers.

Substituting (5) in (4) yields to a polynomial in ε. The first order terms yield the linearized equations for the perturbations.

$$\partial_t r = -2(\gamma_r k^2 + A_0^2)r - 2A_0 k\partial_x\phi - 2c_1 k\partial_x r - c_1 A_0\partial_x^2\phi + \partial_x^2 r\,, \tag{6}$$

$$\partial_t\phi = -2c_2 A_0 r - 2\gamma_i\frac{k^2}{A_0}r - 2c_1 k\partial_x\phi + 2\frac{k}{A_0}\partial_x r + \partial_x^2\phi + \frac{c_1}{A_0}\partial_x^2 r\,. \tag{7}$$

We consider solutions of (6) and (7) proportional to $e^{\eta t + iqx}$, where for periodic boundary conditions q is real whereas η is in general a complex quantity. By substituting in (6) and (7) we obtain the dispersion relation

$$\begin{vmatrix} \eta + 2(A_0^2 + 2\gamma_r k^2) + q^2 + 2ic_1 qk & 2iqk - c_1 q^2 \\ c_1 q^2 + 2c_2 A_0^2 - 2iqk + 2\gamma_i k^2 & \eta + q^2 + 2ic_1 qk \end{vmatrix} = 0\,. \tag{8}$$

The solutions of (8) are

$$\eta = -(A_0^2 + \gamma_r k^2 + q^2 + 2ic_1 qk) \pm \sqrt{u + iv}\,, \tag{9}$$

where u and v are polynomials

$$u = (A_0^2 + \gamma_r k^2)^2 + 4q^2 k^2 - 2c_1 c_2 A_0^2 q^2 - c_1^2 q^4 - 2\gamma_i c_1 q^2 k^2\,, \tag{10}$$

$$v = 4qk(c_1 q^2 + c_2 A_0^2 + \gamma_i k^2)\,. \tag{11}$$

The real part of η indicates the growth rate of the perturbations,

$$\mathrm{Re}(\eta) = -A_0^2 - \gamma_r k^2 - q^2 \pm \sqrt{\frac{u + \sqrt{u^2 + v^2}}{2}}\,. \quad (12)$$

The plus and minus sign ($\pm$) correspond to two different branches. For the negative sign in (12), $\mathrm{Re}(\eta) < 0$, so these perturbations are always damped.

For the positive sign of the square root in (12) $\mathrm{Re}(\eta) = 0$ at $q = 0$, so all the plane wave solutions are marginally stable. The origin of this neutral stability is the phase invariance $A \to Ae^{i\psi}$ of the solutions of Eqs. (1) and (4). For q very large, $\mathrm{Re}(\eta) \simeq -q^2$, so short wavelength perturbations are always damped. However long wavelength perturbations can grow destabilizing the original plane wave solution, to see this we expand (12) for small q.

$$\mathrm{Re}(\eta) = Dq^2 + O(q^4)\,, \quad (13)$$

where

$$D = -1 - \frac{c_1 c_2 A_0^2}{a} + 2\left(1 + \frac{c_2^2 A_0^4}{a^2}\right)\frac{k^2}{a} + \gamma_i\left(-\frac{c_1 k^2}{a} + 4\frac{c_2 k^4 A_0^2}{a^3}\right) + 2\gamma_i^2 \frac{k^6}{a^3}\,. \quad (14)$$

and

$$a = (A_0^2 + \gamma_r k^2)\,. \quad (15)$$

If this coefficient is positive, there is a range of long wavelength perturbations that grow. The condition $D < 0$ is necessary for stability but not sufficient, since the growth coefficient obtained from the full expression (12) can be positive for some finite value of q despite the coefficient D being negative. However, for the values of c_1 and c_2 considered in this work the requirement $D < 0$ gives a very good limit for the stability region.

For the unperturbed CGLE ($\gamma = 0$) the condition $D < 0$, leads to the standard Eckhaus instability limit: $|k| < k_E$ with k_E given by (3). Since the control is done through a diffusive term, the added term never changes the stability of the homogeneous solution $k = 0$. For an arbitrary plane wave of wave number k one has to solve the cubic equation $D = 0$ to find explicitly the range of values of k for which the plane wave is stable. In Figs. 2 and 3 we plot this range as a function of the parameter c_1 for several values of γ and c_2. When no control is applied ($\gamma = 0$) the stability region in the k–c_1 plane is limited by a branch of Eq. (3) (dashed line in Figs. 2 and 3) whose vertex corresponds to the BFN point. Decreasing the value of c_1 the width of the stability region $|k| < k_E$ increases, and for $c_1 \to -\infty$, $k_E \to 1$.

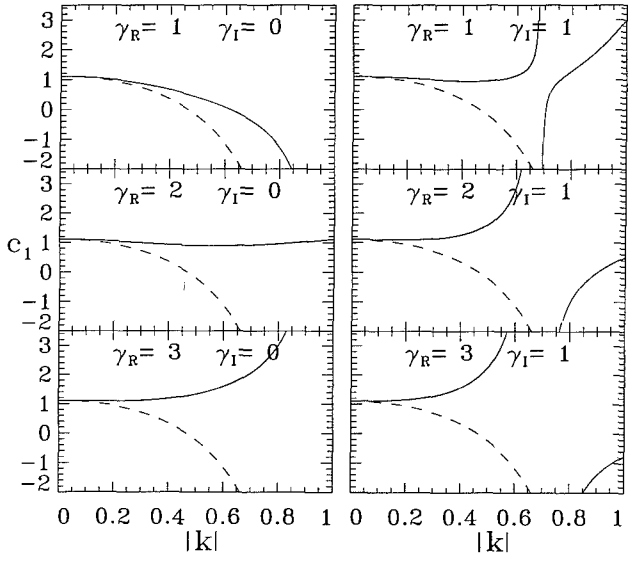

Fig. 2. The shadowed zone shows the stability region for the plane wave (2) for $c_2 = -0.9$. Left column and from top to bottom, $\gamma_i = 0$ and $\gamma_r = 1, 2, 3$. Right column and from top to bottom, $\gamma_i = 1$ and $\gamma_r = 1, 2, 3$. For comparison, the boundary of the stability region for $\gamma = 0$, given by Eq. (3), is shown in all the figures as a dashed line.

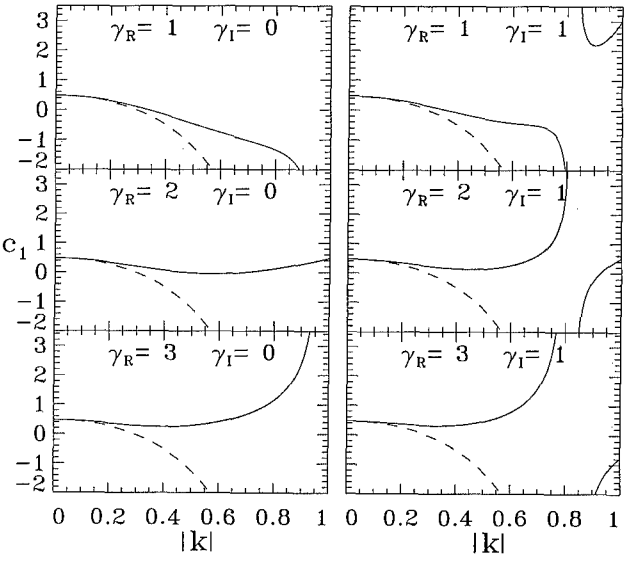

Fig. 3. The shadowed zone shows the stability region for the plane wave (2) for $c_2 = -2.1$. Left column and from top to bottom, $\gamma_i = 0$ and $\gamma_r = 1, 2, 3$. Right column and from top to bottom, $\gamma_i = 1$ and $\gamma_r = 1, 2, 3$. For comparison, the boundary of the stability region for $\gamma = 0$ is shown in all the figures as a dashed line.

As $|\gamma|$ is increased the stability region changes its shape, so that it is possible to stabilize plane waves which were unstable without control. Increasing the value of $|\gamma|$ one finds stabilization of plane waves for values of c_1 well above the BFN line, in the regions of phase turbulence and defect turbulence of the original CGLE. In particular, for $c_2 = -0.9$ the BFN line corresponds in Fig. 2 to a horizontal line at $c_1 = 1.11$. Below this value for c_1, plane waves with a large wavevector (outside the dashed line) are unstable without control. As shown in Fig. 2 they can be easily stabilized with a real control parameter. For $c_1 > 1.11$ we are in the phase turbulence regime up to $c_1 \approx 2.3$ (see Fig. 1). For larger values of c_1 we enter in the defect turbulence region. It is possible to stabilize plane waves in the region of phase turbulence taking $\gamma_r \geq 3$ and $\gamma_i = 0$, or $\gamma_r \geq 1$ and $\gamma_i = 1$. For $c_2 = -2.1$ the BFN line corresponds in Fig. 3 to a horizontal line at $c_1 = 0.476$. Below that level

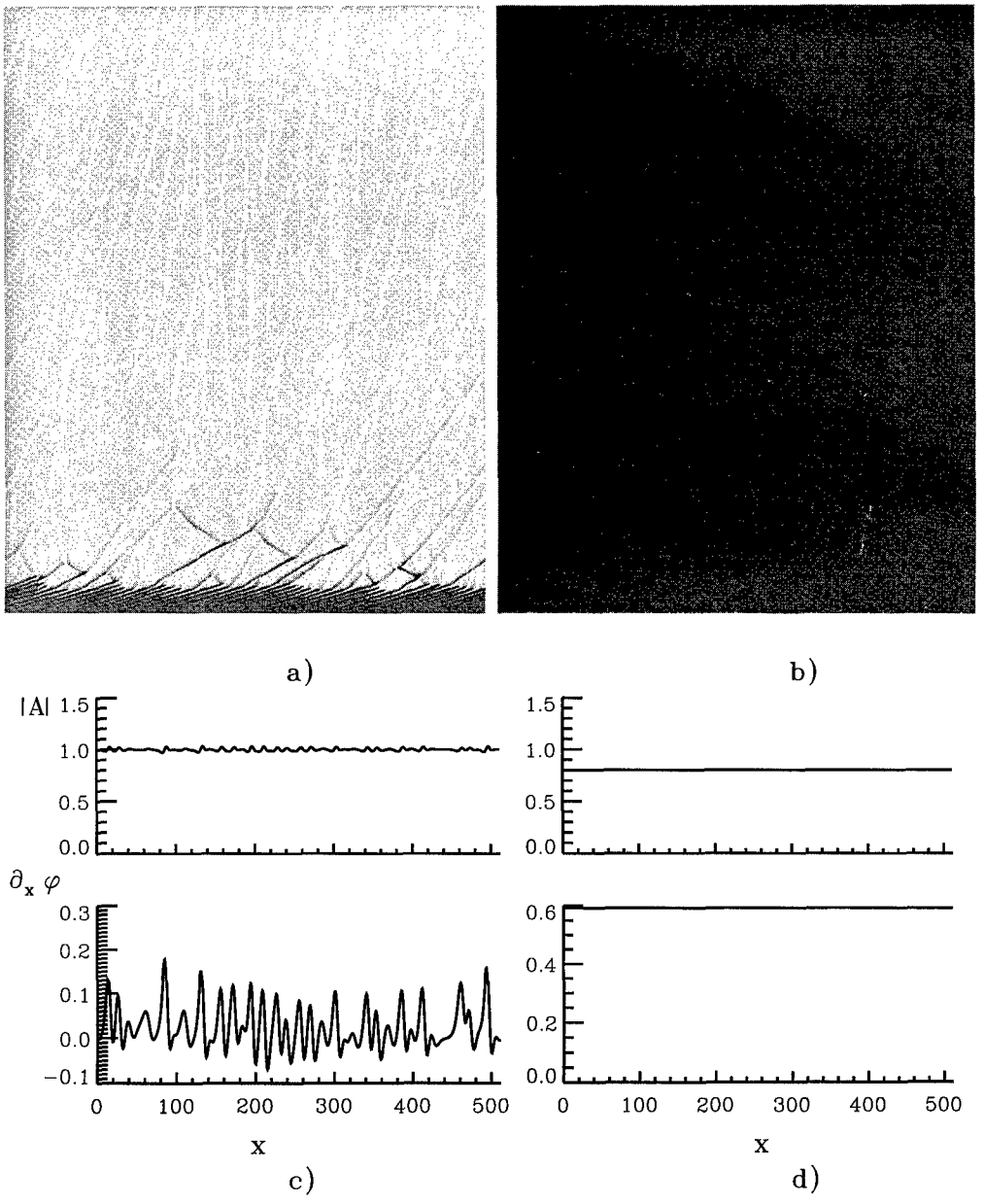

Fig. 4. Spatiotemporal evolution of the CGLE (4) for $c_1 = 1.5$, $c_2 = -0.9$ starting from a perturbed plane wave (16) with $k = 0.5$ and $\sigma = 0.007$. Figures (a) and (b) show $|A(x, t)|$ with time running upwards from $t = 0$ to $t = 1000$ and x in the horizontal direction for $\gamma = 0$ and $\gamma = 3 + 0i$, respectively. The absolute value of the field $|A(x, t_0)|$ and the phase gradient $\partial_x \phi(x, t_0)$ at $t_0 = 950$ are displayed in (c) and (d) for $\gamma = 0$ and $\gamma = 3 + 0i$, respectively.

there are the coexistence of stable plane waves and spatiotemporal intermitency. Plane waves with wavevector outside the dashed line are unstable and will lead to spatiotemporal intermitency without control. As shown in Fig. 3 the real part of γ is very effective in the stabilization of these plane waves. For $c_1 > 0.476$ we are above the BFN line, and increasing c_1 we enter first in the bichaos regime and later in the defect turbulence regime (see Fig. 1). As shown in Fig. 3, stabilization of plane waves in both regions is possible using for example $\gamma = 1 + i$.

In general, the real part of γ is specially effective in extending the stability region to plane waves of a large wave number. We should stress that stabilization of plane waves with wavevector close to one was extremely difficult to achieve using only an imaginary nonlinear diffusion term, even taking large values for γ_i, as shown in [Montagne & Colet, 1997]. Above the BFN line, stabilization of unstable plane waves in the regions of phase and defect turbulence can be achieved taking γ to be purely real (left column in Figs. 2 and 3) or purely

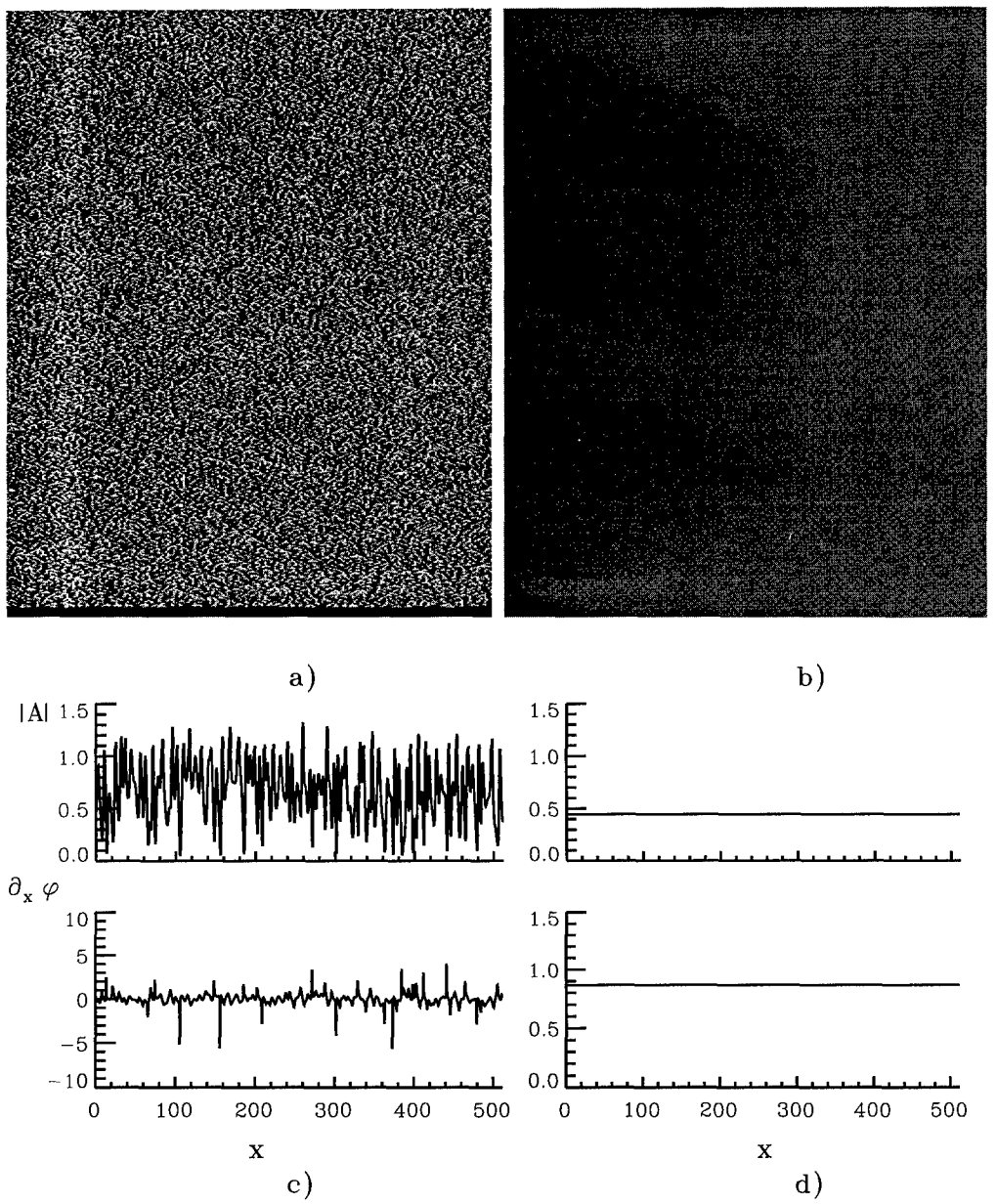

Fig. 5. Spatiotemporal evolution of the CGLE for $c_1 = 2.5$, $c_2 = -2.1$ starting from a perturbed plane wave with $k = 0.9$. Figures (a) and (b) show $|A(x, t)|$ for $\gamma = 0$ and $\gamma = 1 + i$, respectively. The values of $|A(x, t_0)|$ and $\partial_x \phi(x, t)$ at $t_0 = 950$ are displayed in (c) and (d) for $\gamma = 0$ and $\gamma = 1 + i$, respectively. Other parameters are as in Fig. 4.

imaginary (see ref. [Montagne & Colet, 1997]). However, it is more efficient to take γ complex, since one can achieve stabilization with smaller values of $|\gamma|$.

4. Numerical simulations

We have integrated numerically Eqs. (1) and (4) using a pseudospectral code with periodic boundary conditions and second-order accuracy in time. Spatial resolution was typically 1024 modes. Time step was typically $\Delta t = 0.001$. The system size was always taken as $L = 512$. The details of the numerical method can be seen in [Montagne *et al.*, 1997]. We start from an initial condition which corresponds to a plane wave plus a small random perturbation

$$A(x, t = 0) = \sqrt{1 - k^2} e^{ikx} + \sigma \xi(x) \qquad (16)$$

where $\xi(x)$ is a complex Gaussian random perturbation of zero mean and variance $\langle \xi(x) \xi^*(x') \rangle = 2\delta(x - x')$.

We have performed numerical simulations in different regions of the phase diagram (Fig. 1) to verify the results obtained from the linear stability analysis when finite size perturbations are applied. We have found a very good agreement between the prediction of the linear stability analysis and the numerical simulations. As characteristic examples we show the following results.

Figure 4 shows the stabilization of a plane wave for parameter values $c_1 = 1.5$ and $c_2 = -0.9$. This corresponds to the phase turbulence regime (see Fig. 1), where no plane waves are stable for the original CGLE. As predicted by the linear stability analysis, a perturbed plane wave with $k = 0.5$ can easily be stabilized with $\gamma_r = 3$ and $\gamma_i = 0$ while for $\gamma = 0$ the same initial condition decays in time $t = 80$ (approx.) to phase turbulence.

Figure 5, obtained for parameter values $c_1 = 2.5$ and $c_2 = -2.1$, shows stabilization of plane waves in the region of defect turbulence, where for the unperturbed CGLE there are no stable plane waves and the field A shows a strongly disordered STC state characterized by the presence of defects. As predicted by the linear stability analysis, a perturbed plane wave with $k = 0.9$ can be stabilized with $\gamma_r = 1$ and $\gamma_i = 1$.

5. Concluding Remarks

Our study of the dynamics of the CGLE with a nonlinear diffusion term demonstrates the possibility of stabilization of an unstable plane wave in different regimes of STC. Since the added term vanish for the stabilized plane wave, this plane wave is exactly the same unstable solution of the original CGLE. Although our method does not change the stability of the homogeneous solution $k = 0$, it is quite effective in stabilizing plane waves with nonzero wavevector. We have shown that the real part of the nonlinear diffusive term is specially effective for stabilizing plane waves with wavevector close to one. Also, in general it is more efficient to use a nonlinear diffusive term with both real and imaginary parts, in the sense that stabilization can be achieved with a control parameter with smaller absolute value.

Finally, we have studied numerically the stability of the plane waves when finite size perturbations are applied. The results are in excellent agreement with the analytical predictions of the linear stability analysis.

Acknowledgments

Financial support from Dirección General de Investigación Científica y Técnica (DGICYT, Spain), Projects PB94-1167 and PB94-1172, is acknowledged. R. Montagne also acknowledges partial support from the Programa de Desarrollo de Ciencias Básicas (PEDECIBA, Uruguay).

References

Aranson, I., Levine, H. & Tsimring, L. [1994] "Controlling spatiotemporal chaos," *Phys. Rev. Lett.* **72**, 2561–2564.

Battogtokh, D. & Mikhailov, A. [1996] "Controlling turbulence in the complex Ginzburg–Landau equation," *Physica* **D90**, 84–95.

Bleich, M. & Socolar, J. E. S. [1996] "Stability of periodic orbits controlled by time-delay feedback," *Phys. Lett.* **A210**, 87–94.

Bleich, M. E., Hochheiser, D., Moloney, J. V. & Socolar, J. E. S. [1997] "Controlling extended systems with spatially filtered, time-delayed feedback," *Phys. Rev.* **E55**, 2119–2126.

Chaté, H. [1994] "Spatiotemporal intermittency regimes of the one-dimensional complex Ginzburg–Landau equation," *Nonlinearity* **7**(1), 185–204.

Chaté, H. [1995] "Disordered regimes of the one-dimensional complex Ginzburg–Landau equation," in *Spatiotemporal Patterns in Nonequilibrium Complex Systems*, Vol. XXI of Santa Fe Institute in the Sciences of Complexity, eds. Cladis, P. & Palffy-Muhoray, P. (Addison-Wesley, NY), pp. 5–49.

Cross, M. & Hohenberg, P. [1993] "Pattern formation outside of equilibrium," *Rev. Mod. Phys.* **65**, 851–1112 and references therein.

Cross, M. & Hohenberg, P. [1994] "Spatiotemporal chaos," *Science* **263**, 1569–1570.

Eckhaus, W. [1965] *Studies in Nonlinear Stability Theory* (Springer, Berlin).

Gang, H. [1993] "Controlling chaos in systems described by partial differential equations," *Phys. Rev. Lett.* **71**, 3794–3797.

Gollub, J. [1994] "Spirals and chaos," *Nature* **367**, 318.

Lu, W., Yu, D. & Harrison, R. [1996] "Control of patterns in spatiotemporal chaos in optics," *Phys. Rev. Lett.* **76**, 3316–3319.

Mertens, F., Imbihl, R. & Mikhailov, A. [1994] "Turbulence and standing waves in oscillatory chemical reactions with global coupling," *J. Chem. Phys.* **101**, 9903–9908.

Montagne, R. & Colet, P. [1997] "Nonlinear diffusion control of spatiotemporal chaos in the complex Ginzburg–Landau equation," *Phys. Rev.* **E56**, 4017–4024.

Montagne, R., Hernández-García, E., Amengual, A. & San Miguel, M. [1997] "Wound-up phase turbulence in the complex Ginzburg–Landau equation," *Phys. Rev.* **E56**, 151–167.

Newell, A. C., Passot, T. & Lega, J. [1993] "Order parameter equations for patterns," *Annu. Rev. Fluid Mech.* **25**, 399–453.

Shraiman, B., Pumir, A., van Saarloos, W., Hohenberg, P., Chaté, H. & Holen, M. [1992] "Spatiotemporal chaos in the one-dimensional complex Ginzburg-Landau equation," *Physica* **D57**, 241–248.

van Saarloos, W. [1995] "The complex Ginzburg–Landau equation for beginners," in *Spatiotemporal Patterns in Nonequilibrium Complex Systems*, Vol. XXI of Santa Fe Institute in the Sciences of Complexity, eds. Cladis, P. & Palffy-Muhoray, P. (Addison-Wesley, NY), pp. 19–31.

van Saarloos, W. & Hohenberg, P. [1992] "Fronts, pulses, sources and sinks in generalized complex Ginzburg–Landau equations," *Physica* **D56**, 303–367; (Errata) [1993] *Physica* **D69**, 209.

SUBSCRIPTION INFORMATION

Home Page: **http://www.wspc.com.sg**

USA **World Scientific Publishing Co., Inc.**
1060 Main Street, River Edge, NJ 07661, USA
Toll-Free-Tel: 1-800-227-7562 Toll-Free-Fax: 1-888-977-2665 E-mail: sales@wspc.com

UK **World Scientific Publishing (UK) Ltd.**
57 Shelton Street, Covent Garden, London WC2H 9HE, UK
Fax: 44-171-836-2020 Tel: 44-171-836-0888 E-mail: sales@wspc2.demon.co.uk

SINGAPORE **World Scientific Publishing Co. Pte. Ltd.**
Farrer Road, P O Box 128, SINGAPORE 912805 Cable Address: "COSPUB" Telex: RS 28561 WSPC
Fax: 65-382-5919 Tel: 65-382-5663 E-mail: sales@wspc.com.sg

HONG KONG **World Scientific Publishing (HK) Co. Ltd.**
P O Box 72482, Kowloon Central Post Office, HONG KONG
Fax: 852-2-771-8155 Tel: 852-2-771-8791 E-mail: wsped@hk.super.net

INDIA **World Scientific Publishing Co. Pte. Ltd.**
4911, 9th Floor, High Point IV, 45 Palace Road, Bangalore 560 001, INDIA
Telex: 0845-2900- PCO IN **Fax: 91-80-334-4593** Tel: 91-80-220-5972

TAIWAN **World Scientific Publishing Co. Pte. Ltd.**
5F-6, No. 88, Sec 3, Hsin-Sheng S Road, Taipei, Taiwan, ROC
Fax:886-2-2366-0460 Tel: 886-2-2369-1366 E-mail: wsptw@ms13.hinet.net

❑ Please enter my subscription:

IJBC (ISSN: 0218-1274)	Vol. 8/1998 (12 issues)		
Institutions/libraries	❑ US$1399	❑ DM2331	❑ S$1888
SPECIAL RATES			
Institutions/libraries from developing countries	❑ US$803	❑ DM1398	❑ S$1133
Individuals	❑ US$536	❑ DM932	❑ S$755
For airmail, please add	❑ US$96	❑ DM167	❑ S$135
For surface mail, please add	❑ US$55	❑ DM96	❑ S$78

- *Customers from Europe, please pay in DM.*
- *Customers from Asia-Pacific and Australasia, please pay in Singapore dollars (S$)*
- *Customers from America and the rest of the world, please pay in US$.*

❑ **Please send me a complimentary copy of *International Journal of Bifurcation and Chaos in Applied Sciences and Engineering***

Name:_____ Organization/institution:_____

Address:_____ E-mail:_____

City:_____ State:_____ Zip:_____ Country:_____

METHODS OF PAYMENT

- For cheque payment in USA, please make cheque payable to "World Scientific Publishing Co. Inc."
- For cheque payment from the rest of the world, please make cheque payable to "World Scientific Publishing Co. Pte. Ltd."
- **Please enclose your personal cheque or details of your credit card for INDIVIDUAL subscription.**

❑ Cheque/bank draft enclosed for the amount of _____

❑ Charge my ❑ Visa ❑ MasterCard ❑ Amex ❑ Diners Club

Card No:_____ Expiry date:_____

Signature:_____ Tel:_____

❑ Bill my company/institution:_____ (Please attach purchase order.)

Please add my name to your mailing list. My field of interest is_____

RUSH ORDERS
In USA and Canada,
☎call toll-free:
1-800-227-7562
In Europe, fax:
44-171-836-2020
In other countries, fax:
65-382-5919

SINGAPORE • NEW JERSEY • LONDON • HONG KONG • BANGALORE • TAIPEI

Preparation of Manuscript

(a) The whole manuscript should be written in proper English and typed single-sided on letter-size paper with double spacing and wide margins around the text. All pages should be numbered consecutively. Type references, tables and figure captions on separate pages.

(b) The first page of the manuscript should contain the title of the paper, the name(s), affiliation(s) and address(es) of the author(s) and the abstract. The abstract should be less than 500 words. A shortened version of the title of the paper (less than 50 characters) should be provided. This will be used as the running title.

(c) There is no artificial limit to the length of a paper, but letters to the Editor should preferably be restricted to four printed pages in order to speed up the refereeing process.

(d) The words "section"/"sections," "figure"/"figures" and "equation"/"equations" should be abbreviated to Sec./Secs., Fig./Figs. and Eq./Eqs., respectively, whenever they occur within a sentence, e.g., Eq. (24), Eqs. (7)–(10), Fig. 11, Figs. 12–13, Sec. 5. They should, however, be written in full when they occur at the beginning of a sentence.

(e) Number sections, figures and tables using arabic numerals. Subsections should be numbered using the decimal system (e.g., "3.2" means subsection 2 under section 3). To avoid cumbersome numbering, sub-subsections may be labeled as, for example, "3.2(A)," "3.2(B)," etc.

(f) For section headings, capitalize the first letter of each word except for articles, conjunctions and prepositions (e.g., Bifurcation and Chaos in the Synaptic Circuit Model). For subsection headings, only the first letter of the first word is capitalized.

(g) Equations are labeled with arabic numbers which are enclosed within parentheses and set on the right-hand margin, e.g.,

$$x_{n+1} = -(ax_n + b) \bmod 1 \quad . \tag{7}$$

When an equation is cited in the text, the equation number should be in parentheses, e.g., Eq. (7), not Eq. 7.

(h) All mathematical symbols should be easily recognizable. Identify symbols in the margin if confusion might arise, e.g., between certain capital and lower-case letters, the letter O and zero, etc. Italics should either be typed as such or underlined.

(i) References cited in the text should be placed within square brackets and stated as [surname of author(s), year of publication], e.g., [Smith, 1964], [Smith & Thomas, 1964] and, with three or more authors, [Smith *et al.*, 1964]. If the reference reads as part of the sentence, the square brackets enclose only the year of publication, e.g., "According to Smith [1964], ... "

A complete list of references cited, arranged in alphabetical order according to the surname of the first author, should be provided. References by the same author will follow a chronological sequence, i.e., Smith [1969] precedes Smith [1971]. Article titles should be stated in full but standard abbreviations should be used for journal names.

Examples

Journal reference:

Sharkovsky, A. N. & Romanenko, E. Y. [1992] "Ideal turbulence: attractors of deterministic systems may lie in the space of random fields," *Int. J. Bifurcation and Chaos* **2**(1), 31–36.

Book reference:

Hao, B.-L. [1989] *Elementary Symbolic Dynamics and Chaos in Dissipative Systems* (World Scientific, Singapore) Chap. 2, pp. 25–100.

Kaplan, J. L. & Yorke, J. A. [1979] "Chaotic behavior of multi-dimensional differential equations," in *Functional Differential Equations and Approximations of Fixed Points*, eds. Peitgen, H. O. & Walther, H. O. (Springer-Verlag, Berlin) pp. 228–237.

Proceedings reference:

Barnsley, M. & Demko, S. [1985] "Iterated function systems and the global construction of fractals," *Proc. Roy. London* **A399**, 243–275.

(j) Indicate all footnotes in the text with superscript arabic numerals. Type each footnote at the bottom of the page where it is called for, and separate it from the text by a short bar, e.g.,

---

[2]This equation will be solved in Sec. 5.

(k) Figures, including all labeling, should be professionally done and provided in the form of glossy prints or Indian ink drawings. Low-resolution computer-generated charts or graphics should be avoided. All essential details (e.g., labeling) must be legible after a reduction of at least 50%. Each figure should occupy a separate page with the author's name and figure number clearly stated.

(l) High-quality color pictures will be reproduced by the four-color process. For best results, authors should send transparencies (35 mm slides or preferably larger ones) for reproduction, but color prints should also be provided for color matching and quality control purposes. All color pictures in each paper will be printed on one page or on selected pages.

(m) All acknowledgments (for individuals, organizations or funding agencies) should appear as a separate section before the list of references.

(n) Appendices, if any, should be placed at the end of the paper, after the list of references. Subsections within the appendix should be numbered as A.1, A.2, etc.

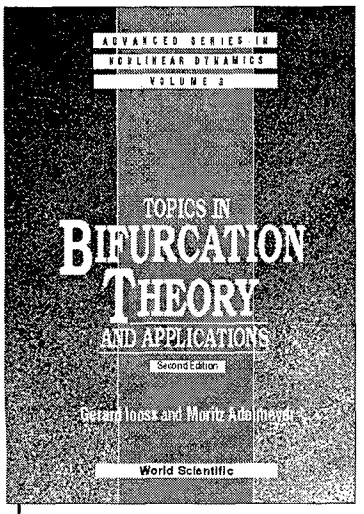

Advanced Series in Nonlinear Dynamics – Vol. 3

TOPICS IN BIFURCATION THEORY AND APPLICATIONS

Second Edition

by **Gérard Iooss** *(Institut Universitaire de France)* &
Moritz Adelmeyer *(ETH Zürich)*

196pp

Pub date: Dec 1998

981-02-3728-6

US$34 • £23

This textbook presents the most efficient analytical techniques in the local bifurcation theory of vector fields. It is centered on the theory of normal forms and its applications, including interaction with symmetries.

The first part of the book reviews the center manifold reduction and introduces normal forms (with complete proofs). Basic bifurcations are studied together with bifurcations in the presence of symmetries. Special attention is given to examples with reversible vector fields, including the physical example given by the water waves. In this second edition, many problems with detailed solutions are added at the end of the first part (some systems being in infinite dimensions). The second part deals with the Couette–Taylor hydrodynamical stability problem, between concentric rotating cylinders. The spatial structure of various steady or unsteady solutions results directly from the analysis of the reduced system on a center manifold. In this part we also study bifurcations (simple here) from group orbits of solutions in an elementary way (avoiding heavy algebra). The third part analyzes bifurcations from time periodic solutions of autonomous vector fields. A normal form theory is developed, covering all cases, and emphasizing a partial Floquet reduction theory, which is applicable in infinite dimensions. Studies of period doubling as well as Arnold's resonance tongues are included in this part.

Contents: ***Center Manifolds, Normal Forms, and Bifurcations of Vector Fields Near Critical Points:*** Unperturbed Vector Fields; Perturbed Vector Fields; ***Couette–Taylor Problem:*** Formulation of the Problem; Couette Flow; Bifurcations from Couette Flow; Bifurcations from Taylor Vortex Flow; ***Center Manifolds, Normal Forms, and Bifurcations of Vector Fields Near Closed Orbits:*** Preliminaries; Adaptation of Floquet Theory; Unperturbed Case; Perturbed Case.

Readership: Scientists and engineers who face qualitative changes in dynamical behavior.

World Scientific
An International Publisher

Home Page:
http://www.worldscientific.com/

For price information, please contact your nearest World Scientific office:

USA office: 1060 Main Street, River Edge, NJ 07661, USA
Toll-free Fax:1-888-977-2665 Toll-free: 1-800-227-7562 E-mail:sales@wspc.com

UK office: 57 Shelton Street, Covent Garden, London WC2H 9HE, UK **Fax: 44-171-836-2020**
Tel: 44-171-836-0888 E-mail:sales@wspc2.demon.co.uk

Singapore office: Farrer Road, P O Box 128, Singapore 912805 Cable: "COSPUB"
Fax: 65-466-5775 Tel: 65-467-7667 E-mail:sales@wspc.com.sg

INSTRUCTIONS FOR CONTRIBUTORS

Organization of Manuscript

To promote the cross-fertilization of ideas among different disciplines, all manuscripts should preferably be organized so that the main results, as well as their significance and potential applications, appear in the earlier sections. Terminologies not generally known outside a main discipline should be defined at the outset. An introductory textbook and/or tutorial paper reference for readers outside the main discipline should also be provided. The technical details, mathematical proofs, and experimental procedure should preferably be given in the latter sections so that a nonspecialist interested only in learning the main results and potential applications need not plow through the complete manuscript in order to filter out this information. Long mathematical proofs should preferably be decomposed into several propositions and/or lemmas so that the main idea of the proof can be understood without having to sift through the fine details.

Submission of Manuscript

Manuscripts should be submitted in **four** copies to:

Professor Leon O. Chua
Editor, *International Journal of Bifurcation and Chaos*
University of California, Berkeley
Dept. of Electrical Engineering & Computer Sciences
Berkeley, CA 94720, USA

To expedite publication, manuscripts of letters to the Editor must include all original line drawings, figures, and photographs.

The cover letter for each contribution should include the author's full postal address, telephone number, computer mail address (if available) and fax number (if available). In the case of a multi-author paper, the cover letter should designate a single author responsible for all future communications.

If available, computer text files ($\TeX$, $\LaTeX$, ASCII or Microsoft Word) should be submitted in a diskette together with the final, revised manuscript.

All manuscripts will be refereed, but they will not be returned to the authors.

Detailed instructions for the preparation of manuscripts are given on the final two printed pages of this issue.

INTERNATIONAL JOURNAL OF
BIFURCATION AND CHAOS
IN APPLIED SCIENCES AND ENGINEERING

MITA (P) No. 310/05/98